Slovak University of Technology

Faculty of Chemical and Food Technology

Polymer Institute
Slovak Academy of Sciences

in cooperation with

INCHEBA EXPO BRATISLAVA

4th International Conference

Polymeric Materials in Automotive

PMA 2011

&

European Collaborative IRCO Conference

RubberCon 2011

12 - 14 April, 2011

Conference Center of hotel Bonbon

Bratislava,

Slovak Republic

In May 2005, the first International Conference on Polymeric Materials in Automotive was organized in Bratislava followed by the second and third PMA in 2007 and 2009. The events reflected steeply rising importance of automotive industry in Slovakia, derived from the presence of dominant investors in Slovakia, namely Volkswagen, PSA and Kia together with a number of other companies – suppliers of plastics and rubber parts being a significant part of them – building up their new facilities in the country. Almost 500 participants from 25 countries attended the three conferences which were ranked as successful and interesting. The appreciated feature consisted in a fact that, although targeted to polymeric materials used in automotive industry, the scope of the conference was kept highly scientific. Thus, new ideas have been presented, many of these being far away from industrial application, still contributing significantly to a progress in the area.

Similar to the PMA 05, PMA 07 and PMA 09 the upcoming conference PMA 2011 is targeted at various aspects related to plastics and rubber in the automotive industry, with the aim to exchange the innovative approaches towards new polymer products increasingly having a decisive influence on the design and appearance of new generation of cars. Developing goals such as aesthetic appeal and comfort, safety and lightweight construction, as well as quality and cost are affected directly by the material concept and the corresponding processing and product technology.

International scientific conference on rubber, Slovak Rubber Conference, has been organized by the Rubber Research Institute of Matador Púchov. From 2005 this traditional event is organized as a part of the International Conference on Polymeric Materials in Automotive. In 2011 the 21th Slovak Rubber Conference will be held as the European Collaborative IRCO Conference RubberCon 2011.

This year the International Conference Polymeric Materials in Automotive PMA 2011 & RubberCon 2011 will be held together with CARPLAST- International Fair of Plastics, Rubbers and Composites for Car Industry and Chemistry Slovakia fair. Considering this, as well as the fact that the year 2011 is the International Year of Chemistry, a first year of a new fair Chemistry Slovakia 2011 is taking place based upon 37 year old tradition of the INCHEBA international fair. The 21th International Car Show AUTOSALON which ranks among significant motoring events in Central Europe will be running in parallel.

Prof. Ivan Hudec
Chairman of the Organizing Committee

Prof. Ivan Chodák, DSc.
Chairman of the Program Committee

MAIN LECTURES

ML-01
CURRENT AND NEXT GENERATION IN-MOULD COATINGS FOR AUTOMOTIVE EXTERIOR TRIM

W. (VOYTEK) S. GUTOWSKI, SHENG LI, GARY TOIKKA, and MARK SPICER

CSIRO Materials Science & Engineering, Functional, Interphases & Coatings and Intelligent Materials, Graham Road (PO Box 56), Melbourne-Highett, Vic. 3190, Australia
Voytek.Gutowski@csiro.au

Abstract

Currently, the most common method of surface finishing plastic automotive exterior trim components is post-mould painting which provides the desired aesthetic and functional attributes to the moulded product (colour, surface gloss, wear & weather resistance). If uncoated, plastics would exhibit substandard durability on exposure to environmental and service elements, e.g.: UV radiation, rain erosion, fuel residues, thus compromising product's visual attributes.

Whilst post-mould coating adds value, improves aesthetics and extends the life of plastic components, it also adds significant costs and additional production steps. It also creates hazardous solid waste and VOCs. In the automotive industry, painting and associated operations account for 30–50 percent of the component's cost, and are a significant source of defects and unrepairable rejects.

This paper addresses the followings:

1. Reviews alternative surface finishing techniques used by auto- and other industries focussing on feasible means for overcoming current challenges and attaining:
   - High-performance automotive quality exterior surface finish through a single-step *'in-mould processing'* comprising coating co-cure with the moulded product, and
   - Single step *'fusion & co-cure'* of surface finishing topcoat material with the substrate, i.e. simultaneous consolidation into a "coated plastic trim component"
2. Describes successful development of an in-mould coating process for plastics which offers the following advantages over the currently used wet-paint finishes:
   - Primer-less in-mould coating (ability to produce 'service-ready' parts),
   - Significantly reduced manufacturing time,
   - Total elimination of hazardous wastes (VOC's and solid waste),
   - UV and wear protection to composite parts during transport and assembly.

REFERENCES

1. Fernholz K. (Ford): *New options for exterior colour*, PCI Paint & Coatings Industry 2006.
2. Grefenstein A., Kaymak K.: Kunststoffe *8*, 37 (2003).
3. Kappacher J., Hollebauer A., Schweighofer L.: Kunststoffe *3*, 112 (2005).
4. Manolis S. L.: Plastics Technol. 2004.
5. BASF: *Advances in automotive coatings technology*, Presentation at Trace Evidence Symposium. Clearwater, Florida, 2009.

ML-02
SPECIAL-PURPOSE RUBBERS REQUIRE SPECIAL CROSS-LINKING SYSTEMS. AN OVERVIEW

HANS MAGG

C/o Lanxess Deutschland GmbH, Chempark, Building K 10
D-51369 Leverkusen, Germany
hans.magg@lanxess.com

Abstract

This report will attempt to provide a brief review of the state-of-the-art in cross-linking systems for non-tire rubbers.

The most important conditions that cross-linking systems are required to meet are functional, process-related and generally "toxicological" in nature, and only to a limited extent economic.

The polymer backbone and cross-linking agent must be matched to one another.

Increased crosslink stability requires polymers with a backbone of increased stability, possibly achieve by the "hydrogenation" of the double bonds.

A classic example of this is the formal transition from IR (or NR) to EPM, being now cured by peroxides. However, since this means that the polymer suffers a significant loss of reactivity for the "classic" cross-linking agents and can therefore no longer be cross-linked sufficiently, new routes must be found to overcome the apparently contradictory effects. The problem is solved by reactive monomers ("cure site" monomers).

Peroxides are comparable to sulfur in terms of their versatility as cross-linking agents, since they are capable of reacting both with double bonds and with systems lacking double bonds, and are essential cross-linking agents for HNBR, FPM, EVM, CM and EPM. The mechanism of peroxide cross-linking systems are shown in detail.

Resin cross-linking is as the third variant of proven curing systems. This involves the use of resoles of *p*-octylphenol or *p*-tert-butylphenol as crosslinking agents, which selectively crosslink polymers with double bonds to form elastomers, with or without chlorine-containing activators depending on their structure.

Another possibility are cross-linking systems involving halogens, which are suitable hetero atoms for activating stable and polar or non-polar polymers of poor reactivity. When modified by these cure sites, such polymer become accessible

for a variety of cross-linking agents since the carbon-halogen bond can readily be cleaved heterolytically or homolytically.

Heterolytic cleavage is promoted by metal oxides (zinc oxide and/or magnesium oxide) or metal soaps, for example, enabling a consecutive reaction to take place with classic sulfur systems, thiourea derivatives and cross-linking agents derived from these, triazine thiols, thiadiazoles and others.

With homolytic cleavage, the polymer can be cross-linked with peroxides. This reaction is similar to the cross-linking of EPM with peroxides outlined above.

Various routes lead to the halogen modification of polymers, i.e.

(1) Halogens as randomly distributed ligands in the polymer backbone (CM, CSM, ECO, CO),
(2) Halogens as cure sites which are formed statically during polymerization (CR),
(3) Halogens as cure sites which are formed by polymer-analog reaction (IIR),
(4) Halogens as cure sites which are used as special co-monomers during polymerization (FPM, ACM).

Further improves stability is generated by halogen-free systems and cross-linking via nucleophilic reaction steps.

For carboxylated diene rubbers and for ethyl acrylate and acrylate rubbers (AEM, ACM) and FPM, acrylic acid or methacrylic acid are among the monomers used as cure site monomers. These create additional possibilities for cross-linking by reaction with metal oxides, preferably zinc oxide thus opening up new application opportunities for the elastomer thanks to improved tensile and wear properties.

There is a need for – naturally polyfunctional – crosslinking agents capable of building up a covalent bond to the polymers. Suitable examples include nucleophilic reactants for electrophilic cure sites or conversely electrophilic reactants for nucleophilic cure sites. A diamine derivative, hexamethylenediamine carbamate (Diak No. 1), has proved most suitable for this purpose.

In fluororubbers too, nucleophilic attack on a double bond activated *in situ* is utilized.

Copolymers of vinylidene fluoride (VDF) / hexafluoropropylene (HFP) can therefore also be cross-linked with hexamethylenediamine carbamate.

The cross-linking of FPM (VDF/HFP) with "alcohols" is largely replacing diamine cross-linking owing to its good processing safety and high degree of cross-linking. The only cross-linking agent used here is bisphenol AF, chemically 2,2-bis(4-hydroxyphenyl)hexafluoropropane.

Isocyanates, for example, react electrophilically with the double bonds of diene rubbers, thus forming stable cross-linking bridges.

Similar – "inverse" systems, as it were – are also possible in heat-resistant rubbers. For example, urethanes are formed under vulcanization conditions if blocked di- or polyisocyanates are present. Polyfunctional carboxylic acids could also conceivably be used as cross-linking agents for amine or hydroxyfunctional cure sites.

ML-03
NEW ASPECTS OF POLYMER ALLOYS AND TPES REVEALED BY POLYMER NANOTECHNOLOGY

TOSHIO NISHI*[a], KEN NAKAJIMA[a], and HIROSHI JINNAI[b]

[a] *WPI Advanced Institute for Materials Research, Tohoku University, 2-1-1 Katahira, Aoba-ku, Sendai 980-8577 Japan,*
[b] *Department of Macromolecular Science and Engineering, Graduate School of Science and Engineering, Kyoto Institute of Technology, Kyoto 606-8585, Japan*
nishi.toshio@wpi-aimr.tohoku.ac.jp

1. Introduction

In order to satisfy industrial demands for various purpose, vigorous research and development have been done on polymer alloys, blends and polymer composites. Recently the characteristic sizes of phase structures of such materials can be as small as on nanometer scale. Especially in the case of thermoplastic elastomers (TPEs), nano-scale microphase-separated structures play an intrinsic role in controlling their mechanical properties. However, the relationship between macroscopic physical properties and microscopic morphological structures was still obscure. In order to boost efficient development and promote creation of novel materials, it is important to develop techniques to evaluate nano-distribution directly. We categorized the required methods into three; nano-three dimensional (3D) measurement, nano-physical properties evaluation systems and nano-spectroscopy. We introduce the first two techniques in this paper.

Transmission electron microtomography (TEMT) is an ideal tool for characterization of polymer nanostructures[1], and as such, it has proven useful for providing high-resolution 3D information on a variety of polymeric structures, *e.g.*, block copolymer nano-scale microphase-separated structures[2–8], etc. Some of these studies provided not only clear 3D pictures but also quantitative structural information. In what follows, we briefly show some examples of structural studies carried out using TEMT to show possible future applications of the methods in polymer science.

For the purpose of evaluating local physical properties, atomic force microscopy (AFM) has a great advantage. While AFM can capture surface morphology on nanometer-scale lateral resolution, it can detect interactive force, which works between a sample and a probe. AFM is mostly used in intermittent contact mode in order to observe surface morphology and phase image was thought to be responses of mechanical properties. However, to derive some physical properties from a phase image is quite difficult[9]. On the other hand, force-distance curve measurement has an advantage that it can obtain quantitative mechanical properties such as Young's modulus. A force mapping measurement is a method to measure force-distance curves at each point after dividing a sample surface into a grid. We combined force mapping measurement with force-distance curve analysis and succeeded in visualizing distribution of various properties such as Young's modulus, adhesive energy on high lateral resolution[10–15]. We show the recent progress on the application of this technique

to block copolymer nano-scale microphase-separated structures.

2. TEMT on block copolymers

Following the classic study carried out by Spontak *et al.*[3], a couple of morphological studies were carried out in the 1990s (ref.[4,16,17]). The numbers of studies using TEMT on block copolymers are increasing rapidly, especially in the past couple of years. This technique has been mainly used for structural investigations due to its 3D visualization capability[6,7].

An interesting example of visualizing complex 3D morphology by TEMT is the double-helical structure of polystyrene-block-polybutadiene-block-poly(methyl methacrylate) triblock terpolymer (SBM)[5]. Since the discovery of the double-helical structure of DNA, the helix has been an attractive subject for investigations of molecular structure[18]. In materials science, numerous studies have investigated the artificial creation and control of helical structures. Because of their sophisticated self-assembling capabilities, block copolymers have been used to mimic the well-known biological architecture, the helix[18,19].

Fig. 1 shows TEM micrographs of the SBM triblock terpolymer, in which the dark gray regions correspond to the OsO_4-stained PB micro domains. The white and light gray regions are the poly(methyl methacrylate) (PMMA) and PS micro domains, respectively. The TEM images reveal that the PS cylinders along with the PB helical micro domains are hexagonally packed in the PMMA matrix. The PS cylindrical micro domains are not completely covered by the PB micro domains, as shown in Fig. 1a. Although the nanostructure of the SBM triblock terpolymer is quite interesting, the 2D projection of the 3D structure did not provide adequate structural information.

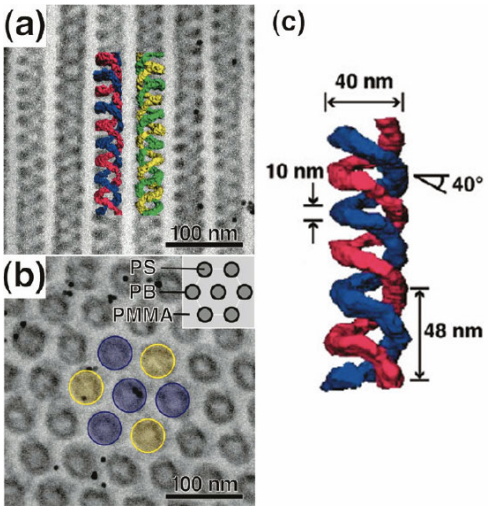

Fig. 1. **TEM micrographs of SBM triblock terpolymer showing its two representative morphology.** OsO_4-stained PB micro domains appear in black. (a, b) Two representative morphologies of SBM terpolymer. (c) Structural dimensions, *e.g.*, pitch of helix, *d*, diameter of helix, *D*, etc.

Both left- and right-handed double-helical structures could be clearly visualized by TEMT (Fig. 1a). Contrary to the previous report on the same triblock copolymer by Krappe *et al.*[18], it was found that the SBM triblock terpolymer has a simple "double"-helical structure and not a four-stranded (*i.e.*, "double double") helical structure. Interestingly, the number of left- and right-handed helical structures was the same. Although the structural order in terms of the helical sense appears to be random, at least at first glance, it is likely that an adjacent pair takes opposing helical configurations (see Fig. 1a). Such detailed but important features of the helical structures can be obtained only by TEMT. It appears that with helical"mesoscale" structures are becoming popular, TEMT will be one of the essential tools for studying the helical morphology as well as complex microphase-separated structures in general.

The TEM and TEMT 3D observations were carried out using a JEM-2200FS (JEOL Co., Ltd., Japan) operated at 200 kV. A series of TEM images were acquired at tilt angles ranging from ±75 at an angular interval of 1°. The experimental details can be found elsewhere[5].

3. Nanomechanical mapping on block copolymers

Block copolymers have attracted increased interest in recent years. The highly ordered nanostructures formed by self-assembly can be found in a wide range of promising applications[20–23]. To date, most of the studies on their nanostructures have been done using small angle X-ray scattering (SAXS) and electron microscopy with proper staining techniques[24]. However, each of these techniques has limitations. The radiation and staining of electron microscopy may damage and change the delicate structure of these Block copolymers, while neither SAXS nor electron microscopy techniques can be used to determine mechanical information on such materials. In order to understand and develop advanced block copolymer-related materials, there is great importance to investigate these samples for identifying phase separated topography, composition, and mechanical properties of individual blocks.

In this work, we report a quantitative method to obtain nanomechanical mapping data of poly(styrene-b-ethylene-co-butylene-b-styrene) (SEBS) triblock copolymers. Our method emphasizes the AFM force volume imaging technique together with Johnson-Kendall-Robert (JKR)[25] analysis. With our technique, high-resolution maps of Young's modulus, adhesive energy, and topography can be obtained simultaneously in a single scan. In addition, we introduce a procedure to rebuild a true height image by which the real surface topography of samples can be determined.

A SEBS sample was supplied by Asahi KASEI Corp. without further treatment. The number average molecular weight, Mn, and the weight fraction of polystyrene (PS) are 50 000 and 0.30, respectively. The film samples with thickness about 10 μm were prepared by solvent-casting a 0.04 g mL^{-1} SEBS toluene solution onto cleaned glass slides. The as-prepared films were first dried in a fume hood for 1 day and then in vacuum at room temperature for another 3 days to remove residual solvent.

Nanomechanical measurements were operated in force volume (FV) mode on a commercial AFM system (Multi-Mode with a NanoScope V controller) under ambient conditions. The samples were scanned at constant force using an E scanner and triangular Si_3N_4 cantilevers with nominal spring constant of 0.32 N m^{-1} (SNL-10, Veecoprobes). An actual spring constant of 0.397 ± 0.005 N m^{-1} was measured by the thermal tune method. Force curves were collected over selected surface areas of 1 μm × 1 μm at a resolution of 128 × 128 pixels. In order to eliminate the effect of substrate stiffness, the value of the trigger set point (3.0 nm) was far less than the 1 % of the film thickness. The obtained force curves were analyzed using JKR contact mechanics to obtain mappings of Young's modulus E and adhesive energy w (ref.[11,12]).

Fig. 2 shows the generated original height, sample deformation, and true height images[26]. Shown in Fig. 2a is the original height image directly obtained from the FV mode. It contains artifacts due to the low elastic modulus of rubbery poly (ethylene-co-butylene) (PEB) component. The sample deformation δ is calculated by subtracting the cantilever deflection Δ from the scanner displacement z ($\delta = z - \Delta$). Then, two dimensional arrays of sample deformation values can be regarded as a sample deformation image (Fig. 2b). The true height image can be considered as the superimposition of the original height image and the sample deformation image. The weak contrast of the true height image is due to large compensation of the deformation at soft PEB regions. Even though, it reveals the real surface topography of the SEBS films prepared by solvent casting technique. By comparing the section analysis of the original height and true height images, it is found that the topography is totally reversed. The higher and lower regions in the original height image become lower and higher regions in the true height image. The height contrast reverses is due to the large deformation caused by the force between the probe tip and the sample.

Fig. 3 shows simultaneously generated maps of the Young's modulus and adhesive energy. Both the Young's

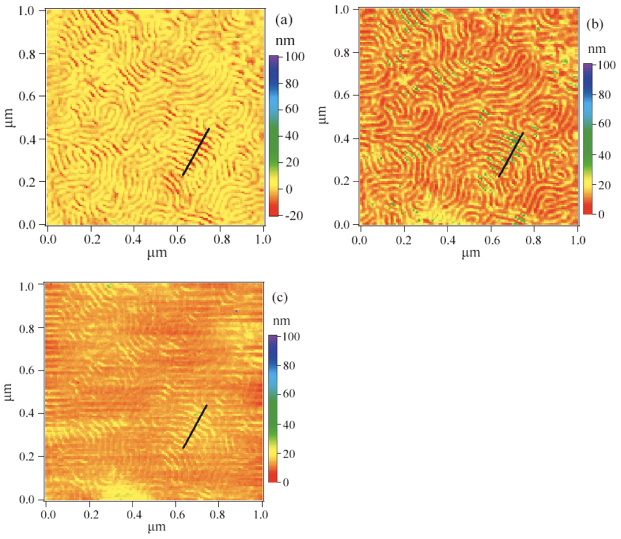

Fig. 2. **Nanomechanical mapping results:** (a) original height image, (b) deformation image, and (c) true height image of SEBS film prepared by solvent-casting technique

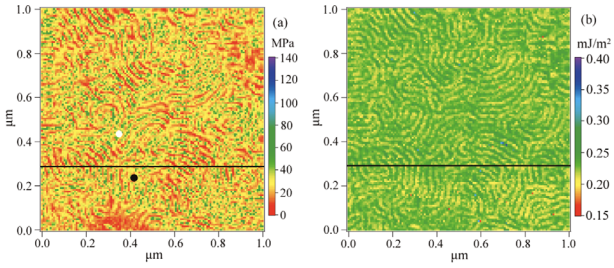

Fig. 3. **Nanomechanical mapping results:** (a) Young's modulus distribution image and (b) adhesive energy distribution image of SEBS film

modulus and adhesive energy distribution images show phase-separated lamellar morphology. The corresponding modulus and adhesive energy profile across a section reveals the two chemical blocks have a large difference in modulus and adhesive energy values. In the Young's modulus image, the light green areas with higher Young's modulus are considered to be the hard PS blocks, while the red areas with lower Young's modulus are considered to be the soft PEB blocks. The Young's modulus is calculated as 53.3 ± 5.4 MPa for white circle and 10.6 ± 3.2 MPa for dark circle. We thus further demonstrate that the light green areas correspond to PS blocks and the red areas to PEB blocks. Using the same evaluation method, we also investigate the Young's modulus of bulk PS and PEB films. The measured modulus value of glassy PS and rubbery PEB is 2.23 ± 0.51 GPa and 13.64 ± 0.68 MPa, respectively. Therefore, the observed modulus on PEB block agrees with bulk value, while PS block's demonstrates a dramatic decrease in stiffness. This decrease may be due to the microstructure effect that the soft PEB blocks surround and support the PS blocks underneath[27]. Other possibilities are that there are some uncertain factors such as the contact area, tip geometry, and the local value of Poisson's ratio.

The adhesive energy image also differentiates the two chemical blocks of the copolymer. However, the adhesive energy contrast between the hard PS and soft PEB blocks is inverted in comparison to the Young's modulus map. The stiffer PS blocks provide lower adhesive energy than the soft PEB blocks. The calculated adhesive energy of PS and PEB components corresponding to the two points indicated in the Young's modulus image is 0.210 ± 0.004 and 0.243 ± 0.006 J m^{-2}, respectively. Comparing with the measured adhesive energy of the bulk PS (0.457 ± 0.037 J m^{-2}) and PEB (1.942 ± 0.094 J m^{-2}), the big discrepancy may relate to the interaction between tip and sample surface. The determined adhesive energy in this work includes all interactions between the tip and sample surface, such as capillary force, which makes the measured adhesive energy very high.

4. Conclusion

We showed several example studies of polymer nanotechnology for TPEs. We will show more examples at the site including TEMT observation of interfacial structure during the well-known order-order phase transitions[28], Nanomechanical mapping of SEBS with the different composition[29], with the different process condition as shown in Fig. 4.

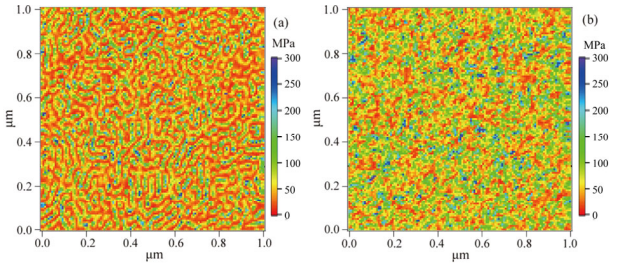

Fig. 4. **Nanomechanical mapping results:** (a) Young's modulus distribution image of spin-cast thin film specimen and (b) that of high-shear treated specimen with twin-screw extruder

The authors thank Dr. Kazuya Nagata of the Asahi Kasei Chemicals Corp. for technical assistance.

REFERENCES

1. Jinnai H., Spontak R. J., Nishi T.: Macromolecules *43*, 1675 (2010).
2. Jinnai H., Nishikawa Y., Ikehara T., Nishi T.: Adv. Polym. Sci. *170*, 115 (2004).
3. Spontak R. J., Williams M. C., Agard D. A.: Polymer *29*, 387 (1988).
4. Radzilowski L. H., Carragher B. O., Stupp S. I.: Macromolecules *30*, 2110 (1997).
5. Jinnai H., Kaneko T., Matsunaga K., Abetz C., Abetz V.: Soft Matter *5*, 2042 (2009).
6. Yamauchi K., Takahashi K., Hasegawa H., Iatrou H., Hadjichristidis N., Kaneko T., Nishikawa Y., Jinnai H., Matsui T., Nishioka H., Shimizu M., Furukawa H.: Macromolecules *36*, 6962 (2003).
7. Wilder E. A., Braunfeld M. B., Jinnai H., Hall C. K., Agard D. A., Spontak R. J.: J. Phys. Chem., B *107*, 11633 (2003).
8. Dobriyal P., Xiang H., Matsunaga K., Chen J.-T., Jinnai H., Russell T. P., Macromolecules *42*, 9082 (2009).
9. García, R., Pérez, R., Surf. Sci. Rep., 47, 197 (2002).
10. Nukaga H., Fujinami S., Watabe H., Nakajima K., Nishi T.: Jpn. J. Appl. Phys. *44*, 5425 (2005).
11. Nishi T., Nakajima K.: *Current Topics in Elastomers Research* (Bhowmick A. K., ed.) CRC press, 2008.
12. Nakajima K., Nishi T., *Polymer Physics* (Utracki L. A., Jamieson A. M., ed.) J. Wiley, Hoboken, New Jersey 2010.
13. Wang D., Fujinami S., Liu H., Nakajima K., Nishi T.: Macromolecules *43*, 5521 (2010).
14. Wang D., Fujinami S., Nakajima K., Inukai S., Ueki H., Magario A., Noguchi T., Endo M., Nishi T.: Polymer *51*, 2455 (2010).
15. Nishi T., Fujinami S., Wang D., Liu H., Nakajima K.: Chinese J. Polym. Sci. *29*, 43 (2011).
16. Spontak R. J., Fung J. C., Braunfeld M. B., Sedat J. W., Agard D. A., Kane L., Smith S. D., Satkowski M. M., Ashraf A., Hajduk D. A., Gruner S. M.: Macromolecules *29*, 4494 (1996).
17. Laurer J. H., Hajduk D. A., Fung J. C., Sedat J. W., Smith S. D., Gruner S. M., Agard D. A., Spontak R. J.: Macromolecules *30*, 3938 (1997).
18. Krappe U., Stadler R., Voigt-Martin I. : Macromolecules *28*, 4558 (1995).
19. Tseng E.-H., Chen C.-K., Chiang Y.-W., Ho R.-M., Akasaka S., Hasegawa H. : J. Am. Chem. Soc. *50*, 1067 (2009).
20. Park C., Yoon J., Thomas E. L.: Polymer *44*, 6725 (2003).
21. Ludwigs S., Böker A., Voronov A., Rehse N., Magerle R., Krausch G.: Nat. Mater. *2*, 744 (2003).
22. Park S., Lee D. H., Xu J., Kim B., Hong S. W., Jeong U., Xu T., Russell T. P.: Science *323*, 1030 (2009).
23. Bang J., Kim S. H., Drockenmuller E., Misner M. J., Russell T. P., Hawker C. J.: J. Am. Chem. Soc. *128*, 7622 (2006).
24. Lynd N. A., Meuler A. J., Hillmyer M. A.: Prog. Polym. Sci. *33*, 875 (2008).
25. Johnson K. L., Kendall K., Roberts A. D.: Proc. R. Soc. London *A324*, 301 (1971).
26. Wang D., Fujinami S., Nakajima K., Nishi T.: Macromolecules *43*, 3169 (2010).
27. Zhou T., Zhang A. M., Zhao C. S., Liang H. W., Wu Z. Y., Xia J. K.: Macromolecules *40*, 9009 (2007).
28. Park H.-W., Jung J., Chang T., Matsunaga K., Jinnai H.: J. Am. Chem. Soc. *131*, 46 (2009).
29. Wang D., Fujinami S., Liu H., Nakajima K., Nishi T.: Macromolecules *43*, 9049 (2010).

ML-04
OVERVIEW OF BIOFOAMS FOR LIGHTWEIGHT AUTO PARTS

MOHINI SAIN*

Centre for Biocomposites and Biomaterials Processing, Faulty of Forestry, University of Toronto, 33 Willcocks Street, Toronto, Canada M5S 3B3
m.sain@utoronto.ca

More lightweight auto parts help save fossil fuels. Biofoams are moving into the mainstream for the auto industry recently because renewable biomasses replace for petrochemicals to make vehicles more environmentally friendly. Biofoams are entirely new sustainable and biologically degradable polymer made from renewable bio-sources. In addition, biomass consumes less energy associated with the energy required for the fabrication process and reduces CO_2 emissions by absorbing greenhouse gas during the plant lifecycle. In the auto parts market, biofoams are mostly biopolyurethane foam with increased content of biomass due to its good quality. The foamed PLA only gains a small proportion.

Bio-polyol is pursued to fabricate polyurethane foam by a foaming process. Most bio-polyol is derived from the production of plant seeds, which is refined to oil. The large output of soybean oil is motivating the use of soy-based polyol, typically in polyurethane foam. Soy-based polyol is made from soybean oil by adding hydroxyl groups at the unsaturated sites. Thus, it has very similar structures to petroleum-based polyol and could react with isocynates to produce foam (Fig. 1).

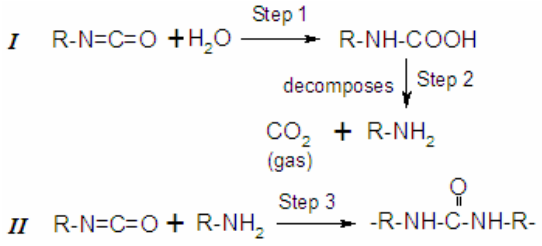

Fig. 1. **Preparation of Polyurethane foams**

High performance polyurethane biofoam could be used to replace traditional petroleum-based polyurethane foams in automotive parts (over 20 kg each car), including seat system, panel, under the hood parts, bumper fascia, and other interior parts etc.

In Canada, the Woodbridge Group has developed soy-based polyurethane foam used in automotive seat cushions, head restraints and arm rests of several popular vehicles, such as 2009 Ford Escape. Biofoam developed by Woodbridge offers up to 25 % bio-based content. We have achieved 100 % bio-polyol substitution with acceptalbe tensile strength in laboratory trials. Ford is weeding out petroleum-based foams in favor of bio-based alternative helping reduce the environmental impacts of its vehicles.

The Ontario BioAuto Council is committing a 4-year, $18 million program to support the research and commercialization of bio-based auto parts, including $1 million in polyurethane automotive seats and interior pieces. There are also more efforts to get bio-based isocyantes to produce absoutely bio-based polyureathne foam. The ongoing project of soy-based isocyanates is funded by Michigan Soybean Promotion Committee to substitute for traditional isocyanates. All the efforts lead to green vehicles in the future with a great win-win situation both for agriculture and the auto industry.

Still, natural fiber containing hydroxyl groups can also be introduced in foaming reaction mixtures for reinforcement and gains better biodegradation.

The authors would thank the NSERC and BioCar for their financial support. Air Products and Chemical Inc. and Urethane Soy Systems are also acknowledged for their cooperation.

KEY LECTURES

KL-01
BLENDS BASED ON PLA AND PHB WITH IMPROVED PROCESSING AND MECHANICAL PROPERTIES

PAVOL ALEXY, PETER BUGAJ, JOZEF FERANC, MIROSLAVA PAVLAČKOVÁ, KATARÍNA TOMANOVÁ, FRANTIŠEK BENOVIČ, RODERIK PLAVEC, MICHAL MIHALOVIČ, and MONIKA BOTOŠOVÁ

Institute of Polymer Materials, Faculty of Chemical and Food Technology, Slovak University of Technology, Radlinského 9, 812 37 Bratislava, Slovak Republic
pavol.alexy@stuba.sk

Introduction

Increasing ecological problems in the last tenth of years bring new approaches in all spheres of human activities in principal. Rising content of green house gases in atmosphere, increasing of global temperature, deliberation of air pollutants as well as increasing of waste waters volume in rivers and oceans, growing of bigger and bigger waste dumps, various ecological catastrophes connected with industrial human activities etc. force us to finding new solutions how to protect environment. The most of negative effects on environment have origin in industrial activities. Production of polymers dramatically increases in the last 5 decades from 1.5 million tons in 1950 to 245 million tons in 2008 (ref.[1]). Modern polymeric materials exhibit very good application properties, high level of resistance to various type of degradation what is very useful during application life of goods. On the other hand, after lifetime these materials are stable against most forms of degradation (biodegradation include) and they are able to remain in environment many years. There are several manners how to solve problems with polymeric waste, including material recycling and energetic recycling (energy recovery in incinerators). In the modern age only reduction or elimination of plastic waste is not sufficient way to solve the ecological problems connected with production, processing and application of polymeric materials. Sources of raw materials for polymer production represent separate problem. Petrol which is main raw material for plastics production represents big reservoir of green house gases which are deliberated during combustion or also during biodegradation of "petrol" polymers. Therefore not only biodegradability of polymers is necessary for protection of environment against the pollutions originated in produced polymers, but also the sources of raw materials have to be solved. In the present time biopolymers, or polymers based on renewable sources appears as the best alternative to petrol based polymers. Substitution of petrol based polymers by biopolymers is not so simple because of some specifics of biopolymers (or bio based polymers). Biopolymers are usually more sensitive to high temperatures in comparison to petrol polymers. Thermal sensitivity brings problems during its processing in the melt using the conventional technologies for plastics processing. Many biopolymers like starch, cellulose etc. are sensitive to moisture. Their properties are not stable and they vary in dependency on relative moisture of application environment. Biopolymers have also usually semi-crystalline and polar character. This gives them such properties like high stiffness, high modulus, but also high brittleness. All these mentioned specifics are regard more as disadvantages. Also price level of majority of biopolymers (or polymers based on renewable sources) is significantly higher in comparison to petrol based plastics.

With respect to all aspects of application of bioplastics in industrial scale, there are several problems which have to be solving for successful introduction of them into industrial life. Polyesters based on renewable sources which exhibit very similar mechanical and physical properties like PP, PET, PS etc. have potential from this point of view. Polylactide acid and polyhydroxyalcanoates (namely PHB) meet most of these conditions, but price of them is relatively high in the present and also processing parameters as well as some mechanical properties represent the barrier to their wider application. PHB is very sensitive to degradation during melt processing and rapid decreasing of molecular weight causes loss of mechanical properties as well as it becomes unprocessable by extrusion due to very low viscosity of its melt. From this point of view PLA is polymer with much better stability of melt, but films prepared from this polymer is very brittle because of high level of crystalinity and physical ageing. Also some physical properties like permeability to gases are worse in comparison to PET or PP. This disadvantage decreases potential of PLA for its application in food packaging where protection of foods against oxygen is important.

The possibilities how to solve mentioned problems can be found in modification of these polymers by addition of modifiers, plasticizers or by blending of two or more polymers together. By this way new materials with new properties can be designed. Possibilities for preparation of polymer blends based on PLA, PHB and starch are investigated in our work with aim to prepare more stable polymer blends during melt processing with better combination of final mechanical properties. Starch as cheap nature polymer was used namely for price reduction of final material.

Materials and methods

PLA 4042D from NatureWorks, LLC, USA was used as polylactide acid, PHB from Biomer, Germany was used as polyhydroxybutyrate, Triacetine was used as plasticizer and Joncryl ADR-4368 and Joncryl ADR - 4300 from BASF, Asia were used as modifiers (styrene-acrylate copolymers containing epoxy groups). Glycerol (GL) from H. C. I. Slovakia was used as starch plasticizer.

All blends were prepared using twin screw extruder L/D=40, diameter = 16 mm, Labtech, Thailand. Tensile tests were done according to ISO 527 standard using Zwick machine at cross-head speed 1 mm min^{-1} in the deformation

range of 0–3 % and after this value of elongation the speed was 50 mm/min. Rheological parameters of blends were measured using oscillation rheometer RPA 2000 from Alpha Technologies. Two types of tests were used in our work – strain sweep for flow curves measurement and timed test for processing stability evaluation. Frequency was set up to 50 cpm during the strain sweep, while angle of strain varied from 0–60°. Timed test was done at constant angle of strain 30° and constant frequency 60 cpm. Time period of test was 20 min. Temperature of measurement for all tested blends was 200 °C.

Results and discussion

Processing stability of PLA and PHB was studied using oscillation rheometer RPA 2000. The dependency of relative values of complex viscosity on time during the timed test was evaluated at various temperatures. Relative values of complex viscosity were calculated according to formula:

$$\eta^*_{rel} = \frac{\eta^*}{\eta^*_0} - 1$$

where η^*_{rel} is relative value of complex viscosity, η^* is complex viscosity at time t, and η^*_0 is complex viscosity at the start of test. Results are presented in Fig. 1. It can be seen that PHB is much more sensitive to thermal degradation than PLA. Both polymers undergo to degradation process rapidly with temperature rising. Decreasing viscosity is connected with decreasing of molecular weight which was confirmed by determination of limiting viscosity number of prepared samples of PLA using Ubelohde viscometer.

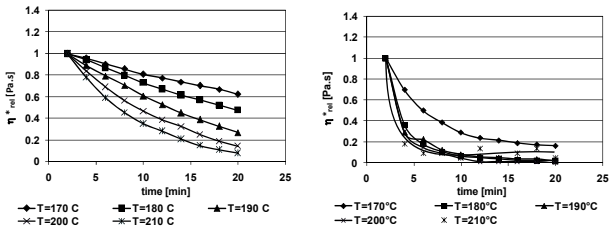

a b

Fig. 1. **Dependency of relative complex viscosity on time and temperature during timed test for PLA (A) and PHB (B)**

Possible stabilisation of biopolyesters during melt processing was tested using copolymer styrene-acrylate which contains epoxy groups (commercial name Joncryl ADR 4368 and Joncryl ADR 4300 from BASF). Effect of used chain extenders on PLA melt viscosity is shown in Fig. 2.

Joncryls are able significantly improve processing stability of PLA during its melt processing. Effectiveness of Joncryls depends on concentration of epoxy groups on polymer chain (in case of Joncryl ADR 4368 it is higher). Effect of Joncryls on PHB was not so strong probably due to much higher rate of degradation of PHB but positive effect was observed in case of PLA/PHB blend if triacetine was used as plasticiser. Flow curves as well as dependencies of relative complex viscosity for PLA/PHB and PLA/PHB/TAC with or without Joncryl ADR 4368 are shown in Fig. 3 and 4.

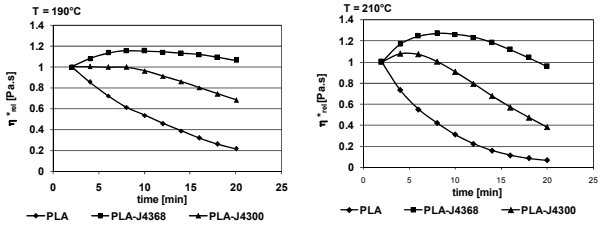

a b

Fig. 2. **Effect of Joncryls on thermal degradation of PLA at 190 °C and 210 °C**

Effect of triacetine on processing stability is weak but addition of Joncryl ADR 4368 significantly improves processability of PLA/PHB as well as PLA/PHB/TAC blends. While TAC slightly decreases processing stability of PLA/PHB/J4368 blend, it is useful to apply it because of improving

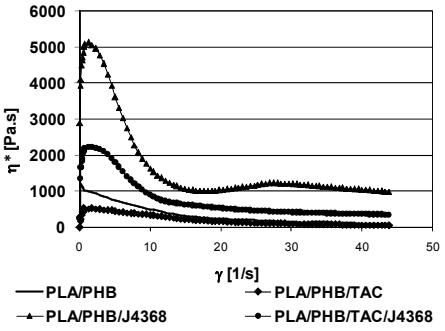

Fig. 3. **Flow curves for PLA/PHB blends (weight ratio 70/30) and PLA/PHB/TAC (TAC content 10 wt.%) with or without Joncryl ADR 4368**

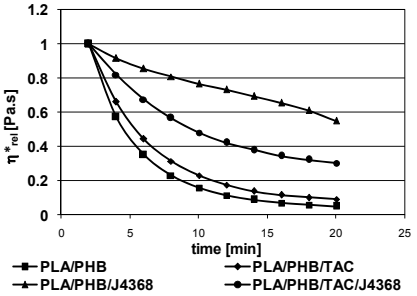

Fig. 4. **Dependency of relative complex viscosity on time for PLA/PHB blends (weight ratio 70/30) and PLA/PHB/TAC (TAC content 10 wt.%t) with or without Joncryl ADR 4368**

of mechanical properties. Dependencies of tensile strength at yield, tensile strength at break as well as elongation at break are shown in Fig. 5–7.

Elongation at break increases (approx. from 200 % to 400 %) in whole range of PHB concentration in PLA/PHB/TAC/J4368 blends. Tensile strength at break and tensile strength at yield reached approximately the same values (up to 50 MPa). Obtained results show that combination of two bio-based polymers PLA and PHB with suitable additives and modifiers can be optimised to blends with balanced properties include processing as well as mechanical properties.

The other possibility how to improve application potential of PLA in industrial scale is decreasing of price of final material. Starch can be considered for such applications which do not need very high values of tensile strength (packaging films for example). We try to applied starch plasticized with glycerol in PLA. Dependencies of tensile strength at break, tensile strength at yield and elongation at break are shown on Fig. 8–10. Various concentration of glycerol was used.

Application of TPS logically decreases tensile strength

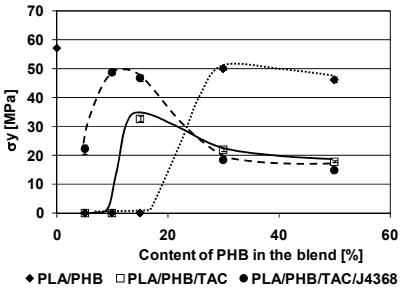

Fig. 5. **The dependency of tensile strength at yield on PHB content in polymer blends;** *PLA/PHB/J4368 blends exhibit no yield point. Zero values mean also that samples exhibit no yield points

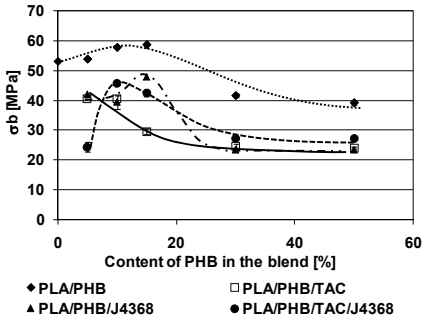

Fig. 6. **The dependency of tensile strength of break on PHB content in polymer blends**

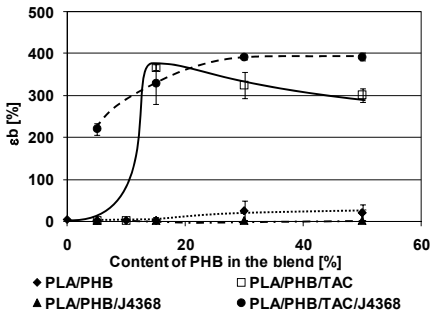

Fig. 7. **The dependency of elongation at break on PHB content in polymer blends**

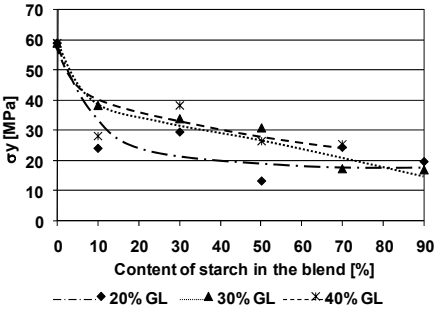

Fig. 8. **Dependency of tensile strength at yield on TPS content in PLA/TPS blend**

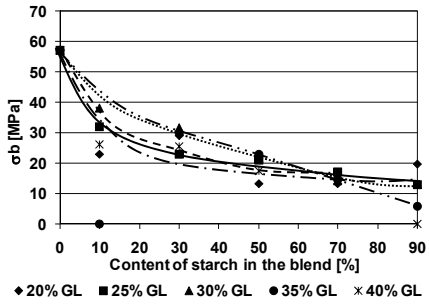

Fig. 9. **Dependency of tensile strength at break on TPS content in PLA/TPS blend**

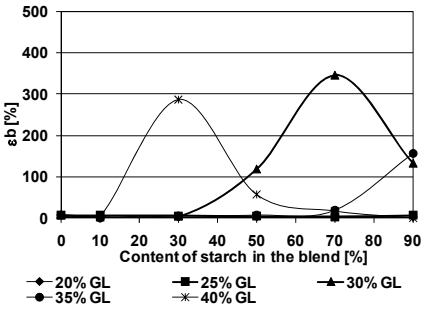

Fig. 10. **Dependency of elongation at break on TPS content in PLA/TPS blend**

at break and tensile strength at yield but real values can be adjusted higher than 20 MPa. Such values are sufficient for common application in packaging. On the other hand by application of TPS much better elongation at break can by obtained if suitable concentration of TPS is used. The maximum of elongation at break reached values about 300−400 % in comparison to values of the pure PLA which are very low near to 0. Position of maximum of elongation at break on axis of TPS concentration can by adjusted by concentration of glycerol in TPS. Obtained results show that there are possibilities to design biodegradable material based on renewable sources with required mechanical properties. Starch satisfy price decreasing as well. These results give better chance to indtroduce such materials into real market.

Conclusion

Results obtained in our work show possibilities how to improve processing as well as some mechanical properties of PLA/PHB blends. Thermal stability and elongation at break were significantly improved if plasticizer triacetine and modifier Joncryl were used. Thermoplastic starch in suitable concentration in dependency on glycerol content is able to improve elongation at break of PLA simultaneously with price decreasing of final material.

This project is supported by Norwegian Financial Mechanism, Financial Mechanism of EEA and State budget of Slovakia – project No. SK 0094.

REFERENCE

1. Chanprateep S.: J. Biosci. Bioeng. *2010*, 621.

KL-02

PROCESSABILITY AND STATE-OF-MIX OF RUBBER COMPOUNDS: A THOROUGH INVESTIGATION BY EXTENSIONAL RHEOLOGY

FABIO BACCHELLI, MARIA FRANCESCA PIRINI, and SALVATORE COPPOLA

ENI-Polimeri Europa, Elastomers Research Centre, Via Baiona 107, 48100 Ravenna, Italy
fabio.bacchelli@polimerieuropa.com

Whatever the chemical nature and composition, rubber compounds are reinforced system of complex heterogeneous nature. They are consisting of several phases and at least one phase is a viscoelastic material. As a consequence, particular morphologies are observed, arising from interactions between the polymer matrix and the reinforcing network. The resulting structure strongly affects flow properties and rheological response. Addition of fillers into polymers is a common industrial practice and, among factors that basically determine the behavior of filled polymers, like the structure of the filler, the viscoelasticity of the polymer matrix and the interfacial interactions, the state of dispersion is known to be extremely important. Active fillers interact both with the polymer matrix and with each other. Physical adsorption of rubber molecules takes place on the filler surface occluding part of the polymer in internal voids. This results in a partial immobilization of the elastomer and an apparent increase of the filler volume fraction. Moreover, filler particles form aggregates and agglomerates resulting in a secondary structure represented by a filler-filler network.

Rheology is the science of deformation and flow of matter, whose investigation tools essentially result from continuum mechanics considerations. The presence of a reinforcing filler is known to induce dramatic changes in the rheological behavior of a polymer and this effect is generally attributed to three main contributions: the hydrodynamic effect of the filler in the molten polymer, the change of the relaxation times of the matrix and the building of a filler network. Strong nonlinear viscoelastic behavior is then observed both in shear and extension.

Among flow kinematics, the extensional contribution proves to be essential in filler wetting and dispersive mixing. The use of this experimental approach reveals to be very sensitive to the state-of-mix in terms of effective filler volume fraction.

A commercial high-cis-polybutadiene (high-cis-BR) was investigated (Neocis BR40, Polimeri Europa). The polymer, nearly linear, has an average molecular weight of 420 000 g mol^{-1} and a polydispersity index of 3.8. Two series of compounds were prepared in a laboratory Brabender Plasticorder using different mixing procedures. The first was obtained by adding a nearly spherical carbon black (N990) and other high structure grades (N330, N121). The second was obtained with the N330 at two different times of mixing. The added volume fraction of filler was 0.21 for all compounds.

The linear viscoelasticity of high-cis-BR was investigated by means of a stress controlled Anton Paar Physica MCR 501 and a strain controlled Rheometrics Ares A11. The investigated frequency range was extended by performing stress relaxation and creep experiments and by converting data by means of Schwarzl formulas[1]. The software used for the calculation of relaxation spectra was the Anton Paar Rheoplus/32 v. 2.62. Large amplitude strain sweep experiments were performed using an Alpha Technologies RPA2000 closed chamber rheometer, equipped with serrated biconical geometry.

Stress growth experiments on unfilled and filled polybutadiene were performed in uniaxial extension at constant deformation rate using a home made assembly based on a four wheels Rheotens 71.97 tensile tester produced by Göttfert[2]. Extruded cylindrical specimens for extensional measurements were prepared by means of a Göttfert Rheograph 6000 capillary rheometer and relaxed for at least three days before measurement.

The reinforcing action of carbon black can be described by analyzing the relaxation dynamics of the filled systems. In Fig. 1 the relaxation spectra of carbon black compounds are reported and compared to that of the pure elastomer.

Large differences are observed at longer times, were the filler contribution in slowing down the terminal relaxation is particularly effective. The spectrum of the N990 based compound is qualitatively similar to that of the polymer matrix, accounting for a dominant effect of hydrodynamic reinforcement. The introduction of the high surface area N330, with his important secondary structure, completely changes the shape

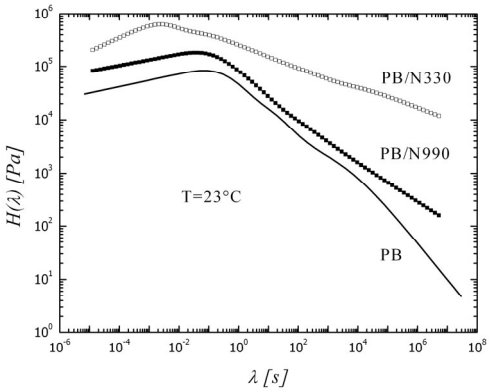

Fig. 1. **Relaxation spectra of high-cis-polybutadiene and related carbon black compounds**

of the relaxation spectrum, moving the characteristic maximum of the pure elastomer to shorter times and enlarging the range of very long relaxation dynamics. This result should be discussed in terms of transient rheological response, a concept very close to the compound processability. Dimensionless parameters, as for example the Deborah and Weissenberg numbers, commonly used to compare the characteristic time of the material with the characteristic times of experimental practice, are obviously governed by the reported relaxation behavior.

The decrease in elastic modulus upon increasing strain amplitude, attributed by Payne to the structure of the carbon black, may be visualized as filler–filler linkages of physical nature which are broken down by straining[3]. The breakdown of the filler network by increasing strain amplitude would release the immobilized rubber so that the effective filler volume fraction and hence, the modulus would decrease.

This mechanism suggests that the Payne effect can serve as a measure of filler networking which originates from filler–filler interaction as well as polymer–filler interaction. A typical graph showing the shear modulus variation with strain amplitude of filled high-cis-polybutadiene (normalized using the plateau modulus of the pure polymer) is shown in Fig. 2 and compared with the contribution of the pure elastomer. As expected, the normalized shear modulus decreases with increasing the amplitude of oscillation. The effect is more pronounced with carbon black of high surface area and is then associated with the properties of filler particles. The normalized shear modulus has been found to have a limiting value both at low strains and at high strains, when further changes of modulus with strain are negligible. The quantity at very high strains represents the dynamic shear modulus when all the carbon black structure has been broken down. This is higher than the gum modulus due to hydrodynamic effects plus the filler-polymer contribution.

The differences in filler networking associated with the filler structure are depicted in Fig. 3, where the AFM technique has been used to produce the reported images of polybutadiene/carbon black compounds. Isolated nearly spherical particles of N990 are clearly visible, while aggregates are observed in the case of N330.

Simple shear is the customary mode of deformation for the study of rheology. However, simple shear experiments do not provide all the information necessary to describe processability of rubber compounds. The milling behavior of gum elastomers and filled rubber was first studied by Tokita and White who distinguished four characteristic milling regions that can be readily interpreted in terms of extensional flow properties of rubbers associated with convergent flows such as that at the approach to the nip[4]. Similar arguments can be used to describe milling in an internal mixer: as the rotor advances, the rubber passes successively through extensional flow and high shear regions to reach the void behind the rotor. In general the mixing process involves both extensional and shear flows, where the extensional flow is more efficient in the dispersion and break-up of rigid aggregates during filler dispersion.

The significance and importance of the extensional flow investigation in the processing of rubber was discussed by Nakajima, who pointed out that the elongational behavior plays an important role in mixing elastomers with carbon-black[5]. Cotten and Thiele, working on extensional behavior of carbon black filled SBR rubber at constant deformation rate, found that the composite curve showed no tendency to reach a steady state viscosity even at the lowest strain rate of $1.8 \cdot 10^{-4}$ s^{-1}

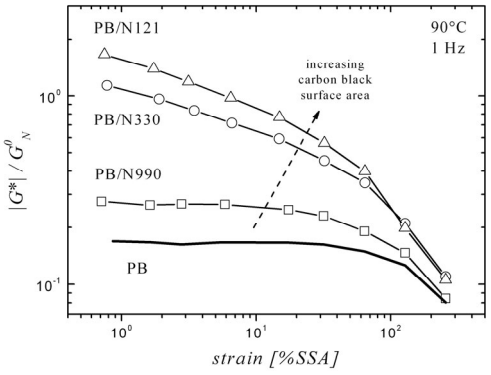

Fig. 2. **Strain dependence of the normalized shear modulus for polybutadiene and related compounds obtained with carbon black of different surface area**

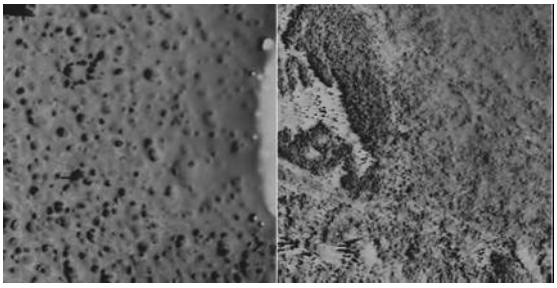

Fig. 3. **AFM images (20 μm) of polybutadiene compounds with different filler structure, BR/N990 (left) and BR/N330 (right)**

and some upward curvature continued to persist. In analogy with shear behavior, they observed a viscosity decrease with increasing the strain rate and with decreasing the carbon black loading[6]. They also reported that, while higher carbon black loading or different carbon black structure caused an increase in viscosity without changing the transient plot shape, an increase in carbon black surface area was responsible of both an increase in viscosity and in the upward curvature of the transient stress growth.

Fig. 4 concerns with the transient extensional response of polybutadiene/carbon black composites obtained at different mixing time. The hydrodynamic effect can be deduced from the difference between the linear viscoelastic envelope of the compounds and three time the transient shear viscosity of the pure elastomer, according to the Trouton rule. Both systems exhibit strong nonlinearities and a pronounced strain hardening is observed, to be intended as the upward detachment from the linear viscoelastic response. At shorter mixing time, a less efficient carbon black dispersion is expected together with a higher effective filler volume fraction and, consequently, a more pronounced strain hardening is observed. This is particularly true at low deformation rates, where the filler network disruption due to the extensional flow is less effective.

According to Medalia and Tokita and Pliskin, the dependence of the compound rheology on the state-of-mix can be related to the presence of immobilized polymer in the form of occluded rubber[7,8].

Occluded rubber is a geometrical concept and refers to rubber, which is situated within the irregular contours of a filler aggregate and it is thus shielded from stress. In the well-dispersed stage, the carbon black particles are individually isolated or grouped in small aggregates while at an earlier stage of mixing the particles at the same filler loading are not well dispersed and can be found to be agglomerated with one another. Each agglomerate contains not only filler particles, but also has rubber occluded between the particles. When stress is applied, the entire filler agglomerate with its occluded rubber behaves as a single filler particle so that the effective filler volume fraction in the early stages of mixing is

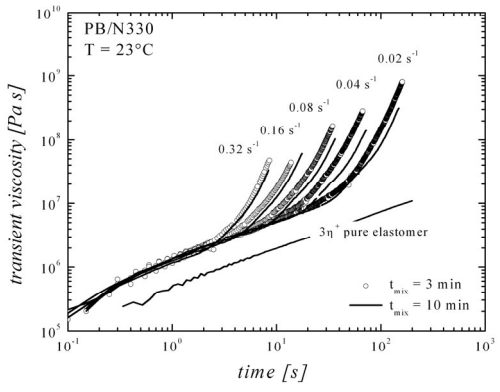

Fig. 4. **Transient extensional behavior of polybutadiene/N330 compounds at different state-of-mix and various deformation rates. The linear viscoelastic response of the pure elastomer according to Trouton rule is also reported**

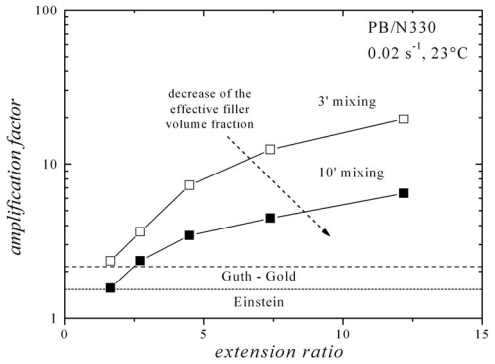

Fig. 5. **Amplification factors in uniaxial extension for polybutadiene/carbon black compounds obtained at two different mixing times**

always larger than that of the well-mixed compound.

The amplification factor in uniaxial extension can be used to represent the variation in occluded rubber as a function of carbon black dispersion. In Fig. 5, the ratio between the tensile stress of pure polybutadiene and that of the N330 compound is reported for the two investigated times of mixing. As expected, the optimization of carbon black dispersion leads to a strong decrease of the amplification factor, accounting for a large decrease of the effective filler volume fraction.

In conclusion, rubber compounds represent highly concentrated suspensions characterized by complex interactions between filler particles and between particles and polymer. A very long memory of the deformation history together with a strong nonlinear viscoelastic response is observed as a consequence of restructuring phenomena. Reinforcement in a carbon black filled polybutadiene is due to hydrodynamic effects together with the build-up of a secondary particulate structure within the rubber matrix and a consequent amount of occluded and immobilized polymer. In this frame, rheology proves to be a powerful tool for investigating the complex behavior of rubber compounds. Among rheological techniques, the transient extensional response results to be very sensitive to the filler network as a function of the state-of-mix.

The authors wish to thank Polimeri Europa for the permission to publish this paper. The authors are also indebted to Danilo Visani for the AFM contribution. Alberto Abbondanzieri and Pier Dante Tavolazzi are acknowledged for their technical support.

REFERENCES

1. Schwarzl F.: Rheol. Acta *8*, 6 (1969).
2. Bacchelli F.: Rheol. Acta *46*, 1223 (2007).
3. Payne A. R.: Rubber Chem. Technol. *39*, 365 (1966).
4. Tokita N., White J. L.: J. Appl. Polym. Sci. *10*, 1011 (1966).
5. Nakajima N.: Rubber Chem. Technol. *53*, 1088 (1980).
6. Cotten G. R., Thiele J. L.: Rubber Chem. Technol. *51*, 749 (1978).

7. Medalia A. I.: Rubber Chem. Technol. *45*, 1171 (1972).
8. Tokita N., Pliskin I.: Rubber Chem. Technol. *46*, 1166 (1973).

KL-03
NEW RAPID METHOD FOR TESTING THERMOPLASTIC ELASTOMERS

JOHN S. DICK and HENRY A. PAWLOWSKI

Alpha Technologies,3030 Gilchrist Road,Akron, OH 44305 USA
john.dick@dynisco.com

Abstract

In the last two decades, thermoplastic vulcanizates (TPVs) and other thermoplastic Elastomers (TPEs) have significantly increased their usage in the rubber industry. New concerns regarding variability in processing characteristics and product performance have emerged and new methods to effectively and quickly predict these differences among different lots or different grades of TPEs have been developed using the Advanced Polymer Analyzer with parallel plate dies. Also this paper explores the advantages of different sample preparation techniques.

Experimental

Much of the testing performed in this study was done with the Alpha Technologies APA 2000® Advanced Polymer Analyzer. The APA is very similar to the RPA 2000® Rubber Process Analyzer, except that it possesses the software and hardware to test with parallel plate dies instead of only biconical dies. The parallel plate dies are used for TPE testing because when cooling the specimen from the hot melt, parallel plate dies allow for even cooling across the interface as the specimen solidifies, which does not happen as well with the biconical dies. Also when testing TPE hot melts, there occasionally are times when the ring procedure needs to be used to assure that sufficient sample pressure is maintained so that slippage does not occur

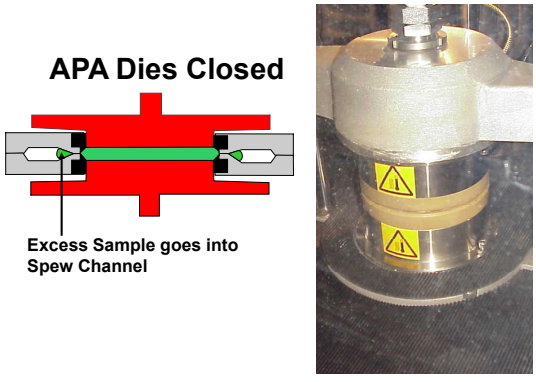

Fig. 1. **APA Dies Closed**

Fig. 2.

This VTM is an automated "viscosity, transition, modulus" rheometer. Just as with the APA, the VTM can measure the **v**iscosity, the thermal **t**ransition, and the **m**odulus of TPEs and other thermoplastics as well. In addition, testing was also conducted on the Alpha Technologies ARC 2020 capillary rheometer to compare the viscosity measurements from the APA with those measured by the capillary rheometer under conditions of steady state shear.

Discussion

A series of measurements were performed on the rheological properties of the TPEs in their melt state and their dynamic properties in their congealed solid state. The three groups of TPE materials that were compared in this study were EPDM / Polypropylene Thermoplastic Vulcanizates, Styrenic Block Copolymer Thermoplastic Elastomers, and ACM / Nylon Thermoplastic Vulcanizates.

Fig. 3 displays the differences in shear thinning profiles observed from the complex dynamic viscosity (η*) measurements obtained from 10-point frequency sweeps of the polymer melts at 215 °C. The APA frequency sweep is a very rapid method for measuring differences in shear thinning profiles among grades of TPVs. All TPEs are non-

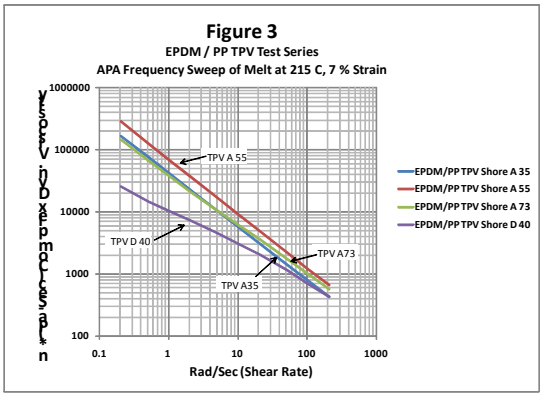

Fig. 3.

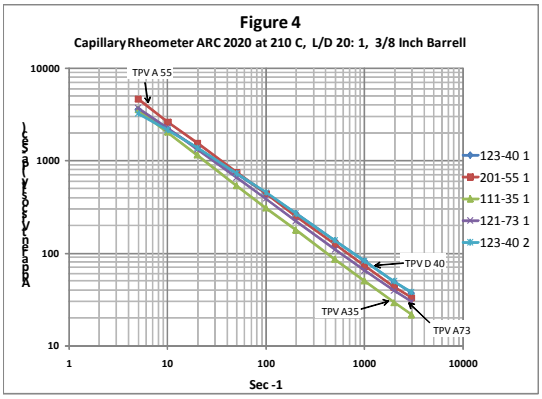

Fig. 4.

Newtonian, meaning that their viscosity (or resistance to flow) will decrease with a rise in applied shear rate (such as a faster extruder speed, etc.). By using the Cox-Merz Rule, one can assume that 1 radian / second under sinusoidal oscillation is equivalent to 1 sec^{-1} under steady state flow conditions (such as with a capillary rheometer or a factory extruder). Fig. 4 shows the shear thinning relationship of these same materials when compared by the capillary rheometer (ARC2020).

Higher durometer EPDM / PP TPVs usually contain more polypropylene in relation to the EPDM rubber content. The polypropylene melt functions somewhat like a "lubricating agent" at low shear rates. Therefore at low shear rates, the particles of vulcanized EPDM rubber are spaced more widely apart and are more free to move, resulting in a relatively lower viscosity. However, these TPVs are actually heterogeneous nanocomposites of vulcanized EPDM particles (representing the discontinuous phase) dispersed in the polypropylene continuous phase. The other "softer" TPV grades contain more of the dispersed, vulcanized EPDM rubber particles which imparts more of a pseudoplastic (shear thinning) effect on the TPV at higher shear rates, causing it to drop its viscosity faster than TPVs (such as the D40 grade), which are not as shear thinning at the higher shear rates. This may explain why the ordinal relationship for ranking of viscosity values becomes inverted when a comparison is made between low shear rate measurements vs. high shear rate measurements. This results in "crossovers" for both the APA profiles as well as the capillary rheometer profiles.

Conclusions

1. A consistent test configuration and test method was established which has broad applicability across a broad range of thermoplastic elastomers.
2. This test procedure displayed very good statistical test sensitivity (discerning power) regarding TPE quality differences in both the melt state and congealed state.
3. This test procedure displayed very good test repeatability for both the melt state and the congealed state.
4. This system can measure changes in shear thinning profiles due to TPE compositional changes.
5. Changes in melt elasticity caused by TPE compositional changes were effectively measured as well.
6. The elastic modulus of the congealed TPE could be effectively measured by this test procedure.
7. Hysteretic differences of the congealed specimens were also effectively measured.
8. Differences in strain softening profiles of the congealed specimens were also effectively measured as well.

KL-04
AGING MECHANISMS OF ELASTOMERS AND EFFECTIVENESS OF ANTIOXIDANTS

ULRICH GIESE* M. SANTOSO and Y. NAVARRO TORRÉJON

Deutsches Institut für Kautschuktechnologie e. V., Eupener Str. 33, 30519 Hannover, Germany
Ulrich.Giese@DIKautschuk.de

1. Introduction

The service life of elastomer components is determined largely by aging processes. Over the course of time mechanical-dynamic (fatigue), oxidation processes, temperature and exposition to UV light lead to irreversible changes in the physical and chemical properties of an elastomer material[1,2]. Alongside the selection of polymers, the aging process is determined mainly by the use of anti-aging agents – e.g. *p*-phenylenediamines or by substituted phenols[3,5–8]. This work focuses specifically on temperature dependency and kinetic aspects of thermal-oxidative aging, on the influence of polymer structure and on the consumption and mechanistic aspects of antioxidants (*p*-phenylenediamines)

2. Theoretical aspects of thermal-oxidative aging

Thermal-oxidative aging is described by means of a (three-phase) radical mechanism[9–13]. The chain reaction is terminated by recombination reactions with the formation of stable compounds, such as, for instance, the constitution of C-C or C-O-C bonds from two macroradicals, tantamount to an increase in crosslinking density. An embrittlement of the material is the macroscopic consequence. On the polymer, there is also formation of polar oxygenic side groups, which likewise have a stiffening effect due to inter- and intramolecular interactions. As a function of aging conditions and the microstructure of the polymers, chain scission can also be observed, accompanied by elastomer viscosity[11,17]. The two reaction channels compete with one another[18–22] Antioxidants are usually used to avoid aging processes. The antioxidants have different effectiveness in dependency on their molecular structure and chemical reactivity. Considering chemical reaction mechanism in the subject of thermal-oxidative aging two groups of antioxidants are exists, the primary (chain breaking) and secondary antioxidants[10,26–28].

3. Methods and materials

For systematic investigations on aging stability of polymers and on mechanisms as well on effectiveness of antioxidants. Were carried out by means of rheometry, chemiluminescence (CL) (ref.[27]), ATR-FT-IR spectroscopy, in combination with CL, extraction, extract analyses by means of GC-MS and LC-MS and analyses of squalene model systems by means of LC-MS. The investigations on polymers were performed with technical grades of three both polydienes (SBR, BR, and NR) used in technical scale and laboratory grades of S-SBR prepared by anionic polymerization with different vinyl content. For systematic investigations on antioxidants on one hand unvulcanized model compounds with polyisoprene rubber (IR) or polybutadiene rubber (BR) with different *p*-phenylene diamines (PPDs) with concentrations in the range from 1 to 7 phr and on the other hand a model substance system consisting of squalene and 10 phr p-PPDs were used.

4. Results

4.1. Investigations on polymers

The thermal oxidation aging of polydienes is significantly influenced by the double bond concentration in the main chain (1,4 units). The OIT value of the polymer, measured by means of Chemiluminescence is also influenced by the addition of stabilizers and by the types of processing. Changes occurring in the polymer structure during the thermal oxidative aging processes can be traced by coupling CL with IR spectroscopy methods. This yields semi-quantitative measurements of the decrease of 1,4-trans units of SBR during the thermal oxidation reaction. These measurements also confirm that this aging process occurs mostly at the double bonds in the main chain, because the decrease of 1,2 units is significantly lower than a decrease of 1,4-trans units.

4.2. Investigations on *p*-phenylenediamines in dependency on molecular structure

The systematic investigation of the influence of the moleculare structure of used p-PPD in dependency on concentration (1 to 7 phr or 10 to 70 g kg^{-1}) in IR results in OIT-values (oxygene induction times), which characterize the thermal-oxidative stability (see Fig. 1) .

A high OIT correlates with a high stability. The efficiency, that means OIT-shift per concentration p-PPD, is given by the slope of the linear function in Fig. 1. So the following sequence is resulting: 77PD < 6PPD < DPPD. The p-PPD -type with the highest amount of aryl-aryl-substituted nitrogene has the best efficiency.Reaction products of p-PPD`s in IR are identified using GC-MS in combination of CL-measurements and extraction. Extracts were produced in dependency of the shape of the CL curve at different times. The CL-curves shows two signals, where the first one is asigned to the antioxidant and the second one to the polymer. After the decay of the first peak no anitoxidant could be detected, but some reaction products, mainly *N*-formyl-derivates or *N*-alkanone-yl-derivates of the p-PPD appear during the

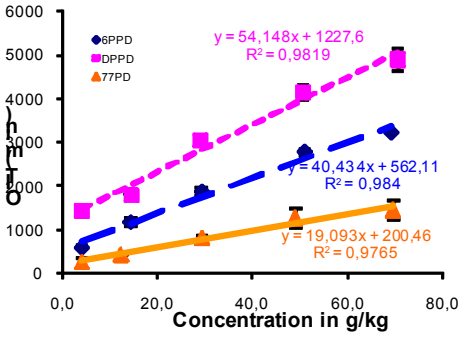

Scheme 1. **OIT-values as function of concentration and structure of *p*-phenylenediamine (DPPD, 6PPD and 77PD) in IR at 150 °C**

increase of the polymer signal. After decay of the polymer signal, for example in the case of the system DPPD/IR after 120 h no antioxidant and no reaction products could be detected. So it could be concluded, that the reaction products are reactive under aging conditions. Systematic investigations on the model system squalene/6PPD using aging at 150 °C in CL and LC-MS analyses in dependency of the aging time had the main objective to identify from reaction mechanism possible pendant groups of antioxidant/squalene, where squalene should act as polymer model. the question is the fate of the antioxidant. The LC-MS -analyses result in the typical above mentioned reaction products of 6PPD and in hydroxylated squalene. The dependency of the yield of different reaction products on aging time are shown in the following selected LC-Ms chromatogram:

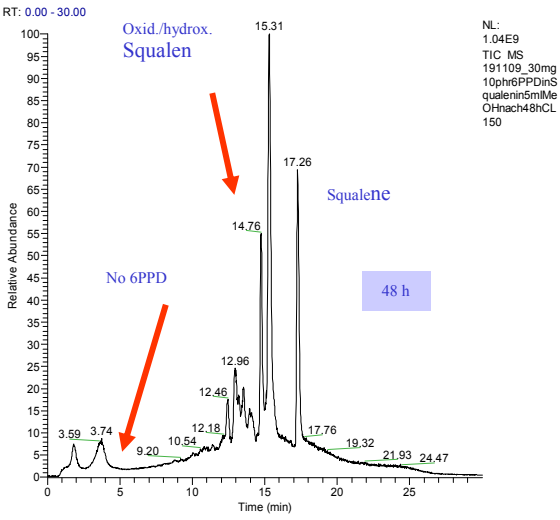

Scheme 2. **LC-MS analyses of model system 6PPD/squalene after after 48 hours aging in CL**

6. Summary

The results of the systematic investigations are summarized as follows:

The stability of polymers could be quantified using CL-measurements. The double bonds in the main chain of the polymer are responsible for the aging stability

The efficiency and effectiveness of the investigated p-PP`s correlate with the molecular structure. The aryl-aryl types have the more stabilizing effect: DPPD > 6PPD > 77PD.

Reaction products have higher mol masses than the origin antioxidant from recombination of antioxidant-radicals with Carbonyl-radicals.

The authors deeply acknowledge the Deutsche Kautschuk Gesellschaft (DKG e.V.) for the support of this work.

REFERENCES

1. DIN 50035 (1972)
2. IUPAC Recommendations-Definitions of Terms Relat ing to Degradation Ageing and Related Chemical Transformations of Polymers (1996)
3. Engels H. W., Hammer H., Brück D., Redetzky W.: Rubber Chem. Technol. *62*, 609 (1989).
4. Sampers J.: Polym. Deg. Stab. 76, 455 (2002).
5. Parra D. F., De M. T., Freire A., De Paoli M.-A.: J. Polym. Sci. *75*, 670 (2000).
6. Ambelang J. C., Kline R. H., Lorenz O. M., Parks C. R., Wadelin C.: Rubber Chem. Technol. *36*, 1497 (1963).
7. Boxhammer J.: Material Test. Prod. Tech. News (Atlas Sun SP) 30 (2000) 1.
8. Krüger R. H., Boissiere C., Klein-Hartwig K., Kretzschmer H. J.: Food Addit. Contam. 22, 968 (2005).
9. Scott G.: Chem. Industry *16*, 271 (1963).
10. Scott G.: *Mechanismen of Polymer Degradation and Stabilisation*, p. 170. Elsevier Applied Science, London-New York 1990.
11. Hoff A., Jacobsson S.: J. Appl. Sci. *27*, 2539 (1982).
12. Scott G.: *Developments in Polymer Stabilisation*, p. 145. Applied Science Publishers LTD, London 1981.
13. Snijders E. A., Boersma A., van Baarle B., Noor J. dermeer: Polym. Degrad. Stab. *89*, 200 (2005).
20. Santoso M., Giese U., Schuster R. H.: Rubber Chem. Technol. *81*, 762 (2007).
21. Santoso M., Giese U., Schuster R. H.: KGK, Kautsch. Gummi Kunstst. *60*, 192 (2007).
22. Bender H., Campomizzi E.: KGK, Kautsch. Gummi Kunstst. *54*, 14 (2001).
23. Bhattacharjee S., Bhowmick A. K., Avasthi B. N.: Polym. Degrad. Stab. 31 (1991).
24. Scott G.: Rubber Chem. Technol. *58*, 269 (1985).
25. Modrow H., Zimmer R., Visel F., Hormes J.: KGK, Kautsch. Gummi Kunstst. *53*, 328 (2000).
26. Ferradino A. G.: Rubber Chem. Technol. *76*, 694 (2003).
27. Engels H.-W.: KGK, Kautsch. Gummi Kunstst. *47*, 12 (1994).
28. Brück D., Engels H.-W.: KGK, Kautsch. Gummi Kunstst. *44*, 1014 (1991).

KL-05

SHEAR-INDUCED METASTABLE STATES OF END-GRAFTED POLYSTYRENE

LESLIE A. SASA, ERIC J. YEARLEY, MICHAEL S. JABLIN, ROBERT D. GILBERTSON, JAROSLAW MAJEWSKI, and REX P. HJELM

Los Alamos National Laboratory, Los Alamos, New Mexico, 87545
hjelm@lanl.gov

The conformational changes of end-grafted polymers, attached at one end to a surface or interface and entangled with free polymer in the bulk, have been of interest in theoretical and experimental studies of non-linear viscoelastic properties, such as shear thinning. This effect may be related to slip-shear observed in the bulk[1,2], which has been proposed to result from disentanglement of surface-bound polymer from the bulk[3], changes in the local conformations of the polymer in the bulk[4]; exchange of polymer at an interface[5]; or a combination of the aforementioned phenomena. However, discrimination between these models are lacking. Resolution will lead to more accurate physics models for non-linear effects polymers, which are important in many of their applications.

Whereas there are a number of theoretical and experimental studies on end-grafted polymer in static contact with solvent and under flow[6,7] , and some modeling studies of a grafted polymer in contact with a polymer melt[8], there has been no work published on the molecular response of a grafted polymer against a melt under shear. In this work we measure fort the first time the *in situ* response of end-grafted polystyrene against a deuterated polystyrene melt with neutron reflectometry as a function of shear rate.

Protonated PS with a molecular weight of 82 kDa and polydispersity index of 1.05, measured by gas phase chromatography, calibrated for PS, was end-grafted onto the surface of a quartz wafer[9] and placed in contact with a deuterated polystyrene (dPS) melt with a molecular weight of 34.1 kDa and a polydispersity index of 1.19. The neutron reflectometry (NR) experiments were performed using the Surface Profile Analysis Reflectometer (SPEAR) at the Los Alamos Neutron Science Center. The interfacial region between the end-grafted PS in contact with the dPS melt was studied as a function of shear rate using the Los Alamos Neutron Science Center neutron rheometer in the cone and plate geometry.

The scattering from the end-grafted PS was first measured in air, and then, the grafted PS was placed in contact with the dPS melt at 190 °C. Neutron reflectivity measurements were done with the sample at rest and at rates between 1.44 and 30.24 s^{-1} with intervening measurements with the sample at rest. Figure 1 shows the brush volume fraction profiles fort the various measurements.

The $\phi(z)$ for the grafted PS are sigificantly different from the parabolic forms predicted[1] and observed[6] for grafted polymers in a good solvent. There is only a small region ($z <$ 25 Å) that might have the predicted parabolic form. Beyond this domain the brushes show a long tail followed by a mushroom like domain extending out to approximately 500 Å at rest and at all shear rates.

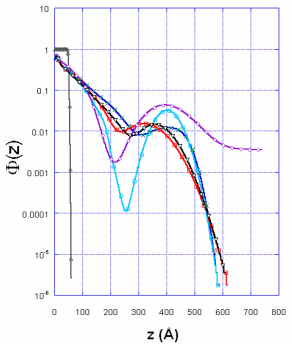

Fig. 1. **Volume fraction profiles of** end-grafted PS as a function of depth, z, from the quartz substrate. End-grafted PS in air (grey triangles); state 0 (green plus symbols): initial no shear state which follows the same curve as state 1 except at very low z values; state 1 (blue crosses): sheared at $1.44s^{-1}$ as well as at other shear rates and at rest, state 2 (red squares): sheared at various rates; state 3 (turquoise circles): at rest after sheared at a low rate; and state 4 (purple diamonds): at rest after a moderate shear and state 5 (black inverted triangles): the final state at rest.

Metastability of the grafted PS chains was indicated by the observation that states where dependent on shear history. While the initial shear rate did not lead to a significant change in the $\phi(z)$ and hence, chain extension (Fig. 1), the higher shear rates did. However, during one particular experiment with a high shear rate, the grafted PS chain profile reverted back to its original state. Additionally, the states with the larger mushroom-like regions were not observed again when the system was returned to rest after low or high shear rates.

The derived grafted polymer density profiles showed that the grafted polymer was retained on the quartz wafer. Furthermore, the profiles suggest that the end-grafted polymer response to polymer melt shear exhibit metastable states, rather than equilibrium states assumed in the current theory (ref.[1–3,8]). Except for some possible extension and/or contraction of the grafted polymer with shear, there was not an obvious direct correlation of the structure and the shear thinning behavior observed in these samples. Within the context of the observed shear thinning, neither polymer exchange[5] of the grafted PS chains with the dPS melt chains nor disentanglements[8] were observed.

This work was supported by the use of the Lujan Neutron Scattering Center at LANSCE, which is funded by the Department of Energy's Office of Basic Energy Sciences. Los Alamos National Laboratory is operated by Los Alamos National Security LLC under DOE Contract DE-AC52-06NA25396.

REFERENCES

1. Milner S. T.: Science *251*, 905 (1991).
2. Zhao B., Brittain W. J.: Prog. Polm. Sci. *25*, 677 (2000).
3. de Gennes P. G.: Macromolecules *13*, 1069 (1980).
4. Bent J. *et al.*: Science *301*, 1691 (2003).
5. Sternstein S. S., Zhu A.-J.: Macromolecules *35*, 7262 (2002).
6. Karim A. *et al.*: Phys. Rev. Lett. *73*, 3407 (1994).
7. Baker S. M. *et al.*: Rev. Sci. Instrum. *65*, 412 (1994).
8. Brochard F., de Gennes P. G.: Langmuir *8*, 3033 (1992).
9. Sasa L. et al.: Rev. Sci. Instrum. *81*, 055102 (2010).

KL-06
RHEIN CHEMIE´S OFFER TO MANAGE YOUR RUBBER MAKING PROCESS EFFICIENTLY

DIETMAR HOFF

Rhein Chemie Rheinau GmbH, Düsseldorfer Str. 23-27, 68219 Mannheim,Germany
Dietmar.Hoff@rheinchemie.com

- Processing promoters to enable processing of high performance rubber compounds.
- Rhenogran products to control optimum dispersion, work safety and environmental protection.
- ICOM to reduce process costs significantly without compromising quality.
- Release agents to improve process efficiency of rubber compounds and goods.
- Rhenomark to eliminate mix-ups within tire making process.
- Rhenoshape high performance bladders for a smooth tire curing process.

KL-07
DISPERSION AND PHASE SELECTIVE DISTRIBUTION IN CARBON BLACK AND SILICA FILLED RUBBER COMPOUNDS FOR TIRES

HANS-JOACHIM RADUSCH[a], SYBILL ILISCH[a], HAI HONG LE[a], EVEMARIE HAMANN[b], and DANIEL HEIDENREICH[b]

[a] Martin Luther University Halle-Wittenberg, Center of Engineering Sciences D-06099 Halle (Saale), [b] Styron Deutschland GmbH, R&D Synthetic Rubber D-06258 Schkopau, Germany
hans-joachim.radusch@iw.uni-halle.de

Introduction

In the Kyoto Protocol a reduction of greenhouse gases, like CO_2 was fixed. This results a.o. in a proposal from the Commission to the European Parliament and Council for a regulation to reduce CO_2 emissions from passenger cars dated from December 2007. Many efforts have been made to develop energy efficient tires. The main way thereby is the reduction of the rolling resistance. Such a reduction can be reached via the tire dimensions, mass and profile and/or via the tire mixture including new or modified filler, rubber and rubber-filler compatibilizer.

The majority of tire treads is built on basis of carbon black and/or silica filled blends from natural rubber (NR), styrene-butadiene rubber (SBR) and butadiene rubber (BR). The properties of such composites depend strongly on the

morphology and localization of the filler in the blend phases. For carbon black and silica filled natural rubber/solution styrene-butadiene rubber (S-SBR) blend systems the wetting, infiltration, dispersion and distribution of the filler during the mixing process were investigated by online measured electrical conductance test (OMEC), as described in our earlier works[1−9], solubility measurements on the raw mixture[10,11], thermogravimetry[11] and infrared spectroscopy[12] on the rubber filler gel, as well as optical microscopy and atomic force microscopy in dependence on the mixing time. For the carbon black filled mixtures the phase selective filler distribution as a function of the styrene and vinyl content of the S-SBR as well as the influence of additives on the filler dispersion was investigated.

Since the introduction of the silica-silane technology in the early 1990s carbon black was partly or nearly totally substituted by precipitated silica in tire tread mixtures for high performance passenger tires. With this technology a optimization of tire properties, like rolling resistance and wet grip further became possible, but the compounding is much more complicated than for carbon black filled rubber mixtures.

In silica filled rubber compounds organosilane based coupling agents have to be used. During the compounding process, a chemical reaction between silane and silica is necessary for the improvement of viscoelastic properties of the vulcanizates. Furthermore, the time of adding of process oil and additives influences the wetting behavior of the rubber. Therefore, the ingredients and the mixing regime of the rubber compounds are key factors for the performance characteristics of the vulcanizates.

Experimental

Carbon black filled mixtures

For the investigation of carbon black filled mixtures commercial solution styrene-butadiene rubber S-SBR (Sprintan SLR-4601, S21/ V62, MU 45, Styron Deutschland GmbH) and experimental S-SBR (MU 61 +/−3, Styron Deutschland GmbH) were used. The material parameters are given in Table I. SMR 10 was used as NR phase, masticated to the MU of the S-SBR. Carbon black Corax N220 (Evonik Industries GmbH) was used as filler; in all cases 50 phr (32 wt.%). The ingredients of CB filled mixtures, for which the phase selective filler distribution were estimated, are shown in Table II.

Table I
Styrene and vinyl content of experimental S-SBR

S-SBR type	Styrene [%]	Vinyl [%]
S0/V67	0	67
S14/V61	14	61
S21/V61	21	61
S30/V62	30	62
S48/V10	48	10
S49/V22	49	22
S49/V30	49	30
S50/V33	50	33

Table II
Ingredients of carbon black filled mixtures

Ingredients	Content, phr
Rubber	100
N 220	50
Stearic acid/ZnO	6
Antioxidants	3,5
Sulphur/Accelerator	2,8

It was found that a strong influence of the styrene content on the phase specific localization of the carbon black exists in the binary 50/50 S-SBR/NR blends. An increased CB content in the NR phase results with increasing styrene content. No influence of the vinyl content on the phase specific CB distribution was observed within the series with varied vinyl content, but including all investigated samples a certain trend is to observe. Increasing vinyl content results in an increased CB content within the S-SBR phase, contrary to the influence of the styrene content.

Both styrene and vinyl content influence the compatibility of the S-SBR with NR, but in opposite direction. The solubility parameters of the S-SBRs were calculated in dependence on styrene and vinyl content according to Schuster[13]. If the phase specific distribution of the CB is brought in correlation with the difference of the solubility parameters of S-SBR and NR ($DSP_{(SSBR-NR)}$), it becomes obvious that the main influence factor on the phase specific CB distribution in the 50/50 S-SBR/NR blends is the compatibility between both rubbers[14].

Latest investigation of nanofiller containing rubber single mixtures and blends shows the essential influence of type, amount and input moment of additives on the dispersion and distribution behavior of the filler. In the case of carbon black filled S-SBR, some additives, like stearic acid, accelerate the filler dispersion, others act retarding[15].

The normalized online conductance curves with respect to the conductance value measured at the BIT G/G_{BIT} of CB filled SBR SLR-4601 without and with additives (stearic acid, zinc oxide, sulphur, accelerator) were analysed in dependence on mixing time (Fig. 1).

The curves show the typical shape as received in[1]. The onset time t_{onset} of the conductance is observed at about 5.3 min and the BIT at 10.2 min for the mixture without additive and 3.5 min and 7.2 min for the other one. As discussed in our previous works[1,5,6] the macrodispersion and the online conductance correlate closely to each other in the period between the t_{onset} and BIT. The largest change of the size of CB agglomerates takes place in this range. Passing the BIT the macrodispersion increases slightly but the conductance started to decrease gradually. As discussed before the main reason for the decay of conductance is related to the distribution process of small aggregates throughout the matrix that is described by

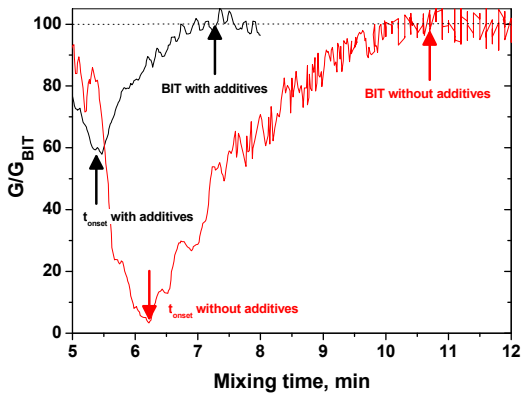

Fig. 1. **Normalized OMEC for carbon black filled S-SBR with and without additives**

the microdispersion[1,5,6]. It was found that for a certain material system the macrodispersion obtained at the BIT is approximately the same for different mixing conditions. Thus, the BIT can be used to compare the dispersion behavior of different mixtures with each other.

In the present work a small quantity of each mixture was taken out during the mixing process and investigated by optical microscopy (OM). Dispersion degrees of 90 % and 99 % were calculated for the mixture without additives and with all additives, respectively, at 11 min.

The effect of any single additive on the online conductance G/G_{BIT} was investigated. It is obviously seen that the addition of ZnO shows no effect on the BIT. Sulphur and CBS slightly prolong the BIT, whereas addition of stearic acid or DPG leads to a significant shortening of the BIT[15].

Silica filled mixtures

The used rubbers were solution styrene-butadiene rubber (S-SBR) (Sprintan SLR-4601, S21/ V62, MU 45, Styron Deutschland GmbH) and natural rubber (NR) SVR-L (Phuoc Hoa Rubber Company). The used silica was Ultrasil 7000 GR (Evonik Industries GmbH) with specific surface area CTAB = 160 $m^2 g^{-1}$ and BET = 170 $m^2 g^{-1}$, pH-value = 6.8. Bis-[3-(triethoxysilyl)-propyl]-tetrasulfide (TESPT) Si 69 (Evonik) was used as coupling agent. Mixing experiments were performed by a Poly Lab System Rheocord 300 p with a 75 cm^3 mixing chamber Rheomix 610 p (Thermo Haake).

Silica filled S-SBR- and NR-compounds were prepared without and with silane in a three-step mixing process. In step 2 the chamber temperature T_A was varied stepwise from 50 °C to 175 °C in order to accelerate the chemical reaction between silane and silica and to characterize the effect of temperature on the wetting process.

The dependence of the rubber-layer L[10,11] on the mixing time of filled S-SBR and NR-compounds prepared at T_A = 50 °C without and with silane is presented in Fig. 2. Without silane the rubber-layer L^{SBR} of SSBR and L^{NR} of NR increase with different rates. With increasing mixing time the infiltration of S-SBR and NR molecules and the dispersion of silica agglomerates take place simultaneously. L^{SBR} and L^{NR} reach a level-off value after about 10 min and 6 min mixing, respectively.

The rubber-layer L^{NR} of NR increases very fast in comparison to SBR, that is related to the high mobility of the linear and flexible NR molecules *vs.* S-SBR molecules containing sterically hindered phenyl rings. The fast wetting behavior of NR was also found in carbon black and carbon nanotubes (CNT) filled rubber compounds as reported in our previous works[11,16].

In S-SBR/NR blends in the earlier mixing stage the NR phase wets silica very fast compared to S-SBR. In the subsequent mixing stage the loosely bonded component of rubber-layer $L^{B(NR)}$ is replaced by SBR molecules because of the better affinity of SBR to silica. The tightly bonded component of $L^{B(NR)}$ remains permanently on the silica surface. Using the wetting concept[10,11] the kinetics of the phase selective silica localization in rubber blends could be characterized. During the first mixing stage, silica localization is strongly affected by the wetting rate ratio of the rubber blend components.

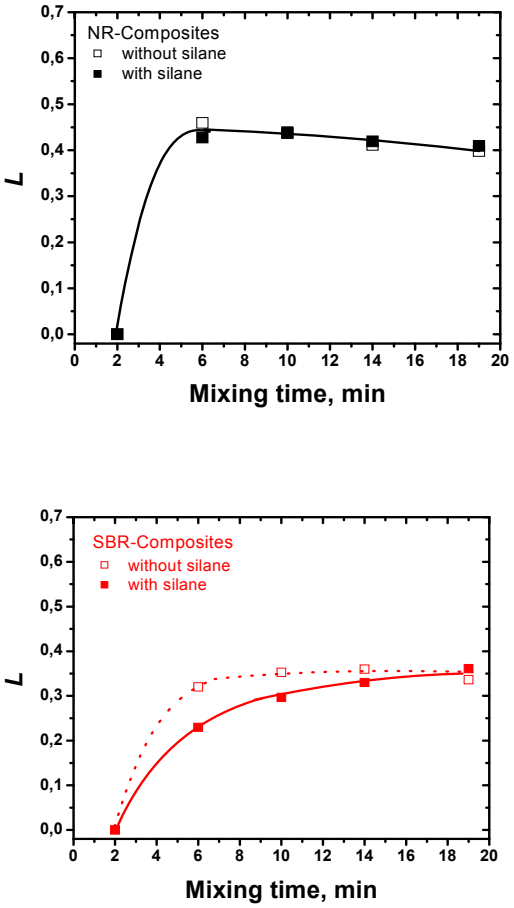

Fig. 2. **Rubber layer L of silica filled NR (above) and SSBR (below) for three mixing steps** (1. T_A=50 °C, n=50 rpm, φ=0,73, t=10 min / 2. $T_{var.}$ (50 °C), n=30 rpm, φ=0,73, t=4 min / 3. T_A=50 °C, n=50 rpm, φ=0,73, t=5 min)

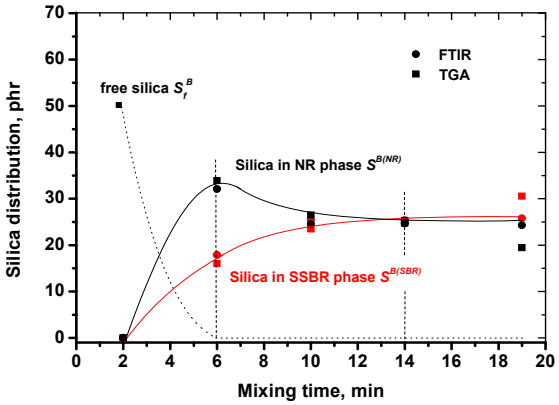

Fig. 3. **Phase specific silica distribution in 3-step random mixed blend** (with silane)[12]

Because of the higher wetting rate of the NR phase more silica is located in the NR phase than in S-SBR. In the next stage, the rubber filler interaction dominantly influences the localization kinetics. As a result, silica is transferred from the NR phase toward the S-SBR phase until the loosely bonded component of $L^{B(NR)}$ is fully replaced by S-SBR (Fig. 3). The increasing chamber temperature increases the rubber layer L, but does not influence the phase selective silica distribution in the investigated blends[12].

Conclusions

With the application of the *wetting concept* based on the analysis of bonded rubber by solubility analysis of raw compounds and TGA and/or FTIR analysis of the rubber-filler gel of filled rubber blends, a deep insight into the morphology development during the mixing process is possible, as well as the quantitative analysis of the phase selective filler localization during the mixing process. The measure of rubber-layer *L* was introduced to describe the wetting behavior of rubber to filler. NR shows a significantly higher wetting rate than SBR. This result was found for CB and silica filled mixtures and does not depend on the addition of silane.

The authors thank the German Research Foundation (DFG) and Deutsche Kautschuk-Gesellschaft (DKG) for the financial support of this work.

REFERENCES

1. Le H. H., Ilisch S., Jacob B., Radusch H.-J.: Rubber Chem. Technol. *77*, 147 (2004).
2. Le H. H., Prodanova I., Ilisch S., Radusch H.-J.: Rubber Chem. Technol. *77*, 815 (2004).
3. Le H. H., Tiwari M., Ilisch S., Radusch H.-J.: Kautsch. Gummi Kunstst. *58*, 575 (2005).
4. Le H. H., Tiwari M., Ilisch S., Radusch H.-J.: Plastics Rubber Composites *35*, 410 (2006).
5. Le H. H., Tiwari M., Ilisch S., Radusch H.-J.: Rubber Chem. Technol. *79*, 610 (2006).
6. Le H. H., Qamer Z., Ilisch S., Radusch H.-J.: Rubber Chem. Technol. *79*, 621 (2006).
7. Le H. H., Ilisch S., Radusch H.-J., Steinberger H.: Plastics Rubber Composites *37*, 367 (2008).
8. Ali Z., Le H. H., Ilisch S., Busse K., Radusch H.-J.: J. Appl. Polymer Sci. *113*, 667 (2009).
9. Ali Z., Le H. H., Ilisch S., Radusch H.-J.: J. Mater. Sci. *44*, 6427 (2009).
10. Le H. H., Ilisch S., Kasaliwal G. R., Radusch H.-J.: KGK, Kautsch. Gummi Kunstst. *60*, 241 (2007).
11. Le H. H., Ilisch S., Kasaliwal G. R., Radusch H.-J.: Rubber Chem. Technol. *81*, 767 (2008).
12. Le H. H., Ilisch S., Heidenreich D., Wutzler A., Radusch H.-J.: Polymer Comp. *31*, 1701 (2010).
13. Schuster R. H.: Gummi Fasern Kunstst. *49*, 966 (1996).
14. Hamann E., Ilisch S., Le H. H., Radusch H.-J.: KGK, Kautsch. Gummi Kunstst., in press.
15. Le H. H., Ilisch S., Hamann E., Radusch H.-J.: Rubber Chem. Technol., submitted.
16. Le H. H., Kasaliwal G. R., Ilisch S., Radusch H.-J.: KGK, Kautsch. Gummi Kunstst. *62*, 326 (2009).

KL-08
TEMPERATURE STABILITY OF IRRADIATED POLYMERS

MIROSLAV MANAS, MICHAL STANEK, DAVID MANAS, STEPANS SANDA, ZDENEK HOLIK, and MICHAL DANEK

Tomas Bata University in Zlín, nám. TGM 5555, 760 01 Zlín, Czech Republic
sanda@ft.utb.cz

Abstract

Radiation processing involves the use of natural or man-made sources of high energy radiation on an industrial scale. The principle of the radiation processing is the ability of the high energy radiation to produce reactive cations, anions, and free radicals in materials. The industrial application of the radiation processing of plastic and composites includes polymerization, cross-linking, degradation and grafting. Radiation processing involves mainly the use of either electron beams from electron accelerators or gamma radiation from Cobalt-60 sources. Tested polymers (PE, PP, PA) show significant changes of temperature stability after irradiation. From this point view new application could be seen also in areas with service temperature much higher than their former melting point. The comparison of temperature stability of irradiates and not irradiated PE, PP and PA is presented in this paper.

Introduction

The cross-linking of rubbers and thermoplastic polymers is a well-proven process of the improvement of the thermal

properties. The chemical cross-linking or rubber vulcanization is normally induced by the effect of heating after processing with the presence of a curing agent. The cross-linking process for thermosets is very similar. In thermosets the polymer molecules are also chemically linked due to heat after processing. Cross-linked rubbers have a wide-meshed molecular network that keeps them soft and their properties change only slightly on a wide temperature scale. On the other hand, thermosets are characterized by a very narrow-meshed network. Due to this fact they hardly change their high level of stiffness on a wide temperature scale. The irradiation cross-linking of thermoplastic materials via electron beam or cobalt 60 (gamma rays) is proceeding separately after the processing. The cross-linking level can be adjusted by the irradiation dosage. The main difference between beta and gamma rays lies in their different abilities of penetrating the irradiated material. Gamma rays have a high penetration capacity. The penetration capacity of electron rays depends on the energy of the accelerated electrons. Due to electron accelerators, the required dose can be applied within seconds, whereas several hours are required in the gamma radiation plant.

Beta and gamma rays can be used for irradiation of polyolefines, polyesters, halogen polymer and polyamides from thermoplastics group, elastomers and thermoplastic elastomers. Some of them need the addition of cross-linking agent. The dimensional stability, strength, chemical resistance and wear of polymers can be improved by irradiation. Irradiation cross-linking normally creates higher strength as well as reduced creep under load and leads to a huge improvement in resistance to most of the chemicals and it often leads to the improvement of the wear behaviour.

The thermoplastics which are used for production of various types of products have very different properties. Standard, engineering and high performance thermoplastics differ in their properties both mechanical and thermal. In comparison with other construction / engineering materials, mainly metals, polymers have limited level of both mechanical and thermal properties. These limitations significantly reduce the application area of polymers. Every improvement of these properties of course makes the application wider. Irradiation of thermoplastics is the important way to change of thermal properties. From the point of use, mainly the temperature stability is very important factor.

Experimental

The thermal stability of irradiated PE, PP and PA after irradiation has been tested. Injection molding machine ARBURG Allrounder 420C Advance has been used for sample preparation.

Used polymers:

- PE: DOW – HDPE 25055 E
- PE: DOW – LDPE 780 E
- PP: PTS – Crealen EP – 2300L1 – M800 (unfilled PP)
- PP: PTS – Crealen EP8G5HS* M0083 (PP filled 25% glass fibers)
- PA: PTS – Duramid

TMA test:

- Equipment: Perkin – Elmer Thermal Analyser TMA 7
- Heat from 50°C to 400°C at 20°C/min
- Hold for 1 min at 50°C

Results

Polyethylene both HDPE and LDPE show significant changes of thermal properties after irradiation. The range of changes strictly depends on the dose of applied radiation and the best result are observed by the dose of 196 kGy (HDPE) and 165 kGy (LDPE).

The temperature stability of polypropylene is also affected by the irradiation. The doses of irradiation have only

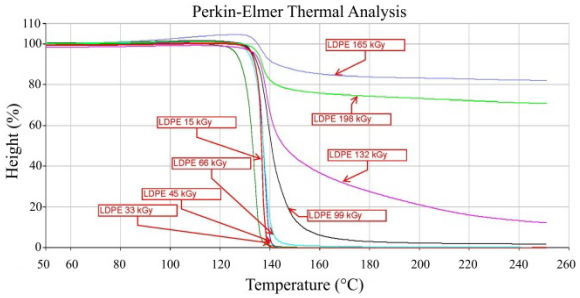

Fig. 1. **Temperature stability of LDPE**

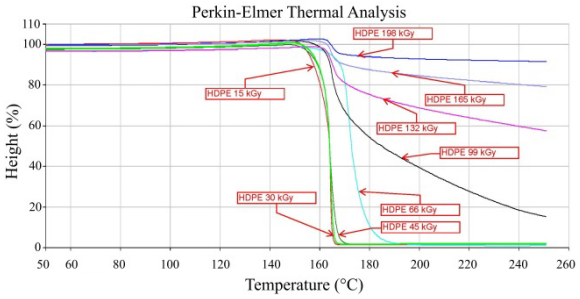

Fig. 2. **Temperature stability of HDPE**

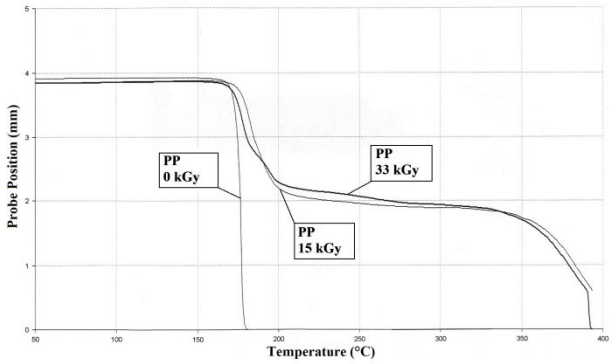

Fig. 3. **Temperature stability of PP**

limited effect on thermal stability of not filled PP (Fig. 3).

In case of PP with reinforcement (PP 25% GF) the dose of irradiation is very significant. The raising dose of irradiation can influenced the temperature stability negatively (Fig. 4).

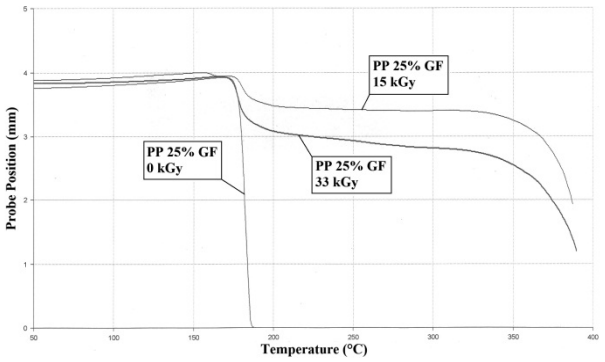

Fig. 4. **Temperature stability of PP 25 % GF**

Very similar results have been obtained by the irradiation of polyamide. The graph of TMA of Duramide is in Fig. 5.

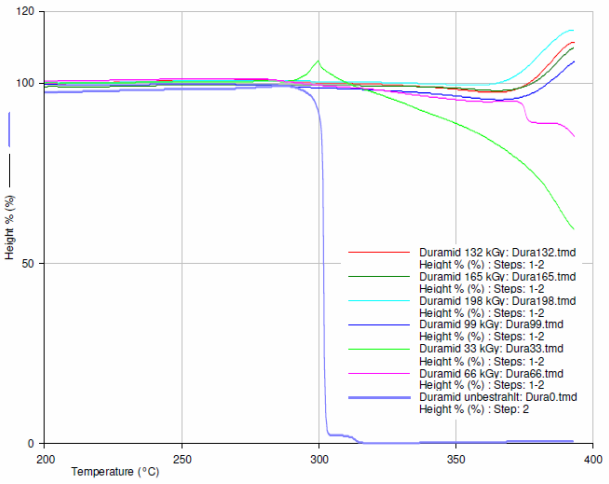

Fig. 5. **Temperature stability of PA**

Conclusion

Irradiation improves the thermal properties of polymer. All tested polymer (PE, PP and PA) show better temperature stability after irradiation. Irradiation significantly extends the application area of polymers. The service temperature can be higher than the melting point of not irradiated polymers.

This article is financially supported by the Czech Ministry of Education, Youth and Sports in the R&D projects under the titles 'Modelling and Control of Processing Procedures of Natural and Synthetic Polymers', No. MSM 7088352102 and 'CEBIA Tech', No. CZ.1.05/2.1.00/03.0089.

REFERENCES

1. Manas D., Stanek M., Manas M., Pata V., Javorik J.: KGK, Kautsch. Gummi Kunstst. *62*, 240 (2009).
2. Maňas M., Staněk M., Maňas D., Daněk M., Holík Z.: Chem. Listy *103*, 24 (2009).
3. Manas D., Manas M., Stanek M., Zaludek M., Sanda S., Javorik J., Pata, V.: Chem. Listy *103*, 72 (2009).
4. Šanda Š., Maňas M., Staněk M., Maňas, D., Rozkošný L.: Chem. Listy *103*, 140 (2009).
5. Kyas K., Stanek M., Manas M., Manas D., Krumal M., Cerny J.: *21st International DAAAM Symposium, 2010, Zadar, Croatia*, p. 1081.

KL-09
OPTIMIZATION OF MIXING CONDITIONS FOR SILICA-REINFORCED NATURAL RUBBER COMPOUNDS

W. KAEWSAKUL[a,b], K. SAHAKARO[a,b], J. W. M. NOORDERMEER[b]

[a] *Centre of Excellence in Natural Rubber Technology (CoE-NR), Department of Rubber Technology and Polymer Science, Faculty of Science and Technology, Prince of Songkla University, Pattani 94000, Thailand,* [b] *Department of Elastomer Technology and Engineering, University of Twente, P.O. Box 217, 7500 AE Enschede, the Netherlands*

Abstract

It is well accepted that mixing conditions are of paramount importance for the properties of silica-filled rubber compounds. The dump temperature and mixing interval between rubber, silica and silane coupling agent, prior to adding other ingredients for silica-filled natural rubber (NR) compounds using bis-triethoxysilylpropyl tetrasulfide (TESPT) as coupling agent were optimized. Mooney viscosity, cure characteristics, silica dispersion (as indicated by the reinforcement parameter, flocculation rate constant and Payne effect), loss tangent at 60 °C (indication of rolling resistance of tires) and mechanical properties: tensile strength, elongation at break, reinforcement index and tear resistance were investigated. The dump temperature is the key parameter governing the properties of the silica-filled NR compounds. The increase in viscosity of the compounds by changing the dump temperature from 100–150 °C indicates that inevitably some crosslinking occurs of NR by sulfur contained in TESPT, simultaneous with the silanization reaction between silica and silane. However, the viscosity decreases again when dump temperatures above 150 °C are applied, indicating a dominant occurrence of degradation of the NR molecules. The results are in good agreement with bound rubber contents. The overall properties

indicate that a dump temperature in the range of 135–150 °C and a silica-silane-rubber mixing interval of 10 minutes are the most appropriate mixing conditions for silica-filled NR compounds with TESPT as coupling agent.

KL-10
POLYMER SCIENCE IN SERVICE OF AUTOMOTIVE INDUSTRY

MARTIN OBADAL* and THOMAS WAGNER

Borealis Polyolefine GmbH, Business Unit Mobility, St-Peter-Strasse 25, 4020 Linz, Austria
martin.obadal@borealisgroup.com

Isotactic polypropylene (iPP) is one of the most important industrially used polymers (not only) for automotive applications. Today, each passenger car contains more than 60 kg of polypropylene based material. This fact is mainly arising from a variety of iPP modifications based on the molecular and supermolecular design, use of fillers, additives and nucleating agents or even on a blending with other polymers – these factors all together make from iPP the material interesting also scientifically, which favorably contributes in the increase of technical understanding. Such a relation is a closed loop in which developments of new applications can be based on a solid polymer science background. Several examples of these interrelations allowing a design and construction of engineering applications, such as innovative bumpers, fenders, seat carriers or air-intake-manifolds will be presented.

The structure property interrelations in PP can be gathered from the individual structural levels. On the supermolecular level, the variation between the crystalline and amorphous phases, resulting mainly from the material stereoregularity, can be first considered. In addition at this level (within the crystalline portion), iPP exhibits polymorphic behavior as it crystallizes into four different crystalline modifications, namely monoclinic α, trigonal β, orthorhombic γ and mesomorphic smectic forms[1]. The α-crystalline form is the most common and predominant in common iPP processed by standard conditions; to obtain higher amounts of β-form, the use of specific nucleation is essential – such material shows then favorably enhanced toughness and drawability as compared to common α-form iPP[2,3] and is used also industrially (see Beta (β)-PP™ BE60 in Ref.[4]). Coming from the supermolecular to the next structural level – spherulitic, where the lamellae are organized in complex aggregates, also here their size and organization can be influenced by several ways, eg. by using of nucleating agents or clarifiers. These help to fasten the crystallization (ie. processing) but also favorably adjust mechanical properties and even improve organoleptics by increased transparency: presently transparent iPP is an essential material related to the packaging (and other) industry, see eg. Ref.[5]. Another structural level is created by morphology being created by crystallization of two or more mutually immiscible materials where individual phases creates a system of two (or more) separated morphologies. Typical example is the iPP material called heterophasic or impact copolymer having the iPP matrix while the softer inclusions are based on ethylene-propylene copolymer; impact strength even at low temperature is significantly enhanced[6]. Such material is a key material for automotive applications. Its subsequent modification with other components like external rubber, fillers and other additives creates another structural level encompassing the morphology of the base material with the relation to other individual components; see the example in Fig. 1, top. Interfaces between them play then a critical role when adjusting material properties to a given application, see eg. a fender application in Fig. 1, bottom left. Another example is the iPP based composite filled with glass fibers – here the use of appropriate compatibilizer in a given concentration must guarantee a proper interface between the glass fiber and the polymer resulting in a large enhancement of the material stiffness but yet taking into account to keep rather high impact strength. As a consequence, such compounds move iPP from the field of commodity polymeric materials into full-value member of the engineering plastic material pool next to polyamides, polyesters and others. Consequently, resulting applications can range from structural carriers and covers, fan shrouds, front-end and seats carriers up to motor parts like air intake manifold[7], see Fig. 1 bottom right – offering better technical functionality (optimized air flow), design freedom (integration of functions), reduction in weight and at the end also lower costs. The knowledge of all the interrelations briefly mentioned above are critical when developing improved iPP based materials for demanding automotive applications.

Fig. 1. ***Top*: electron microscopy micrograph of the morphology of heterophasic mineral filled PP after RUO4 staining; *Bottom left*: Fender Application for BMW X5 (mineral filled iPP compound Daplen™ EF341AE); *Bottom right*: Air Intake Manifold (glass-fibre filled iPP compound XMOD™ GB306SAF)**

REFERENCES

1. Turner-Jones J. M., Aizlewood D. R. Beckett: Makromol. Chem. *75*, 134 (1964).
2. Grein C.: Adv. Polym. Sci. *188*, 43 (2005).
3. Obadal M., Čermák R., Baran N., Stoklasa K., Šimoník J.: Int. Polym. Proc. *19*, 35 (2004).
4. www.borealisgroup.com/datasheets/10021259
5. www.foodqualitynews.com/Innovation/Borealis-

develops-clear-freezable-packaging
6. Gahleitner M., Hauer A., Bernreitner K., Ingolic E.: Int. Polym. Proc. *17*, 318 (2002).
7. www.reinforcedplastics.com/view/11141/volkswagen-switches-to-polypropylene-composite-for-air-intake-manifolds/

KL-11
FACTORS DETERMINING THE PROPERTIES OF PLA/WOOD COMPOSITES: PARTICLE CHARACTERISTICS, INTERACTIONS, REINFORCEMENT

GÁBOR DORA, GÁBOR FALUDI, KÁROLY RENNER, JÁNOS MÓCZÓ, and BÉLA PUKÁNSZKY

[a] *Laboratory of Plastics and Rubber Technology, Budapest University of Technology, 1521 Budapest, P.O.Box 91, Hungary,* [b] *Institute of Materials and Environmental Chemistry, Hungarian Academy of Sciences, 1525 Budapest, P.O.Box 17, Hungary*
bpukanszky@mail.bme.hu

The interest in compostable and biodegradable materials increases continuously shown also by the increased production and consumption of PLA. This polymer is used in increasing quantities in packaging applications, but also in the automotive industry. Unfortunately, PLA has several disadvantageous properties like fast physical ageing and limited impact resistance. Attempts are made to improve PLA properties by fillers, impact modifiers, plasticizers and various reinforcements. Mostly structural materials are needed in automotive applications and the use of natural reinforcements may result in stiffer materials with improved dimensional stability, which is fully compostable at the same time. Commercial wood flour and other lignocellulosic reinforcements are available in a wide range of particle characteristics and prices. However, the chemical composition of the fillers and especially their particle characteristics influence properties considerably and an optimum must be found to achieve the property combination needed for a certain application. The goal of the study reported in this communication was to determine the effect of particle characteristics of lingocellulosic reinforcements on the mechanical properties of PLA/wood composites. Six reinforcements with widely differing particle sizes and aspect ratios were compounded with PLA in an internal mixer. Mechanical properties were studied by tensile testing as a function of wood content. The extent of reinforcement was determined by modeling from the tensile strength of the composites. Micro-mechanical deformation processes occurring during deformation were followed by acoustic emission measurements. The results were compared to those obtained on PP composites. Both modeling and micromechanical testing indicated strong adhesion between ligno-cellulosic fibers and the PLA matrix. The results clearly proved that the final strength of the composites is determined by micromechanical processes as shown by Fig. 1, in which composite strength is plotted against the initiation stress of the dominating micromechanical deformation process.

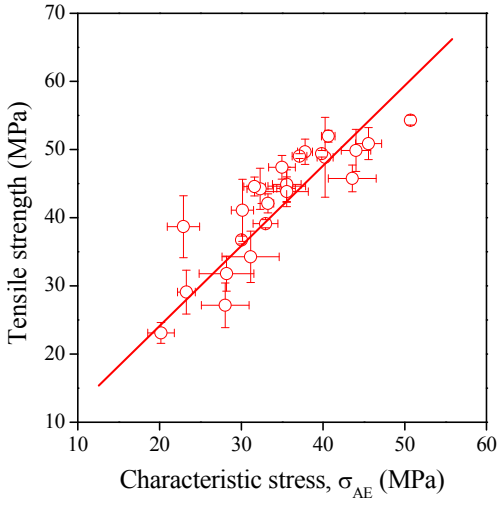

Fig. 1. **Close correlation between composite strength and the initiation stress of fiber failure in PLA/wood composites**

KL-12
CHANGES IN ENVIRONMENTAL LEGISLATION BOOST DEMAND FOR ECOLOGICALLY SOUND PRODUCTS

HEINZ UNTERBERG, HERMANN-JOSEF WEIDENHAUPT, and MELANIE WIEDEMEIER

Lanxess Deutschland GmbH, 51369 Leverkusen, Germany
melanie.wiedemeier@lanxess.com

Abstract

This paper considers the impact of changes in legislation for the production of environmentally friendly rubber-goods.

The REACH regulation is in force since June 1st 2007. REACH is the new European Chemicals Regulation, which replaces the current policy with different systems for “new” and “existing” chemicals. REACH regulates the handling with chemical substances either on their own, in preparation or in the final rubber-articles. REACH covers all chemical substances, dangerous or not. For dangerous chemicals like substances of very high concern (SVHC) the regulation demands a substitution in a very narrow timeframe. The first list of SVHC was published on October, 28th 2008 and updated on December, 15th 2010 which includes plasticizers such as DEHP (di-2-ethylhexylphthalate) or DBP (di-butyl-phthalate). Addressing this challenge the LANXESS Business Unit (BU) Rubber Chemicals has replaced all phthalates in its portfolio by safe alternatives without any negative impact on rubber compounding and performance.

Starting from 2012 a new EU tire labelling will force the tire industry to increasingly focus on silica filled tread compounds in order to fulfil the demand for tires with a good

rolling resistance label and well balanced other properties like wet grip and abrasion. DPG (diphenylguanidine) is the most common used secondary accelerator in tire compounds,mainly used in silica filled passenger car tread compounds. Beside its function as secondary accelerator DPG acts in this application also as a processing aid for the silica compound. A problem accompanied with DPG is its release of toxic aniline during the vulcanization process. A solution to overcome this problem is the use of Vulcuren® as secondary accelerator. Vulcuren® can be used beneficially in state-of-the-art crosslinking systems for

silica compounds. Furthermore, it also improves the so-called "new silica systems" based on silanes with reduced volatile organic chemicals (VOC). The reduction of VOC´s is a requirement of the authorities in the USA and now in consequence a challenge for the automotive industry.

Ultimately, the LANXESS BU Rubber Chemicals again reconfirms its position as a strong contributor to environmentally sound and sustainable rubber chemicals usage for its customer base.

KL-13
HIGH-PERFORMANCE MATERIALS AND NEW PROCESS SOLUTIONS

RALF ZIMNOL*

Lanxess Deutschland Gmbh
ralf.zimnol@lanxess.com

LANXESS is a worldwide operating chemical company. We are producing high tech polymers, chemical intermediates and basic chemical raw materials.

Innovations in the form of high performance plastics and high performance applications are a common goal of LANXESS and its business partners. We will show some examples of new products with special stabilizations and special processing characteristics.

The easy flowing grades and the new high modulus materials with their high amount of glass fibres can make it possible to produce thin parts at low costs.

Modern tools and modern calculating methods make it possible to design parts with thin walls and few gating points. These require, however, plastics with a better flowability. It would be easy to produce such a material, just by using polymers with lower molecular weights. This, however would have a big disadvantage, because the impact resistance would be much lower. LANXESS has managed to develop materials with a much increased flowability without losing much impact resistance. Our so called Durethan Extreme Flow grades achieve almost the double flow length than standard grades.

Temperatures unter the hood of automotives are rising due to, e.g., noise encapsulations and aerodynamic optimizations. Plastics with higher long term thermal resistancies are therefore required. LANXESS has developed a special heat stabilization.

Blow molded nylon tubes are more and more important for engines with turbo loaders. Nylon is a good material for such applications because of its high resistance to the high temperature of the compressed air inside the tubes.

The shown LANXESS specialities are based on structural viscous polymers. They are available in various stiffnesses, so that they can be used for tubes with rigid and flexible elements.

The water injection technology improves the inner surfaces and, due to the injected water, the cycle time.

The WIT process is, however, much more difficult to control and requires special materials with a likewise controlled quality.

CONTRIBUTED LECTURES

CL-01
CONSTITUTIVE EQUATION FOR RUBBER ELASTICITY WITH THE CHANGE IN INTERNAL ENERGY AND ENTROPY

KEIZO AKUTAGAWA*, SATOSHI HAMATANI, and HIROSHI KADOWAKI

Bridgestone corporation, Ogawahigashi-cho, Kodaira-shi, Tokyo, 187-8531, Japan
akutag-k@bridgestone.co.jp

Abstract

For the design of the rubber products, the finite element analysis, FEA, is one of important technique to model the behaviours of rubbers stressed in complex manner. On the other hands, the energy loss properties of tyre compounds are empirically used as important design parameters to satisfy their performances such as rolling resistance, friction and durability. But most of the constitutive equations for FEA are based only on the entropic origin of rubber elasticity and can not describe the energy dissipation process. The purpose of this study is aiming at understanding the origin of the energy loss of the deformed rubbers. The derivation of a constitutive equation is based on the change in both energy and entropy, which represents the non-equilibrium behaviours of rubber in deformation. This equation was derived from the statistical thermodynamics with Hamiltonian equations and it showed a good agreement with the experimental result.

From global warming concern a tyre rolling resistance is one of the important performances in the tyre industry. In general, tyre rolling resistance is responsible for 10 % of passenger car fuel consumption and 20 % in the case of fully loaded heavy trucks[1]. Approximately 90 % of tyre rolling loss may be attributed to viscoelastic behaviours of the cord and the rubber component of tyre materials[1]. For tyre tread compounds the energy loss properties can be empirically correlated with tyre performance characteristics. It has been shown, for example, that the wet traction and the rolling resistance are best correlated with the dynamic mechanical loss properties at the temperature of around 0 °C and 60 °C, respectively.

For tyre applications the finite element method is one of important tool to model the behaviour of tyre components stressed in a complex manner. Recently this method was applied to the meso-scopic analysis of the filled rubber and it can provide the meso-scopic stress-strain behaviour of rubber phase and filler phase separately[2]. To carry this out successfully it was also needed to develop a constitutive equation to represent the stress-strain behaviour of a rubber phase, preferably at least up to the glass transition temperature of rubber phase encountered in many tyre tread applications.

The mean energy of a system in thermal equilibrium can be represented by

$$U = \frac{1}{Z}\sum A_\alpha e^{-\beta A_\alpha} = -\left(\frac{\partial \log Z}{\partial \beta}\right)_{\{V\}} \qquad (1)$$

where A_α is the energy level of the microstate labeled by α and Z is the partition function as a function of temperature.

From the statistical thermodynamics it can be assumed that the energy function of A_α can be described by a function of the Hamiltonians, H.

$$A_\alpha = f(H_{interacton}, H_{trans}, H_{rot}) \qquad (2)$$

where the Hamiltonian for the system can be assumed as a function of temperature and constrains due to stretching the chain molecules with transversal motion, H_{trans}, rotational motion, H_{rot} and molecular interaction, $H_{interacton}$.

For the model of the temperature dependence of the rubber elasticity it can be thought of as two distinguishable molecules, each of which can be in either of two different

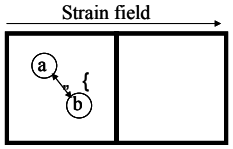

strain states as shown as follows.

The system has 2 × 2 = 4 microstates. The strain energy of each molecule can be assumed to be the strain invariants, I_{1a} and I_{1b}, more in one state than in the other state. There has to consider the attractive energy[3] or interaction energy term, which lowers the energy of the system by κ of the two molecules are in the same strain state.

The Helmhortz free energy change of the rubber elasticity,ΔA, can be described as[4]

$$\Delta A_1 = U_1 - T\cdot S_1 = \frac{e^{\beta'\cdot\kappa}\left\{\kappa\cosh\left(2\beta'\left(I_1'-3\right)\right)+2\left(I_1'-3\right)\cdot\sinh\left(2\beta'\left(I_1'-3\right)\right)\right\}}{e^{\beta'\cdot\kappa}\cosh\left(2\beta'\left(I_1'-3\right)\right)+1} \qquad (3)$$
$$-\frac{N}{\beta}\cdot\left\{\frac{1}{2}I_1+\frac{3}{100n}\left(3I_1^2-4I_2\right)+\frac{99}{12250n}\left(5I_1^3-12I_1I_2\right)\right\}$$

where β' is 1/kΔT and n is the number of statistical links between crosslinks. The first term of the equation (*3*) represents the internal energy of the elasticity and the second term represents the entropy of the rubber elasticity described by the inverse Langevin function[5]. The theoretical curves showed a good agreement with the experimental results to represent the temperature dependence and strain induced crystallization.

This study was partially supported from New Energy and Industrial Technology Development Organization (NEDO).

REFERENCES

1. Willett P. R.: Rubber Chem. Technol. *47*, 118 (1974).
2. Akutagawa K., Yamaguchi K., Yamamoto A., Heguri H.,

Jinnai H., Shinbori Y.: Rubber Chem. Technol. *81*, 182 (2008).
3. Thomas A. G.: Trans. Faraday. Soc. 569 (1954).
4. Heinrich G., Kaliske M., Lion A., Reese S.: *Proceedings of the 6th ECCMR*, Taylor & Frances, 185 (2010).
5. Wang M. C., Guth E.: J. Chem. Phys. *20*, 1144 (1952).

CL-02
ENERGIZING CHEMISTRY - LANXESS INNOVATING FOR THE GLOBAL MEGATRENDS

FLEMMING BJØRN BJØRNSLEV

LANXESS Central Eastern Europe s.r.o, Stetinova 4, 811 06 Bratislava, Slovakia
flemming.bjoernslev@lanxess.com

Tomorrow's world will be shaped, above all, by the four megatrends: mobility, urbanization, a responsible use of the precious resource water and the provision of enough food to feed the global population. The chemicals industry has already developed innovative products to serve these megatrends, ranging from fuel-saving tires to the removal of arsenic from drinking water.

CL-03
KINETICS OF THE SILICA-SILANE REACTION

ANKE BLUME

Evonik Degussa GmbH, Harry-Kloepfer-Str. 1, 50997 Köln
anke.blume@evonik.com

Abstract

The introduction of the silica/silane system in the tire industry has changed the demands of the mixing process dramatically. Thenceforth, the rubber manufacturers have to control a chemical reaction during the mixing process. Only a detailed knowledge of the influencing parameter will enable them to gain an optimum silanization of the silica surface and afterwards a more controlled linkage to the polymer. This study was carried out to determine the reaction kinetic of different silanes. It is shown that varying functional groups at the silane have a big influence on the rate of reaction of the silica-silane coupling.

Introduction

The increasing extension of the use of the silica/silane technology in tires implies that rubber manufacturers have to control to a greater extent a chemical reaction during the mixing process. Only a detailed knowledge of the influencing parameter will enable them to gain an optimum silanization of the silica surface and afterwards a more controlled linkage to the polymer. TESPT has been for a long time the standard silane in the tire industry. In order to cover the demands for further rolling resistance reduction, new silanes like VP Si 363® have been developed. A basic study has been carried out to determine the reaction kinetic of different silanes in comparison to TESPT and VP Si 363®. The influence of different functional groups at the silane on the rate of reaction of the silica-silane coupling is evaluated.

Scope of the study

The kinetic behavior of the reaction of different silanes with ULTRASIL® 7000 GR was studied with the below described experimental set-up. The goal of this study was to understand the differences between the mercapto- and an alkylgroup, to clarify the influence of the size and shape of the silane, to identify the different behavior of methoxy and ethoxy and to evaluate the influence of different functional groups.

Experimental set-up

The study was carried out in a model system. The rubber matrix was replaced by decane in order to analyze the reaction between silica and silane without interferences. The detailed experimental set-up is shown in Fig. 1.

The reaction at 120 °C was started by adding the silane to the silica / decane solution. The reaction was stopped according to a fixed time schedule by freezing the sample in liquid nitrogen. Afterwards, the adsorbed EtOH or MeOH at the silica surface area were desorbed by adding 10 ml DEGMBE (Diethylenglycol-monobutylether) and analyzed by GC. The amount of remaining silane was analyzed by GC, HPLC or GPC.

The rate of recovery of EtOH were determined by adding different amounts of EtOH to 1 g ULTRASIL® 7000 GR in 10 ml decane without adding silane. The rate of recovery was determined to be ca. 80 % after one hour reaction time at 120 °C. The rate of recovery of MeOH was evaluated in the same way. It is ca. 10 % lower than for EtOH. This has to be taken into account by discussing the maximum of reacted alkoxy groups of a silane.

Furthermore, it was shown that all investigated silanes are stable at 120 °C (measurement of the amount of silane after stirring at 120 °C in decane without silica) and the resulting effects were not overlaid by degradation phenomenons.

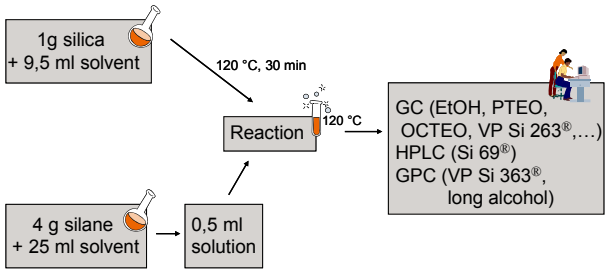

Fig. 1. **Experimental set-up**

Comparison of mercaptosilanes with alkylsilanes

Different silanes with mercapto function (VP Si 363® with long dialkoxy-ethoxy-silyl group and VP Si 263® with triethoxy-silyl group) were compared with an experimental alkylsilane (XP Si 303: propyl-dialkoxy-ethoxy-silane with a relation of alkoxy to ethoxy of 2,3:0,7 or 2,9:0,1 respectively) and Dynasylan® PTEO (propyltriethoxysilane). The resulting rate of reaction –dc/dt is shown in Fig. 2 versus the remaining concentration c of the silane.

The silane which reacts most slowly is PTEO, the silane which shows the highest reaction rate is VP Si 363®: The ascending order of the reaction rates is the following: PTEO < VP Si 263® = Si 303 < VP Si 363®. This shows that the chemical structure of the whole silane influences its kinetic behavior although all molecules react via the triethoxy-group. The presence of a SH-group or a long alkoxy-group increases the rate of reaction in comparison to an alkyl-group. The presence of a SH- and a long alkoxy-group enhances the rate of reaction most significantly. An explanation for the higher rate of reaction of a mercaptosilane could be the additional adsorption possibility to the silanol group of the silica not only via the ethoxy group but also via thiol. And an adsorption via thiol could stabilize also the intermediate product during the silica-silane reaction. VP Si 363® reacts faster than Si 263 probably due to an increasing possibility of adsorption of the different oxygen atoms inside the long alkoxy chain to the silanol groups of the silica via hydrogen bonding.

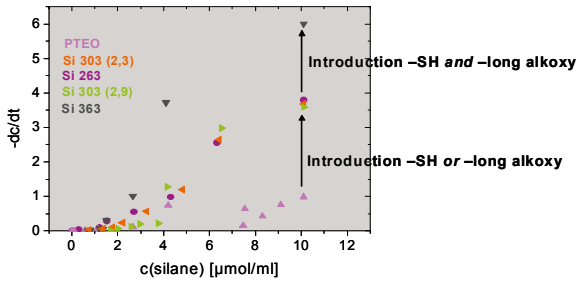

Fig. 2. **Rate of reaction of mercaptosilanes in comparison to alkylsilanes**

Kinetic Behavior of Triethoxyalkylsilanes

The influence of the length and branching of the alkyl-chain of different triethoxyalkylsilanes on the rate of the reaction with the silanol groups of the silica was tested: Dynasylan® MTES (methyltriethoxysilane), Dynasylan® PTEO (propyltriethoxysilane), Dynasylan® OCTEO (octyltriethoxysilane), HDTEO (hexadecyl-triethoxysilane) and Dynasylan® IBTEO (isobutyl-triethoxysilane). Fig. 3 shows the different turnovers of the silane (c_0-c) with c_0 as the initial concentration versus the rates of reaction (--dc/dt).

The ascending order of the rate of the start reaction is the following: MTES > PTEO > OCTEO > HDTEO > IBTEO. This leads to two general conclusions: The shorter the alkyl chain of the silane the higher is the rate of reaction. Linear

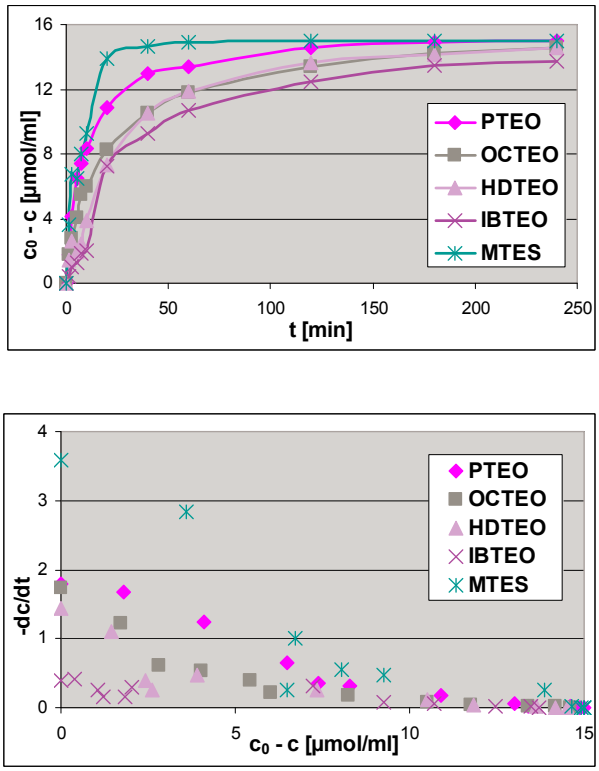

Fig. 3. **Rate of reaction of different alkyltriethoxysilanes**

alkyl silanes react faster than branched ones. This shows that the stearic hindrance of the alkyl chain of the silanes plays an important role in the reaction mechanism. The higher the effectivity of a longer or even branched alkyl chain to shield the silanol group of the silica the lower is the possibility for an adsorption of the triethoxy-group to a silanol group.

Kinetic Behavior of Trimethoxyalkylsilanes

The influence of the length and branching of the alkyl-chain of different trimethoxyalkylsilanes was tested: Dynasylan® MTMS (methyltrimethoxysilane), Dyna-sylan® PTMO (propyltrimethoxysilane), Dynasylan® OCTMO (octyltrimethoxysilane), Dynasylan® 9116 (hexadecyltrimethoxysilane) and Dynasylan® IBTMO (isobutyltrimethoxysilane).

Fig. 4 shows the different turnovers of the silane (c_0-c) versus the rates of reaction (-dc/dt).

The most obvious is that all methoxysilanes are reacting significantly faster than ethoxysilanes. The ascending order of the rate of the start reaction is as follows: MTMS > PTMO > OCTMO > IBTMO > 9116. This means that the same conclusions are true as for the alkyltriethoxy-silanes. A longer or even branched alkyl chain can shield the silanol groups of the silica more effectively. Therefore, the rate of reaction slows down with increasing chain length and degree of branching.

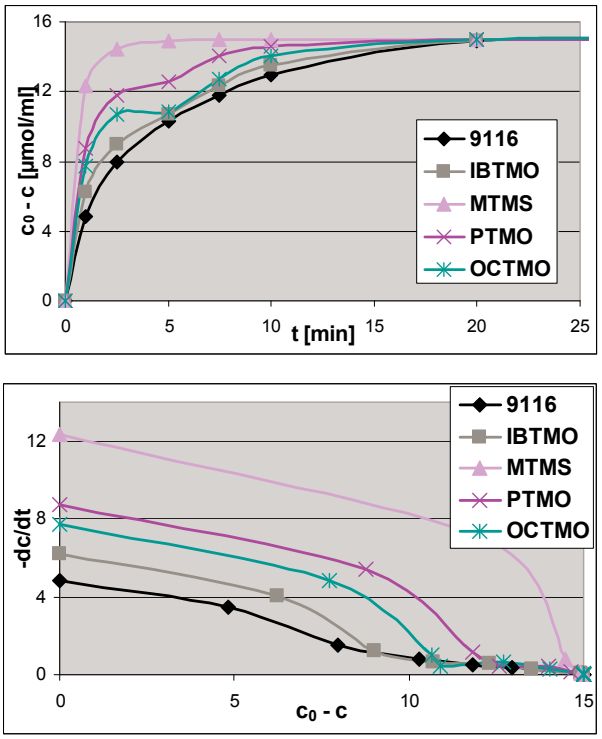

Fig. 4. **Rate of reaction of different alkyltrimethoxysilanes**

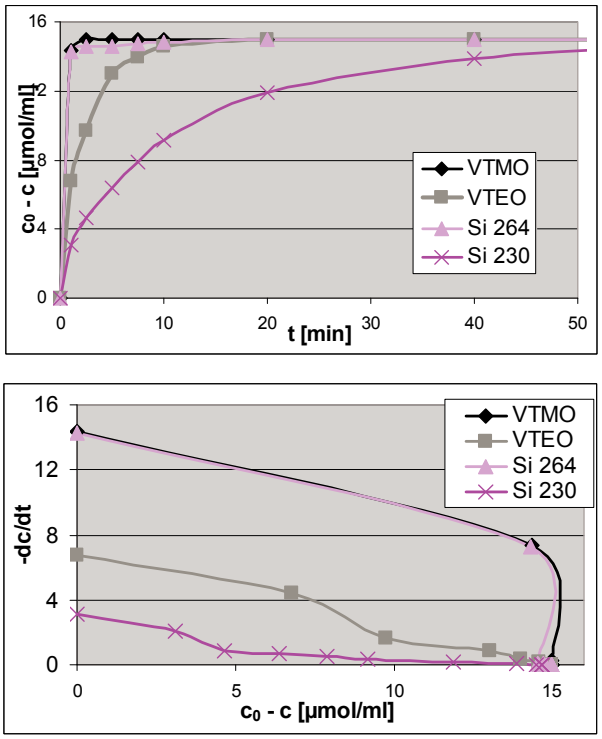

Fig. 5. **Rate of reaction of further functional silanes**

Kinetic Behavior of further functional silanes

Additionally, further silanes with different functional groups were tested: Dynasylan® VTMO (vinyltrimeth-oxysilane), Dynasylan® VTEO (vinyltriethoxysilane), Si 264 (Thiocyanatopropyltriethoxysilane) and Si 230 (Chloropropyltriethoxysilane). Fig. 5 shows the reaction curves.

The ascending order of the rate of the start reaction is the following: VTMO = Si 264 >> VTEO >> Si 230. VTMO reacts with its vinyl group and a trimethoxysilyl-group as fast as Si 264 with a triethoxysilyl group but with a thiocyanato group. This shows that the thiocyanato group has the highest tendency to adsorb on the silica surface and therefore leads to the fastest reaction rate even in combination with a triethoxysilyl group.

Comparison of all investigated silanes

A comparison of all investigated silanes shows that in this basic study at least two alkoxy groups per Si unit have reacted, often even three. Taken into account that the rate of recovery for MeOH is lower than for EtOH (EtOH: ca. 80 %; MeOH: ca. 70 %) and both are not 100 %, nearly all alkoxy groups have reacted.

Fig. 6 shows the comparison of the rate of the start reactions of all investigated silanes. VTMO and Si 264 has the highest start reaction rate, alkylsilanes with a triethoxy-group the lowest. Fig. 7 gives an overview of all rates of the start reaction beginning from the slowest reaction rate to the fastest.

The start reaction of a triethoxysilane is the slowest with a isobutyl-group, the fastest with a thiocyanato-group. The ascending order for the different alkyl groups is the following: isobutyl < hexadecyl < octyl < propyl < methyl. The branching of the alkyl chain hinders the adsorption of the silane on the silica surface most effectively. The shorter the linear alkyl chain is the lower the stearic hindrance for an adsoption and the faster the rate of reaction.

The ascending order for the rate of the start reaction for the different functional groups is as following: Cl < S_x < Mercapto < Vinyl < Thiocyanato. The thiocyanato group has the

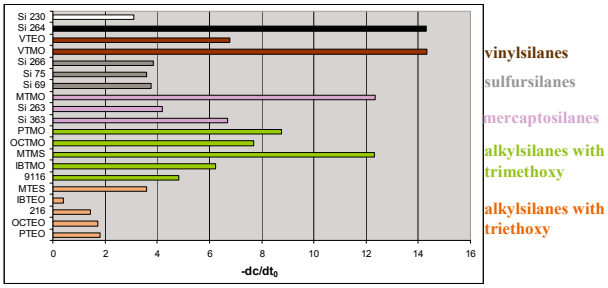

Fig. 6. **Rates of the start reaction of all investigated silanes**

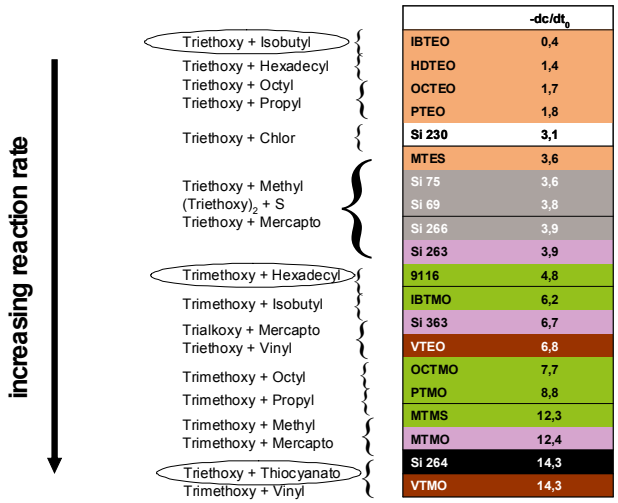

Fig. 7. **Rates of the start reaction of all investigated silanes in ascending order**

highest tendency to adsorb on the silica surface and therefore leads to the fastest reaction rate of all investigated silanes.

Trimethoxysilanes are reacting much faster than triethoxysilanes. Therefore, a trimethoxysilane with a hexadecyl-group reacts even faster than a triethoxysilane with mercapto! A methoxysilane with a thiocyanato function should be the fastest silane.

Summary

The kinetic behavior of different silanes with varying functional groups was investigated in a basic study. Although only the trimethoxy- or triethoxy-group reacts with the silanol group of the silica, the chemical structure of the whole silane determines the rate of the reaction. The following trends were obvious:

- The trimethoxy-group reacts significantly faster than the triethoxy-group.
- The shorter the alkyl chain of the silane the higher is the rate of reaction. Linear alkyl silanes react faster than branched ones.
- The presence of a SH- and a long alkoxy-group enhances the rate of reaction significantly.
- The thiocyanato-group leads to the fastest reaction rate of all investigated silanes.

Outlook

The mixing process of silica/silane compounds is still one of the most ambitious tasks in the rubber industry. The knowledge of the different kinetic behavior of different silanes from this basic study can help to adjust the mixing process more precisely. For example, combinations of the slower reacting alkylsilanes with faster reacting sulphur- or mercaptosilanes are possible.

REFERENCES

1. Hunsche A., Görl U., Müller A., Knaack M., Göbel T.: KGK, Kautsch. Gummi Kunstst. *50*, 881 (1997).
2. Hunsche A., Görl U., Koban H.G., Lehmann T.: KGK, Kautsch. Gummi Kunstst. *51*, 525 (1998).
3. Görl U., Parkhouse A.: KGK, Kautsch. Gummi Kunstst. *52*, 493 (1999).
4. Görl U., Münzenberg J., Luginsland D., Müller A.: KGK, Kautsch. Gummi Kunstst. *52*, 588 (1999).
5. Dubois L. H., Zegarski B. R.: J. Phys. Chem. 97, 1665 (1993).

CL-04
WEAR OF OFF – ROAD TIRES EVALUATION

DAVID MANAS, MIROSLAV MANAS, MICHAL STANEK, STEPAN SANDA, JAKUB CERNY, MARTIN OVSIK, and VLADIMIR PATA

Tomas Bata University in Zlin, Faculty of Technology, Department of Production Engineering, TGM 275, 762 72 Zlin, Czech Republic
dmanas@ft.utb.cz

Abstract

Wear of tire treads is an important factor in the lifespan of tires. Tire wear of passenger cars is characterized by abrasiveness as the tire tread is exposed to abrasive effect of the road on which the car is used. The process of wear for off-road vehicles is, however, completely different. Bits of tire tread compound are chipped off by sharp edges of stones and roughness of the terrain in which the tire is used. The article describes what properties the tire tread used should have.

1. Introduction

Rubber industry often faces the problem of wear of rubber parts. Some forms of wear, especially the wear of tyre tread or conveyor belts, are very similar to working itself. The tire tread is the part of tyre which secures contact of vehicle with road and is directly involved in the transfer of driving power. The wear of tire treads of passenger car and freight vehicles moving on usual roads, is characterised by its abrasion. Tire tread of a vehicle is exposed to abrasive effect of the road it moves on. However, the mechanism of wear of tires working in very hard terrain conditions is absolutely different. Sharp stone edges and terrain irregularities gradually cut (tear off) parts of the rubber tread surface, which can be understood as a way of working. There is also some similarity to milling, although under very specific conditions. The mechanism of tire tread wear working in hard terrain conditions is technically called Chipping-Chunking effect and it can be considered as “workability” of rubber surface.

The tests for wear are usually performed on finished products under running conditions, but these are usually very

time demanding and expensive. It would be very useful for technical practice to find a quick test of wear which could be carried out on small samples. Creating a model predicting the behavior of tire tread mixtures and specifying the characteristics (tensile strength, elongation, tear strength, hardness etc.) which affect the wear dramatically, would improve the development of wear research in this field.

2. Experiment

2.1. Used materials (compounds)

Thirteen kinds of tire tread compounds used for motorcycle treads subjected to high stress, treads for technical, agricultural and multipurpose vehicles were experimented. All compounds represent real products and are produced and machined.

2.2. Test of wear

The tests of tire (tread) wear are time and money consuming. They are carried out using real tires in testing rooms or directly in the terrain during driving tests. That is one of the reasons for searching a method that would in a very short time (in minutes) and on small samples test the wear for a comparison of the different kinds of compounds.

Based on these requirements an equipment seen on Fig. 2 was designed. The Chip – Chunk wear testing machine (J. R. Beatty and B. J. Miksch in RCHT, vol. 55, p. 1531.) was used for basal measurements. A new machine enabling changing the tested parameters and true simulations of the process conditions was designed, see Fig. 1.

When it drops on the revolving wheel, the ceramic tool gradually chips the material and creates a groove on the wheel. The size of the groove chipped by the ceramic tool in a given time is the scale of wear.

The ceramic edges proved a perfect resistance to wear. If the tool was well manipulated there was no difference between original and "worn" plate.

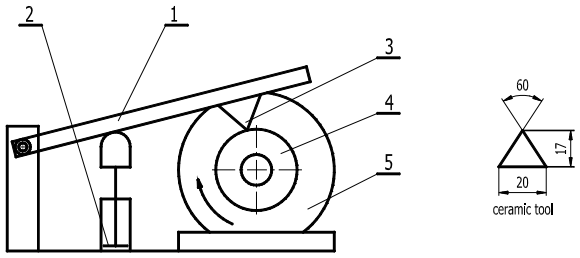

Fig. 1. **Design of testing equipment;** 1 – Arm, 2 – Pneumatic cylinder, 3 – Ceramic tool, 4 – Rubber sample, 5 – Electric motor

3. Results and discussion

The influence of drop of the ceramic tool on the surface of the testing sample is crucial. If the sample were rigid, the evaluation of the impact of dropping force would be quite easy. The elastic properties of the testing sample however cause a series of other effects of smaller intensity (jumping on the surface) apart from the main effect (the first drop of the ceramic tool on the testing sample). The main effects of the ceramic tool have only partial influence on the total wear. It turned out that evaluating total work needed for wear (i.e. creating a groove on the testing sample) only by the energy of the drop would be biased. After the first testing of the experiment equipment, it was clear that the results in a given series of measurements would be comparable if the experiments ran under the same conditions.

The actual contact surface between the surface of the tested rubber sample and sharp edges of stones and terrain irregularities is very small during the process of wear. Stress develops in this spot during rotation (rotary movement) of the test sample. When the ceramic tool is dropped on the circumference of the test sample the tool is forced against the surface layer of the rubber, which causes tensile stress behind the head of the deformation on the sides of the groove (Fig. 2 and Fig. 3). If the tensile stress exceeds the mechanical strength of the rubber material, a part of rubber is ripped off, either completely or partly. Stress and deformation in the area around the ceramic tool are reduced and the process can repeat a bit further away.

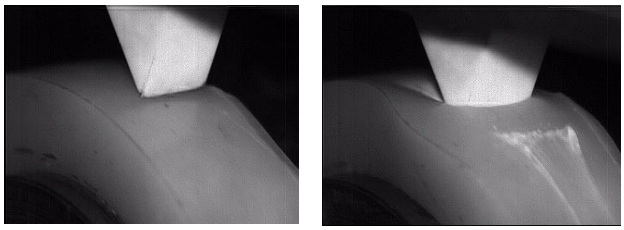

Fig. 2. **Tool penetration during the drop** (hard compound)

Tread compounds of off-road tires are subjected to harsh terrain conditions (construction sites, quarries) being stressed by sharp edges and terrain irregularities. Their high load contributes greatly to the deformation when the tires move on a stony surface. If a high resistance to wear is required, the tires must resist cutting tools such as sharp edges of stones and terrain irregularities, which tool the surface of the tread compound. The compounds with high value of hardness, resilience and dynamic complex module will easily manage to roll round the sharp bits on the surface. Their greater values of elongation strength will ensure better toughness and thus a high resistance against damage of the surface of tread compound, which would cause micro and macro cracks, which are sources for avalanche effect of wear. Hard compounds with smaller elongation strength and high values of resilience and dynamic complex module E* will be more susceptible to crumbling when in contact with irregular surface (Fig. 4). This leads to the damage of the surface of the compound,

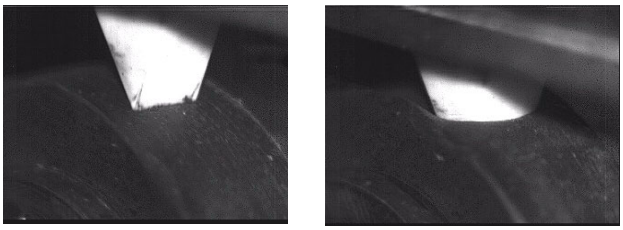

Fig. 3. **Tool penetration during the drop** (soft compound)

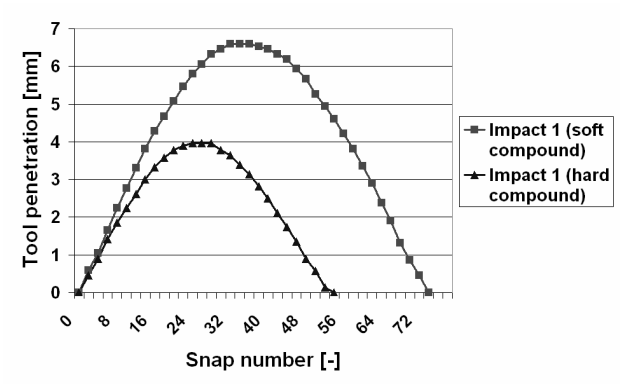

Fig. 4. **Tool penetration during the drop**

which creates ideal conditions for more cracks resulting in the avalanche effect of wear.

4. Conclusion

Tire wear is a rather complicated matter. It is not entirely clear which tire tread compound is the most effective and which will show poorer qualities in respect of wear. The character of wear should always be taken into account and the right properties of a given compound selected accordingly. For movements on standard roads and highways where the tread is exposed to abrasion, it is be more suitable to select a compound which is harder, more resistant to the abrasive effect of the road. On the other hand a softer compound is a better choice for tires used in harsh terrain conditions.

This article is financially supported by the Czech Ministry of Education, Youth and Sports in the R&D project under the title 'Modelling and Control of Processing Procedures of Natural and Synthetic Polymers', No. MSM 7088352102 and 'CEBIA Tech', No. CZ.1.05/2.1.00/03.0089.

REFERENCES

1. Manas D. et al.: KGK, Kautsch. Gummi Kunstst. *62*, 240 (2009).
2. Kaszonyiová M. et al.: J. Macromol. Sci., Phys. *B44*, 377 (2005).
3. Stanek M. et al.: Chem. Listy *103*, 88 (2009).
4. Stanek M. et al.: Chem. Listy *103*, 91 (2009).
5. Sanda S. et al.: Chem. Listy *103*, 140 (2009).
6. Manas M. et al.: Chem. Listy *103*, 24 (2009).
7. Kaszonyiová M. et al.: J. Macromol. Sci., Phys. *46*, 1 (2007).
8. Javořík J. et al.: KGK, Kautsch. Gummi Kunstst. *60*, 608 (2007).

CL-05
LIQUID ELASTOMERS: SCIENCE AND TECHNOLOGY

JIRI GEORGE DROBNY*

Drobny Polymer Associates, 11 Quails Way, Merrimack, NH, 03054 USA
jdrobny@drobnypolymer.com

The term "Liquid Elastomers" or "Liquid Rubbers" refers to low molecular weight polymers with molecular weight of only several thousands, which can be pumped or cast at room or slightly higher temperatures (i.e. their viscosity does not exceed about 150 Pa.s)[1]. These oligomers can be vulcanized in some way, either by extending chains, by cross-linking or by both reactions combined.

Generally, liquid elastomers can be classified into two groups, depending on whether their terminal groups are non-reactive or reactive. This contribution will focus on the group with reactive terminal groups, often referred to as telechelic oligomers[2].

When combining terminal reactive groups, a linear high molecular weight polymer is formed. If the functionality of the liquid oligomers or other reagent present is more than 2, branching and cross-links are formed during the reaction and a three-dimensional network results. Theoretically, more perfect three-dimensional structures could be obtained by this process than those generated by cross-linking of high molecular weight of currently available elastomers. However, in reality, this is not the case and the final products from liquid systems generally do not attain properties of conventional vulcanized rubber

Typical reactive groups in liquid elastomers are: –OH, –COOH, –Br and –SH[3]. The polymers terminated by hydroxyl groups can be cross-linked with diisocyanates. An example is the reaction of hydroxyl-terminated polybutadienes with MDI to form polyurethanes.

In general, this type of rubber can be used for applications, where there are not high demands on mechanical properties. Some of them can be reinforced by addition of reinforcing fillers. The incorporation of such fillers requires a very intensive shearing in mixers of special construction to achieve good dispersion[4]. The mixture obtained is a paste that has a low cohesion and is sticky; it cannot be processed in the traditional way as milleable rubbers. Otherwise, the advantages of liquid elastomers are that they generally require lighter machinery, which is less expensive and requires less power. The process requires less labor, which results in a higher productivity.

There are essentially four types of commercially available liquid elastomer systems[5,6]:

– polysulfides,
– silicones,
– polyurethanes,
– terminally reactive butadiene-based polymers.

This contribution will review the current state of the art in the liquid elastomer science and technology, major applications and current trends.

REFERENCES

1. Mesissner B., Schätz M., Brajko V., in: *Elastomers and Rubber Compounding Materials* (Franta I., ed.), p. 294, Elsevier, Amsterdam 1989.
2. Edwards D. C., in: *Handbook of Elastomers,* Second Edition (Bhowmick A. K., Stephens H. L., eds.), p. 133, Marcel Dekker, New York 2001.
3. Mesissner B., Schätz M., Brajko V., in: *Elastomers and Rubber Compounding Materials* (Franta I., ed.), p. 297, Elsevier, Amsterdam 1989.
4. Mesissner B., Schätz M., Brajko V., in: *Elastomers and Rubber Compounding Materials* (Franta I., ed.), p. 298, Elsevier, Amsterdam 1989.
5. Edwards D. C., in: *Handbook of Elastomers,* Second Edition (Bhowmick A. K., Stephens H. L., eds.), p. 136, Marcel Dekker, New York 2001.
6. Saskar A., in: *Rubber Technologist's Handbook,* Volume 2 (White J., De S. K., Naskar K., eds.), p. 405, Smithers Rapra Technology, 2009.

CL-06
A SINGLE TESTING INSTRUMENT WITH MULTIPLE TESTING CAPABILITIES FOR RUBBERS AND ELASTOMERS

ARNAUD FAVIER

01dB-Metravib 200 chemin des Ormeaux 69760 Limonest-France
arnaud.favier@areva.com, www.dma-instruments.com

Dynamic mechanical Analysis of rubbers are a very particular issue: contrarily to most other polymer materials, they exhibit very singular behaviour, which makes it complex to characterize. Their properties are sensitive to various different parameters: temperature, frequency, strain, heat build up and even the dynamic history of the sample itself! Rubber samples are available with different geometry and state. In each case, it is necessary to propose the adequate interface in order to adapt easily the sample on the testing instrument.

Following a development of 40 years, 01 dB-Metravib is proposing a set of powerful instruments, including innovative and unique capabilities. The different instruments are covering a unique frequency range from static up to 10,000 Hz. Thanks to high force capabilities (up to +/–450 N), it is possible to understand strain dependence of the material up to very high dynamic strain (+/–300 % and higher) and also to propose on the same instrument, complementary tests such as: fatigue, heat build up, crack growth, excitation waveform control, automated glass transition detection and optimization of measurement, … .

This presentation illustrates some of the capability of the DMA+ range of instrument applied to different kind of rubbers and elastomers material.

CL-07
TIRE PYROLYSIS – EFFECT OF PARTICLE SIZE

JUMA HAYDARY, JURAJ SÁGHY, and ĽUDOVÍT JELEMENSKÝ

Institute of Chemical and Environmental Engineering, Faculty of Chemical and Food Technology, Slovak University of Technology, Radlinského 9, 812 37 Bratislava, Slovak Republic
juma.haydary@stuba.sk

Prolysis is considered as an effective method for disposal of waste tires. In a pyrolysis reactor, waste tire is decomposed into pyrolysis products in form of solid char, liquid oil, and gases. Distribution of material into the pyrolysis yields and composition of individual fractions depends on the composition of the feed material, used pyrolysis technique and process conditions applied. Temperature, heat and mass transfer conditions, the use of catalysts and particle size are the main factors affecting the behavior of thermal decomposition and the amount and composition of the pyrolysis products.

Tire rubber is a material with low thermal conductivity, for this reason, the size of tire particles can significantly influence the time required for complete decomposition of the material. Many papers have been devoted to the influence of process conditions such as temperature or heating rate on the yield of pyrolysis products and their composition. Thermogravimetric analysis of thermal decomposition kinetics was applied by different authors. However, the number of papers studying heat conduction in particles and the influence of particle size on process duration is very limited although a real model of the pyrolysis process should take into account the size of particles. Authors of papers[1–3] have considered the effect of heat conduction and analyzed the influence of particle size.

This work aims to determine the effect of particle size on the conversion of thermal decomposition of tire pyrolyzed in a flow reactor under isothermal conditions.

Experimental setup

A laboratory pyrolysis unit with a screw type flow reactor for pyrolysis of rubber samples with sizes between 2 and 8 millimeters (weight of 50 to 500 mg) was used. The pyrolysis apparatus is in detail described in ref.[4]. The sizes and shapes of the used samples are illustrated in Scheme 1. The samples contained also textile cords, but steel cords were removed.

Scheme 1. **Illustration of tire rubber samples**

Temperature of the reactor was set to 550 °C. This temperature was selected based on our previous study on the influence of temperature on pyrolysis conversion[4]. Each type of the sample was pyrolyzed for a different residence time in the range from 15 to 300 seconds. Residence time was controlled by the frequency of rotation of the screw. Conversion of thermal decomposition was obtained by two methods: by comparison of the weight of the virgin sample and the residue char and by comparison of the TG curves of the residue char and the virgin material. Termogravimetric analysis of virgin rubber and residue char was provided using a NETZSCH STA 409 PC Luxx TG/DSC analyzer.

Separate thermogravimetric experiments using small samples (around 10 mg) were carried out to obtain kinetic parameters of thermal decomposition. For details on the method for kinetic data estimation see our previous paper[5].

Mathematical model

For mathematical modeling, a spherical particle with an equivalent diameter $de=2r_A$ was considered. Based on the solid char characteristics it was assumed that in the first step, rubber changes into a porous material which is further decomposed based on a shell model (reacted part of the particle creates a shell around the unreacted part as shown in Scheme 2).

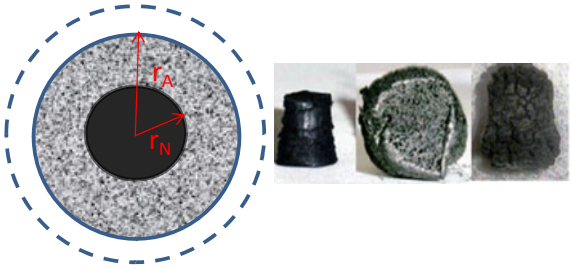

Scheme 2. **Behavior of rubber particle pyrolysis**

Based on these considerations and on the isothermal conditions in the reactor, for kinetics of thermal decomposition and heat conduction in the particle it can be written:

$$\frac{d\alpha}{dt} = A\exp\left(\frac{-Ea}{RT}\right)(1-\alpha)^n \qquad (1)$$

$$\lambda\left[\frac{1}{r^2}\frac{\partial}{\partial r}\left(r^2\frac{\partial T}{\partial r}\right)\right] + Q_R = \rho c_p \frac{\partial T}{\partial t} \qquad (2)$$

Initial and boundary conditions with respect to the technical aspects of the experiment are:

$$T\,(r,\ t=0) = T0 \qquad (3)$$
$$T\,(r=r_A,\ t>0 = T_R$$

$$\left.\frac{\partial T}{\partial r}\right|_{r=0} = 0$$

Results and discussion

The used laboratory pyrolysis reactor provides ideal heat and mass transfer conditions. A sample with the equivalent diameter of 4 mm was pyrolyzed completely during 15 seconds while for complete pyrolysis of an 8 mm sample, more than 120 seconds were required. Scheme 3 shows conversion of all samples at different residence times.

The pyrolysis conversion was predicted also by mathematical modeling. Kinetic parameters (activation energy, pre-exponential factor and reaction order) were estimated using the method described in ref.[5]. For thermal conductivity of tire rubber and for thermal conductivity of residue char an average value of 0.2 W/mK and a value of 0.1 W/mK were considered, respectively. Average values of specific heat of 1800 J/

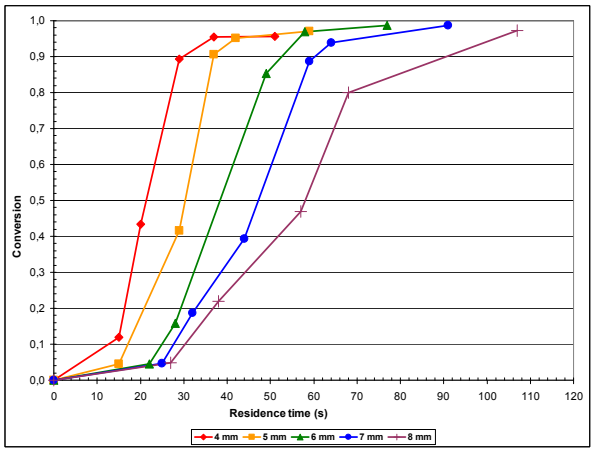

Scheme 3. **Conversion of samples with different sizes at different residence times**

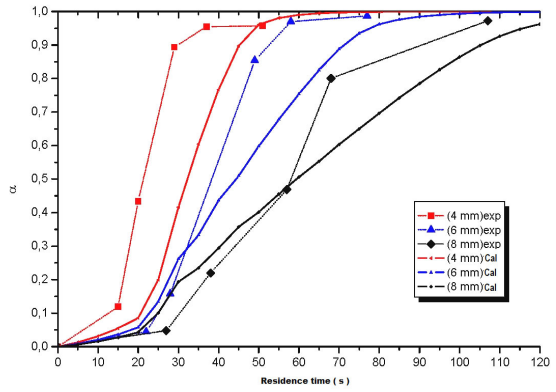

Scheme 4. **Comparison of experimental and model data**

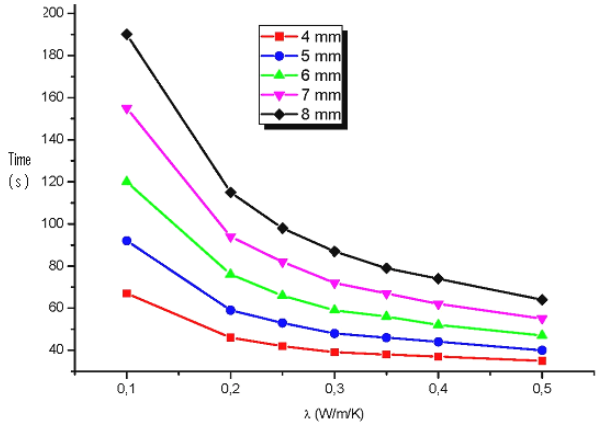

Scheme 5. **Influence of thermal conductivity**

kgK and decomposition reaction heat of 300 kJ/kg were applied. Scheme 4 shows the comparison of predicted and experimental conversions for different particle sizes. Generally, good coherence between predicted and experimental data was observed. However, the model data show slower thermal decomposition than experimental data.

Also the influence of thermal conductivity was analyzed. The values of thermal conductivity from 0.1 to 0.5 W/mK were used in the model; time needed for 90 % conversion at different thermal conductivities and sample sizes is shown in Scheme 5.

Both experimental and mathematical model results show that particle size and heat conduction have a crucial effect on the pyrolysis time of waste tire. By increasing the size of particles from 4 mm to 8 mm, the time needed for pyrolysis increased eight times.

This work was supported by the Grant VEGA No. 1/0796/10 from the Slovak Scientific Grant Agency.

Nomenclature

A – pre-exponential factor, c_p – specific heat, Ea – activation energy, n – reaction order, Q_R – heat of reaction, R – gas constant, r_A – radius of particle, r_N – radius of unreacted part of particle, T – temperature, T_R – reactor temperature, t – time, λ – thermal conductivity, ρ – density

REFERENCES

1. Juan F. González, Jose´ M. Encinar, José L. Canito, Juan J. Rodríguez: J. Anal. Appl. Pyrolysis, *58–59*, 667 (2001).
2. Morten Boberg Larsen et al.: Fuel *85*, 1335 (2006).
3. Siyi Luo, Bo Xiao, Zhiquan Hu, Shiming Liu: Int. J. Hydrogen Energy *35*, 93 (2010).
4. Haydary J., Jelemenský Ľ., Markoš J., Annus J.: KGK, Kautsch. Gummi Kunstst. *62*, 661 (2009).
5. Korenova Z., Juma M., Annus J., Markos J., Jelemenesky L.: Chemical Papers *60*, 422 (2006).

CL-08

EFFECT OF IRRADIATION CROSS-LINKING ON MECHANICAL PROPERTIES OF SELECTED TYPES OF POLYMER

ZDENEK HOLIK, MICHAL DANEK, MIROSLAV MANAS, ROMANA LAMBOROVA, JAKUB CERNY, KAMIL KYAS, MARTIN KRUMAL, and MARTINA MALACHOVA

Tomas Bata University in Zlin, Department of Production Engineering, Nam. T.G.Masaryka 275, 762 72 Zlin, Czech Republic

Abstract

The main objective of the study is an investigation of mechanical properties of selected polymers. These properties were examined in dependence on the dosage of the ionizing electron beam radiation.

1. Introduction

Polymers are more and more replaced by other materials; this is due to a huge range of their properties and processability in a liquid state. Demands on their properties rise with increase of application of these materials. Therefore it is necessary to find new methods of improving the polymer properties to replace expensive construction materials by affordable polymer materials.

Method of improving the polymer properties is based on creating of a network between the polymer chains by energy supplied to the material by ionizing beta radiation as can be seen at Fig. 1. Then the material reaches better mechanical, chemical and thermal properties. The process of irradiation is also carried out on final products without additional stress. A range of irradiation parameters can also vary according to

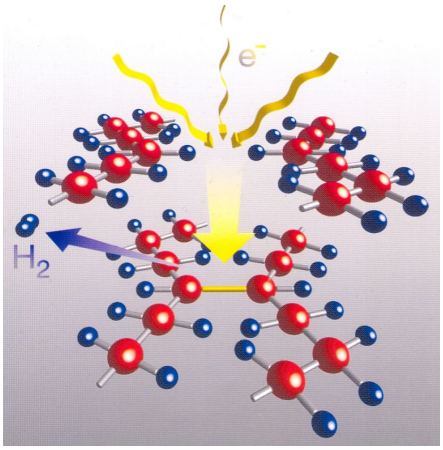

Fig. 1. **Principe of radiation cross-linking (5)**

the cross-linking degree and thus the desired material properties can be achieved.

2. Experiment

The samples were made by the injection moulding machine (ARBURG ALLROUNDER 420 C 1000-350).

The sample material was chosen polyamide 6.6 (PA 6.6), unfilled and filled with 25 % glass fibers.

– PTS Creamid-A3H2G5FR – PA6.6 25%GF
– PTS Creamid-A3H2 – PA6.6

Processing conditions during the injection moulding were set according to the recommendation of the producers.

All samples were irradiated with electron rays (electron energy 10MeV, dosage: 33, 66, 99, 132, 165 and 198 kGy) in the firm BGS Beta Gamma Service GmbH & Co, Saal am Donau – Germany.

The following equipment was used during testing:

– Tensile test, according to standard CSN EN ISO 527-1, 527-2 was carried out on the tensile machine ZWICK 1456; used rate: PA 6.6 – 100 mm/min; test data was processed by Test Xpert Standard software; modulus (E [MPa]) and tensile stress (σ_M [MPa]) were determined.
– Gel content according to standard CSN EN 579.

3. Results

At each irradiated test specimens the gel content was measured which is presented in the table I and in the table II. Here you can see that the gel content is stable from dosis 99 kGy (in case of PA 6.6) and from dosis 33 kGy (in case of PA 6.6 with 25 % glass fibres).

Comparison of tensile strength and E – modulus of polyamide 6.6 (PA66) measured at 23 °C is given in the Fig. 2 and at 80 °C in the Fig. 3. It is evident that cross-linking improves the tensile strength (σ_M) and E – modulus at of both temperatures, but the improvement in case of evaluated temperature is much higher. The best improvement is reached for test specimens irradiated by dosis 132 kGy (70 %). However, as can be seen in Fig. 3, the highest value of doses does not mean the highest value of tensile strength.

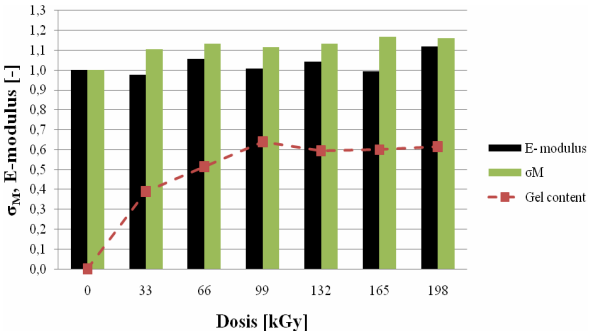

Fig. 2. **Comparisons of tensile strength and E – modulus of PA 6.6 at 23 °C**

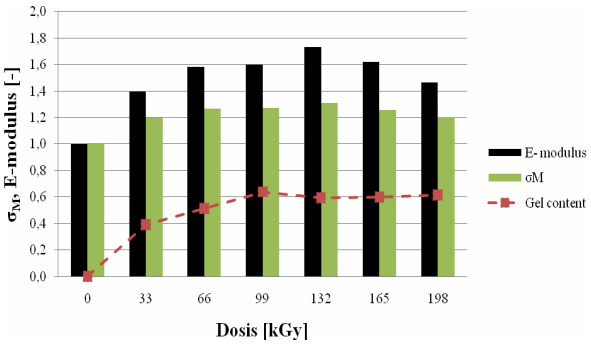

Fig. 3. **Comparisons of tensile strength and E – modulus of PA 6.6 at 80 °C**

Comparison of tensile strength and E – modulus of polyamide 6.6 with 25 %GF measured at 23 °C is given in the Fig. 4 and at 80 °C in the Fig. 5. Here we can see the stagnation of tensile strength after irradiation but opposite to un-

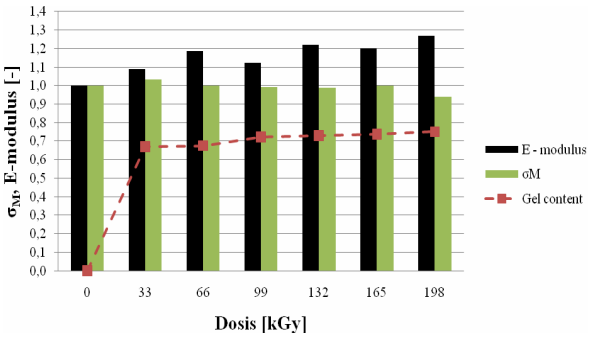

Fig. 4. **Comparisons of tensile strength and E – modulus of PA 6.6 25 % GF at 23 °C**

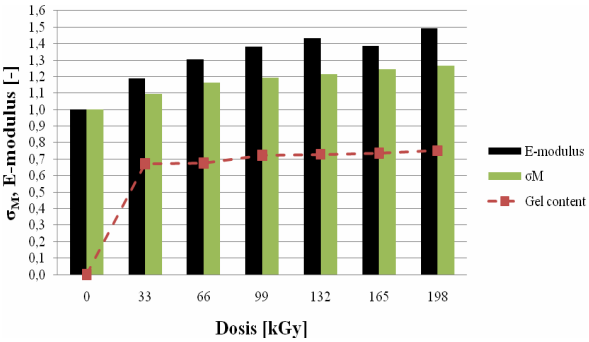

Fig. 5. **Comparisons of tensile strength and E – modulus of PA 6.6 25 % GF at 80 °C**

Table I
Gel content of PA 6.6

PA 6.6	
Dosis [kGy]	Gel content [%]
0	0
33	39,0
66	51,4
99	63,9
132	59,4
165	60,0
198	61,5

Table II
Gel content of PA 6.6 with 25 % GF

PA 6.6 25 % GF	
Dosis [kGy]	Gel content [%]
0	0
33	67,1
66	67,5
99	72,3
132	72,9
165	73,7
198	75,1

filled PA 6.6 there is higher increase of E-modulus (of about 25 % against non-cross-linked samples). Raise of mechanical properties can be given by cross-linkage of polymeric matrix on fibres.

4. Conclusion

As can be seen from the tests results, the irradiation cross-linking improves the mechanical properties of each polyamide. The improvement is more considerable in case of higher temperature (80 °C), as a consequence of creation of cross-link (during irradiation cross-linking) resulting in protraction of macromolecular string, which is thus more flexible during thermal load than individual shorter macromolecular strings.

This article is financially supported by the Czech Ministry of Education, Youth and Sports in the R&D projects under the titles 'Modelling and Control of Processing Procedures of Natural and Synthetic Polymers', No. MSM 7088352102 and 'CEBIA Tech', No. CZ.1.05/2.1.00/03.0089

REFERENCES

1. Woods R. J.: *Applied radiation chemistry: radiation processing*, 1994.
2. Drobný J. G.: *Radiation Technology for Polymers*, CRC Press, Boca Raton 2003.
3. Zyball A.: *Strahlungsenergie zur Modification von Kunststoffen – Industrielle Anwendungen der Bestrahlungstechnik*, In: Strahlenvernetzte Kunstoffe, Springer VDI verlag, Dusseldorf 2006.
4. http://www.pts-marketing.de
5. http://www.bgs.com/

CL-09
POSSIBLE METHOD OF RECYCLATION OF SELECTED TYPES OF CROSSLINKED POLYMERS

ROMANA LAMBOROVA, MICHAL DANEK, and ZDENEK HOLIK

Tomas Bata University in Zlin, Department of Production Engineering, Nam. T. G. Masaryka 275, 762 72 Zlin, Czech Republic

Abstract

The main objective of this article is a study of the possible use of irradiated polymer products after their lifetime period. Irradiated HDPE pipes were used for this research; the main advantage of cross-linking polyolefins is their cross-linking ability without the need of the cross-linking agent. However, the main problem is that the cross-linked material cannot be reprocessed by method of plastification. Focus of research lies in a study of mechanical properties.

1. Introduction

With increasing trend of using the plastic materials and demands on their properties in economic point of view and also in term of their usage arises the question of their reuse after the life-time period.

In some cases there is limited recyclability of plastic materials. There is a range of methods for reusing the thermoplastic materials, which are remeltable after processing unlike materials, in which the three-dimensional net is created in the

final product after processing, for instance curing at thermosets or rubber compounds.

The three-dimensional net is also created by application of radiation cross-linking, which is used for enhancement of wide range of properties, not only mechanical but also chemical and thermal properties as well. This can be utilized with great benefit for cross-linking of commonly used materials and for their subsequent substitution for more expensive constructional materials or materials for special applications.

The change of properties after radiation cross-linking entails the question of reuse of these materials since due to cross-linking an originally thermoplastic material becomes thermoelastic, thus is the possibility of direct recycling by remoulding analogically closed.

2. Experiment

In order to determine the possibility of reusing products made of polyethylene modified by irradiation, material of the Slovnaft Petrochemicals s.r.o. LDPE BRALEN VA 20 – 60 was applied as a virgin polyethylene and irradiated high-density polyethylene pipes were used as a filler. The virgin material of these pipes is HDPE Lupolen 4261 A Q 416. These materials were finely ground.

HDPE pipes were cross-linked by accelerated electrons of the energy of 10 MeV and dosage of 139 kGy radiation by BGS Beta-Gamma-Service GmbH & Co. KG. The crosslinking-degree of this pipes used for heat exchanger was measured 64 %. Irradiation by β rays is a process by which a material is absorbing energy of high-accelerated electron beams. Energy absorption initiates chemical processes in material. By penetration of electrons in material comes to activation and ionisation of molecules, which are joining and thereby reaching the cross-linking.

Furthermore the mixtures of virgin LDPE and cross-linked HDPE powder were prepared from 0 to 50 % amount of filler and finally the specimens were moulded for the tensile test under room and higher temperature and appropriate tests were executed and evaluated.

3. Results and discussion

During the tensile test several parameters were observed, especially modulus of elasticity, tensile strength or relative elongation at break. Obtained values were processed into tables depending on the measurement temperature and the amount of cross-linked HDPE filler. For every mixture was testing of thirty specimens accomplished.

When comparing values of unfilled and filled specimens the modulus of elasticity is increasing markedly up to 280 % from 132.9 N mm^{-2} (10 % of HDPE filler) to 298.62 N mm^{-2} (50 % of HDPE filler) (Fig. 1).

Analogous to the previous graph, also tensile strength (Fig. 2) grows steadily in whole 10 to 50 % fillers interval, although the growth is more gradual from 9.19 N mm^{-2} (10 % of HDPE filler) to 12.38 N mm^{-2} (50 % of HDPE filler).

Similar results can be observed from the tensile test at elevated temperature. The raise of modulus of elasticity up to

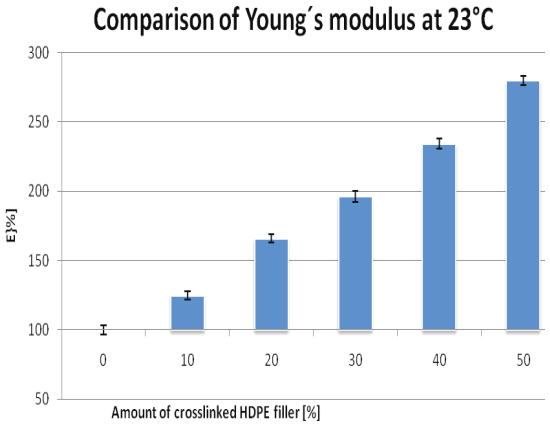

Fig. 1. **Comparison of modulus of elasticity for mixtures of virgin LDPE and crosslinked HDPE at 23 °C**

85 % can offer interesting applications of recycled HDPE pipes (Fig. 3).

In the case of the tensile strength at elevated temperature (Fig. 4), values of filled specimens show also higher values than unfilled, where the highest growth goes up to 32 % by specimens formed of 50 % of fillers and 50 % of virgin material.

4. Conclusion

It is evident from the measured data, that investigated material can be reused as fillers in all measured concentrations without any appreciable loss of observed mechanical properties.

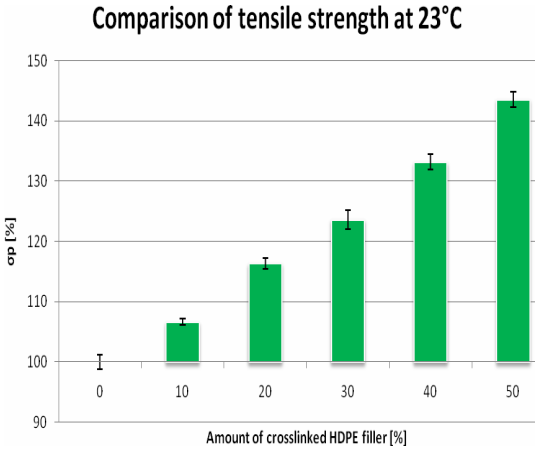

Fig. 2. **Comparison** of tensile strength for mixtures of virgin LDPE and crosslinked HDPE at 23 °C

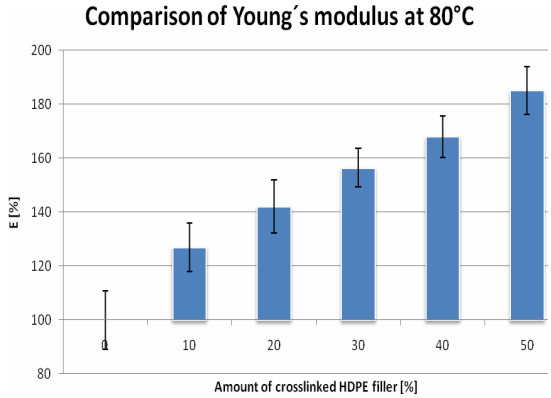

Fig. 3. **Comparison of modulus of elasticity for mixtures of virgin LDPE and crosslinked HDPE at 80 °C**

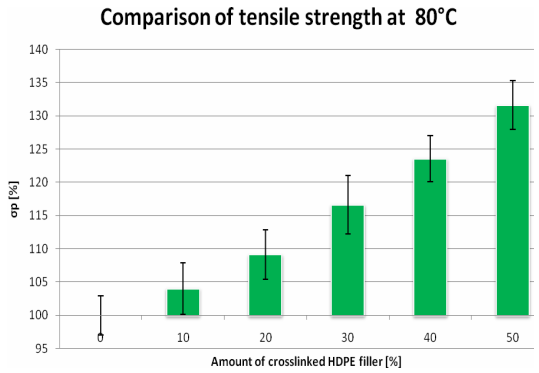

Fig. 4. **Comparison of tensile strength for mixtures of virgin LDPE and crosslinked HDPE at 80 °C**

Opposite to this, higher amount of filler comes a increase tensile strength and modulus of elasticity.

Another good result is the possibility of mixture LDPE and HDPE which are in normal state miscible with difficulties.

These results are significant for both the engineering practice, where product price can be reduced by the filler addition with increase in their properties, furthermore thus contribute to a possibility of recycling the radiation crosslinked products and also consequently for the consumer.

This article is financially supported by the Czech Ministry of Education, Youth and Sports in the R&D projects under the titles 'Modeling and Control of Processing Procedures of Natural and Synthetic Polymers', No. MSM 7088352102 and 'CEBIA Tech', No. CZ.1.05/2.1.00/03.0089

REFERENCES

1. Woods R. J.: *Applied radiation chemistry: radiation processing*, 1994.
2. Zyball A.: *Strahlungsenergie zur Modification von Kunststoffen – Industrielle Anwendungen der Bestrahlungstechnik*, In: Strahlenvernetzte Kunstoffe, Springer VDI verlag, Dusseldorf 2006.
3. Drobný J. G.: *Radiation Technology for Polymers*, CRC Press, Boca Raton 2003.
4. BGS - Beta-Gamma-Service. [online]. http://www.bgs.de

CL-10
THE TESTING OF HYPERELASTIC PROPERTIES OF THE RUBBER MATERIALS

JAKUB JAVORIK* and ZDENEK DVORAK

Tomas Bata University in Zlin, nam. T.G. Masaryka 5555, 760 01 Zlin, Czech Republic
javorik@ft.utb.cz

Abstract

The aim of our work is to set up nonlinear material parameters of elastomers for numerical simulation of these materials. For this purpose, it is necessary to test material in three different modes: uniaxial tension, equibiaxial tension and pure shear. The equibiaxial elastomer characterization is the object of this paper. A bubble inflation technique was used for this characterization. We use data from this test and from uniaxial test to create the FEM models of elastomer.

Introduction

Thanks their special properties we can find the elastomers in almost all areas of human doings (let us remember their sealing and damping properties)[1,2]. A need of exact description of the highly nonlinear mechanics of this material arises still more often.

Our aim is to set up nonlinear material parameters of elastomers for numerical simulations. The measuring the engineering constants for nonlinear material models is demanding more special equipment than the measuring the constants for previously used linear material models. For accurate evaluation of hyperelastic material constants we need to test material in all deformation modes that will occur during simulation. Usually three basic deformation modes are tested: uniaxial tension, equibiaxial tension and pure shear[3,4]. The uniaxial tension is easy to perform on standard testing machines[5]. But the special equipments are necessary for next two deformation modes.

One of the suitable methods for equibiaxial characterization of elastomers is the bubble inflation technique in which an elastomer is inflated to the shape of bubble[6].

Experimental

A uniform circular specimen of elastomer is clamped at the rim and inflated using compressed air to one side. The specimen is deformed to the shape of bubble. The inflation of the specimen results in a biaxial stretching near the pole of the

bubble and the planar tension near the rim.

Thanks to the spherical symmetry we can consider equibiaxial stress at the pole of the bubble. The thickness of specimen is small and the ratio between the thickness of the inflated membrane t and the curvature radius r is small enough, then the thin shell assumption allows us to neglect the radial stress in the specimen. With consideration of material incompressibility we can express the thickness of inflated

$$t = \frac{t_0}{\lambda_{\theta\theta}^2}$$

specimen as:

where t_0 is the initial thickness of specimen (unloaded state). Further we have to measure the stretch $\lambda_{\theta\theta}$ at the pole of inflated material. Generally stretch λ is the ratio between the

$$\lambda = \frac{l}{l_0}$$

current length l and the initial length l_0:

We can use some of optical method for measurement of stretch $\lambda_{\theta\theta}$ and curvature radius r (camera, video camera, laser etc.).

Finally we can compute the hoop stress $\sigma_{\theta\theta}$ on the pole

$$\sigma_{\theta\theta} = \frac{pr\lambda_{\theta\theta}^2}{2t_0}$$

of the inflated specimen as ref.[6]:

The specimen of 2 mm thin elastomer is fixed between two rings with inner diameter 40 mm. Rings are clamped in a support.

Next function of the support is distribution of the compressed air to one side of the specimen. The current value of applied pressure is recorded using a pressure sensor. The inflation of the specimen is recorded using a high resolution CCD video camera. A computer is used to control the pressure.

The white strips were drawn in the central area of specimen for stretch measurement. It is important to measure elongation and curvature radius only in the area near to pole (between the strips) of inflated specimen and not on entire bubble contour because only on the pole the equibiaxial state of stress occurs.

The common SBR compound for tire manufacturing was tested. The material was loaded until failure. We obtained values of stretch ratios $\lambda_{\theta\theta}$ and curvature radii r from image analysis of video record.

Results

The equibiaxial stress-strain diagram of tested material is shown in Fig. 1. Also the uniaxial stress data are presented in this diagram for comparison. We can see generally known fact[3], when equibiaxial stress values are 1.5-2 times greater than uniaxial.

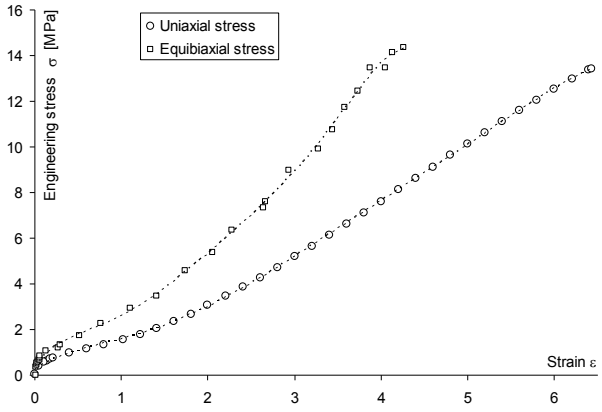

Fig. 1. **Stress-strain diagram of tested material**

The FEM model of specimen inflation (based on 5-terms Mooney-Rivlin hyperelastic model) was created and compared with experiment.

Conclusions

It is not possible to predict biaxial behaviour of elastomer from uniaxial data only. When both uniaxial and biaxial data are used, the material models closely follow both uniaxial and biaxial experimental data[6]. The bubble inflation technique is very suitable method for the equibiaxial tension test of elastomers and for the accurate description of hyperelastic behaviour of material.

This work is financially supported by the Czech Ministry of Education, Youth and Sports in the R&D project under the title 'Modelling and Control of Processing Procedures of Natural and Synthetic Polymers', No. MSM 7088352102.

REFERENCES

1. Manas D., Stanek M., Manas M., Pata V., Javorik J.: KGK, Kautsch. Gummi Kunstst. *62*, 240 (2009).
2. Manas D., Manas M., Stanek M., Zaludek M., Sanda S., Javorik J., Pata, V.: Chem. Listy. *103*, 72 (2009).
3. Ogden R. W.: *Non-linear Elastic Deformations*, Dover Publications, Mineola 1997.
4. Kohnke P.: *ANSYS – Theory reference*, Ansys Inc., Canonsburg 1998.
5. Smith L. P.: *The language of Rubber,* Butterworth-Heinemann, Oxford 1993.
6. Reuge N., Schmidt F. M., Le Maoult Y., Rachik M., Abbé F.: Polymer Eng. Sci. *41*, 522 (2001).

CL-11
EFFECTS OF CRYOGENIC TREATMENT ON THE PROPERTIES OF TYRE PRUDUCTION WASTES

BAĞDAGÜL KARAAĞAÇ*[a], VELİ DENİZ[a], and MURAT ŞEN[b]

[a] Kocaeli University, Engineering Faculty, Chemical Engineering Dept, Umuttepe Campus, 41380 Kocaeli / Turkey,
[b] Hacettepe University, Faculty of Science, Chemistry Dept. Beytepe Campus, 06800 Ankara / Turkey
bkaraagac@kocaeli.edu.tr, vdeniz@kocaeli.edu.tr, msen@hacettepe.edu.tr

Recent waste management strategies focus on the prevention of wastes. Therefore, any kind of wastes should be reduced as much as possible where they are produced. Wastes of tyre industry can be classified as used tyres, green tyre wastes, unvulcanized tread wastes, laboratory wastes, inner tube and bladder scraps, reinforcing material wastes and other compound scraps. In recycling plants, each kind of vulcanized and unvulcanized wastes can be recycled by various techniques[1]. In reinforcing materials group, textile fabric wastes can be recycled as regenerated rubber after removing the textile component[2]. It is difficult to separate the rubber compound and metallic cord in the calendered fabric and/or green tyres due to its sticky character. In many applications, these wastes are vulcanized in autoclave and then recycled with the other vulcanized wastes, i.e. with used tyres. In some cases, metallic fabric wastes are burned in the field to recover metallic cord, illegally and environmentally unfriendly. It has not been reported any methodology in literature for recycling of calendered metallic fabric and green tyre wastes, produced in tyre industry.

In this study, the conditions of cryogenic recycling of metallic fabric wastes and the possibility of reuse their compound part have been investigated. Metallic fabric wastes used in this study were obtained from the local tyre manufacturing factories in Kocaeli. Solid CO_2 and liquid N_2 were used as coolant. Cold and brittle material was separated into two phases as rubber compound and steel by mechanical treatment. The conditions of cryogenic recycling and the possibilities of reusing rubber compound of these wastes were investigated. The changes in physical, mechanical, and rheological properties of the compounds after cryogenic treatment were investigated.

It has been observed that the adhesion values, rheological and mechanical properties of compounds obtained from wastes were worsened by a maximum of %10 with decreasing dispersion quality. It has been concluded that cryogenic technique can be used for recycling of reinforcing materials such as calendered metallic fabric and green tyre wastes without any decreasing in their commercial values.

REFERENCES

1. Adhikari B., De D., Maiti S.: Prog. Polym. Sci. *25*, 909 (2000).
2. Schafer R., Isringhaus R. A., in: *Introduction to Rubber Technology*, Van Monstrand Reinhold Co., UK, 1959.

CL-12
CHARACTERIZATION OF ELASTOMERS BY WETTING: ROUGHNESS AND CHEMICAL HETEROGENEITY

CHRISTIAN W. KARL* and MANFRED KLÜPPEL

German Institute of Rubber Technology, Eupener Strasse 33, 30519 Hannover, Germany
christian.karl@dikautschuk.de

An advanced method of describing the impact of roughness on contact angles of different rough and varnished elastomers is presented here. The composition of coated elastomers was analysed by ATR-IR and SEM-EDX. The topography and coating thickness were examined by SEM and digital microscopy. Dynamic contact angles were estimated for solvents of different polarity by using the Wilhelmy method. The hysteresis of the contact angles was correlated with roughness parameters which were obtained by white light interferometry and measurements with the stylus instrument. From the contact angles, the polar and disperse parts of the surface energy were calculated by the OWRK method.

Introduction

The characterization of solids by wetting experiments has attracted a lot of attention over many years. Wettability plays a very important role in the fields of adhesion, printing, cleaning and lubrication. Many different systems have been investigated so far. It is difficult to have a physically and chemically inert, smooth, homogenous and rigid solid which is necessary to measure Young`s contact angle[1]. Such conditions are rarely encountered in many practical situations. The contact angle is influenced by surface patches having different chemical composition and the roughness of the surface[2]. Up to now, it has not been fully explained how physical roughness and chemical heterogeneity, especially with isolated defects, affect the contact angle which is an important parameter to calculate the surface energy of solids[2−4]. Little work has been done to correlate contact angle hysteresis with roughness parameters, such as fractal dimension and height profile data[5,6]. The change of a contact angle at a certain roughness paramter has not yet been investigated. Only the mean roughness index represents a parameter which is widely used in literature to describe the roughness of a surface[7]. To address this issue, we used different smooth and rough elastomers with coated laquers to investigate the influence of roughness and surface composition on contact angles, contact angle hysteresis and surface energy.

Experimental

The samples were prepared as follows: S-SBR (VSL-2525-0) filled with 50 phr of carbon black N 339 was prepared via a conventional sulphur vulcanization system. Four surfaces with different textures of vulcanization plates were processed, cleaned with isopropanol and coated entirely with one of the four varnish systems: PTFE (polytetra-

fluoroethylene), TPU (thermoplastic polyurethane), PDMS (poly-dimethylsiloxane) and PU (polyurethane). Subsequently, the samples were heated up to 120–140 °C for 2–5 minutes. The roughness of the samples was studied using a white light interferometry instrument (FRT). A velocity of 0.1 mm s^{-1} and an area of 4 mm^2 were employed. Additionally, a stylus instrument UST 1000 (Innowep) was used with the following conditions: distance: 40 mm, velocity: 3 mm s^{-1}, force: 10 mN, stylus: 90° diamond. For performing wetting experiments with the Wilhelmy method, the DCAT 11 (Data Physics Instruments GmbH) was applied. A set of different test liquids over a wide range of polarities was used to obtain advancing and receding contact angles. Three different samples for each solvent were taken into account. Contact angle hysteresis, being a measure for roughness, was calculated as the difference from advancing and receding contact angles for each sample. Digital microscopy and SEM were used to determine the coating thickness and the topography of the elastomer composites. The composition of the lacquers was analysed by ATR-IR and EDX mapping.

Results and discussion

To investigate the roughness of the coated and reference samples, white light interferometry measurements were carried out. Fig. 1 represents a white light interferometric micrograph of a smooth SBR sample (left) and the corresponding rough sample (right) both coated with a PTFE varnish. The coating of the lacquer on the rough surface reveals that the height differences increase significantly as opposed to the smooth equivalent. Possibly, the varnish does not penetrate fully into the surface grooves.

For the evaluation of the white light interferometry height data, a Gaussion fit was used. As shown in Fig. 2, the fit curve describe the data points quite well.

The parameter σ representing the half width of a height distribution is regarded as a parameter for the roughness of a surface. Advancing and receding contact angles of the four different varnishes on smooth and rough SBR were measured by the Wilhelmy method as previously shown[9]. Contact angle hysteresis values correlate quite well with the σ-values as it is revealed in Fig. 3. In addition to this, σ values are also in good accordance with values of the mean roughness index R_a measured by a stylus intrument. As expected, Δθ-values for the very smooth SBR surface (reference) are very low in contrast to the varnished samples and rough SBR. The latter shows a significant decrease of hysteresis values (Fig. 3) with

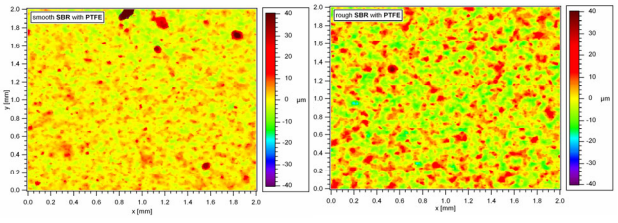

Fig. 1. **White light interferometric micrographs of a smooth (left) and rough (right) SBR sample coated with PTFE varnish**

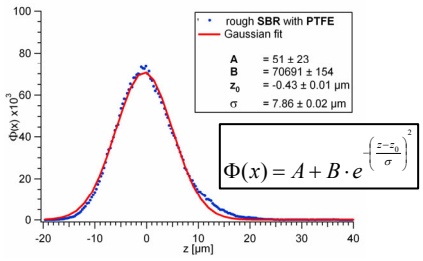

Fig. 2. **Histogram of the height differences versus the z-height and the Gaussian fit curve for a rough SBR sample coated with PTFE varnish**

decreasing polarity of the solvents due to a strong roughening effect. Surface casting with PTFE implies a higher σ-value as shown in Fig. 2 and 3. This is also confirmed by the fact that the σ-value for the rough SBR sample increases from 4.5 (Fig. 3) to 7.9 (Fig. 2) for the rough sample with PTFE coating. This is due to the fact that the roughness as well as the surface composition contribute to the roughness of the sample.

The PTFE and the TPU lacquers exhibit the biggest differences with respect to the roughness parameters because of the particles in the PTFE varnish and the surface patches of TPU. PU shows the highest values due to the formation of spherical structures which occur during the drying of the lacquer film.

Fig. 4 shows the plots of the dynamic water and thiodiethanol contact angles as a function of the dynamic hysteresis for SBR filled with carbon black with varied surface roughness. Water is the most polar among the five and thiodiethaol the most unpolar solvent. For both solvents there is no relevant difference as far as the wetting behaviour is concerned. A linear extrapolation (solid lines) to the intercept with the y-axis indicates the equilibrium contact angle at which no influence of roughness can be verified[10]. Furthermore no difference is observed between dynamic angles for surfaces with

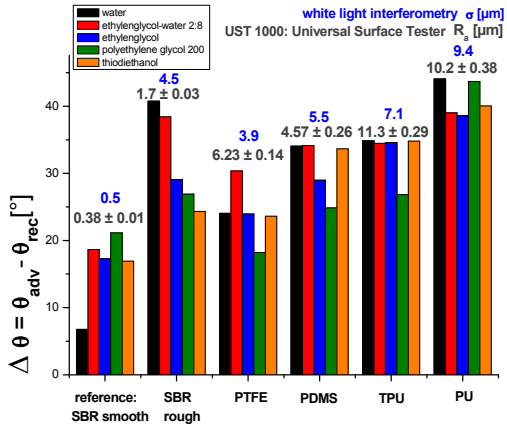

Fig. 3. **Contact angle hysteresis values of the lacquers coated on smooth SBR (reference) and the corresponding roughness parameters**

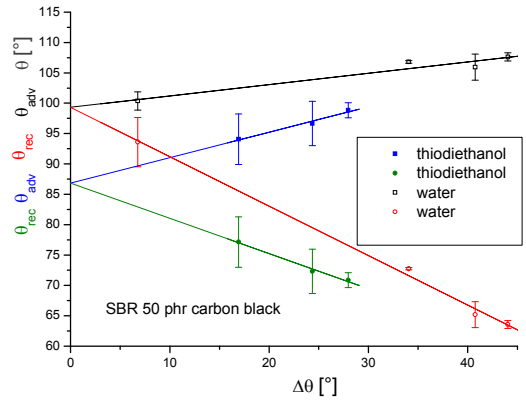

Fig. 4. **Advancing and receding contact angles versus the hysteresis for the systems SBR/water and SBR/thiodiethanol at 20 °C**

dynamic hysteresis and thus roughness of less than 5°. This is in good accordance with previous investigations[10].

Conclusions

The varnished elastomer composites were analysed with respect to their chemical composition which influences contact angles. Advancing and receding contact angles as well as the correlation of hysteresis values with roughness parameters are reproducible. Roughness analysis is necessary, because it influences the surface energy and friction behaviour[9]. It is found that a rougher sample causes a rise in the contact angle hysteresis. An analysis of this effect by the method of Kamusewitz et al.[10] gives further evidence of surface roughness on contact angle measurements allowing for an estimation of the equilibrium contact angle.

This work was supported by the Arbeitsgemeinschaft industrielle Forschung (AiF-grand 15810 BG). The sample preparation by the Forschungsinstitut für Leder- und Kunststoffbahnen e. V. (FILK Freiberg) is highly appreciated.

REFERENCES

1. Marmur A.: Annu. Rev. Mater. Res. *39*, 473 (2009).
2. McHale G.: Langmuir *23*, 8200 (2007).
3. Stöckelhuber K. W., Das A., Jurk R., Heinrich G.: Polymer *51*, 1954 (2010).
4. Owens D. K.: J. Appl. Polym. Sci. *13*, 1741 (1969).
5. Grythe K. F., Hansen F. K.: Langmuir *23*, 6109 (2006).
6. Persson B. N. J., Albohr O., Tartaglino U., Volokitin A. I., et al.: J. Phys.: Condens. Matter *17*, 1 (2005).
7. De Gennes P. G.: Rev. Mod. Phys. *57*, 3 (1985).
8. Palzer S., Hiebl C., Sommer K., et al.: Chemie Ing. Technik *73*, 1032 (2001).
9. Karl C. W., Busse L., Klüppel M., Giese U.: *9th Fall Rubber Colloquium* (2010).
10. Kamusewitz H., Possart W., Paul D.: Colloids Surf., A *156*, 271 (1999).

CL-13

POLYPROPYLENE NANOCOMPOSITES BASED ON HALLOYSITE AND MONTMORILLONITE: THE EFFECT OF DIMALEINIMIDE REACTIVE MODIFIERS ON STRUCTURE AND PROPERTIES

VIERA KHUNOVÁ[a], JÁNOS KRISTÓF, and JANA KOZÁNKOVÁ[a]

[a] The Slovak University of Technology, Faculty of Chemical and Food Technology, Institute of Polymer Materials, Radlinského 9, 812 37 Bratislava, Slovakia, [b] University of Pannonia, Department of Analytical Chemistry, Egyetem 10, H-8200, Veszprém, Hungary

Introduction

The extensive research efforts devoted to the development of polymer nanocomposites during the last decade made available a number of new materials with exceptional properties. The most explored one is polymer nanocomposites based on layered clay mineral montmorillonite (MMTs) and carbon nanotubes (CNTs). Surprisingly, halloysite (HNTs) with its unique crystal structure has until recently not been considered as an alternative to MMTs and CNTs.

Halloysite (HNTs) is a natural layered 1:1 aluminosilicate ($Al_2Si_2O_5(OH)_4 \cdot 2\ H_2O$) clay mineral. The most common halloysite particle morphology is an elongated hollow tubular structure with a large aspect ratio, similar to that of CNTs (ref.[1]).

Advantage of HNTs as opposed to MMTs is that in high polar polymer matrix composites efficient dispersion of the nanotubes and significant improvement of strength and toughness can be achieve by using unmodified halloysite[3,4].. Contrary, in nonpolar polymer matrix in addition of chemical modification/intercalation of clay (MMTs and HNTs), it is necessary to apply interfacial modifiers (i.e. MAPP) to achieve improvement of end use properties [5,6].

In our earlier work it was found that 1,3-phenylene dimaleimide (BMI) is a highly effective interfacial modifier for non polar polymer (PP, PE) composites based on unmodified (Na-MMTs) as well as organically modified (o-MMTs) montmorillonite. In addition to a significant increase of interface interactions in o-MMTs nanocomposites, reactive processing with BMI supports the delamination of MMTs tactoids together with improving the degree of platelet dispersion[7].

This work highlights the role of another dimaleinimide derivate, 4,4'-diphenylmethylene-dimaleinimide (DBMI) as a reactive modifier on structure and properties of montmorillonite and halloysite nanocomposites.

Materials

Polypropylene homopolymer SABI 575 P [Melt flow rate 11.0 dg min^{-1}(230 °C/2.16 kg)]. Two layered silicate nanofillers have been evaluated:

– organically modified MMT (o-MMT) Nanoblend™ Concentrate (NB1001) obtained from PolyOne Corp, (USA),
– tubular untreated halloysite from location Biela Hora,

(Slovakia).

As a reactive modifier DBMI from VUCHT, Bratislava, Slovakia has been used:

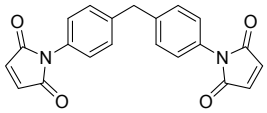

Analysis and characterisation

The composites were formed from polypropylene and MMT (5–40 wt.%) together with DBMI (0.5 to 3 wt.%) via melt mixing in a Brabender W50-E chamber fitted with cam blades. Mixing temperature was 200 °C and rotor speed was 180 rpm.

Structure of nanocomposites has been studied by wide-angle X-ray diffraction patterns (WAXS) using a powder diffractometer (the HZG/4A Präzisionsmechanik GMBH, Germany). Composite fracture surfaces were examined using a TESLA BS 300 combined scanning and transmission electron microscope. For transmission electron microscope (TEM) observations ultrathin (60 nm) sections were cut under liquid N_2, from a stained (RuO_4 vapor for 90 min) sample using an Ultracut UCT (Leica) ultramicrotome. Tensile tests were carried out at 22 °C using an Instron 5800 tensometer at a crosshead speed of 50 mm min^{-1}

Effect of DBMI on structure of PP/MMT and PP/HNTs nanocomposites

The effect of DBMI on dispersion of MMTs tactoids is clearly evident from WAXS observations. Fig. 1 shows data for composites based on PP containing 5 wt.% NB1001.

Addition of DBMI resulted in reductions of the intensity of the (001) reflections and improved also the degree of platelet dispersion. This effect is even higher than it was observed in other BMI modified PP/ o-MMTs (Nanocor, Cloisite 30B, Nanofil 5) nanocomposites[6].

As it is evident from the TEM images of cryo-microtomed sections of PP/NB1001 nanocomposites, the addition of DBMI resulted in reduction of clay tactoids size.

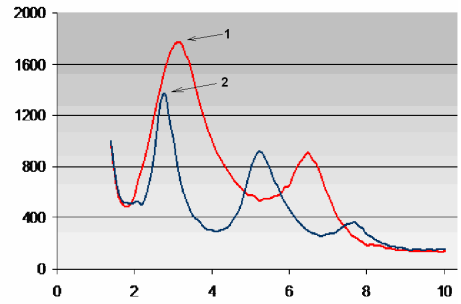

Fig. 1. **XRD patterns for (1) PP containing 5 % w/w NB 1001 and (2) PP containing of 5 % w/w NB 1001 and 1 % w/w DBMI**

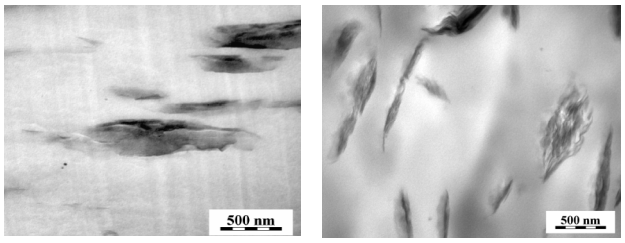

Fig. 2. **TEM images of PP/Nanoblend 1001 nanocomposites; (a) without DBMI and (b) with DBMI**

The effectiveness of DBMI in increasing the level of filler-matrix interaction can be readily seen in SEM images of fracture surfaces PP/NB1001 nanocomposites. In the unmodified composite (Fig. 3a) relatively poor filler matrix interaction is manifested, whilst in DBMI modified composites much better adhesion of clay particles to the matrix is evident (Fig. 3b).

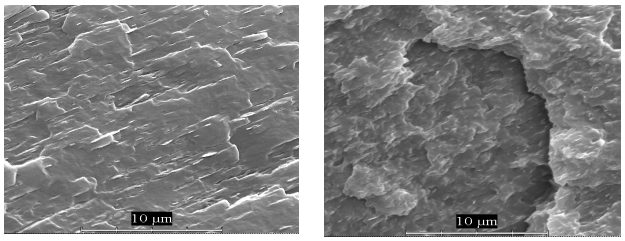

Fig. 3. **SEM images of fracture surfaces PP/Nanoblend 1001 nanocomposite; (a) - without DBMI, (b) with DBMI**

The addition of DBMI to the PP/HNTs composite had no effect on the crystallographic properties as shown in Fig. 4. It means that the coupling of the clay particles to the polymer via DBMI is an interfacial reaction.

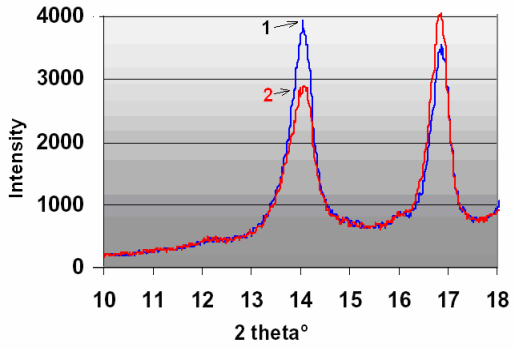

Fig. 4. **XRD patterns for (1) PP containing 5 % w/w halloysite and (2) PP containing of 5 % w/w halloysite and 1 % w/w DBMI**

Effect of DBMI on properties of PP/HNTs nanocomposites

In our previous work[8] BMI has been shown to be effective at improving the properties of composites based on high inorganic filler loadings. The evaluation of effect of DBMI on mechanical properties of PPHNTs composites with low and high HNTs content is presented in Table I and Fig. 5.

Table I
Influence of 5 %w/w untreated halloysite and 1 %w/w DBMI

Sample	s_b [MPa]	E [MPa]	ε [%]
Neat PP	35,4	1340	8.6
PP/5% HNTs	36,5	1440	4,9
PP/5% HNTs/1 % DBMI	38,6	–	4,4

The results in the Table I confirm that by reactive processing with DBMI simultaneous improving of HNTs dispersion and interfacial adhesion (observed by SEM) leads to higher strength and stiffness.

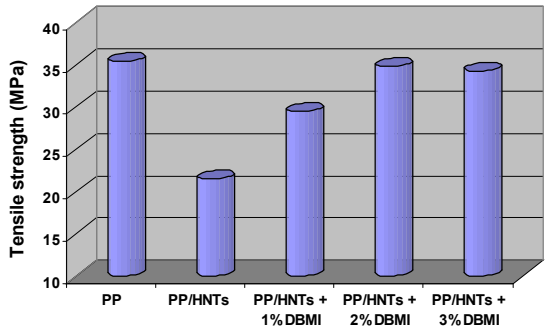

Fig. 5. **Influence of DBMI content on tensile strength of PP composites containing 40 % w/w untreated halloysite**

In composites with high halloysite content even much significant effect of DBMI on mechanical properties has been observed. As it is evident from Fig. 5, addition 1 % w/w DBMI improved the tensile strength nearly at 50 %. When 2 % w/w DBMI has been used, the tensile strength increasing of up to that of the unfilled matrix.

Conclusions

In the paper the effect of dimaleimide type reactive modifier on structure and properties of melt prepared PP nanocomposites has been studied. It was found that 4,4'-diphenylmethylene-dimaleinimide (DBMI) acts as a very effective coupling agent for montmorillonite and halloysite based PP nanocomposites. Reactive processing by DBMI led to significant improving of interface and fillers dispersion. The effect of DBMI was confirmed by improving mechanical and thermal properties both PP/MMTs and PP/HNTs nanocomposites.

This project was supported by the Hungarian Ministry of Culture and Education under grant TÁMOP-4.2.2-08/1/2008-0018. The financial and infrastructural support of the State of Hungary and the European Union in the frame of the TÁMOP-4.2.1/B-09/1/KONV-2010-0003 is also gratefully acknowledged.

REFERENCES

1. Joussein E., Petit S., Churchman J., Theng B., Righi D.: Clay Minerals *2005*, 383.
2. Lecouvet B., Gutierrez J. G., Sclavons M., Bailly C.: Polym. Degrad. Stab. *96*, 226 (2011).
3. Hedicke-Höchstötter K., Lim G., Altstädt V.: Compos. Sci. Technol. *69*, 330 (2009).
4. Liu M., Jia Z., Liu F., Jia D., Guo B.: J. Colloid Interface Sci. *350*, 186 (2010).
5. Marney D., Russell L. J., Wu D. Y., Nguyen T.: Polym. Degrad. Stab. *93*, 1971 (2008).
6. Nan-ying Ning, Qin-jian Yin, Feng Luo, Qin Zhang, Rongni Du, Qiang Fu: Polymer *48*, 7374 (2007).
7. Khunová V., Kelnar I., Liauw C. M.: Compos. Interfaces 2011, in press
8. Khunová V., Liauw C. M.: *Property Tailoring of Particulate Polymer Composites by Reactive Processing*, Macrom. Symp, 170, 2001, 197–204.

CL-14
COMPARISON OF DIFFERENT TESTING METHODS IN STABILIZATION OF ELASTOMERS

K. KOŠÁR[a], P.LEHOCKÝ[a], J. UHLÁR[a], M. KRÁLIK[a], and P. ŠIMON[b]

VUCHT a.s. (Research Institute of Chemical Technology), Nobel Str. 34, SK-83603 Bratislava, [b] Slovak University of Technology, Faculty of Chemical and Food Technology, Radlinského 9, SK-812 37 Bratislava, Slovakia
kkosar@vucht.sk

Abstract

The results of measuring the antioxidative efficiency of stabilizers by the viscosity changes of a polymer and by the protection factor determined from differential scanning calorimetry (DSC) tests were compared. Both methods showed relatively good correspondence for most of the tested antioxidants.

Introduction

A considerable part of antidegradants in rubber industry are used as stabilizers added to elastomers after polymerization in order to protect them against thermo-oxidative effects

during their production, drying, storage and processing by the end-user during compounding. As our aim is to find balance between efficiency, cost and all the other properties, it is important to have rapid and reliable test methods for evaluation of their efficiency in elastomers. We have tested the efficiency of stabilizers in emulsion type butadiene-styrene rubber (E-SBR) through viscosity changes of rubber measured at different stages of its thermooxidative aging on one hand and on the other hand by DSC measurement to find the so-called protection factor of the tested stabilizers.

Experimental

To test the methods of evaluation of antioxidants, samples of E-SBR were prepared with various substances (more than 60 chemicals, mostly derivatives of diphenylamine and *p*-phenylenediamine, but also other groups of chemicals). In parts of the tests the stabilizers were added to the unstabilized latex before its coagulation. Preparing the rubber samples in this way the concentration dependence of efficiency of stabilizers in the rubber could be clearly recognized by both methods, however, in these cases a certain part of the stabilizers did not enter the coagulated polymer, but remained in waters. So, to get more accurate results, we tried to get the stabilizers into in advance isolated unstabilized SBR in a mixing chamber.

Results and discussion

The differences in the efficiency of various stabilizers were assessed through changes in the viscosity of SBR before and after chosen times of thermooxidative aging. Taking into consideration the large amount of prepared rubber samples, in order to increase the productivity of testing and to make it possible to distinguish better between the activities of stabilizers, mostly higher temperature (130 °C) has been used for thermooxidative aging. The viscosity measurements were carried out by using Mooney viscosimeter[1], and RPA[2] (Rubber Process Analyzer) at 100 °C. Both instruments measure the resistance of rubber against shear force. During the first stages of propagation of thermooxidative degradation of SBR, the chain scission occurs resulting in a reduction of chain length and average molecular weight, and subsequently in lower viscosity. During later stages of ageing as a sign of termination of thermal degradation, through the interaction of macro radicals the crosslinking appears, resulting in a three-dimensional structure, in higher molecular weight and consequently in higher viscosity. During these tests the stabilizing efficiency of the tested chemicals we tried to express by the time ($t_{15\%}$) of thermo-oxidative aging of SBR, during which the viscosity of the rubber does not fall by 15 % from the "unaged" value. Some results measured by the applied viscosity method (RPA) can be seen on Fig. 1.

Simultaneously with the viscosity tests, the oxidation onset temperature (OOT, T_i)[3] of the prepared SBR samples (containing different "stabilizers") was measured at various heating rates (β) on DSC. The results measured for an unstabilized and a stabilized SBR can be compared on Fig. 2.

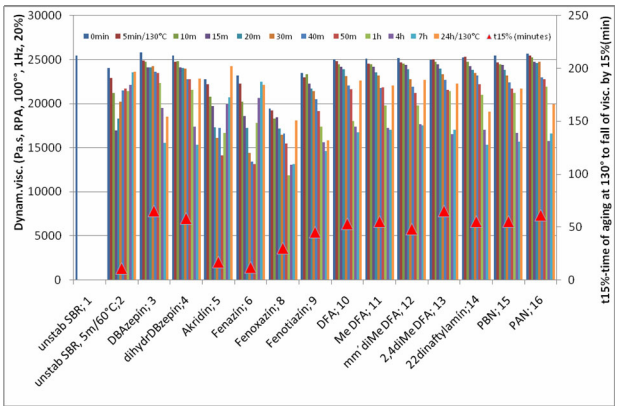

Fig. 1. **The viscosity changes of unstabilized SBR (No 2) and stabilized SBR (No 3-16) during thermooxidative aging at 130 °C with expression of $t_{15\%}$** (time during which the viscosity of the rubber does not fall by 15 % from the unaged value), RPA

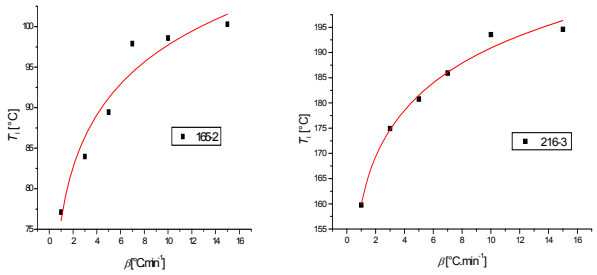

Fig. 2. **Dependence of oxidation onset temperatures (T_i) for unstabilized (on the left) and for stabilized SBR on heating rate β, DSC**

From the dependence of T_i on heating rate the values of parameters *A* and D were calculated for each tested antioxidant (equation (*1*)).

$$T_i = \frac{1}{D}\ln\left(AD\,\beta + 1\right) \qquad (1)$$

Then, by using the above mentioned parameters A and D the induction period of oxidation (oxidation induction time,t_i) for each "stabilizer" was calculated for a large scale of temperatures by using equation (*2*).

$$t_i = A\,e^{-DT} \qquad (2)$$

By comparing the values of t_i for stabilized rubber to that of unstabilized SBR sample, we have calculated the protection factor (*PF*) for each tested antioxidant for the chosen temperature range:

$$PF = \frac{t_i(\text{SBR stabilized})}{t_i(\text{SBR unstabilized})} \qquad (3)$$

Fig. 3 shows the differences in temperature dependence of the efficiency of some of tested chemicals. These results could be helpful in development of mixtures of stabilizers efficient in the desired temperature range.

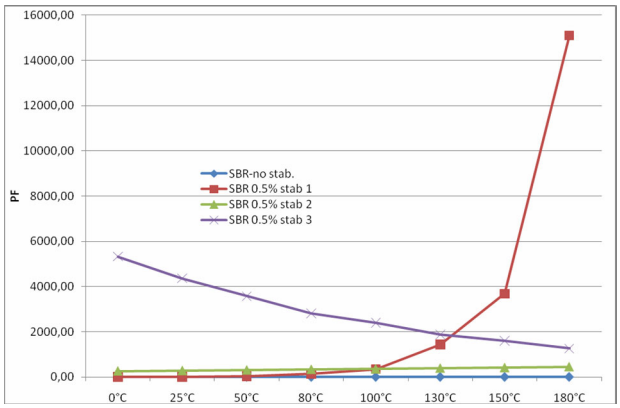

Fig. 3. **The obtained temperature dependence of efficiency (protection factor, PF) of some of the tested stabilizers in SBR**

We have compared the results of viscosity and DSC test. On Fig. 4 the time of thermo-oxidative aging of SBR, during which the dynamic viscosity of the rubber (RPA) does not fall by 15 % ($t_{15\%}$) is compared to the calculated protection factor for the chosen stabilizers at 130 °C. Both methods confirmed the excellent stabilizing efficiency of amine type stabilizers on one hand (especially of derivatives of *p*-phenylenediamine) and on the other hand, despite our expectations, all the synthesized triazine structures proved to be very poor stabilizers.

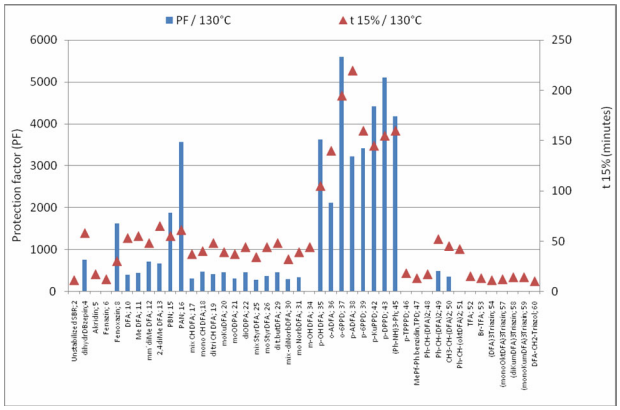

Fig. 4. **Comparison of the calculated values of protection factor (PF) for 130 °C obtained by DSC and values of $t_{15\%}$ (time of thermo-oxidative aging of SBR, during which the dynamic viscosity of the rubber (RPA) does not fall by 15 %) for different stabilizers**

Conclusions

The comparison of the tested methods showed, that they both can be successfully applied in evaluation of antioxidative efficiency of stabilizers. The viscosity tests are more productive and closer to industrial practice. The DSC measurements enable to extrapolate the results to lower temperatures, i.e. to assess the lifetime of rubber compounds for a chosen temperature. Both of them can be very useful in research and development of new stabilizing systems for elastomers.

This work was supported by the Slovak Research and Development Agency under the contract No APVV: 0446-07 and by Duslo a.s.

REFERENCES

1. *ISO 289*-1:2005
2. ASTM D 6204-07
3. Cibulková Z., Šimon P., Lehocký P., Balko J.: Polym. Degrad. Stab. *87*, 479 (2005).

CL-15
FUNCTIONALIZATION OF FIBROUS MATERIAL SURFACES

SILVIA PODOBEKOVÁ and MICHAL KRIŠTOFIČ

Department of Fibres and Textile Chemistry, Institute of Polymer Materials, Faculty of Chemical and Food Technology, Slovak University of Technology in Bratislava, Radlinského 9, 812 37 Bratislava, Slovakia
silvia.podobekova@stuba.sk

Abstract

Polyethyleneterephthalate (PET) fabric surfaces have been treated by deposition of pigment pastes and sol-gel method. The effect of used fixing agents on improvement of adhesion and selected end-use properties has been studied. The improvement of adhesion (according to dry and wet rubbing fastness), the contact angle of wetting and UV resistance were evaluated.

Introduction

Fibers and fibrous materials have high potential for their modification. The functionalization of fibrous material surfaces can be provided by physical, chemical or/and physical-chemical modifications in order to reach qualitatively new properties. The purpose of the fibrous material surfaces functionalization is that this material obtains some new properties, while conserves its original important properties. Producers try to produce goods according to special acquirements of customers and with minimal financial claims. The advantage of surface modification is maximal if it can be shifted to end of the technological process of production[1].

One of several possible surface modifications is the pigment printing. The absence of chemical bonds between the pigment and the substrate is overcome by addition of auxiliary fixing agents.

The surface modifications of textile materials by inorganic-organic nano-sol create transparent, elastic and solid

surfaces with an added value. Silicon-organic compositions provide the hydrophobic surface[2].

Experimental

Materials used

Standard PET fabrics were pigmented on their surfaces with pigments based on carbon, titanium and aluminum having pigment particles size in nano- and micro- dimensions. The pigments were implemented into a pigment paste. Composition of the pigmenting paste:

1. 1–5 wt.% of pigment referred to the fabric's weight – Printex L-6 (PL6), graphite (G), Hombitec S-100 (HS100), ALBO 615 (A615);
2. 10 wt.% of fixing agent referred to the fabric's weight – acrylate (AK), polyvinylacetate (DX), styrenacrylate copolymer – Sokrat 4924 AF (ST);
3. 10 wt.% of thickener (0.8 wt.% sodium alginate solution) referred to the fabric's weight;
4. Novanik 1010 and Slovafol 909 wetting reagents.

The pigment paste was applied on to the PET fabrics by stippling by laboratory foulard with a 100 % wring. The fixation of the modified fabrics on their surfaces was carried out at elevated temperature T_1 = 150 °C for 30 s and T_2 = 200 °C for 60 s.

Consequently, the testing material was covered with the sol prepared from SiO_2 ($Si(OEt)_4$ + EtOH +HCl). The sol was applied by a dip-coating technique at the constant temperature, constant speed of extending and atmospheric pressure.

Method used

Determination of rubbing fastness

According to this method the stability of dyed textile materials dry and wet rubbing fastness are determined. Samples of fabric (white or black) are tested with a dry cotton fabric (dry rubbing fastness) and wet cotton fabric (wet rubbing fastness). Staining of the pigment into the comparative cotton fabric is assessed by a five step gray scale, and thus determines the stability of the coloring. Both, dry and wet rubbing were evaluated in accordance with STN EN 20105-A03 and STN EN ISO 105-X12. Satisfactory levels of dry and wet rubbing fastnesses are 4–5 for dry rubbing and 3–5 for wet rubbing fastnesses.

Assessment of the contact angle of wetting

The See System[3] contact method based on monitoring testing liquid's drop sitting on the surface of testing sample by camera system and measurement the contact angle of wetting via a computer program was used to asses the contact angle of wetting. The water was used as testing liquid.

Barrier properties of fabrics against UV radiation

The barrier properties of treated and untreated PET fabric were measured with Libra S12 spectrophotometer equipped with deuterium lamp. The barrier properties were determined on the basis of STN EN 1378-1:2001. The textile sample was stick on the special metal frame, put into spectrophotometer and the UV radiation throughputs were measured in the range 200–400 nm five times in four different positions. The program Acquire Toolbar was used for determination of the UPF factor for each fabric[1].

Results

According to references[4,5] three fixing agents were selected; two of them commonly available multi-purpose agents based on acrylate (AK) and industrial PVAc derivative (BD Duvilax 20, DX). The third one was styrene-acrylic fixing agent (Socrates, ST) specially designed for textile materials.

PET fabrics modified with pigment pastes have better dry rubbing fastness in comparison with wet ones. Dry rubbing fastness of 58 % samples meet the standard while in wet rubbing fastness it is only about 28 % of samples (Table I).

From the point of pigment used the effectiveness of pigments decreases according to the following sequence: PL6 < A615 < G << HS100.

Table I
Dry and wet rubbing fastness of PET textiles modified by pigment printing (2 wt.%)

Pigment	Fixing agent	Rubbing fastness	
		dry	wet
PL6	AK	2	1
	DX	2	1
	ST	4	3
G	AK	2	1
	DX	4	1
	ST	5	1
HS100	AK	4	–
	DX	5	–
	ST	5	–
A615	AK	2	1
	DX	3	2
	ST	5	4

Table II
Dry and wet rubbing fastness of PET textiles modified by sol-gel method, 2 wt.% of pigment

Pigment	Fixing agent	Rubbing fastness	
		dry	wet
PL6	AK	3	2
	DX	3	2
	ST	4	4
HS100	AK	4	–
	DX	5	–
	ST	5	–
A615	AK	4	3
	DX	4	3
	ST	4	4

From the Table I is evident that the best dry and wet rubbing fastnesses are reached if the pigment pastes were fixed with agents ST or DX.

According to Table II, when sol-gel method was used, one can observes about 78 % accordance with the standard for dry rubbing of the samples treated with 2 wt.% of pigment in the pigment paste.

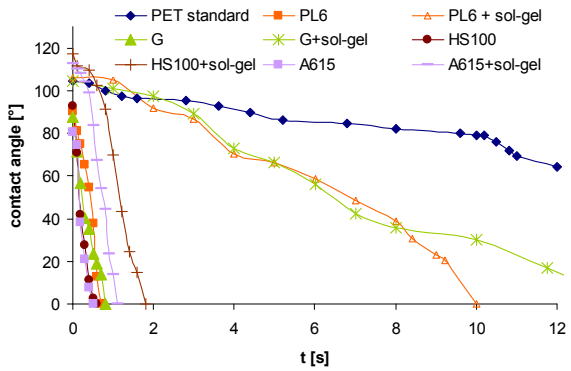

Fig. 1. **Dependency of contact angle of sol-gel modified fabrics from the time,** fixing agent – ST, content of pigment – 3 wt.%

The measurement of contact angle of wetting water was used as testing liquid. The comparison of effectiveness of three used fixing agents in pigmenting paste (AK, DX and ST) shows that fixing agent ST mostly influence the contact angle and water drops were absorbed the slowest. On the contrary fabric modified with the pigment paste containing agent DX was the most hydrophilic.

As it is clear from Fig. 1 sol-gel treatment provides the hydrophobic textile surface.

Among used pigments the pigment HS 100 acts as a UV absorber therefore samples modified with it and all three auxiliary agents were examined from the point of barrier properties. Best results were obtained with the pigment HS100 and Sokrat 4924 AF (Fig. 2).

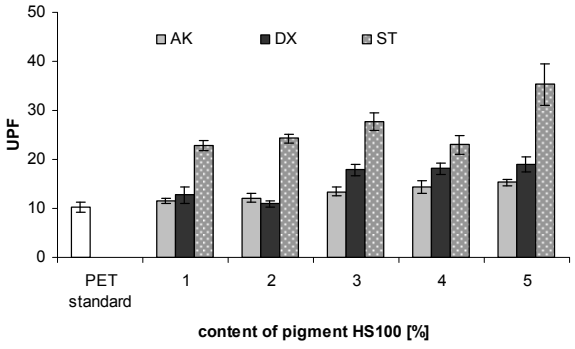

Fig. 2. **UPF factor of fabrics modified with pigment HS100**

Conclusion

1. PET fibrous materials modified with pastes containing four different pigments and three different auxiliary agents exhibit better dry and wet fastnesses. The best results are reached mainly with pigment ALBO 615 and Printex L-6 and auxiliary agent Sokrat 4924 AF. Moreover sol-gel method positively influences fastnesses.
2. The contact angle of modified PET fibrous materials was the highest if auxiliary agent Sokrat 4924 AF was used and the lowest if auxiliary agent polyvinylacetate was applied.
3. The highest UPF factor exhibits pigment HS 100 in combination with auxiliary agent Sokrat 4924 AF.

This work was supported by the Slovak Research and Development Agency under the contract No. VMSP-P-014-09.

REFERENCES

1. Dulíková M.: *PhD work*, Bratislava, p. 3, (2010).
2. Exner P.: Technická univerzita v Liberci, ISBN 80-7372-063-9, (2006).
3. www.seesystems.wz.cz
4. Rusnák A., Murárová A., Ďurman V.: Chem. Listy *100*, 746 (2006).
5. Murárová A., Podobeková S., Jakubíková Z., Rusnák A.: Fibre and Textile *13*, 23 (2006).

CL-16
ELASTOMERIC MATERIALS FILLED WITH MAGNETIC HARD FILLERS

JÁN KRUŽELÁK[a]*, IVAN HUDEC[a], and RASTISLAV DOSOUDIL[b]

[a] Slovak University of Technology in Bratislava, Faculty of Chemical and Food Technology, Institute of Polymer Materials, Department of Plastics and Rubber, Radlinského 9, 812 37 Bratislava, [b] Slovak University of Technology, Faculty of Electrical Engineering and Information Technology, Ilkovičova 3, 812 19 Bratislava, Slovakia jan.kruzelak@stuba.sk

Elastomeric magnetic composites are possible to prepare by incorporation of magnetic fillers in polymer matrix[1,2]. The two different elements are attended to one structural unit, what brings new technological abilities and properties. The advantage of elastomeric magnetic composites are that their properties can be modified for the requirements of specific applications. Because of their elasticity and easy mouldability there are suitable for additive devices, where elasticity and flexibility are additional and important parameters. Moreover, they have very good magnetic properties. Rubber magnets can absorb shock and sound, so they can be applied in dc-motors, motor parts, memo holders, intelligent tyres, in microwave and radar technology, also in other technological applications.

Ferrites represent well established family of magnetic materials. Metal ferrites with general formula $MFe_{12}O_{19}$ (M is divalent cation such as Ba, Sr, ect.) belong to the widely used magnetic materials. High values of magneto-crystalline ani-

sotropy and saturation magnetization allow wide application of these materials as permanent magnets. Because of low price and very good chemical stability, ferrites are included in the most important magnetic materials, which cannot be easily replaced.

In this work a preparation of elastomeric magnetic composites and evaluation of magnetic filler influence on curing characteristics, physical-mechanical and magnetic properties of prepared composites were studied.

Elastomeric magnetic composites were prepared by incorporation of ferrite (F) as well as ferrite in combinations with carbon black (CB) in the rubber blend based on natural rubber. A standard sulfur-based vulcanization system was used. In the first type of composite, filled only with ferrite (type A), the content of magnetic filler was changed in range from 0 to 100 phr. Anisotropic strontium hexaferrite was prepared by wet milling. Detailed characterization of applied ferrite is mentioned in Table I.

Table I
Strontium ferrite characteristics

Characteristics	Values
Density ρ [g cm^{-3}]	4.73
Specific surface area [m^2 g^{-1}]	4.06
Total porosity [%]	55.62
Coercivity [kA m^{-1}]	117
Remanent magnetic induction [T]	0.170

Elastomeric composites, specified as B, were filled with combinations of ferrite and carbon black. The total content of both fillers was kept constant (85 phr), only the weight fraction of ferrite in combination of both fillers ($w_f = F/(F+CB)$) was changed.

The influence of ferrite on basic curing characteristics, e.g. the scorch time t_{S1} and the optimum cure time t_{C90} was investigated. From Fig. 1 it is clearly seen that the presence of feromagnetic filler in rubber matrix leads to a decrease of optimum cure time as well as the scorch time of rubber compounds A. The t_{C90} of maximum filled rubber compound decreased in about 10 % and the t_{S1} in about 21 % in comparison with t_{C90} or t_{S1} of ferrite free sample.

By contrast, the optimum cure time as well as the scorch time of rubber compounds B was found to increase with increasing content of ferrite in combinations of applied fillers (Fig. 2). The most significant increase of both curing characteristics was observed in case of rubber blend filled only with magnetic filler. The t_{C90} of sample filled only with ferrite increased in about 11 minutes, the t_{S1} in 7 minutes in comparison to evaluated parameters of sample filled only with carbon black.

The results of study of physical – mechanical properties of composites A showed that ferrite present in rubber matrix has an influence on moduli especially, which increase substantially with increasing of magnetic filler loading. On the other hand the elongation at break was found to decrease with increasing amount of ferrite. At maximum ferrite loading there was recorded about 17 % of elongation at break in comparison to unfilled sample (Fig. 3). From Fig. 3 also becomes evident, that the influence of magnetic filler content on the tensile strength at break was insignificant.

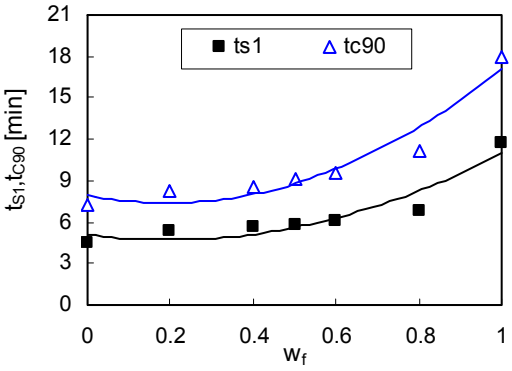

Fig. 2. **Influence of ferrite weight fraction w_f on scorch time t_{S1} and optimum cure time t_{C90} of rubber compounds B**

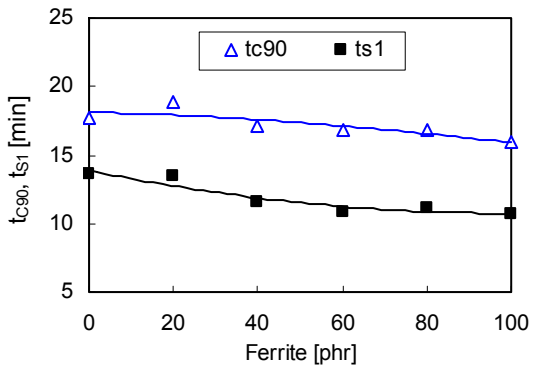

Fig. 1. **Influence of ferrite content on scorch time t_{S1} and optimum cure time t_{C90} of rubber compounds A**

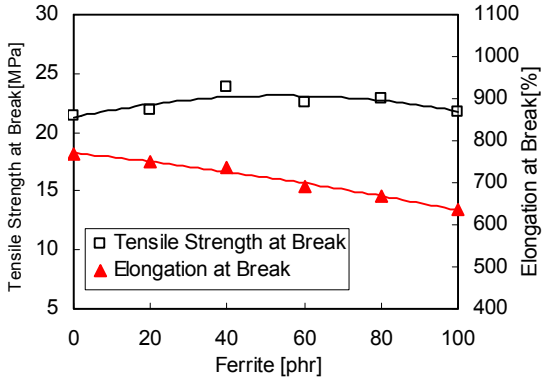

Fig. 3. **Influence of ferrite content on tensile strength at break and elongation at break of composites A**

As seen in Fig. 4, the elongation at break exhibits non-linear increasing tendency with increasing of ferrite content in fillers combinations in vulcanizates B. In case of sample filled with 85 phr of magnetic filler there was observed nearly 165 % increase of elongation at break in comparison with elongation at break value of sample with equivalent content of carbon black. In contrast to vulcanizates A, the tensile strength of vulcanizates B also increases in the whole examined ferrite concentration range. There was possible to see the decline of moduli with increasing of ferrite weight fraction in vulcanizates filled with fillers combinations.

The magnetic characteristics, namely the remanent magnetic induction B_r, the maximum magnetic induction B_m and the maximum magnetic polarization J_m show significant non-linear increasing tendency with increasing of ferrite content in vulcanizates A as well as with increasing of ferrite content in fillers combinations in vulcanizates B (Fig. 5, 6).

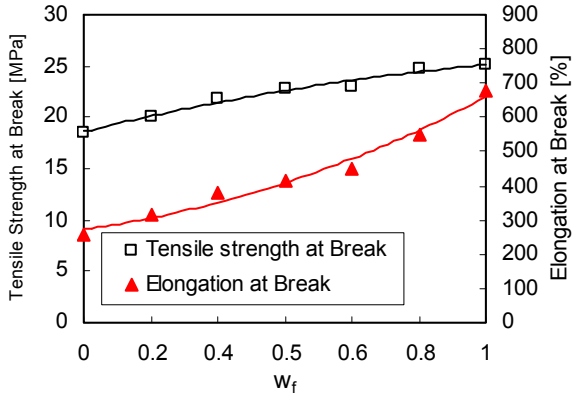

Fig. 4. **Influence of ferrite weight fraction w_f on tensile strength at break and elongation at break of composites B**

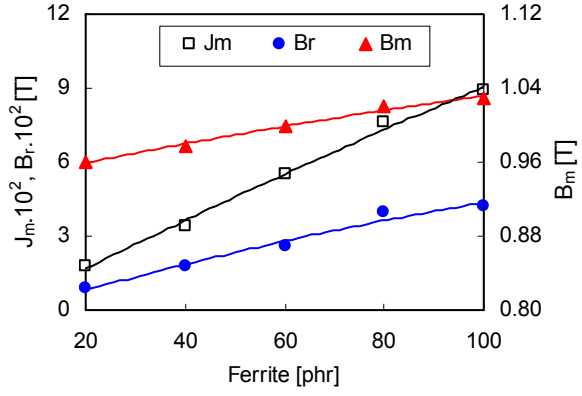

Fig. 5. **Influence of ferrite content on remanent magnetic induction B_r maximum magnetic induction B_m and maximum magnetic polarization J_m of composites A**

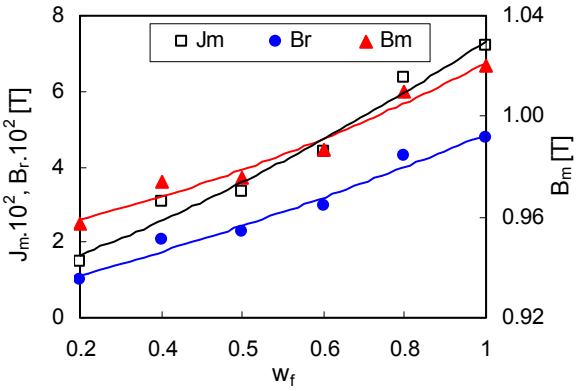

Fig. 6. **Influence of ferrite weight fraction on remanent magnetic induction B_r, maximum magnetic induction B_m and maximum magnetic polarization J_m of composites B**

The results achieved by the study point out the possibilities of preparation of elastomeric magnetic composites by the progresses generally used in rubber technologies. The prepared materials have suitable magnetic and elastic properties.

This work was supported by grant agency VEGA, project No.1/0575/09.

REFERENCES

1. Paul K. B.: Physica B *388*, 337 (2007).
2. Bellušova D., Alshuth T., Schuster R. H., Myndyk M., Šepelak V., Hudec I.: KGK, Kautsch. Gummi Kunstst. *61*, 118 (2008).

CL-17

PREDICTION OF FILLER LOCALIZATION IN HETEROGENEOUS PHASES OF RUBBER BLENDS

H. H. LE[a]*, K. OSSWALD[b], S. ILISCH[a], and H.-J. RADUSCH[a]

[a] *Center of Engineering Sciences, Martin Luther University Halle-Wittenberg, D-06099 Halle (Saale),* [b] *University of Applied Sciences, D-06217 Merseburg, Germany*
hai.le.hong@iw.uni-halle.de

Abstract

For rubber compounds and blends, carbon black (CB) and silica are the most widely used fillers in the rubber industry to improve the static and dynamic mechanical properties like, modulus, tear strength, abrasion, and fatigue resistance. In the past years works were conducted to characterize the phase selective filler distribution and related mechanical properties of filled rubber blends[1]. The preferred localization of the filler is actually governed by thermodynamics as soon as rheological effects do not play a significant role. In the present paper we propose a model for a quantitative prediction of the filler distribution in rubber blends at a thermodynamic equilibrium state. Using this model the physical background

of the filler distribution under influence of the addition of curing additives and coupling agent will be discussed.

Model and experimental

The filler fraction $\varphi_{B\text{-}F}/\varphi$ in the phase B can be calculated as followed:

$$\frac{\varphi_{B-F}}{\varphi} = \frac{\omega}{\omega+1}100\% \quad \text{with} \quad \omega = \left(\frac{\gamma_A + \gamma_F - 2\sqrt{\gamma_A \gamma_F}}{\gamma_B + \gamma_F - 2\sqrt{\gamma_B \gamma_F}} \right)^2$$

and $\varphi = \varphi_{A-F} + \varphi_{B-F}$

where $\varphi_{B\text{-}F}$ is the part of the filler *F* in the phase *B* and φ is the total weight of filler in the blend A/B. γ_A, γ_B and g_F are the surface tensions of the phase *A, B* and *F*, respectively.

The dependence of filler loading in the NR phase $\varphi_{NR\text{-}F}/\varphi$on γ_F shows different behaviour in three ranges I, II and III (Fig. 1). In the range I, at low filler surface tension far away from γ_{NR} an even distribution of filler is nearly received because filler shows similar bad affinity to both blend phases. With increasing γ_F the filler fraction $\varphi_{NR\text{-}F}/\varphi$ in NR phase increases and reaches 100% when $\gamma_F = \gamma_{NR}$. In the range II, passing γ_{NR} the filler fraction $\varphi_{NR\text{-}F}/\varphi$ decreases because the affinity of the filler to NR becomes worse and to NBR better. When $\gamma_F = \gamma_{NBR}$, a complete localization of filler in the NBR phase is obtained. In the range III, with increasing γ_F the filler loading $\varphi_{NR\text{-}F}/\varphi$ increases and approaches the value 50 % (even distribution) at a high filler surface tension far away from that of both blend phases. From the master curve presented above it is obvious to recognize some features. First, a nearly even distribution of filler can be achieved when the filler surface tension is far away from those of both blend phases (similar bad affinity of filler to both phases), or lies in between them (similar good affinity of filler to both phases). Second, a very strong dependence of the filler distribution on the filler surface tension is obtained in the range II. A small change of filler surface tension in this range can lead to an extremely large change in filler distribution. Third, according to the proposed model a localization of the filler at the interphase is not a thermodynamic equilibrium state. It is only a result of an interplay between thermodynamic driving forces and rheological effects.

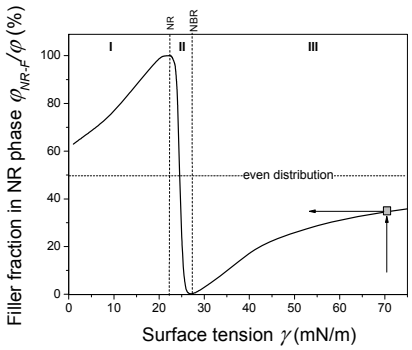

Fig. 1. **Master curve presenting the filler fraction in the NR phase $\varphi_{NR\text{-}F}/\varphi$ in dependence on the surface tension of filler (A = NBR, B = NR and F = silica)**

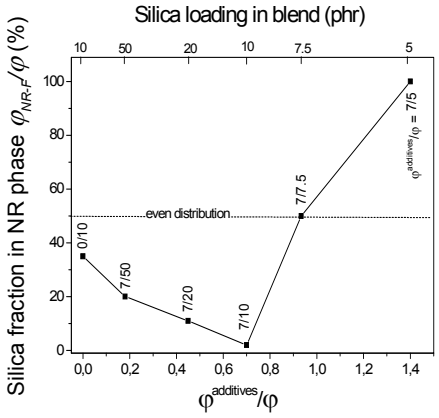

Fig. 2. **Silica fraction in NR phase $\varphi_{NR\text{-}F}/\varphi$ in dependence on the ratio $\varphi^{additives}/\varphi$**

In order to understand the effect of curing additives on the distribution behaviour of silica, NBR/NR blends filled with different silica loading were prepared by keeping constant the loading of curing additives. The silica fraction in NR phase $\varphi_{NR\text{-}F}/\varphi$ of lowly filled blends (silica loading up to 20 phr) was experimentally determined by means of the selective extraction method and of highly filled blends (50 phr silica) using the wetting concept. In Fig. 2 the silica fraction in NR phase $\varphi_{NR\text{-}F}/\varphi$ is presented in dependence on the ratio $\varphi^{additives}/\varphi$ and silica loading. Without curing additives $\varphi_{NR\text{-}F}/\varphi$ = 34 % was determined as discussed above. With increasing ratio $\varphi^{additives}/\varphi$, i.e., with decreasing silica loading the silica fraction $\varphi_{NR\text{-}F}/\varphi$ decreases to zero at $\varphi^{additives}/\varphi$ = 7/10. Passing this value the silica fraction $\varphi_{NR\text{-}F}/\varphi$ strongly increases and reaches a value of 50 % when $\varphi^{additives}/\varphi$ = 7/7.5 and 100 % when $\varphi^{additives}/\varphi$ = 7/5.

The morphological investigation of NBR/NR filled with different silica loading was carried out by AFM and TEM. The images of blends with different ratio $\varphi^{additives}/\varphi$ are presented in Fig. 3 and support very well the silica distribution determined by the selective extraction experiments shown in Fig. 2.

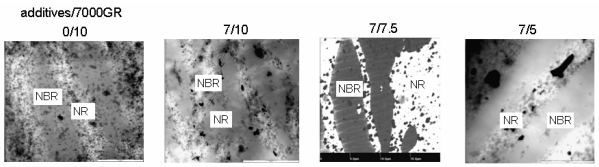

Fig. 3. **TEM and AFM images of blends with different ratio $\varphi^{additives}/\varphi$**

We believe, that this behaviour is related to the fact that the adsorption of curing additives like stearic acid, ZnO and CBS on the surface of silica will make it more hydrophobic. The adsorption of them and its impact on the scorch time and reduction of the crosslink density in silica filled rubber compounds have been frequently characterized. Regarding the effect on the filler distribution with increasing silica loading by keeping constant the additive concentration, the surface of silica will be differently modified, that leads to change of the affinity of silica to the blend phases and consequently to change of silica distribution behaviour.

When fitting the values of silica fraction $\varphi_{NR\text{-}F}/\varphi$ observed from Fig. 2 to the master curve as shown in Fig. 4a the correlation between the ratio $\varphi^{additives}/\varphi$, silica surface tension and the silica distribution becomes obvious. The silica surface tension, which was changed by adsorption of curing additives, can be determined from Fig. 4a and presented in dependence on the ratio $\varphi^{additives}/\varphi$ in Fig. 4b. With increasing ratio $\varphi^{additives}/\varphi$ the silica surface tension decays first strongly and then slowly approaches a level-off value when silica surface is saturated. Thus, the surface tension of saturated silica agglomerates is $\gamma_{additives}$, which is considered as the surface tension of the non-polar part of additives. The decrease of g_F with $\varphi^{additives}/\varphi$ follows an exponential decay function and can be empirically described as followed:

$$\gamma_F(\varphi^{additives}/\varphi) = \gamma_{additives} + (\gamma_F - \gamma_{additives}) \cdot e^{-\frac{\varphi^{additives}/\varphi}{a}}$$

where *a* is a factor describing the effectiveness of additives with respect to the reduction of the filler surface tension. Fitting the above equation to the data presented in Fig. 4b by setting surface tension value of silica γ_F = 73 mN/m for blends without additives, we get:

$$\gamma_F(\varphi^{additives}/\varphi) = 22.4 + 50.6 \cdot e^{-\frac{\varphi^{additives}/\varphi}{0.28}}$$

If silica surface is fully covered by additives a surface tension of 22.4 mN/m is observed. Investigation of the effect of each additive on the silica surface tension was not conducted in the frame of the present work.

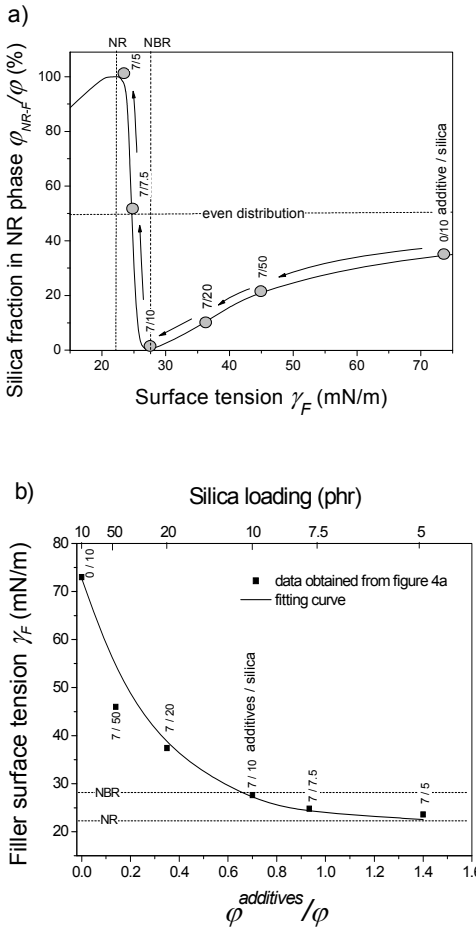

Fig. 4. **Silica fraction in NR phase $\varphi_{NR\text{-}F}/\varphi$ in dependence on the filler surface tension (a), filler surface tension in dependence on the ratio $\varphi^{additives}/\varphi$ and silica loading (b)**

The authors wish to thank the German Research Foundation (DFG) for the financial support of this work.

REFERENCES

1. Le H. H., Ilisch S., Kasaliwal G. R., Radusch H.-J.: Rubber Chem. Technol. *81*, 767 (2008).
2. Le H. H., Ilisch S., Heidenreich D., Wutzler A., Radusch H.-J.: Polymer Comp. *31*, 1701 (2010).

CL-18
EXCELLENT PROPERTIES OF SLOVNAFT′S PETROCHEMICALS IMPACT PP COPOLYMER GRADES PRODUCED BY UNIPOL PP TECHNOLOGY

MARTIN LOVIČ

Slovnaft Petrochemicals, s.r.o., Product and Application Development, Vlčie Hrdlo 4846, 824 12 Bratislava, Slovak Republic
martin.lovic@petchem.sk

Slovnaft Petrochemicals, s.r.o., the member of MOL Group, is producer of polyolefin grades LDPE – registered trademark Bralen and PP homopolymes and ethylene / propylene random and impact (block) copolymers – registered trademark Tatren.

Process of polypropylene production using the Unipol polypropylene gas phase technology provided by DOW Company. The primary reaction in gas-phase Reactor 1 is used for production of homopolymers, random copolymers and the homopolymer segment of impact copolymers. Product properties are controlled by reaction conditions via advanced control computer system. Melt Flow Rate is controlled by adjusting the amount of hydrogen in the cycle gas. Isotacticity is controlled by adjusting the amount of cocatalyst, Internal and External donors.

Impact copolymers are produced in the second fluid gas-phase reactor operating in series with the primary reactor. Homopolymer resin containing active catalyst is transferred from the first reactor to the second where an ethylene/ propylene polymeric mixture is dispersed in the homopolymer base segment. Ethylene incorporation is controlled by adjusting the ethylene content of the cycle gas and partial pressure of propylene and ethylene in Reactor 2. Resin properties do not vary with production rate. The copolymerized part of the material creates rubber phase which is dispersed within PP matrix. Amount and homogenity of dispersion the rubber phase has crucial influence to impact properties of final copolymer grades. Also using twin screw extruder in Unipol PP technology contributes to further improving homogenity of dispersion the rubber phase.

Slovnaft Petrochemicals produces impact copolymers with broad range of MFR (from 6 to 100 g/10 min) with very good balance between the toughness and stiffness. Unipol impact copolymers grades are characterized by high ambient and low temperature impact strength and very good Flexural Modulus. Due to the advantage properties, impact copolymers Tatren have very broad utilization in injection moulding of rigid packaging, storage, medical and transport boxes and containers, household appliances, garden furniture, auto battery cases and other technical items. High MFR of impact copolymers – up to 100 g/10 min provides the possibility to use these copolymers also for high speed thin wall injection moulding products of complicated shapes. Excellent final processing and application properties are multiplied by using of appropriate additives – e.g. antioxidants, nucleating, antistatic agents etc. With new nucleating agents Tatren impact PP copolymers have higher temperature of crystallization – Tc, uniform shrinkage in both direction, better demoulding properties and lower cycle time by injection molding.

Specific of Unipol PP process is possibility to produce the Thermoplastics Polyolefines – TPOs grades with very high rubber content. The process gives the capability to make TPO grades directly in the reactor that in the past could only be produced by past-reactor blending with elastomers. TPOs grade have excellent impact properties, NB at ambient and also at low temperature with Flexural Modulus 900 MPa. Due to excellent impact properties TPOs grades are available for compounding, automotive applications and bumpers.

Unipol PP Technology is available to design production of grades with target properties- tailored according to requirements of market. For example for applications where requirements for Flexural Modulus are higher than we reached with TPOs grades we can offer special grade Tatren IM 25 75 with excellent impact properties at ambient temperature, good at minus temperature as well as with very good stiffness.

Unipol PP Technology also produces control rheology as well as reactor impact copolymer grades with high Melt Flow Rate (up to 120 g/10 min). Advantages of reactor grades are good organoleptic properties, lower Volatile Organic Compounds (especially ketones and other oxygen compounds).

CL-19
COMPUTED TOMOGRAPHY FOR ANALYSIS OF POLYMER COMPONENTS

OLIVER BRUNKE[a] and JENS LÜBBEHÜSEN[b]

[a] GE Sensing & Inspection Technologies GmbH, Niels-Bohr-Str. 7, D-31515 Wunstorf, [b] Jens Lübbehüsen GE Sensing & Inspection Technologies GmbH, Niels-Bohr-Str. 7, D-31515 Wunstorf, Deutschland.
Oliver.Brunke@ge.com, www.phoenix-xray.com, Jens.Lubbehusen@ge.com, www.phoenix-xray.com

Thanks to the knowledge of the 3D microstructure of a specimen by using a high resolution X-ray Computed Tomogaphy (CT) system, it is not only possible to judge the actual state of that specimen, but also predict its characteristics. By means of generating full 3D information with submicron resolution and moving virtually through the inner parts of the object slice by slice, complete new possibilities for analysis are available for research and quality control.

Especially for materials like rubber used in safety relevant applications, CT systems are used more and more often through the complete process of development up to the final quality check of components. With the new nanotom m small objects can be examined with voxel sizes < 300 nm (0.3 μm). Further fields of applications are the analysis of metals, plastic materials and composites, ceramics and much more. Every difference within the specimen with regards to material composition, density or porosity influencing the x-ray absorption can be visualized in the 3D image. This provides exact information about the spatial distribution of different materials, dispersion of additives without destroying the object. In addition defects like cracks, voids or inclusions cannot only be visualized but also their volume can be calculated.

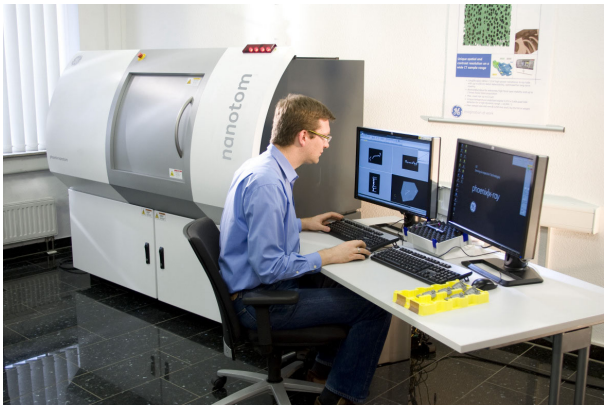

CL-20
A POSSIBILITY OF USING THE FLOTATION PROCESS TO SEPARATE SOLID POLYMERS

JIŘÍ ŠKVARLA*, MARTIN NAGY, and MARTIN SISOL

Institute of Montaneous Sciences and Environmental Protection, Technical University in Košice,
Park Komenského 19, 042 00 Košice, Slovak Republic
jiri.skvarla@tuke.sk

Flotation is a physico-chemical process used traditionally to separate various solid materials, including plastics, basing on a difference in their surface wettability. Unfortunately, the surface of most plastics is hydrophobic which fact makes the selective flotation separation of targeted types of plastics from their mixtures with other types of plastics difficult or even impossible. To render the selectivity of the process itself, the surface of some plastics has to be selectively hydrophilized and so flotationally depressed.

To make the surface of plastics selectively hydrophilic and thus nonfloatable, various methods have been testing such as adsorption of wetting agents[1] or a physical treatment[2,3] (flame, ozonation, plasma, photocatalytic, etc.). However, a potential of selective chemical treatment by incipient alkaline hydrolysis is recently emphasized, as exemplified by analyzing the surface hydrophilization of polyethylene terephthalate (PET) submerged with polyvinylchloride (PVC) in NaOH solutions even at ambient temperature and for a very short period of time[4].

Indeed, the NaOH-pretreated surface of PET foils was found to become hydrophilic (nonfloatable) to such an extent that the flotation recovery and selectivity of PVC foils, whose surface was left almost untouched (and so entirely floatable), increased appreciably[5].

The enhancement of the surface wettability of PET, as measured by contact angle goniometry of water drops, due to the hydrolytic attack is a result of the formation of new hydrophilic groups originating from chain scissions (chemical alteration) as well as of associated dissolution roughening (physical alteration)[6].

At the ambient temperature of pretreatment, a descending sigmoidal dependence between the advancing contact angle on the PET surface and the concentration of NaOH solution was observed, being paralleled with the PET/water interfacial tension-vs-concentration dependence. An increase in the temperature of the pretreatment solution up to the temperature of glass transition (~80 °C for PET) further promotes the hydrophilization process and shifts proportionally the latter dependences. The limiting hydrophilicity θ_a was assessed to occur in 6 % NaOH solution at 60 °C, corresponding to the zero interfacial tension.

The surface roughness and negative charge due to the hydrolytic attack, evaluated by the Atomic Force Microscopy and Streaming Current method, respectively, attain a maximum when pretreated in the NaOH solution whose concentration is exactly the same as that for which the above dependences go through their inflection. This is thought to confirm a general parallelism between the interfacial free energy and the dissolution kinetics.

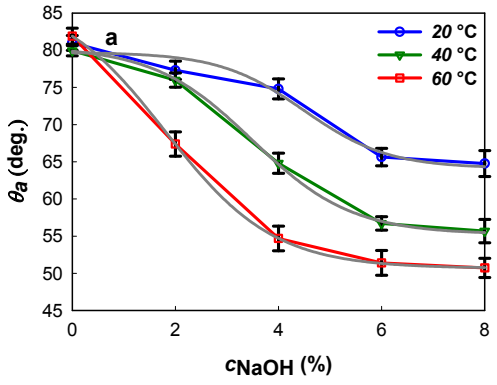

Scheme 1. **Advancing contact angle θ_a of water drops on PET foils as a function of concentration and temperature of the NaOH pretreatment solution**

This contribution is the result of the project implementation Research excellence centre on earth sources, extraction and treatment supported by the Research & Development Operational Programme funded by the ERDF.

REFERENCES

1. Pongstabodee S., Kunachitpimol N., Damronglerd S.: Waste Manag. *28*, 475 (2008).
2. Pascoe R. D., O´Connell B.: Waste Manag. *23*, 845 (2003).
3. Okuda T., Kurose K., Nishijima W., Okada M.: Ozone: Sci. Eng. *29*, 373 (2007).
4. Drelich J., Payne T., Kim J. H., Miller J. D.: Polymer Eng. Sci. *38*, 1378 (1998).
5. Sisol M.: *PhD thesis*, 103 p. Technical University in Košice 2006.
6. Škvarla J., Luxbacher T., Nagy M., Sisol M.: ACS Appl. Mater. Interfaces *2*, 2116 (2010).

CL-21
GENERAL PRINCIPLES OF OPERATION AND CLEANING OF VULCANIZATION MOULDS

KAROL NICIŃSKI* and DARIUSZ M. BIELINSKI

Institute of Polymer Materials & Dyes in Torun, Branch House of Elastomers & Rubber Technology, Harcerska 30, 05-820 Piastów, Poland
k.nicinski@ipgum.pl

It is a well-known fact, mould fouling occurs during vulcanization, what have negative influence on apperance and dimention stability of moulded parts, and also makes manufacturing costs higher[1].

On the basis of conducted analysis hypothesis was accepted, that mould fouling has two stages. In the first stage, insoluble zinc sulphide is formed in the reaction of zinc oxide with sulphur, which makes inorganic deposites on the mould surface. In the second stage, on ZnS crystallites sediment low-

molecular organic ingredients of rubber compound, which carbonize with time[2,3].

Contamination of vulcanizing mould can be observed as change of colour of its whole surface or deposition of the material in some places of the mould surface[4].

The speed of mould fouling depends on various factors. Most important of them are: composition of rubber mix, use of anti-adhesive agents, shape and construction of the moud, vulcanization parameters (temperature, pressure) and different reactions between ingredients of rubber compound[5].

There are several methods which reduce mould fouling and allow to remove easy an end-product. One can mention among them the use of releasing agents:

– internal – added to a rubber compounds,
– external – modifying the surface of a mould (sacrificial, semi-permanent, permanent). All of them will be shortly described[6–8].

Correctly used anti-adhesive agents reduce or even eliminate problem of mould fouling. However, inappropriate selection can generate problems[9].

In Branch House of Elastomers & Rubber Technology an investigations over treatment of mould surface by ion bombardment were made[10]. Due to ion bombardment of metal parts of machines and devices used for compounding, processing or vulcanization of rubber mix, their durability significantly increased. The treatment, preferably of Cr^+ with energy 20–500 keV in $2 \cdot 10^{17}$ cm^{-2} i $5 \cdot 10^{16}$ cm^{-2} dosage carried out under vacuum, makes possible to get rid of the problem arising from adhesion of rubber of its components to metal surface.

Unfortunately, mould fouling occurs sooner or later. Short information about now used methods of cleaning of vulcanization moulds and their efficiency will also be presented[11–15].

REFERENCES

1. Cieślak R., Olszewski J., Pabiś L., Guma – Poradnik Inżyniera i Technika, Wydawnictwa Naukowo-Techniczne, Warszawa 1981, rozdz. 6, str. 553
2. Van Baarle B.: Rubber World *225*, 34 (2001).
3. Van Baarle B.: Rubber World *231*, 25 (2004).
4. McDuff K.: RAPRA Bulletin *6*, 130 (1969).
5. Sommer J. G., Grover H. N., Suman P. T.: Rubber Chem. Technol. *49*, 1129 (1976).
6. www.struktol.de
7. Martin D. L., Hillman S. J.: Rubber World *208*, 32 (1993).
8. Commercial information NEDOX – nedox.com
9. Glanville L. M.: *Injection Molding of Elastomers*, (Penn W. S., ed.), rozdz. 10, p. 129. Gordon & Breach Science Publ., New York 1969.
10. Bieliński D., Pankiewicz D., Ostaszewska U., Machnowski G.: *Sprawozdanie z działalności statutowej Instytutu IMPiB* „Obróbka powierzchni gniazd i elementów roboczych form wulkanizacyjnych metodą bombardowania jonowego w celu poprawy ich trwałości i parametrów eksploatacyjnych” , 2007.
11. Golubski M. A.: Rubber World *213*, 18 (1995).
12. Young F. C.: Rubber World *227*, 39 (2002). www.cryonomic.com
13. Young F.: *State-of-the-art in CO2 blast tire mould cleaning, new nozzles, new techniques, new automation*, Akron, Ohio USA - www.emeraldinsight.com (2000).
14. Philips Electrical Industries, LTD GB 929 998, 1963.
15. Jetter J.: Tire Technol. Int. Annual Rev. *2002*, 136; www.jetlaser.de

CL-22
VISUALIZATION OF THE WEAR TEST OF RUBBER MATERIALS

VLADIMIR PATA, DAVID MANAS, MIROSLAV MANAS, and MICHAL STANEK

Thomas Bata UniversityInstitute, Faculty of Technolog,Department of Production Engineering,TGM 272, 762 72 Zlín, Czech Republic
pata@ft.utb.cz

Abstract

The article describes the problem of dual shooting and evaluation of high-speed time varying phenomena using high-speed camera systems. It describes necessary steps for the preparation of shooting and how to set up the electronic shutter and also focuses on the processes of calibration and final evaluation of the high-speed phenomena. Dual shooting of high-speed phenomena is very modern while still remaining quite an unexplored field and is at present subject of a research at the Institute of Production Engineering ÚTB in Zlín. The published processes particularly for the Chip-Chunk test are brand new and at currently being patented in the Czech republic.

Introduction

High-speed camera systems (hereafter referred to as HSC) are well-known not only for the scientific community but also for people from the technical field. Their use has at present been extended from special applications in the military and automobile industry to the common technical practice.

The requirements to improve production process, lower costs and increase safety are continuously growing and HSC has a lot to offer in this respect. Using the high recording frequency they enable to examine the given phenomenon, stop the image in a set moment and then examine it as well as detecting the problematic sections.

If we want to do this all, we first need to define the concept “speed, high-speed phenomena”. They are such phenomena for the recording of which it is necessary to use the recording frequency ranging from 100 Hz to 1 000 000 Hz. We also need to specify the type of phenomena. In practice they are periodic, aperiodic and stochastic phenomena, for which it is necessary to determine the time and length of shooting.

Next, we have to consider the type of a HSC. At present there is a number of producers of HSC, which, however, have different configurations. It is also worth noting that the market has recently introduced digital cameras with higher speed of

recording. The recording speeds range up to 100 Hz, which enable to make only very basic evaluations. In the case of professional devices we can distinguish between two basic types: It is a compact type, with a display and most control elements are integrated in the HSC and next, a modular type consisting of a number of modules and peripherals enabling the user to make a recording and evaluation according to the given requirements. The compact systems are more economical, but they are very easy in terms of their operation, setting and evaluation. The modular systems can be adjusted exactly to our requirements with the aid of connectable peripherals and methods of shooting but the setting and evaluation are rather complicated, the price very high.

When shooting with the HSC there are often problems with an insufficient angle of view, which is needed to capture the phenomenon. Common lenses working at angles up to 60° are often not capable to capture the scene shot, on the contrary, the wide-angle lens and special lens, such as Fish Eye, which have the angle of view over 180° can capture the scene but with a subsequent image distortion. Hence, there are two high-speed camera systems used in practice which shoot the parallel phenomena. The two high-speed camera systems are used for parallel shooting of phenomena, which would be difficult or impossible to repeat, with lenses with the angles of view up to 60°.

The result of such shooting of one or more phenomena using a set of two camera systems are two films of the same phenomenon, or phenomena from different angles of view according to the position of lenses of the cameras.

The disadvantage is that so far no method has been developed that would combine these separate films, giving a more complex idea about the phenomenon processed. This combination can only be made subjectively in the minds of the viewers watching the films but it is clear that this way of putting images of the two films together may not be precise and sufficiently predicable. So far this process has not been objectivized.

Visualization of the time varying phenomena

This deficiency of the present state of technology can be made up by a method of visualization of the time varying phenomena. The principle of this method is that the images created by shooting a phenomenon with a set of two camera systems (see Fig.1) are put together at a given time into one dual image according to a characteristic trait of the image, such as a characteristic point, edge or angle.

Practical method of visualization

The example of a practical method of visualization of time varying phenomena is shooting a phenomenon, which takes place during the wear test of rubber materials (referred to as Chip-Chunk test), see Fig. 2 during which a rubber sample of cylindrical shape is penetrated by a pointed tool with defined geometry, see Fig. 3.

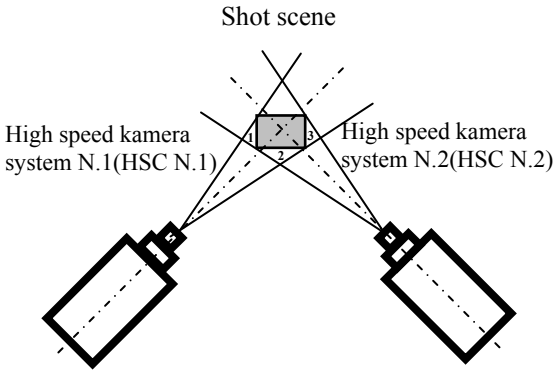

Fig. 1. **Configuration of high-speed camera systems**

A dual image can be created very fast and enables to immediately detect different behaviour of the left and right edges of the sample at the moment of penetration of the test tool, depth of the penetration of the tool inside the sample, speed of revolution of the sample, size and speed of the chipped parts of the rubber test sample, speed of the ceramic tool, etc. (which is one of the main requirements in practice), see Fig. 4.

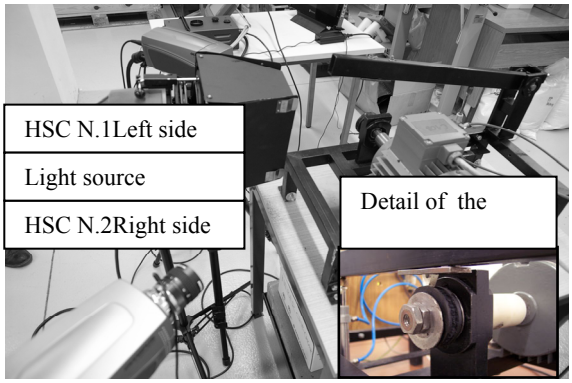

Fig. 2. **Practical configuration of high-speed camera systems with axes of lenses 90°**

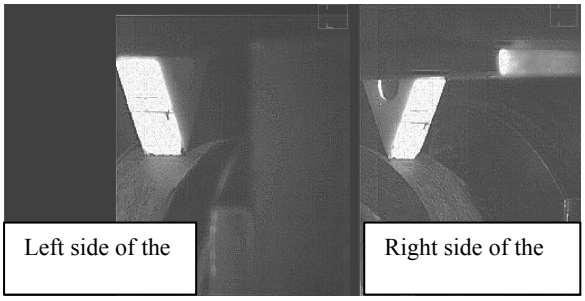

Fig. 3. **Right and right side of the rubber sample obtained from high-speed camera systems**

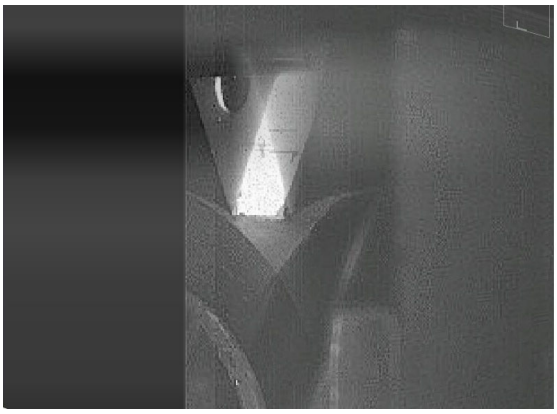

Fig. 4. **Final dual image**

Conclusion

Dual images give us a very precise idea of the limit positions at different time intervals and if the images are arranged in a given time sequence it is possible to demonstrate a visualized dual phenomenon as a filmed scene.

This article is financially supported by the Czech Ministry of Education, Youth and Sports in the R&D project under the title 'Modelling and Control of Processing Procedures of Natural and Synthetic Polymers', No. MSM 7088352102 and 'CEBIA Tech', No. CZ.1.05/2.1.00/03.0089.

REFERENCES

1. Manas D., Manas M., Stanek M., Pata V.: Arch. Mater. Sci. *28*, 81 (2007).
2. Manas D., Stanek M., Manas M., Pata V., Javorik J.: KGK, Kautsch. Gummi Kunstst. *62*, 240 (2009).
3. Manas D., Manas M., Stanek M., Zaludek M., Sanda S., Javorik J., Pata V.: Chem. Listy *103*, 72 (2009).
4. Manas D., Manas M., Stanek M., Pata V.: *International Rubber Conference – IRC 2008*, 20 – 23.10.2008, Kuala Lumpur, Malaysia, p.37–48, CD.
5. Manas D., Pata V., Manas M., Stanek M.: *8th Fall Rubber Colloquium 2008, 26 – 28.11.2008, Hannover, Germany, p.93-94 + CD Proceedings.*

CL-23
MASS SPECTROMETRIC ANALYSIS OF POLYMERIC ADDITIVES IN POLYMER EXTRACTS BY PYROLYSIS-GC-MS

FRANKY PUYPE and JIŘÍ SAMSONEK

Institute for Testing and Certification – Zlín, testing division – laboratory of analytical chemistry, třida T. Bati 299,764 21 Zlín-Louky, Czech Republic
fpuype@itczlin.cz

Introduction

A new trend in polymer additive chemistry is the increasing use of polymeric additives. Mainly in the field of polymeric antioxidants, stabilisers or polymeric flame retardants new polymeric additives are coming up. Polymeric additives have the big advantage to make the final product blooming free and the additives are available all over the polymer. Polymeric additives give nearly no emissions, no migration loss and allow higher application temperatures.

The analysis of polymer additives and application of classical gas chromatography is restricted due to low volatility and high molecular weight of some species. Reliable and rapid analytical methods are often needed for the identification of unknown additives, therefore a best available solution need to be developed. For polymeric additives soft ionization methods like fast atom bombardment (FAB)[1] and matrix-assisted laser desoption/ionization (MALDI)[2] are relatively easy and have the ability to analyze high molecular weight compounds, however these methods have limitations. Concerning polymeric additives, soft ionization methods give no clear structural information. The use of a time-of-flight mass spectrometer (TOF-MS) can give a molecular weight distribution of majorities (which means polymer) but under a concentration of 5 % of additives, it is a difficult task to give proper information of the additive, unless extracted[3].

The main focus stays on difficulties concerning volatility, separation and detection, therfore pyrolysis as sample introduction system was evaluated for characterization of some polymeric additives. Pyrolysis as an injection technique coupled to classical gas chromatography with mass detection (PY-GC-MS) makes firstly fragments from the polymeric additive fraction, which are separated by classical gas chromatography and easily detectable by mass spectrometry. This method can be applied if we are interested into the structure of compounds and not primary in the molecular weight.

Sampling and analysis

This method is based on separation of the polymeric additives from the polymer matrix by a simple static extraction in toluene. Only a few µl of extract was dried and taken to pyrolysis. The principle of pyrolysis is based on radical reactions induced by heat in an inert atmosphere. These radical reactions continue as radical depolymerization raction (also called unzipping or back-to-monomer) and might induce a H-transfer between molecules (inter- and intramoleculair proton transfer). Pyrolysis fragments are mainly volatiles with molecular weight < 1000 Da and are swept into the analytical column for separation. Mass spectrometry is used for the detection and identification of the fragments.

The ions detected by the mass spectrometer at a certain retention time are very specific for one part of the polymeric additive. The obtained chromatogram (further pyrogram) is often based on a large number of peaks, however, if certain ions are known, the method can be automatizted to judge if selected additives are presented or not[4].

Additives with a molecular weight between 900 – 1500 Da have the intention to evaporate partly and pyrolyze slowly. Higher masses (the not volatile ones) degradate according to the pyrolytic fragmentation rules in the furnace. It is expected that there are more than one additive in the extract. Different additives are needed to modify the polymer properties. The additive fraction lower than 900 Da (e.g. Irga-

fos 168, Irganox 1076) is also screened by this method.

All experiments were carried out with an automated pyrolyzer unit (Frontier Laboratories ltd. − Kyoto, Japan) coupled to a GC-MS 2010+ (Shimadzu − Kyoto, Japan) with electron impact ionization mode (70eV). The method was optimized, evaluated and proved to be free from memory effects. The optimal pyrolysis temperature was set to 650 ºC and the sample extracts were injected by a quick free fall injection of special sample cups. By measurement of sample blanks special attention was taken to assure a clean sample path and avoiding adsorption or condensation of fragments along the sample path.

Polymeric brominated flame retardants

Pyrolysis-GC-MS was evaluated for the characterization of polymeric brominated flame retardants (p-BFR). For this the p-BFR needs to be isolated from the polymer matrix. Bromine used as a flame retardant has a long tradition as polymer additive. A recent environmental friendly approach is based on the incorporation of bromine into the polymeric chain (like tetrabromobisphenol A in PC or epoxy resins) or as a polymeric additive (like brominated polystyrene in PET). P-BFRs are mainly used for high-temperature applications like polyesters and polyamides. Flame retardant treated thermoplastics contain generally 5–20 % p-BFR which is for this analytical method an advantage. Most common brominated polystyrenes are produced by the copolymerization of di- and tribromostyrene and are commercialy available (Firemaster PBS-64, Saytex HP-7010P). Poly(dibromostyrene), known as PDBS-80, is also commonly used however only for polyester applications[5,6].

From the legislative point of view, some additive BFRs are restricted to be used. In order to speciate the bromine containing molecule, PY-GC-MS is able to fill this gap in BFR characterization. Here counts the slogan ``no data = no market``, sometimes data is missing concerning additive composition[7].

In Fig. 1 is shown a pyrogram of isolated brominated polystyrene from PA6. Main peaks seen in this pyrogram are the isomers from mono-, di-, tri- and tetra-bromostyrene formed after depolymerization. Further a mixture of cyclic side-products from radical recombination can be seen, mainly brominated polycyclic aromates and cyclic hydrocarbons.

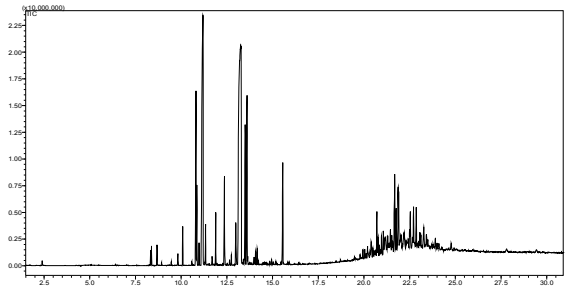

Fig. 1. **Pyrogram of isolated brominated polystyrene from a PA6 sample**

The area ratios between the mono-, di-, tri- and tetra-bromostyrene were used to calculate the degree of bromination in this polymeric additive according the equation given in Fig. 2. The measured brominated polystyrene had a calculated number-average bromine degree of 2,7 (2 % RSD, n=3). Technical data from a supplier confirmed that the p-BFR had an average bromination degree of 2,7 (ref.[8]). Very good match!

$$Bn = \frac{\sum_{\infty}(Bi.Ai)}{\sum_{\infty} Ai}$$

Fig. 2. **Equation used for calculation of number-average bromination degree in brominated polystyrene (B_n).** Where: $\underline{B_i}$ means number of bromine atoms (here used e.i. 1, 2, 3 and 4) $\underline{A_i}$ (peak area) means certain amount of brominated styrene monomer containing the same amount of bromine atoms i

Polymeric hindered amine light stabilizers

Polymeric steric hindered amine light stabilizers (p-HALS) are improving heat and light stability in thin film polyolefins. The average molecular weight of these p-HALS are ranging from 2000 till 4000 Da. They are added to the polymer in a range of 0,1 till 2 % and appear sometimes mixed with other p-HALS. The importance of detecting p-HALS is mainly based on the need for completing documentation and for quality control/quality assurance purpose.

After extraction and analyzing a LDPE sample containing the commercial p-HALS UVINUL 5050H from BASF (Fig. 3), there were seen 2 regions in the pyrogram (Fig. 4).

The first region exist mainly of linear (saturated and unsaturated) hydrocarbons (C_9–C_{24}) with some higher peaks from 2,2,6,6-tetramethylpiperid-4-yl derivates after unzipping of the monoamid side of this monomer (shown with an asterisk). In the second region are nicely seen the distribution of the monomer in its whole. The appearance of the monomer is in analytical pyrolysis no surprise as depolymerization is one of the main processes.

Mass spectrometry is playing a major role for the interpretation of the results. As shown in Fig. 5, by using a selective scan for ion 57 M/z, all hydrocarbon fractions can been taken out and the theoretical C_{17}–C_{21} distribution is appearing more in detail. The maximum of the hydrocarbon distribution is approximately at C_{19}, which is also given in the technical data.

A scan of ions with masses in the monomer range (M/z 500−700) shows nicely the distribution of the monomer (Fig. 6).

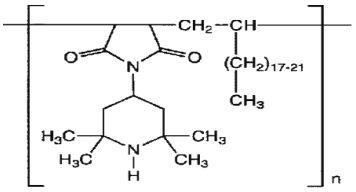

Fig. 3. **UVINUL 5050 (BASF)[9]**

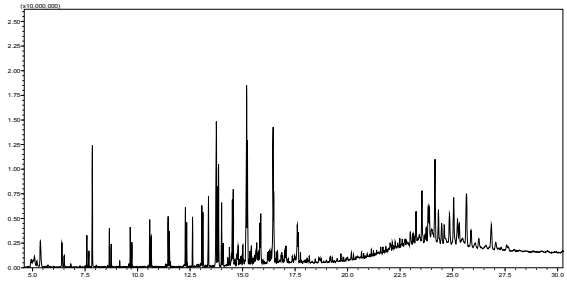

Fig. 4. **Full scan pyrogram of Uvinul 5050H in LDPE**

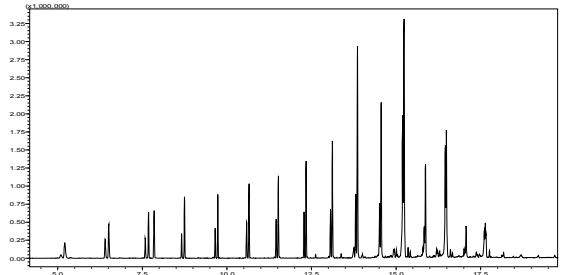

Fig. 5. **Scan for hydrocarbon distribution (M/z 57) in the first region of Uvinul 5050H in LDPE**

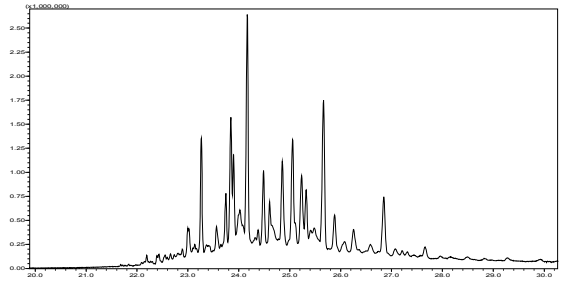

Fig. 6. **Scan for monomer distribution (M/z 500-700) in the second region of Uvinul 5050H in LDPE**

Polymeric hindered amine light stabilizers in a mixture

The depolymerization mechanism of p-HALS is a practical mechanism for identification by monomer composition. The condensed types of p-HALS like the poly(4-hydroxy-2,2,6,6-tetramethyl-1-piperidine-ethanol–alt-1,4-butanedioic acid, further called light stabilizer 622 (Fig. 7) will difficult decompose to monomers.

Due to advantages related to mass spectrometry, these fragments can be fully identified and selected as typical fragmentations for a certain polymeric additive. By use of a spectral database containing reference additives made in-house, mixtures of additives can be detected according to their retention time and mass spectra. Complex mixtures like commercial TINUVIN 783, which is a synergistic mixture of light stabilizer 944 and light stabilizer 622 can be identified using reference pyrograms from both compounds.

For light stabilizer 944 there can be taken one major characteristic peak which is the monomer peak at retention time 24,9 minutes (Fig. 9) with a typical fragmentation ion at

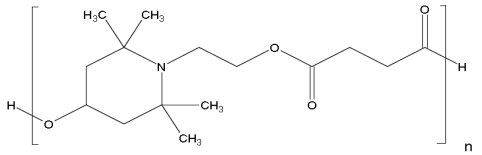

Fig. 7. **Poly(4-hydroxy-2,2,6,6-tetramethyl-1-piperidine ethanol – alt-1,4-butanedioic acid, light stabilizer 622 (ref.[10])**

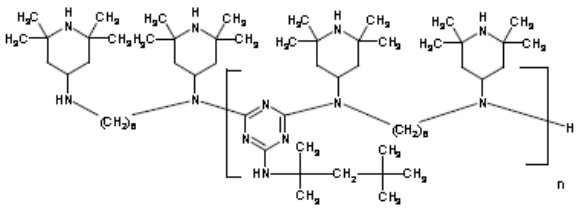

Fig. 8. ***N,N'*-Bis(2,2,6,6-tetramethyl-4-piperidinyl)-1,6-hexanediamine polymer with 2,4,6-trichloro-1,3,5-triazine reaction products with 2,4,4-trimethyl-2-pentanamine , light stabilizer 944 (ref.[11])**

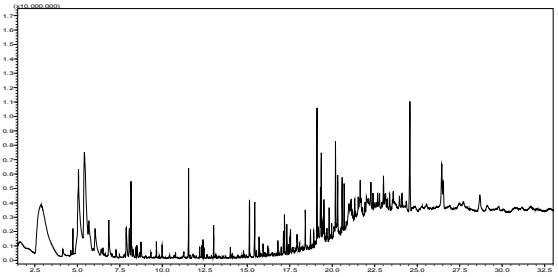

Fig. 9. **Full scan pyrogram of light stabilizer 944**

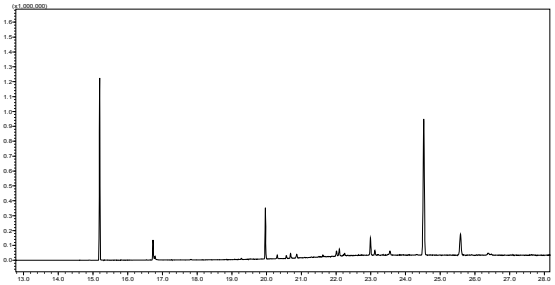

Fig. 10. **Single ion monitoring pyrogram of light stabilizer Tinuvin 783 with selected reference peaks (containing p-HALS light stabilizer 622 and p-HALS light stabilizer 944)**

460 M/z. The light stabilizer 944 is also presented in Tinuvin 783 as shown in Fig. 10, but here are already single ions selected for light stabilizer 944 and light stabilizer 622. Some information is lost but the main conclusion stays, the target analytes are detected and the "noice" from all other fragmentations are reduced.

Conclusion

PY-GC-MS seems to be a useful tool for polymeric additive characterization. Each polymeric additive has its own decomposition mechanism with possibility to get very specific information about the structure. A comparison with reference standards is recommended as well as automatisation of data processing by measuring selected ions.

The extraction procedure seems to give a satisfying sensitivity and suppresses the background sufficiently to make proper conclusions.

The main drawback of PY-GC-MS is that there is no molecular mass detectable; it is up to the customer to decide what is more important, structural information or an average mol weight distribution of used additives.

REFERENCES

1. Juo C. G., Chen S. W., Her G. R.: Anal. Chimica Acta *311*, 153 (1995).
2. Draft international standard ISO/DIS 10927 (2009-09-30).
3. Raquel Rial-Otero, Marco Galesio, Jose-luis Capelo, Jesus Simal-Gandara: Chromatographia *70*, 339 (2009).
4. Puype F., Samsonek J.: Chem. Listy 126 (2009).
5. Gouteux B.: Env. Sci. Technol. *42*, 9039 (2008).
6. Wang F. Cheng-Yu: Anal. Chem. *71*, 2037 (1999).
7. Kemmlein S., Herzke D., Law R. J.: J. Chrom., A (2008).
8. Albemarle corporation, Saytex HP-7010P technical data sheet (2003).
9. BASF, Uvinul 5050H technical data sheet (1996).
10. CIBA, Product range overview, No. 016530.00.040 (2004).
11. CIBA, CHIMMASORB, technical data sheet.

CL-24
REINFORCEMENT OF RECYCLED BUMPER MATERIAL WITH WOOD FIBERS: STRUCTURE DEFORMATION MECHANISMS, PROPERTIES

G. KELEDI[a,b], A. SUDÁR[a,b], C. BURGSTALLER[c], K. RENNER[a,b], and B. PUKÁNSZKY[a,b]

[a] *Laboratory of Plastics and Rubber Technology, Budapest University of Technology, 1521 Budapest, P.O.Box 91, Hungary,* [b] *Institute of Materials and Environmental Chemistry, Hungarian Academy of Sciences, 1525 Budapest, P.O.Box 17, Hungary,* [c] *Transfercenter for Plastics Technology, Upper Austrian Research GmbH, Wels, Austria*
krenner@mail.bme.hu

Recently the production and application of thermoplastics reinforced with forest-derived fibers increased considerably. The application of wood fibers in polymer composites has several advantages: the fibers are obtained from natural resources, they are available in various forms in large quantities, they are light, cheap, and can be added to commodity matrices in considerable amounts. As plastics contribute to the amount of solid waste in increasing volumes, waste utilization has become an attractive alternative to disposal. Today the main application of recycled car bumpers is the production of new bumpers, but the reinforcement of this material with wood fibers could open up new possibilities for the automotive industry and be a solution for an environmentally friendly, high quality and cheap material. Since such a composite consists of at least four components, its structure can be quite complicated. The elastomer added for impact modification and the reinforcement can be distributed in the matrix separately from each other, but the elastomer may also encapsulate the filler. The properties of the resulting composite depend very much on the extent of encapsulation. Stiffness was shown to depend mainly on embedding, while impact resistance was influenced also by other factors[1]. The extent of encapsulation depends on the relative magnitude of adhesion and shear forces acting during homogenization and processing[2]. Since interactions are relatively weak, while the particle size of the reinforcement is quite large, mostly separate distribution of the components is expected in PP/elastomer/wood composites. Structure can be and often must be controlled by the addition of functionnalized components, like MAPP or MAEPDM. However, changing composition and structure modifies the mechanism of deformation, the extent of reinforcement and final properties. In this study composites modeling wood reinforced bumper material as well as actual recycled bumper regrind/wood composites were prepared and studied in detail. Filler content was varied in a wide range. Structure and interfacial adhesion was modified with the use of different functionalized polymers. Mechanical characteristics were studied on injection molded parts by tensile testing and by the measurement of impact resistance. The structure of the composites was analyzed by SEM and model calculations. Deformation mechanism was studied with the help of acoustic emission and volume strain measurements. A wide variety of deformation mechanisms and behaviors were found as composition, interactions and structure changed

REFERENCES

1. Molnár Sz. et al. : Polymer *41*, 1529 (2000).
2. Pukánszky B. et al. : Polym. Compos. *11*, 98 (1990).

CL-25
EU TIRE LEGISLATION - HOW SSBR HELPS TO MEET THE CHALLENGE

SVEN K. H. THIELE, JOACHIM KIESEKAMP, and SASCHA RULHOFF

Styron Deutschland GmbH, PF 1265, D 06202 Merseburg, Germany
srulhoff@styron.com

The Kyoto Protocol as the first globally agreed contract on reducing greenhouse gas emissions requires industrialized

nations to reduce their CO_2- emissions significantly already in near future. In general, Transportation is contributing about 26 % of the overall anthropogenic CO_2 emissions in the EU (Michelin Fact book 2008) and 18 % can be directly correlated to road transport. Thus, tire rolling resistance reflects 4 % of the overall emissions and is a significant contributor to fulfilling the global requirements.

The improvement of the CO_2 balance in Transportation was clearly correlated to tire design and put forward to the tire industry by several legislators worldwide. Tire manufacturers in the European Union are facing challenging target limits required by legislation taking effect as of 2012. The European Regulation (EC) No 443/2009 from 2009 is setting emission performance standards for new passenger cars as part of the Community's integrated approach to reduce CO_2 emissions from light-duty vehicles. Additionally as of 2012 all tires marketed in the European Union will be rated concerning type-approval requirements based on Regulation (EC) No 661/2009 and labelled regarding Regulation No 1222/2009 (Fig. 1) with respect to fuel efficiency, wet grip and external noise.

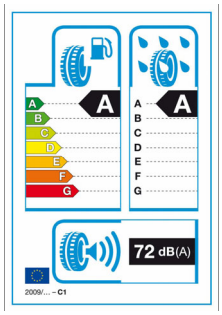

Fig. 1. **Tire label EU (Regulation No 1222/2009)**

As of 2012 the label will increase the level of consumer information on tires regarding wet grip and environmental aspects and increase market transparency. As 2014 tires not meeting the requirements will not be allowed to be sold in the EU. This trend is not limited to Europe. Several countries as Japan, Korea, Canada or US have already or are planning to implement similar schemes.

Major performance targets of tire treads as rolling resistance, wet grip and wear are inversely correlated to each other. The reduction of fuel consumption must be achieved at the expense of neither safety (wet grip) nor wear (Abrasion resistance).

A major contribution to decreasing rolling resistance and optimizing heat built up of tire tread comes from limiting hysteric energy loss and improving filler distribution. A major part of passenger car tread compound is SSBR. The next generation of functionalized SSBR enhances the interaction of polymer chain ends with fillers as silica or carbon black. As shown in Fig. 3 the new functionalization technology leads to an overall expansion of the magic triangle without loosing performance in any of the three categories. Beside DIN abrasion, tan δ 0 °C is reflecting wet grip performance and the rolling resistance is indicated by tan δ 60 °C. As an example the new generation of chain end modified SSBR grades, e.g. Sprintan® SLR 4602-Schkopau, enable in a silica compound (80 phr) a significant improvement of 28 % in tan d 60 °C, enhanced DIN abrasion and heat build up, while maintaining wet grip characteristics.

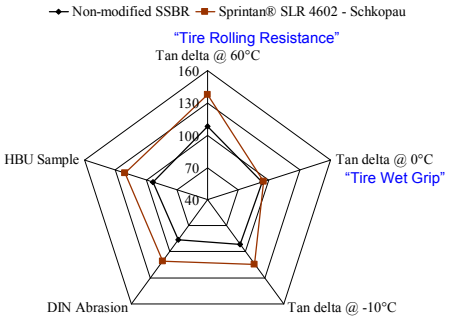

Fig. 3. **Comparison of a non modified SSBR**

In general, improving polymer-filler interaction is leading to increased compound viscosity levels, which could impose limitations regarding compounding or output characteristics depending on mixing and extrusion equipment. However, diverse processing aids could be applied to reduce compound viscosity and assist filler distribution, but these changes may affect compound performance as well as add undesired raw material cost.

In a comparable silica formulation the newest generation of functionalization technology developed by Styron Synthetic Rubber results in enhanced processing index and additional performance regarding rolling resistance and wet grip.

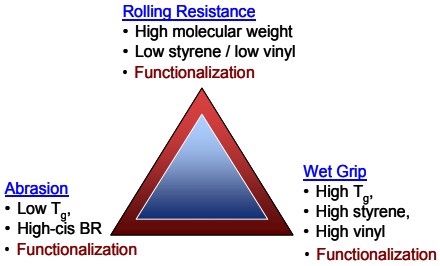

Fig. 2. **Magic triangle for performance characteristics in tread compounds**

CL-26
STUDY OF THERMOELASTIC PROPERTIES OF ACRYLATE COMPOSITES IN AUTOMOTIVE INDUSTRY – PART I

BRANISLAV JURAČKA[a], SOŇA RUSNÁKOVÁ*[b], IVAN LETKO[b], PAVEL KOŠTIAL[c], IVAN RUŽIAK[c], and JANKA JURČIOVÁ[d]

[a] VACUUMSCHMELZE, s.r.o., 916 24 Horná Streda 1325/14, Slovak Republic, [b] Tomas Bata University in Zlín, Faculty of Technology, T. G. Masaryka 275, 762 72 Zlín, Czech Republic, [c] VŠB-Technical university of Ostrava, Faculty of Metallurgy and Material Engineering, 17. listopadu 15/2172, 70833 Ostrava-Poruba, Department of Materials Engineering, Czech Republic, [d] Saar Gummi Slovakia spol. s r.o., Gumárenská 397/21, Dolné Vestenice 972 23, Slovak Republic
rusnakova@ft.utb.cz

Abstract

The wide spectrum of composite materials application in automotive, aerospace and military industry, heterogeneous and their large –scale utilization requires necessary demanding accurate knowledge of material parameters those materials.

The thermal expansion behaviour and elastic properties of acrylate resin MODAR reinforced by glass fibre are studied. MODAR − Modified Acrylic Resins offers a series of unique thermoset polymers used in many markets such as automotive, mass transit, railways, building, rods for optical cable, structural parts and profiles and optical fire retardant/ low smoke / low toxicity composite parts. MODAR resins offers: low viscosity, rapid cure, fast cycle times, superior physical properties, and resistance to cracking, long shelf-life and stability (valuable for hot climate countries).

Introduction

Properly designed composite materials can produce thermal expansion coefficients lying well outside the range shown by homogeneous materials both in a single direction and in a plane. Much lower negative values may be produced compared with single materials as well as larger positive values. Such extreme values may be coupled with a choice of other mechanical properties, e.g., Young's modulus or breaking strength or toughness. In this paper we demonstrate influence of two kind of reinforcement to linear coefficient of expansion and elastic properties, too. The investigated sample contains different kind of reinforcement, UNIFILO and ROVICORE. ROVICORE consists of a non-woven core sandwiched between Chopped Strand Mat (CSM.) This fabric is ideal for Closed Mould production, for example RTM (Resin Transfer Moulding.) Each square metre x 1mm thickness will absorb approx. 600g of resin. UNIFILO is an E-glass continuous strand mat of random orientation in multiple layers and held together by a binder[3]. Dilatometry is a method by which the thermal expansion of a material may be measured. There are many types of dilatometers. Dilatometers may use a pushrod, capacitor, or optical system to sense expansion and

Study of thermoelastic properties

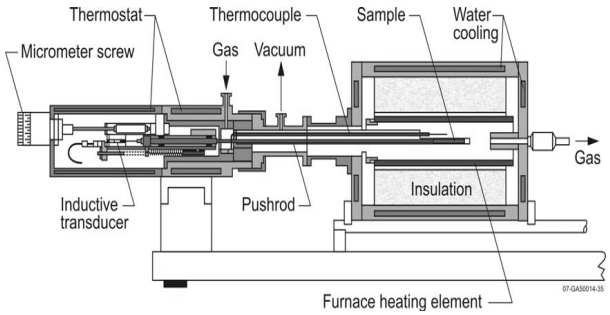

Scheme 1. **Schematic of dilatometer in horizontal configuration[2]**

may be configured in horizontal, vertical, or in-between configurations[1]. Materials expand because an increase in temperature leads to greater thermal vibration of the atoms in a material, and hence to an increase in the average separation distance of adjacent atoms. Thermal expansion of investigated composite materials was measured on the Dilatometer DIL 402 PC, Scheme 1, which is universally applicable instrument for routine investigations of ceramic, glass, and metal samples, this dilatometer meets all normal requisites regarding resolution, calibratability, precision and sample atmosphere. This is an easy-to-operate, entry-level instrument for materials characterization for in-plant quality control.

Dilatometers utilize a Linear Differential Variable Transformer (LVDT) to convert a pushrod displacement to a voltage. This voltage is recorded and converted to a recordable displacement signal by software. By carefully controlling and recording, via thermocouple, the temperature of a sample at the free end of the pushrod, the thermal elongation characteristics of a sample may be determined. When changes in length are driven by changes in temperature, it must be recognized that dilatometer components can also be affected. For that reason, two test runs are required for each experimental sample. The first run is performed using a material with known thermal expansion characteristics. This first "correction" run allows determination of changes in length of the dilatometer components (sample holder and pushrod) by subtracting changes of the known material from the total. The second run is performed with the experimental sample. Changes in length of the experimental sample can be determined by subtracting changes in length of the system components from the total changes in length. Horizontal and vertical dilatometers each have advantages and disadvantages due to orientation. Horizontal dilatometers minimize thermal expansion of components because convection effects are minimized, whereas component expansion in vertical dilatometers may be much greater as heat is carried by convection along the length of the sample holder and pushrod. A disadvantage of horizontal dilatometers is friction. Typically, the sample is placed in contact with the sample holder, and it must expand

along the surface. This is not a problem with vertical dilatometers[4]. The sample is set on a fixed plate, and the pushrod is lowered to contact the sample. On the investigated samples are impose requirements on permanent specific length, eventually only little exchanging, so trust rod was perpendicular on base (cross-sectional area). The measurement can be doing only to critical temperature – gas evolution, burning, diffluence and so on[2]. The software allowed calculates two kinds of thermal expansion coefficient. The first is technical coefficient of thermal expansion, which is calculated by the using equation (*1*), during exactly required value of reference temperature T_0 standardly indicated $T_0 = 20$ °C. The second is physical coefficient of thermal expansion. For both cases is coefficient function of temperature. Consequently is required to find the temperature interval, where the relative displacement is linear function of temperature. We should find so temperature interval where is physical coefficient linear expansion constant or practically constant. The coefficient linear expansion is determined like average value on this interval, more detailed is referred in [1].

$$\alpha = \frac{l}{l_0}.\frac{l - l_0}{T - T_0} = \frac{\varepsilon}{T - T_0} \qquad (1)$$

Results and discussion - part A

The diagrams of work for the sample A are described on the schemes 2, 3, 4, 5.
Sample A: measurement 1,
Mode of heating, T = 50 °C, $\alpha_f = 23{,}070.10^{-6}$ K^{-1},
Mode of cooling T = 52,6 °C, $\alpha_f = 73{,}725.10^{-6}$ K^{-1}.

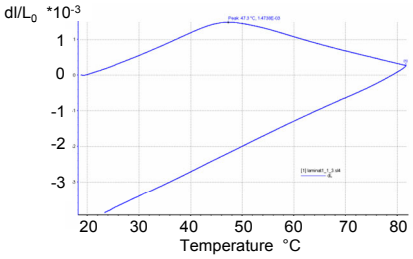

Scheme 2. **Behaviour dependency ε to T, sample A, measurement 1**

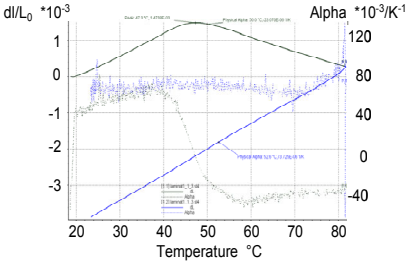

Scheme 3. **Behaviour dependency T to α, sample A, measurement 1**

Sample A: measurement 2,
Mode of heating, T = 50,1 °C $\alpha_f = 61{,}573.10^{-6}$ K^{-1}
Mode of cooling T = 52, 6 °C $\alpha_f = 64{,}347.10^{-6}$ K^{-1}.

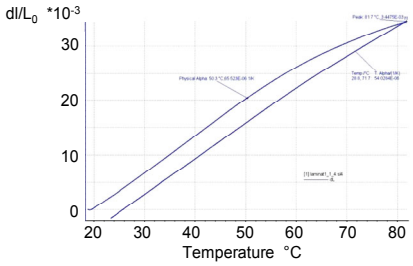

Scheme 4. **Behaviour dependency ε to T, sample A, measurement 2**

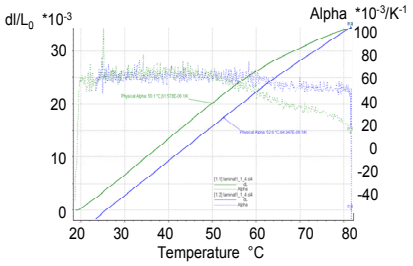

Scheme 5. **Behaviour dependency T to α, sample A, measurement 2**

The diagrams of work for the sample B are described on the schemes 6, 7, 8, 9.
Sample B: measurement 1,
Mode of heating, T = 48,9 °C, $\alpha_f = 39{,}289.10^{-6}$ K^{-1},
Mode of cooling T = 52,6 °C $\alpha_f = 39{,}342.10^{-6}$ K^{-1}.

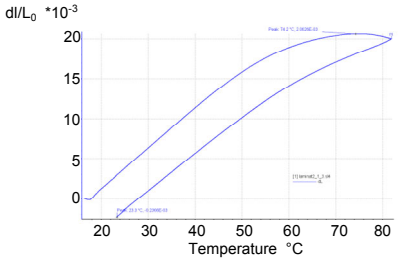

Scheme 6. **Behaviour dependency ε to T, sample B, measurement 1**

REFERENCES

1. Koštial P. and all: *Využitie statických metód a kmitov v diagnostike materiálov*: Diagnostické metódy v materiálovom inžinierstve. UKC ZSVTS, 2009.
2. Daw J. E., Rempe J. L., Knudson D. L., Condie K. G., Crepeau J. C.: *Viability of Pushrod Dilatometry Techniques for High Temperature In-Pile Measurements*.

Idaho National Laboratory, 2008.
3. ASHLAND, Composite polymer division MODAR 835 S CS [online]. http://www.ashchem.com.
4. Dasgupta A., Agarwal R. K., Bhandarkar S. M.: Compos. Sci. Technol. *56*, 209 (1996).
5. Manfredi L. B., Rodríguez E. S., Maria Wladyka-Przybylak M. W., Vázquez A.: Polym. Degrad. Stab. *91*, 255 (2006).

CL-27
DEFECT ANALYSIS FOR AUTOMOTIVE INDUSTRY – FROM THE ANALYTICAL POINT OF VIEW

FRANKY PUYPE and JIŘÍ SAMSONEK

Institute for Testing and Certification – Zlín, Testing division – analytical chemistry, Třida T. Bati 299,764 21 Zlín-Louky, Czech Republic
fpuype@itczlin.cz

Introduction

Already ancient Romans knew that ``making haste slowly`` was not just an aphorism, but a reflection based on experience. Defects always will appear, as they are part of daily life. Nowadays many defects in automotive industry are raising-up caused by higher production speeds, shorter leading times, changing of suppliers or simply human abstraction.

However, sometimes a product looks good during storage but in real use discolors, shows mechanical defects like cracking, blooming or has adhesive problems. It is impossible to keep everything for 100 % under control, therefore production lines count always with a few % of defect end products. If the number of defects are significantly increasing, there is need to investigate the problem. Defects can have a wide range of causes/consequences and should be used as data for continuous quality improvement.

Economical and technical aspects

Defect analysis acts in many cases not to find the ``bad guys and good galls``, but mainly to clearify unexpected inversions which are leading to new approaches and mainly prevention. Analytical chemistry can support the automotive industry to characterize defects if results are properly interpreted. Working out cases scientifically needs afterwards a technical correction by the producer. After characterization a certain defect, conclusions are important for further prevention.

Defect analysis need to be considered as a feedback mechanism to improve the quality and productivity with overall prevention of historically determined mistakes. This prevention can save manufacturers lots of money.

Strategy: comparison and elimination

According to the location and shape of the defect spectral, microscopic or separation techniques can be applied. According to the desired uncertainty of measurement, the best available technology should be chosen.

Basically a defect is best detectable if there is a possible comparison with a reference sample (or more samples). Many methods used in the scientific community are based on this principle. By elimination of possibilities, a solution can be found for further prevention.

Non-destructive first ! - spectral methods

The use of spectral analytical tools is prefered in order to know in which direction the analyst should speciate. Common spectral tools like fourier transformed infrared spectrometry (FTIR) andX-ray fluorescence spectrometry (XRF) can be equiped with a microscope, (e.g. scanning electron microscope coupled to energy-dispersive X-ray spectroscopy / SEM-EDX). From these visualizations lots of basic information can be achieved. Mainly defects like small impurities, spots, adhesive problems and surface defects can be easily characterized. Spectral methods are non-destructive and very quick.

One case of a defect appearing on the surface of a multilayer car profile made from EPDM. On the surface were seen

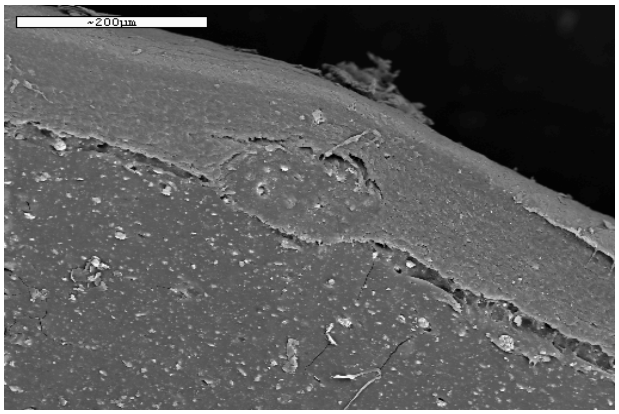

Fig. 1. **SEM picture of a rubber profile with some ``dots`` on the surface**

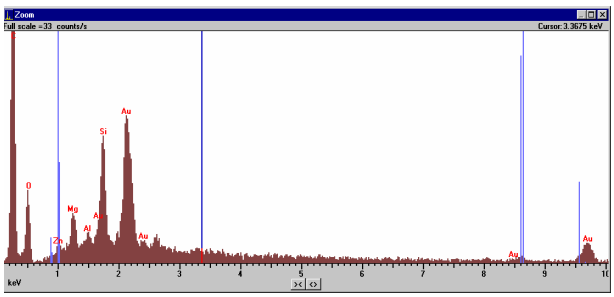

Fig. 2. **Screening element composition of defect test point by SEM-EDX (Mg and Si presence)**

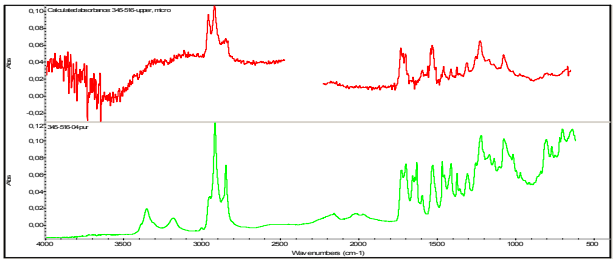

Fig. 3. **Confirmation of talc present in defect test point. Upper is reference spectrum of talc, lower is spectrum from defect measured by microscope-FTIR**

``dots``. In Fig. 1 is seen by SEM that a ``dot`` is located between 2 polymer layers. After gold sputtering for SEM-EDX measurement there was detected that the material is foreign and contains typical elements from talc ($H_2Mg_3(SiO_3)_4$), which the other parts did not have. This was once more confirmed by measurement on FTIR by microscope (Fig. 3). The polymer in the ``dots`` is foreign due to the fact that it contains talc and the other test parts (from the layers) not. All results were obtained by comparison the defect test point with reference test points.

Both spectral methods come to the same conclusion. In many cases these spectral analysis can direct the analyst in the direction of organic defects or inorganic defects.

Separation sciences

To identify a small amount of macromolecules as impurities, pyrolysis-GC-MS can be applied. The power of pyrolysis is that it requires a small amount of sample (0,5 mg) and is able to fully characterize pyrolysis fragments by classsical gas chromatography/mass spectrometry (GC-MS). In Fig. 4 is seen a picture of white fibers coming out of a cover intended to use for car interior. After isolating them, extracting and applying a pyrolysis analysis on this part, this foreign material was identified to be a copolymer PC/ABS.

Fig. 4. **Picture of a defect: white fibers coming out from a black car interior cover**

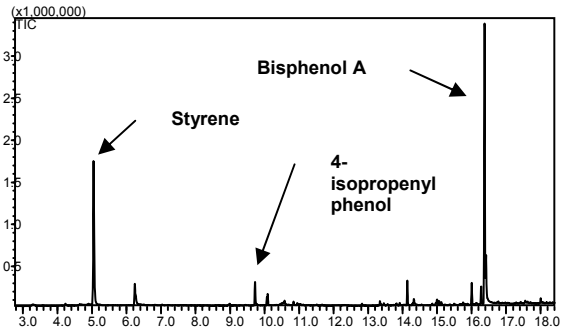

Fig. 5. **Pyrogram of white fiber coming out from a black car interior cover**

For characterization of fogging, thermal desorption (TD) coupled with GC-MS is the best available technique. It is possible to simulate on a test part the whole temperature range over a longer time and identify the emissions produced. Fig. 6 shows a fogging comparison test of 2 car sealants. One sealant (lower chromatogram, Fig. 6) give no emissions while the other/defect one (upper chromatogram, Fig. 6) shows a Gaussian distribution of polydimethylsiloxanes. Such a comparison is commonly done for screening of additives, searching for batch-to-batch differences and looking for foreign reaction products.

Non-adhesive behavior of materials can have a broad range of causes, however, if there is a possibility for comparison with previous batches it makes sence to compare. In the following case a defect with adhesive properties of leather on a steering wheel was solved by thermal desorption. Low molecular weight analytes were expected, therefore thermal desorption GC-MS was applied. The absence of 2 commonly used amine catalysts in the PU-glue at the defect test point prove the bad-adhesive properties on the defect test point (Fig. 7).

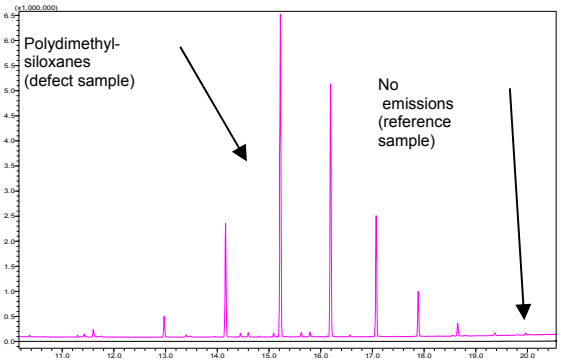

Fig. 6. **Thermal desorption GC-MS chromatogram of 2 sealants for automotive, a comparison (defect sample upper, reference sample lower)**

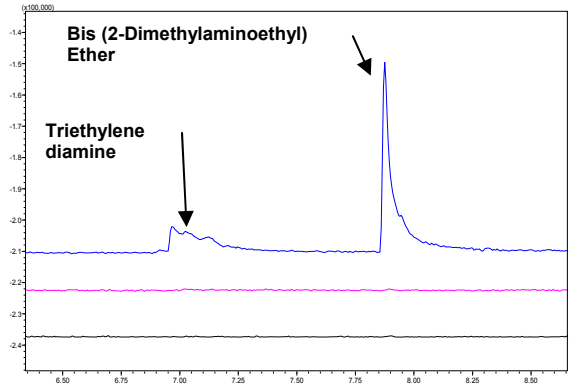

Fig. 7. **Thermal desorption GC-MS chromatogram of PU-glue for production of a steering wheel, a comparison (reference sample upper, defect sample middle, sample blank lower)**

Elements, lower detection limits please !

Element analysis for automotive industry is in evolution toward trace levels. Therefore special analytical tools like inductively coupled plasma spectrometry (ICP) is getting more and more important for defect analysis. Differences between batches for an element like sulfur might be critical fur rubber mixtures.

The use of inorganic additives, fillers, inorganic acid scavengers can be characterized on its element composition. Differences in homogeneity of hydrotalcites used as an acid scavenger in PP pellets can give already huge effects of yellowing, if a phenolic stabilizer is mixed. Therefore the ratio Mg/Al should be screened on raw materials.

Conclusion

New trends in modern analytical chemistry are focussed on many fields in the scientific world. However for automotive industry with common analytical instrumentation and experienced people, defect analysis can support the QA and QC for many automotive applications. As defect analysis is a part of its prevention itself and process optimization, it might not be ignored as defect analysis can save the producer lots of money.

CL-28
GATE EFFECT ON QUALITY OF INJECTED PART

STEPAN SANDA, MIROSLAV MANAS, DAVID MANAS, MICHAL STANEK, and VOJTECH SENKERIK

Tomas Bata University in Zlín, nám. TGM 5555, 760 01 Zlín, Czech Republic
sanda@ft.utb.cz

Abstract

The article describes the influence of the type and location of gates for the properties of injected parts. Test samples were made from injected parts of board shape manufactured by using different types of gates and their location. For the test a polymer (PA 66) was used with a different quantity of reinforcing material (glass fibers) Interesting correlations between the type and location of the gate and selected material were found.

Introduction

The quality of runners in injection moulds considerably influences the product which is being formed in the cavity of the mould. Runners determine the speed of the flow of the melt and thus influence the injection phase. They influence the distribution and orientation of the filler in the product. They decide the efficiency of the holding pressure, which has an influence on the deformation and shrinkage of the product. In addition, they can be agents of residual strain due to exceeding maximum shear rate and the strain in the polymer during the injection.

At the moment the design of runners depends on the experience of the designer of the injection mould and the product specifications. The designer is bound by many circumstances which restrict the selection of the runner in respect of the following:

– The way of filling the cavity and the length of the flow of polymer;
– flaws (flow mark, weld lines, sinks).

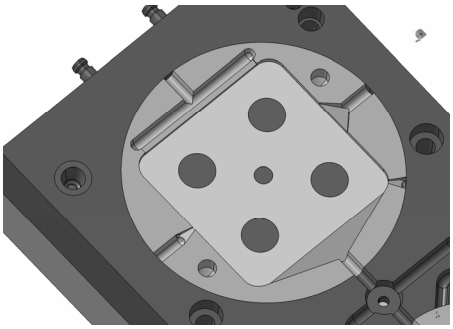

Fig. 1. **The cavity of the injection mold**

At the same time, the designer is expected to design the gate in such a way so that it fulfills its function. It is one of the reasons why it is necessary to study the influence of gates on the injected product. More profound knowledge of this problem can help designers of injection molds to make the right decision.

Experimental conditions

Parts with ejecting mechanism to fit the universal frame of the injection mould were designed for the experiments. The cavity of the mold was of square board shape with the dimensions (100 × 100 × 3) mm. The design of the runner system enabled to fill the cavity by different ways – by different types of gates.

Gates were divided into three groups (A, B and C) according to the way of filling the mold cavity. Out of these groups representative gates were selected in respect of their practical application. In total four gates were selected:

- A1 – film gate on the side of the board;
- A3 – fan gate on the side of the board;
- B1 – fan gate in the corner of the gate;
- C1 – cone gate in the centre of the board.

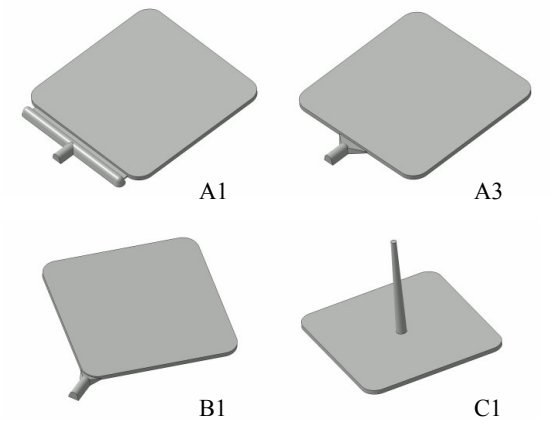

Fig. 2. **Injected board – types of gates**

Square boards from the selected gates were manufactured on the injection molding machine ARBURG Allrounder 420 C. Test samples were cut out of the boards to be used for mechanical tests. The test samples were prepared in two directions:

- In the direction of the melting from the gate – L direction (longitudinal).
- Transversally to the direction of the melt from the gate – T direction (transversal).

The following mechanical tests were carried out on the test samples:

- Tensile test – performed on a universal testing machine ZWICK 1456 according to ČSN EN ISO 527-1 and ČSN EU ISO 527-2. To increase the precision of measurement an extensometer was used during testing.
- Bend test – performed on a universal testing machine ZWICK 1456 according to ČSN EN ISO 178.
- Impact test – performed on the hammer CEAST Resil Impactor Junior according to ČSN EN ISO 179.
- Hardness test – carried out on the hardness testing machine AFFRI using the method of Shore D according to ČSN EN ISO 868.

Polymer material used for the experiments was Polyamid 66 produced by company BASF.

Table I
List of polymers used

Name	Type of filler	Content of filling [%]
Ultramid A3W	No filler	0
Ultramid A3WG3	Glass fibres	15
Ultramid A3WG5	Glass fibres	25
Ultramid A3WG6	Glass fibres	30
Ultramid A3WG7	Glass fibres	35
Ultramid A3WG10	Glass fibres	50

Results and discussion

Tensile test proved the influence of the filler and its orientation. The orientation of fibres is what makes the gate different. In the case of A1 film gate, in which fibres have the greatest possibility of orientation and the gate enables the best balanced application of holding pressure, the influence of the filler on the product properties in the L direction of the flow and T direction of the flow were most visible. In the case of other types of gates this influences is not so apparent and depends on the shape and location of the gate.

The values of tensile modulus obtained from the samples taken in the direction of the flow (L direction) and transversally to the direction of the flow (T direction) were different as expected. The interesting fact was that in the case of 15 % filling and 50 % filling, the values in the T direction were higher than in the L direction. The greatest difference between the L direction of the flow and T flow was shown by 30 % filling. At the same time it was shown that in the case of this filling the type of the gate used made no difference, because the values measured are almost identical in both directions regardless of the type of the gate.

The bend test in many respects confirmed the tendencies found by the tensile test. Also, lower values of flexural modulus of elasticity compared with the tensile test were confirmed. The values were about 10 % to 20 % lower in the L direction than in the tension and in the T direction the values were 30 % to 40 % lower. By comparing the results obtained for all the gates and materials it was found that the values of individual fillings in the T direction do not show any significant difference and therefore the type of gate does not make any difference. However, in the case of filled materials, in the L direction A1 gate is considerably dominant compared to A3 and B1 gates, which show significantly lower values in this direction. It does not apply to 35 % filing which

shows minimal differences in both directions.

In the case of unfilled material the type of the gate showed a great influence during the impact test. A1 film gate showed only minor difference when comparing the values in the L and T directions, only about 6 %, but the difference was quite significant for A3 and B1 gates with approx. 25 %.

In the impact resilience there was an interesting development in the values measured. While at other measurements it is common that the value measured rises in parallel with the increasing amount of filling, there was at first a considerable drop and then a gradual growth to the original value. The reason is the glass fibres. The unfilled material showed its resilience as expected and it was necessary to apply higher energy to fracture the test sample. However, only 15 % of glass was sufficient to decrease the energy needed by as much as 65 %. With the growing content of the filler, material strength was gradually increasing and the values measured slowly approached those of the basic material. The values were, however, leveled at 35 % filling.

The polymer filled with 15 % and 35 % of glass fibres showed the greatest stability of the values measured regardless of the type of the gate used. The difference between the gates was more significant in the other filled materials.

Measurement of the hardness showed the expected fact that the higher the content of the filling, the greater the hardness of the material. The tests further showed that when using A1, A3 and B1 gates the values of hardness are very similar for all materials. C1 gate showed the lowest hardness for all materials, but it is lower by 4 % compared to the other gates, which can in general be considered negligible.

Conclusion

The presented results showed interesting correlations between the type of the gate and the selected material. In general the most suitable material appears to be polymer with the filling of 30% or 35 % of glass fibers. The reason is the greatest stability of values measured for all types of gates. At present it would not be right to make recommendations for designers, because more tests and experiments are in progress.

This article is financially supported by the Czech Ministry of Education, Youth and Sports in the R&D projects under the titles 'Modelling and Control of Processing Procedures of Natural and Synthetic Polymers', No. MSM 7088352102 and 'CEBIA Tech', No. CZ.1.05/2.1.00/03.0089.

REFERENCES

1. Beaumont John P.: *Runner and Gating Design Handbook : Tools or Successful Injection Molding*. 2nd edition. xvi, 308 s. Hanser, Munich 2007.
2. Ducháček V.: *Polymery : výroba, vlastnosti, zpracování, použití*. 2 vyd. 280 s. VŠCHT v Praze, Praha 2006.
3. Pötsch G., Michaeli W.: *Injection Molding : An Introduction.* 2nd Edition. x, 246 s. Hanser, Munich 2008.
4. Rees H.: *Mold engineering*. 2nd edition. xxiii, 688 s. Hanser, Munich 2002.

CL-29

HOW THE FILLER INFLUENCE THE FLUIDITY OF POLYMER

MICHAL STANEK, MIROSLAV MANAS, DAVID MANAS, VLADIMIR PATA, STEPAN SANDA, VOJTECH SENKERIK, and ADAM SKROBAK

Tomas Bata University in Zlin, Faculty of Technology, Department of Production Engineering, TGM 275, 762 72 Zlin, Czech Republic
stanek@ft.tub.cz

1. Introduction

Injection molding is one of the most extended polymer processing technologies. It enables the manufacture of final products, which do not require any further operations. The tools used for their production – the injection molds – are very complicated assemblies that are made using several technologies and materials. Working of shaping cavities is the major problem involving not only the cavity of the mold itself, giving the shape and dimensions of the future product, but also the flow pathway (runners) leading the polymer melt to the separate cavities. The runner may be very complex and in most cases takes up to 40 % volume of the product itself (cavity). In practice, high quality of runner surface is still very often required. Hence surface polishing for perfect conditions for melt flow is demanded. The stated finishing operations are very time and money consuming leading to high costs of the tool production.

Delivery of polymer melts into the mold cavity is the most important stage of the injection molding process. This paper shows the influence of cavity surface roughness and technological parameters on the flow length of polymer melt into mold cavity. The fluidity of polymers is affected by many parameters (mold design, melt temperature, injection rate and pressures) and by the flow properties of polymers. Results of the experiments carried out with polypropylene contained different amount of filler proved a minimal influence of surface roughness of the runners on the polymer melt flow. This considers excluding (if the conditions allow it) the very complex and expensive finishing operations from the technological process as the influence of the surface roughness on the flow characteristics does not seem to play as important role as was previously thought.

2. Injection molding

The injection mold for was designed for the easiest possible manipulation both with the mold itself and during injection while changing the testing plates, size of the mold gate etc. The injection mold is inserted into a universal frame (Fig. 2) which was designed for use with many different injection molds that fit the size of the frame. This makes the change of the separate injection molds easier, because the frame remains clamped to the injection molding machine and only the shaping and ejection parts of the molds are changed. Attaching right and left sides of the frame to fixed and mov-

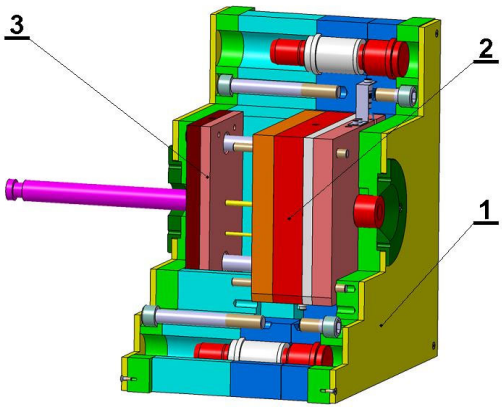

Fig. 1. **Assembly of injection mold;** 1 – frame, 2 – injection mold, 3 – ejection system

ing plates of the injection machine is done using four clamps on each side.

The shaping part of the injection mold is composed of right and left side. The most important parts of the injection mold concerning the measurements are: testing plate, cavity plate and a special sprue puller insert.

The cavity (Fig. 2 – right) of injection mold for is in a shape of a spiral with the length of 2000 mm and dimensions of channel cross-section: 6 × 1 mm. The cavity is created when the injection mold is closed, i.e. when shaping plate seals the testing plate.

Injection mold can operate with 5 exchangeable testing plates (Fig. 2 – left) with different surface roughness. The surface of the plates was machined by four different technologies, which are most commonly used to work down the cavities of molds and runners. These technologies are polishing, grinding, milling and electro-spark erosion (Table I). The testing plates are used for changing the surface of the mold cavity.

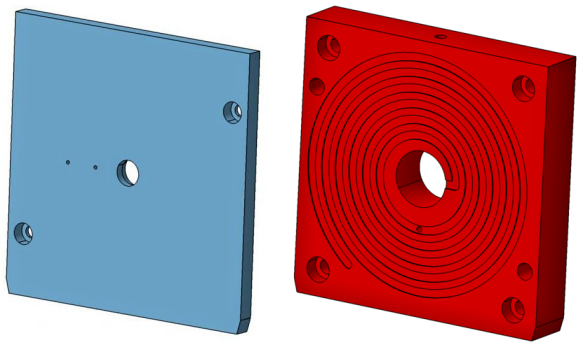

Fig. 2. **Cavity plates (left – testing plate, right – shaping plate)**

Table I
Surfaces of testing plates

Polished plate	Ground plate	Electro – spark machined plate (fine design)	Milled plate	Electro – spark machined plate (rough design)
R_a [μm]	R_a [mm]	R_a [mm]	R_a [mm]	R_a [mm]
0,102	0,172	4,055	4,499	9,566

3. Results

Natural polypropylene and polypropylene with different amount of filler – glass fibers (10 %, 20 %, 30 %, 40 % of GF) has been used for the experiment.

The aim of the measurements was to find out the influence of separate parameters, especially the quality of the injection mold cavity surface and filler amount, on the flow length. The main results are given on the following pictures.

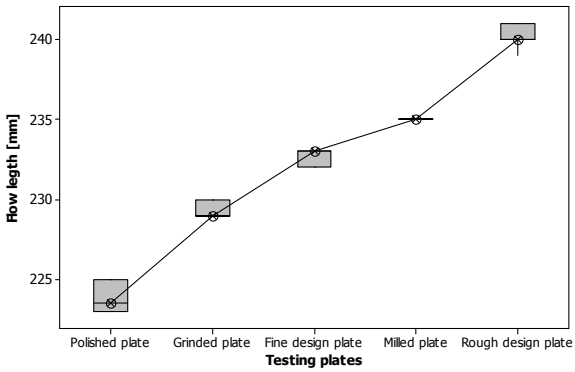

Fig. 3. **Dependence of the flow length on surface quality (0 % GF)**

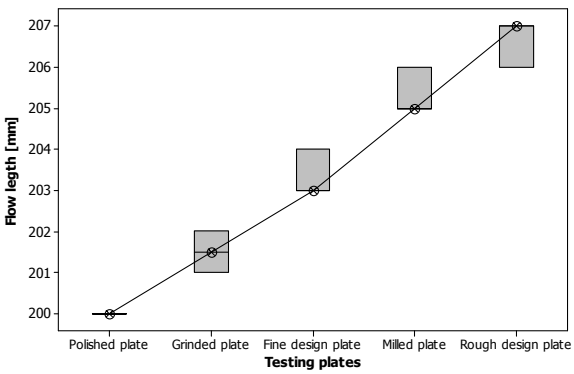

Fig. 4. **Dependence of the flow length on surface quality (20 % GF)**

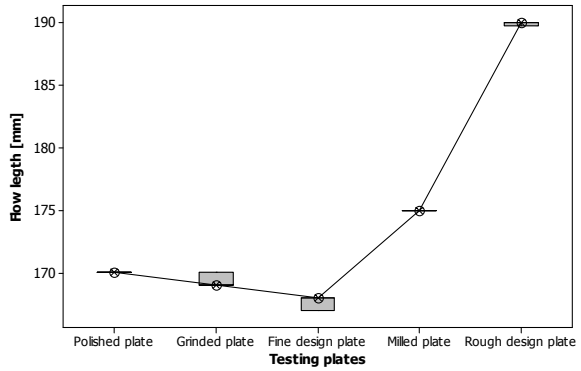

Fig. 5. **Dependence of the flow length on surface quality (40 % GF)**

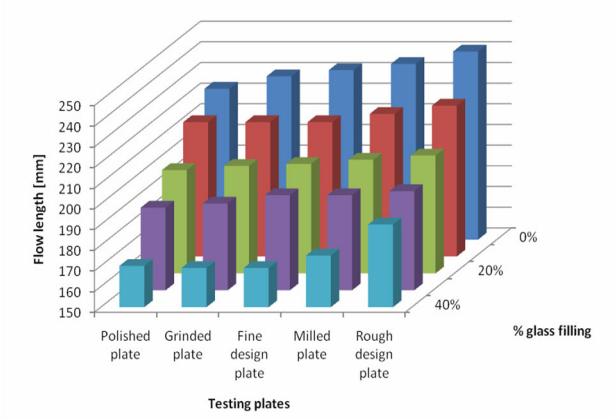

Fig. 6. **Dependence of the flow length on surface quality and filler amount**

4. Conclusion

This research looked into the influence of technological parameters on filling of the injection mold cavity and the flow length respectively. The differences in flow lengths at the testing cavity plates with different surface roughness were very small, rather higher in case of rougher surfaces. But the there is demonstrable difference of worse flow properties on each testing plate with increasing percentage of filler (GF – glass fibers). The measurement shows that surface roughness of the injection mold cavity or runners have no substantial influence on the length of flow. This can be directly put into practice. It also suggests that final working and machining (e.g. grinding and polishing) of some parts of the mold, especially the flowing pathways, are not necessary.

This article is financially supported by the Czech Ministry of Education, Youth and Sports in the R&D projects under the titles 'Modelling and Control of Processing Procedures of Natural and Synthetic Polymers', No. MSM 7088352102 and 'CEBIA Tech', No. CZ.1.05/2.1.00/03.0089.

REFERENCES

1. Manas D., Stanek M., Manas M., Pata V., Javorik J.: KGK, Kautsch. Gummi Kunstst. *62*, 240 (2009).
2. Maňas M., Staněk M., Maňas D., Daněk M., Holík Z.: Chem. Listy *103*, 24 (2009).
3. Manas D., Manas M., Stanek M., Zaludek M., Sanda S., Javorik J., Pata V.: Chem. Listy *103*, 72 (2009).
4. Šanda Š., Maňas M., Staněk M., Maňas, D., Rozkošný L.: Chem. Listy *103*, 140 (2009).
5. Kyas K., Stanek M., Manas M., Manas D., Krumal M., Cerny J.: *21st International DAAAM Symposium, 2010, Zadar, Croatia*, p. 1081.

CL-30
MAGNETO ACTIVE ELASTOMERS AND THEIR APPLICATIONS

T. STEINKE[a], M. MÖWES[a], D. MENZEL[b], T. ALSHUTH[a], and R. H. SCHUSTER[a]

[a] Deutsches Institut für Kautschuktechnologie e.V., Eupener Straße 33, DE-30519 Hannover, [b] Technische Universität Braunschweig, Mendels sohnstr. 3, DE-38106 Braunschweig, Germany
Timo.Steinke@DIKautschuk.de, Robert.Schuster@DIKautschuk.de

Abstract

This article describes the synthesis, functionalization and dispersion of magnetite nanoparticles with superparamagnetic properties in polymeric hybrid materials.

The magnetite particles are synthesized by a coprecipitation method using iron chlorides and are functionalized by different silanes. These silanes contain organic groups adapted to the polymeric matrix in which the particles should be dispersed.

The synthesized particles and hybrid materials are particularly analyzed by TEM, SEM, AFM, TGA, XRD, SQUID and Moessbauer spectroscop.

Introduction

Nanosized particles and structures are currently key materials for advancements in electronics[3], biotechnology[4,5], magnetic storage[6,7], actuators[8] and many other fields of interest. These materials show different physical and chemical characteristics compared to the macroscopic structures of conventional materials and enable the miniaturizing of well-known technologies. Additionally electrical, thermal, magnetic and other characteristics can be changed and even adjusted by the particle size.

Magnetite particles demonstrate a high saturation magnetization at room temperature and the highest ordering temperature among spinel ferrites[9].

Magnetite has been synthesized by many different methods, and various procedures have been developed in order to obtain particles with different sizes, shapes and surface modi-

fications. This procedure uses aqueous[10–12] and organic[13–16] methods. Non-aqueous methods are mostly based on thermal decomposition of organic iron precursors in the presence of a surfactant. The resulting magnetite nanoparticles can be stabilized in water or organic solvents depending on the reaction method.

In this work a simple and direct method for the preparation of magnetite nanoparticles with diameters ranging from 5 to 30 nm is presented.

The synthesized magnetite particles are functionalized with different silanes in ethanol and dispersed in silicon rubber. The physical properties of anisotropic composites are presented.

Eperimental

Synthesis of magnetite nanoparticles

Magnetite particles were prepared by coprecipitation, adding 5 mol l^{-1} NaOH solution at 30 °C into the mixed solutions of 0.25 mol l^{-1} $FeCl_2$*4 H_2O and 0.5 mol l^{-1} $FeCl_3$ (molar ratio 1:2) until the pH reached 11. The slurry was magnetically separated and washed three times with demineralized water until the pH became neutral. The solid was dried at 5 mbar and room temperature[1,2,17].

Functionalization of magnetite nanoparticles

The dry magnetite nanoparticle powder was dispersed in ethanol (96 %) in an ultrasonic bath for one hour. 100 wt.% of silane was added to this dispersion ,stirring rapidly. After 20 h the reaction was quenched with water, washed three times with demineralized water and dried at 5 mbar at room temperature[17].

In this work two silanes were used for functionalization: tetraethyl silicate (TEOS) and triethoxyoctylsilane (Si□208).

Magnetite nanoparticles in silicon

Different amounts of dry, functionalized magnetite nanoparticle powder were dispersed in a two-component silicon in an ultrasonic bath for 30 minutes. The composite was cured at 30 °C for 24 h with and without a magnetic field in a 2 mm Teflon-mould.

Results and discussion

The synthesized magnetite nanoparticles are identified by XRD. The XRD-pattern (Fig. 1) shows the typical structure for magnetite[2] with broad peaks showing the nanoparticularity of the powder. The room temperature Mössbauer spectrum of the magnetite sample is typical for nanocrystalline magnetite particles with a diameter about 10 nm (ref.[18]).

The size of the magnetite particles is measured by TEM and DLS.

The TEM images show a average particle diameter of 17.9 nm. Fig. 3 shows a TEM image and the histogram of the particle size. The unfunctionalized particles have a tendency

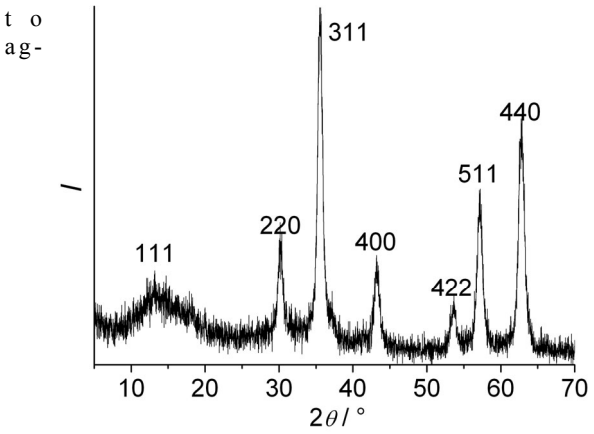

Fig. 1. **XRD-pattern of magnetite nanoparticle powder with assignment of the Miller indices**

glomeration which is confirmed by DLS results. Here the unfunctionalized particles have a solvodynamic average diameter in ethanol of 1.66 μm, the particles which are functionalized with TEOS have a average diameter of 51 nm and the particles which are functionalized with acrylsilane have a average diameter of 35 nm. This tendency shows the deagglomeration of functionalized particles and indicates a monolayer of acrylsilane on the magnetite particle surface instead of a multilayer of TEOS.

The SQUID-measurements (Fig. 2) show a high saturation magnetization and no hysteresis at room temperature this indicates superparamagnetic properties in the material.

The effect of functionalization of the magnetite particles is investigated by TGA and FT-IR. The TGA of the particles functionalized with Si-208 indicate a 4 mass% coverage with organic material, this equates to 5 mass% of silane. The FT-IR spectrum of the functionalized particles shows typical aliphatic bands.

The transition temperature of Fe_3O_4 (magnetite) into Fe_2O_3 is also given by TGA at 168 °C. After functionalization with TEOS the transition temperature rises to 188 °C. This fact indicates a good coating of the surface and a protection of the surface atoms against oxidation by the functionalization.

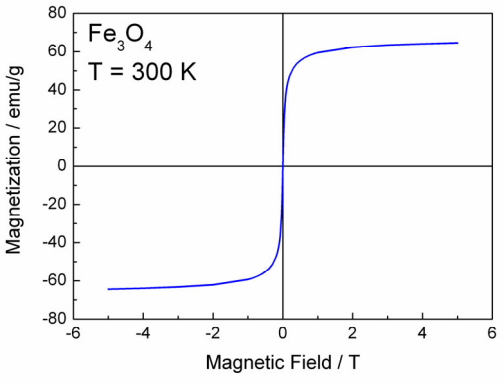

Fig. 2. **SQUID-measurement of magnetite nanoparticles at 300 K**

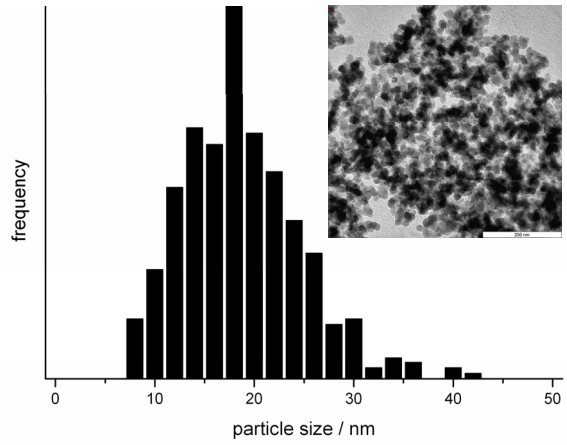

Fig. 3. **TEM image and diameter histogram of magnetite nanoparticles in dry powder**

Magnetite-polymer composites

The magnetite-silicon composites show a switching effect to higher stiffness in presence of an magnetic field as a function of field strength. This property can be used to build actuators and sensors based on elastomers.

Physical properties

During incorporation and curing the magnetic particles can be oriented within the polymer matrix. The orientation is establishing a memory effect in as much as physical properties changes significantly when the composite is deformed in absence or on presence of an external magnetic dynamically field.

Summary and outlook

The combination of magnetic nanomaterials with polymeric matrix materials opens new ways to synthesize different composite materials with adjustable characteristics. These materials can be used for example as new sensors, actuators or in biotechnologies.

The main problem, a good dispersion of the nanoparticles in the polymeric matrix, was solved by functionalization with silanes, which have organic groups that are similar to those used in this work.

A better control of the particle size and particle dispersion will be part of the next steps of this work.

The authors want to thank Prof. V. Šepelák (University of Braunschweig) for the Mössbauer measurements, Dr. Ch. Menneking (Laser Zentrum Hannover e.V.) for the DLS measurements and the BMBF for financial support of this work.

REFERENCES

1. Cushing B. L., Kolesnichenko V. L., O`Conner C. J.: Chem. Rev. *104*, 3893 (2004).
2. Yamamura M., Camilo R. L., Felinto M. C. F. C.: J. Alloys. Compounds *344*, 152 (2002).
3. Gensler R., Goppel P., Muhrer V., Müller N.: Part. Part. Syst. Charact. *19*, 293 (2002).
4. Gupta A. K., Gupta M.: Biomaterials *26*, 3995 (2005).
5. Gamarra L. F., Brito G. E. S., Pontuschka W. M., Amaro E., Parma A. H. C., Goya G. F.: J. Mag. Mag. Mater. *289*, 439 (2005).
6. Hyeon T.: Chem. Commun. (*2003*) 927.
7. Todorovic M., Schultz S., Wong J., Scherer A.: Appl. Phys. Lett. *74*, 2516 (1999).
8. Lu A.-H., Salabas E. L., Schüth F.: Angew. Chem. *119*, 1242 (2007).
9. Smit J., Wijin H. P. J.: *Ferrites: Physical Properties of Ferrimagnetic Oxides in Relation to Their Technical Applications*; Phillips` Technical Library, Eindhoven, NL, 1959.
10. Massart R., Cabuil V.: J. Chim. Phys. *84*, 967 (1987).
11. Lee J., Isobe T., Senna M.: J. Colloid Interface Sci. *177*, 490 (1996).
12. Jolivet J. P., Vayssieres L., Chaneac C., Tronc E. : Mater. Res. Soc. Symp. Proc. *432*, 145 (1997).
13. Shun S., Zeng H.: J. Am. Chem. Soc. *124*, 8204 (2002).
14. Park J. et al.: Nature Mater. *3*, 891 (2004).
15. Pinna M., Grancharov S., Beato P., Bonville P., Antonietti M., Niederberger M.: Chem. Mater. *17*, 3044 (2005).
16. Rockenberger J., Scher E. C., Alivisatos A. P.: J. Am. Chem. Soc. *121*, 11595 (1999).
17. Ma M., Zhang Y., Yu W., Shen H., Zhang H., Gu N.: Colloids Surf., A *212*, 219 (2003).
18. Goya G. F., Berquó T. S., Fonseca F. C., Morales M. P. : J. Appl. Phys. *94*, 3520 (2003).

CL-31
RECYCLING OF PP/EPDM/TALC CAR BUMPERS

MAREK SZOSTAK

Poznan University of Technology, Institute of Materials Technology, Piotrowo street 3, 61-138 Poznan, Poland
marek.szostak@put.poznan.pl

In the work the comparison of mechanical properties of recyclates from Volkswagen car bumpers obtained after the grinding and regranulates from the same wastes but produced in the extrusion process on the twin screws extruder (type ZAMAK, L/D = 40) has been presented. The original bumpers has been produced from the PP blends with 20 % EPDM and 10 % of talc. The example of passenger car bumper is presented on the Fig. 1.

Materials and technology used in car industry were always connected with technical knowledge in the time of its production. First cars were based on wood and steel. In 1930 same elements has been produced from polymeric materials. In 1955 the average car have 5 kg of parts made from plastics. Between the years 1960−1970 the contents of plastics part in

Fig. 1. **The example of passengers car bumper**

the cars increase form 11 kg to 45 kg, but still it were mostly rather the decoration part than constructional one. In next years together with development of polymer processing technologies the car parts produced from plastics became the real construction elements and now we can find about 145 kg of plastics parts in every produced passenger car (it is around 12–15 % of car weight)[1–6]. The amount of plastics used in production of average passenger car is shown on the Fig. 2.

One of the most common application of polymer materials in the car are bumpers. They are produced mostly from modified PP material. The front bumpers are made from PP+EPDM polymer blends (to have more elastic properties) and the rear bumpers are made from PP+EPDM blends modified by some amount of talc (to decrease a cost of production).

The wastes from such a bumpers have been put on the recycling test. The PP/EPDM/Talc recyclates obtained during the grinding process have been compared with PP/EPDM/talc regranulates obtained during extrusion and regranulation process made on the twin screw extrusion line. The static tensile test and dynamic mechanical thermal analysis (DMTA) have been done for both materials. The measurements of melt flow index (MFI) of the PP blends recyclates and regranulates has been made too.

The research results of rheological (MFI) and mechanical properties (max. tensile strength – δ_{max}, elongation at break – ε, Young Modulus – E) are presented in table I while the results of DMTA tests are shown on Fig. 3,4 and in Table II.

The results of the measurements have been presented on the line diagrams (Fig. 3 and 4) of E' and tg δ dependence in a function of temperature. The full line designation the results

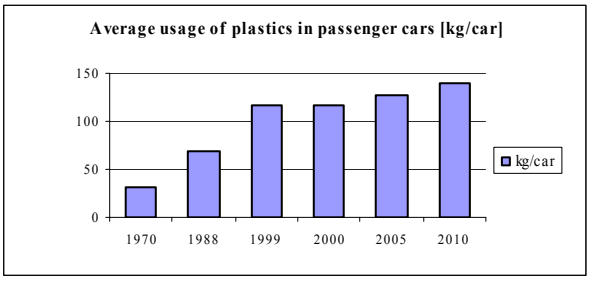

Fig. 2. **The amount of plastics used in production of average passenger car**

Table I
Results of mechanical and rheological properties tests

Type of polymer	Stress at peak [MPa]	Strain at break [%]	Young Modulus [MPa]	MFI [g/10min]
PP blend Recyclate	17,5	167	932	35,5
PP blend regranulate	16,3	168	802	27,5

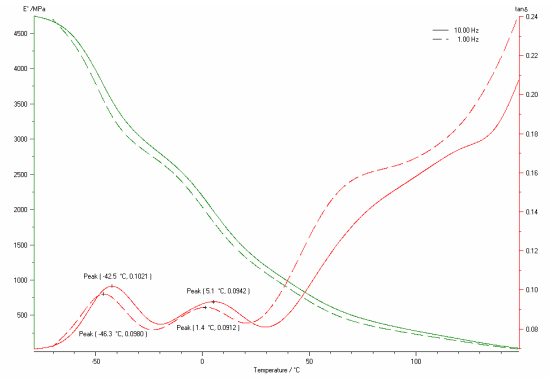

Fig. 3. **DMTA study of E' and tg δ in dependence of temperature for PP+EPDM+talc recyclate.** Full line: f = 10 Hz; broken line = 1 Hz

for 1 Hz frequency testing while the broken line the results for 10 Hz. On the diagrams the T_g temperatures for the components of the blends have been shown. For the sample obtained from PP recyclate the T_g temperature for EPDM component was determined as –42.5 °C for 10Hz frequency and –46.3 °C for 1Hz frequency testing. The T_g temperature for PP in the same sample was found as +5.1 °C for 10Hz and +1.4 °C for 1 Hz frequency. For the sample obtained from PP regranulate the T_g temperature for EPDM was measured as –42.7 °C for 10Hz and –46.8 °C for 1Hz frequency, while the T_g temperature for PP was: +3.4 °C for 10Hz and +0.8 °C for 1 Hz frequency testing.

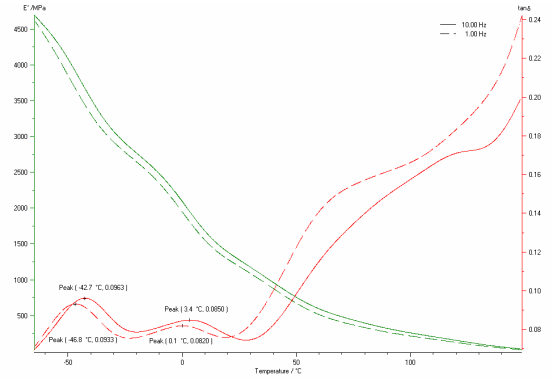

Fig. 4. **DMTA study of E' and tg δ in dependence of temperature for PP+EPDM+talc regranulate.** Full line: f = 10 Hz; broken line = 1 Hz

Table II
Results of DMTA tests

Material	Tg [°C] /freq. = 1Hz/	Tg [°C] /freq. = 10Hz/
EPDM in recyclates	–46,3	–42,5
EPDM in regranulates	–46,8	–42,7
PP in recyclates	1,4	5,1
PP in regranulates	0,8	3,4

The results of the measurements have shown that both materials have good mechanical properties (tensile strength 16−18 MPa, Young Modules 800−930 MPa and elongation above 160 %), good procesability – MFI above 27 g/10 min (recyclate – 35 g/10 min, regranulate – 27 g/10 min) and good thermal behaviour (glass transition temperature 1,4−5,1 °C for PP recyclates and 0,8−3,4 °C for PA regranulates) what is very important for the materials used in the production of car bumpers.

On the basis of the research results it was fund that the differences in samples properties produced from recyclates and regranulates of PP/EPDM/talc blends are very small. The differences in mechanical and rheological properties are negligible only the glass transition temperature for PP regranulates (after the thermal treatment in extrusion and regranulation process) has shown a small shift into the more negative value. Such a results allowed to conclude that regranulation of tested PP/EPDM/talc blends in the recycling process is useless. Due to the lower price of reprocessing of PP/EPDM/talc wastes from car bumpers, for the production purposes, using only the grinding process is more effective than extrusion and regranulation processes of such a wastes and that's why the cheaper material – recyclates, should be selected for further recycling technologies.

The research was financing from European Regional Development Fund – ERDF and Polish Operative Programme Innovative Economy – POIG. Grant no UDA-POIG.01.03.01-00-025/08.

REFERENCES

1. Official Journal of the European Communities L 170, 26.02.2002, (2002).
2. Kozlowski M.: Plastics Recycling in Europe, 217-255, Wroclaw (2006).
3. Phlegem H. K.: *The role of chemist in automotive design*. CRC Press (2009).
4. Kunststoff im Automobil, Einsatz und Verwertung, VKE, Frankfurt/Mainz (2008).
5. Braess H. H., Seiffert U.: *Handbook of Automotive Engineering*, SAE International (2005).
6. Merkisz-Guranowska A.: *Recykling samochodow w Polsce*. Instytut Technologii Eksploatacji, Radom (2007).

CL-32

RHEOLOGICAL AND THERMAL PROPERTIES OF EXTERNALLY PLASTICIZED CELLULOSE ACETATE (CA) FOR PHYSICAL FOAMING

STEFAN ZEPNIK[a,b]*, STEPHAN KABASCI[a], HANS-JOACHIM RADUSCH[b], and THOMAS WODKE[a]

[a] *Fraunhofer Institute for Environmental, Safety and Energy UMSICHT, Osterfelder Straße 3, D-46047 Oberhausen,* [b] *Chair of Polymer Technology, Centre of Engineering Sciences, Martin Luther University, D-06099 Halle/Saale, Germany*
stefan.zepnik@umsicht.fraunhofer.de

Abstract

The influence of plasticizers on thermoplastic processing, rheological and thermal properties of CA necessary for foam sheet extrusion were investigated by rotational and capillary rheometer, rheotens test, melt flow rate (MFR) and differential scanning calorimetry (DSC).

Introduction

Today, oil-based polystyrene (PS) is a standard material for producing thermo-formable extruded foam sheets using physical blowing agents (PBA). PS is a non-biodegradable polymer based on non-renewable resources. Cellulose acetate (CA), as a cellulose ester, is a biodegradable polymer based on renewable resources and therefore particularly suitable for producing sustainable foams and thermoformed trays.

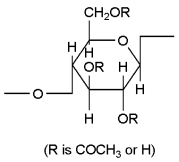

Scheme 1. **Chemical structure of cellulose acetate**

CA exhibits mechanical properties as well as heat distortion resistance comparable to or better than those of PS. Thus, CA is a good candidate to replace PS. Generally, CA has to be modified for thermoplastic processing. The most common way is external or physical plasticization with suitable plasticizers like phthalates[1].

For effective foam sheet extrusion using PBAs, CA has to fulfil specific rheological and thermal properties. In particular a specific melt viscosity, melt elongation and melt strength is required for sufficient nucleation, cell growth and cell stabilisation to prevent cell collapse[2,3]. To adjust these requirements, suitable eco-friendly non-toxic plasticizers like citrates can be used.

Experimental

Cellulose acetate was supplied as white powder with a degree of substitution (DS) of about 2,4 and a solubility parameter δ between 22 to 25 $MPa^{1/2}$ [4,5]. Different types of

Table I
Used plasticizers with short characteristics

Plasticizer	Synonym	M_w [g/mol]	δ [$MPa^{1/2}$]	bp [°C]
Acetate-1	CA-A-1	176,17	23,4	259
Acetate-2	CA-A-2	218,21	21,8	260
Benzoate	CA-B	342,39	19,6	232
Citrate	CA-C	276,28	20,9	294
Phosphate	CA-P	326,00	22,2	370

plasticizer in different concentrations (15, 20, 25 wt%) were used (table I).

An internal mixer (Plasti-Corder® Lab-Station, Brabender) with a chamber volume of approx. 370 cm^3 and a kneader temperature of 180 °C was used for compounding. The plasticizer and the CA powder were premixed and then fed into the chamber. After feeding had been completed, mass temperature and torque were measured as a function of mixing time. To minimize the thermo-mechanical induced degradation of CA, the mixing time was fixed at 3–4 min.

The glass transition temperature T_g was investigated from the second heating cycle of DSC measurements with 10 K min^{-1} heating and cooling rate under N_2 atmosphere. The MFR was measured at 230 °C with 5 kg. Melt viscosity was measured with rotational rheometer (cone-plate modus) and capillary viscosimeter (strand die 30/1). Melt strength was investigated with rheotens test. The temperature of the extruder was set from 210 to 220 °C with a throughput of 0,5 kg h^{-1} and a strand die of 30/2.

Results and discussion

For thermoplastic processing of CA, the addition of an appropriate compatible plasticizer is necessary.

With increasing plasticizer content, maximum torque as well as mass temperature decreased considerably (scheme 2). Thus, thermo-mechanical stress decreased, degradation of CA can be minimized and thermoplastic processing at lower temperatures is possible.

The plasticizer efficiency was studied by measuring the glass transition of CA. The data were extrapolated using the Fox-Flory-Equation. With increasing plasticizer content, the T_g decreased significantly (scheme 3). Therefore, melting and thermoplastic behaviour of CA can be improved. The decrease in T_g is a function of plasticizer type and its compatibility as well as mutual behaviour with CA. The use of the Hansen solubility parameter is one option to predict plasticizer miscibility with a polymer[6]. For good solubility, it is generally accepted that $I\Delta\delta I$ ($\delta_{Poly} - \delta_{Plast}$) ≤ 3. However, this is almost a rough estimation as the solubility depends also on functional groups in the molecules and the diffusion behaviour of the plasticizer into the polymer[6].

The rheological properties are very important for effective nucleation, cell growth and foam stabilisation to prevent cell collapse. Therefore melt viscosity, MFR and melt strength were investigated. The melt viscosity decreased considerably in the low shear region due to lower polymer content and more plasticizer-plasticizer as well as plasticizer-polymer interaction leading to higher free volume in the compound[6]. At high shear rates, the concentration influence diminished due to shear thinning.

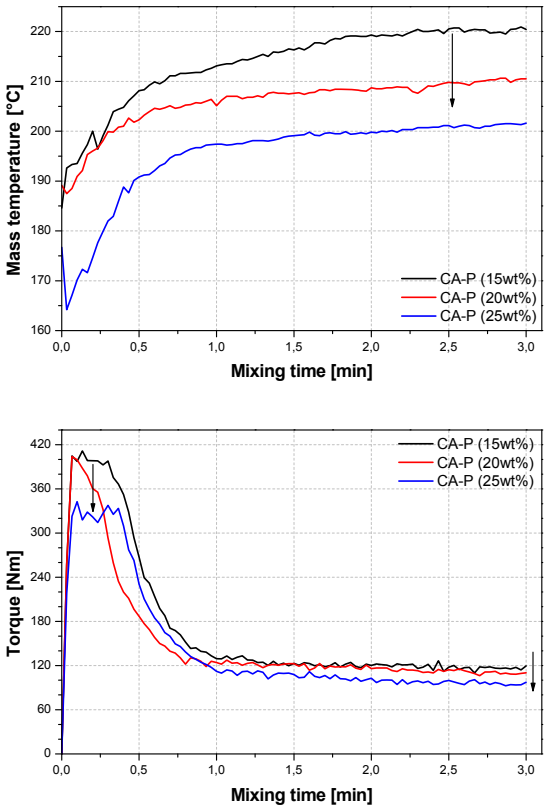

Scheme 2. **Kneader graphs of CA-P as a funcition of plasticizer** content

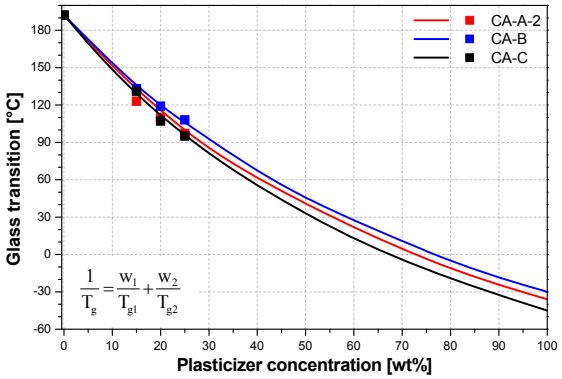

Scheme 3. **Glass transition of selected plasticized CA as a function of plasticizer** type and content (n DSC-data / – Fox-Flory)

As mentioned above, the compatibility between plasticizer and CA has a tremendous influence on the flow behaviour of the polymer (scheme 5).

Generally, the more compatible the plasticizer is with CA, the better the interaction and mutual behaviour. The plas-

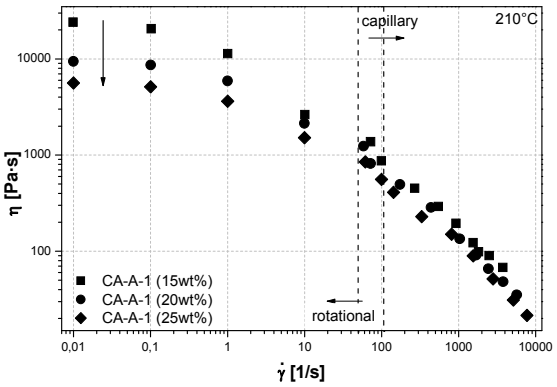

Scheme 4. **Melt viscosity of CA-A-1 as a function of plasticizer content at 210 °C**

ticizer disturbs the structure of loose attachments between polymer chains because of shielding effects and thereby, the intermolecular forces between polymer chains weaken and segmental motion increases[6]. As a result, the free volume increases and improves flow behaviour of CA. The clear increase in MFR with increasing plasticizer content confirms the observed melt viscosity results (Table II).

Melt strength is a key characteristic for stable cell growth. If the melt strength and viscosity is too high, insufficient cell growth occurs due to fast hardening of the melt. If the melt strength is too low, cell collapse (rupture) can occur due to strong biaxial stretching at the growing cell surface. Therefore melt strength was measured with rheotens test. The melt elongation of CA increases significantly with an increase in plasticizer content (scheme 6). The draw resonance (curve oscillation) is diminished compared to lower plasticizer content. Thus, indicating an improvement in melt flowability and melt elasticity with an increase in plasticizer content.

Conclusions

Thermoplastic processing behaviour, rheological and thermal properties of externally plasticized CA were investigated with regards to foam sheet extrusion. Generally, the required properties of CA can be easily adjusted either through plasticizer content or plasticizer type. Plasticizers that are highly compatible with CA lead to higher plasticization effectiveness. Therefore less amount is required to achieve the desired properties.

Further characteristics such as heat conductivity and solubility of different PBAs in externally plasticized CA will be studied in detail. Moreover, foam sheet extrusion tests with different PBAs will be carried out.

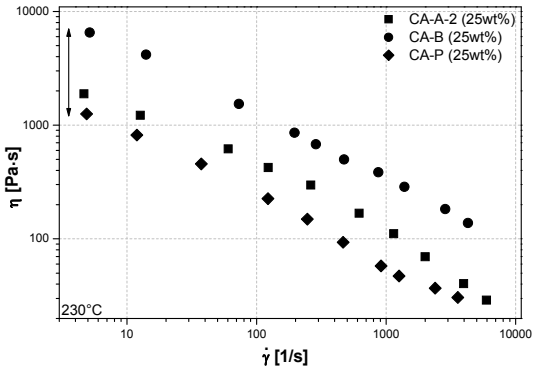

Scheme 5. **Melt viscosity of selected plasticized CA as a function of plasticizer type at 230 °C**

Table II
MFR of selected plasticized CA as a function of plasticizer type and content (230 °C/5 kg)

Compound	15 wt.%	20 wt.%	25 wt.%
CA-A-2	8,0	22,8	50,5
CA-C	4,9	11,4	21,9
CA-P	3,0	4,7	8,2

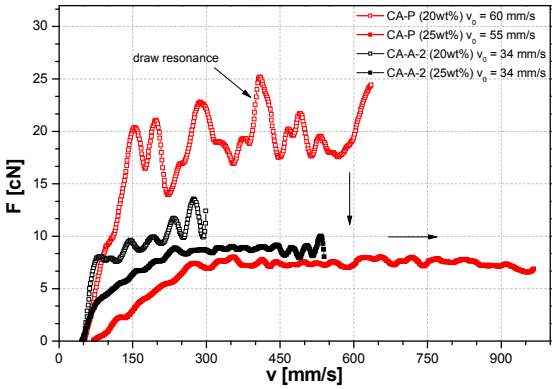

Scheme 6. **Melt strength of selected plasticized CA as a function of plasticizer type and content**

The authors thank the BMELV (federal ministry of food, agriculture and consumer protection) and FNR (agency for renewable resources) for funding the project.

REFERENCES

1. Müller F., Leuschke Ch.: *Organische Celluloseester – Thermoplastische Formmassen*, in: Technische Thermoplaste – Polycarbonate, Polyacetale, Polyester, Celluloseester, Kunststoff Handbuch 3/1, p. 365, Carl Hanser Verlag, (1992).
2. Wang J.: Rheology of Foaming Polymers and its Influence on Microcellular Processing, *PhD Thesis*, (2009).
3. Lee S. T.: *Foam Extrusion – Principles and Practise*, CRC Press, (2000).
4. Hansen C. M.: *Hansen solubility parameters – a user's handbook*, CRC Press, (2000).
5. *Thieme Chemistry: RÖMPP Online Lexikon*, Georg Thieme Verlag, (14.02.2011).
6. Wypych G.: *Handbook of Plasticizers*, ChemTec Publishing, (2004).

POSTERS

P-01
RUBBER FERRITE NANOCOMPOSITES WITH ADAPTIVE PROPERTIES

DENISA BELLUŠOVÁ, MARKUS MÖWES, THOMAS ALSHUTH, and ROBERT H. SCHUSTER*

German Institute of Rubber Technology, Eupener Strasse 33, 305 19 Hannover, Germany
denisa.bellusova@dikautschuk.de

Abstract

In the present work we consider new magnetic field controlled rubber nanocomposite materials prepared by dispersing ultra-fine barium ferrite magnetic particles in polymer matrix based on butadiene rubber. The one of the aims of this work is investigate dispersion of ferrite magnetic particles in butadiene rubber.The silane modification of barium ferrite to achieve better dispersion in rubber matrix was done. The atomic force microscopy and dynamic measurements were used to obtain the results displaying the homogeneity of the magnetoactive elastomers. The influence of testing conditions (with or without magnetic field) on change of the elasticity in a magnetic field is under consideration. It is revealed that the formation of chains of magnetic particles in a magnetic field during samples preparation and testing results in anisotropic nanocomposites with adaptive properties.

Introduction

The new generation of magnetic elastomers and gels represent a new type of composites, consisting of small (mainly nano-and micron-sized) magnetic particles dispersed in a high elastic polymeric matrix. These materials are relatively new and exhibit a great number of fascinating phenomena, which are the subject of intensive theoretical and experimental research. The peculiar magnetoelastic properties may be used to create a wide range of motions and to control the shape change and movement. An understanding of magnetoelastic coupling in polymers will hasten the engineers to develop new type of switches, sensors, micromachines, biomimetic energy transducing devices, and controlled delivery systems[1–4].

Experimental

Barium ferrite (20−60 phr) was embedded in 1.4-cis butadiene as a magnetic filler. The M-type barium ferrite was synthesized from iron and barium chlorides using a chemically reliable co-precipitation method. The introduction of reactive groups onto the magnetic surface was achieved by reaction between silane coupling agent (vinyltrimethoxysilane – Dynasylan 6490 and triethoxy(oktylsilane) – Si208) and the hydroxyl groups on the surface of barium ferrite. The morphology of magnetic powders was studied using a combined field-emission (scanning) transmission electron microscope LIBRA® 120, Zeiss. Magnetic measurements were made using a SQUID magnetometer at 5K. Characterized ferrites powders were incorporated into 1.4-cis butadiene rubber in internal mixer Haake Rheocord System 90 under the following conditions: temperature: 50 °C, rotation speed: 50 min^{-1} and mixing time: 10 min. The elastomers were cured in uniform magnetic field to facilitate the alignment of ferrites particles. For this process, a modified vulcanization press with a magnetic field (applied perpendicular to the plane of vulcanized plate) produced by an electromagnet was used. For the evaluation of the filler-filler interaction, the storage modulus and loss modulus were measured as a function with a Rubber Process Analyser (RPA 2000 – Alpha Technologie) at a temperature 80 °C at strain amplitude from 0.2 to 399 % at 1 Hz. The switching ability of ferrite in silicon oil suspensions was detected using Rotation Rheometer Physica MCR 501 S – Anton Paar with magnetic chamber. The dispersion of the magnetic particles in isotropic and anisotropic magnetoactive composites was observed using high-resolution type of scanning probe microscopy – atomic force microscopy.

Results and discussion

Fig. 1 represents the transmission electron microscope images of the ferrites morphology used for magnetoactive elastomers. The particles of the co-precipitated ferrite were found to be uniform in shape; the majority of them are hexagonal platelet crystals. Whereas the thickness of the ferrite platelets is in the 20–100 nm range, their length ranges from 300 to 400 nm.

The values of the saturation magnetization, the coercive field and the remanent magnetization of the $BaFe_{12}O_{19}$ were found to be M_s = 93.8 emu/g, H_c = 0.335 T and M_r = 44.3 emu/g, respectively.

Non-funcionalizied particles of barium hexaferrite have a tendency to agglomerate (Fig. 1). This tendency can cause poore dispersion in the rubber matrix and a negative influence on the performance of magnetic rubber composites. Function-

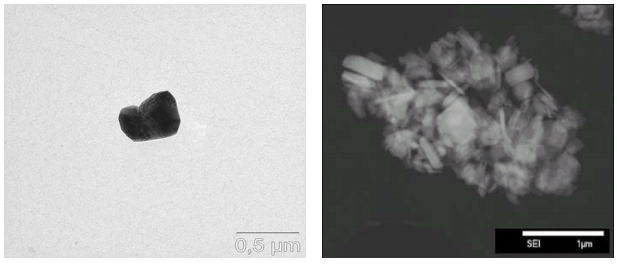

Fig. 1. **TEM images of barium ferrite**

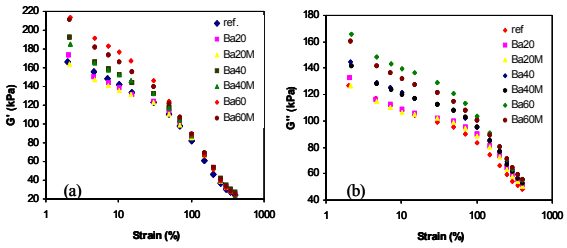

Fig. 2. **(a) The storage modulus and (b) the loss modulus dependency on strain amplitude at 1 Hz frequency of magnetic elastomers with various (0-60 phr) dosage of unmodified and modified (M) barium ferrite with vinyltrimethoxysilane**

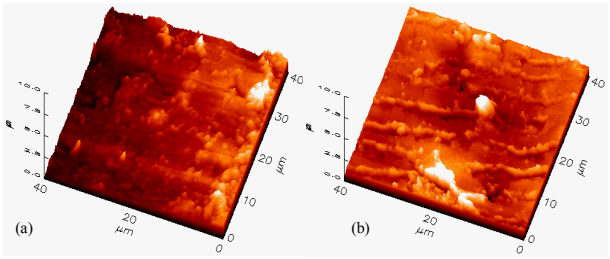

Fig. 4. **AFM images of barium ferrite magnetoactive rubber nanocomposites vulcanized (a) without the presence of the magnetic field, (b) in the presence of the magnetic field**

alization of ferrite particles should be helpful to improve the dispersion of ferrite and enhance the interface interaction of ferrite and matrix. The filler-filler interactions can be seen directly from the dynamic-mechanical properties. (Fig. 2) An increasing dosage of magnetic filler in the butadiene matrix causes an increase of the storage and loss modulus at low strain amplitudes. This behavior seems to be due to hydrodynamic effects at 20 and 40 phr. With higher amounts of ferrite particles 60 phr there seems to be a tendency of the formation of the agglomerates, which results to poor dispersion of the magnetic particles in the rubber matrix. The mixtures with modified barium ferrite show similar viskoelastic behaviour, but there is evident the small improvement approximately 5 % in the dispersion of the modified magnetic particles in the butadiene matrix. Only marginal number of the reactive groups from the vinyltrimethoxysilane were absorbed on the surface of barium ferrite, but the particle size of the barium ferrite is much larger than the small molecules of silane and therefore it is assumed that reaction of silane reactive groups with hydroxyl groups on the surface of barium ferrite was realized.

The rheological and dynamic mechanical properties of composite materials consisting of magnetically active particles strongly depend on the orientation of the magnetic particles. From the Fig. 3 is evident the dependency of the magnetic particle orientation and the switching ability of barium ferrite in silicon oil on the presence and absence of magnetic field.

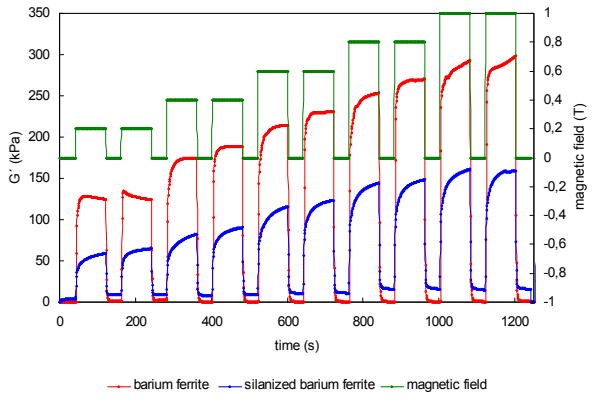

Fig. 3. **Switching ability of the modified (Silane Si208) and unmodified barium ferrite silicon oil suspensions in apllied magnetic field (0-1T)**

The unmodified barium ferrite formed great agglomerates and was insufficiently dispersed in silicon oil. The storage modulus shows the higher value in comparision with silane Si208 modified barium ferrite, which was better dispersed due the functionalization.

Fig. 4 shows atomic force images of rubber ferrite nanocomposites vulcanized (a) without the presence of the magnetic field, (b) in the presence of the magnetic field. In the absence of an applied magnetic field the magnetic moments are randomly oriented and thus the composites has no magnetization.The application of the magnetic field during the vulcanization shows the evidently influence on the particles alignments. Magnetization during the vulcanization leads to the formation of the columnar structure of the magnetic particles in elastomer matrix.

Particles are aligned and fixed to the direction of the applied magnetic field. The anisotropic magnetoactive elastomer with adaptive properties was obtained.

Conclusions

The samples of hard magnetic barium ferrite prepared by using co-precipitation technique showed a high degree of purity and hexagonal structure. Barium ferrite form strong and developed agglomerates. By applying an alkyl chains on the ferrite surface the inter-particle interactions are reduced and the filler dispersion improved. The modified barium ferrite particles with vinyltrimethoxysilane have lower tendency agglomerate, the filler-filler interactions are smaller and therefore the storage modulus and loss modulus of the rubber ferrite nanocomposites demonstrate a steady decrease. The switching ability and the feasibility of barium ferrite controlled orientation in applied magnetic field give us opportunity to prepare the rubber magnetoactive nanocomposites with anisotropic and adaptive properties.

REFERENCES

1. Farshad M., Benine A.: Polym. Test *23*, 343 (2004).
2. Zrínyi M.: Colloid Polym. Sci. *27*, 98 (2000).
3. Zhou G. Y., Jiang Z. Y.: Smart Mater. Struct. *13*, 309 (2004).
4. Bernadek S.: Appl. Phys., A *68*, 63 (1999).

P-02
POLYMER BLENDS BASED ON POLYMERS FROM RENEWABLE RESOURCES

FRANTIŠEK BENOVIČ , KATARÍNA TOMANOVÁ, MIROSLAVA PAVLAČKOVÁ, and PAVOL ALEXY

Ústav polymérnych materiálov, Fakulta chemickej a potravinárskej technológie, Slovenská technická univerzita, Radlinského 9, 812 37 Bratislava, Slovak Republic
frantisek_benovic@stuba.sk

Introduction

Bioplastics represent a relatively new class of biodegradable polymers for industrial applications. Polyhydroxyalkanoates (PHAs) represent one important class of biodegradable polymers. The most common member of the PHAs, poly (3-hydroxybutyrate) (PHB), has several properties such as the melting point and the crystallinity which are similar to the conventional polymer polypropylene (PP). On the other hand it is stiff and brittle which can be for same applications disadvantageous. To improve the mechanical properties the preparation of copolymers and blends of PHB has been proposed[1].

Blending techniques are promising approach which can improve the original properties of the polymers, including biopolymers like PHB.

This study is focused on research of preparation of ternary blends based on polylactic acid (PLA), polyhydroxybutyrate (PHB) and thermoplastic starch (TPS). In this work an influence of thermoplastic starch on properties of PLA/PHB blends was studied. Design of experiment method was used for basic investigation. Influence of blend composition on properties of PLA/PHB/TPS blend was described. Experiments for investigation of interaction TPS/PLA as well as TPS/PHB were realised for better understanding of relations in the multicomponent blend of three polymers and two plasticizers. Conclusions and recommendations for solving of application of TPS in blends containing PHB were done based on results obtained in the presented work.

Experimental

Materials

Polylactic acid (PLA) from NatureWorks LLC, US Tm : 173–178 °C , Tg : 50–80 °C
Polyhydroxybutyrate (PHB) from Biomer, Germany Tm : 168–172 °C
Natural starch from Amylum Slovakia, Slovakia pH : 6,7
Triacetin (TAC) used as PLA plasticizer density : 1,155 g cm^{-3}, boiling point : 258 °C
Glycerin (GL) from H. C. I. Slovakia, used as starch plasticizer

PLA/PHB/TPS blends preparation

We used twin-screw extruder, with parameters L / D = 40, D = 16 mm for polymer mixtures preparation. We set the next temperature profile on twin-screw extruder (in the direction from feeder to die): 140 – 150 – 160 – 160 – 160 – 160 – 160 – 155 – 150 – 140 °C. Screws speed was 100 rpm. Extruded blends were cooled down with cold water and then they were granulated.

PLA/PHB/TPS films preparation

PLA/PHB/TPS films were made using single-screw extruder (d = 19 mm, L/D = 25) with chill-roll technology. Temperature profile during films extrusion was set on 150–160–170–170 °C in the direction from feeder to die and screw speed was 30 rpm. The test pieces in form of strips used for tensile test were cuted in the longitudinal direction, 15 mm wide.

Measurement of mechanical and rheological properties

Tensile strength at yield (σy), tensile strength at break (σb) and the elongation at break (εb) were measured using Zwick machine according to ISO 527. Cross-head speed was 1 mm/min in the deformation range 0–3 % and above 3 % of elongation the speed increased up to 50 mm min^{-1}.

For measurement of rheological properties we used oscillating rheometer RPA 2000 from Alpha Technologies Company. We took deformation test, wich ran at a constant oscillation frequency of 50 CPM, while the oscillation angle varied from 0 to 60°. Measuring chamber had biconical shape. Weight of the sample was 4 grams.

Results and discussion

Based on our previous experiences, we decided to examine the possibilities of application of plasticized starch (TPS) in a mixture of PLA / PHB / TAC which gives material with good mechanical properties at the level of tensile strength at break of 15–30 MPa and the elongation at break 200 % depending on the plasticizer content.

We used in our work Design of Experiment method (four-factor, five level) with following ratios as factors: x1 = PLA/PHB, x2 = TPS/(PLA/PHB), x3 = GL/TPS, x4 = TAC/(PLA+PHB). TPS is natural starch plasticized with glycerol. After preparation of all blends and samples, the ANOVA and regression analysis were done for all measured properties. Based on evaluation of σb results it can be said, that the tensile strength at break is influenced only by factors x2 and x4 (the ratio of starch to both polymers (PLA and PHB) and plasticizer content – triacetin). Others two factors have no statistically significant effect on tensile strength. Response surface is shown on Fig. 1. σb at lower values of x2 strongly decreases with increasing of TAC portion while at higher content of starch this depency is not significant. Increasing content of starch causes decreasing of σb if TAC content is at the lowest level in oposit to its increasing if TAC content is at the highest level. These effects are given by significant interaction between factors x1 and x2.

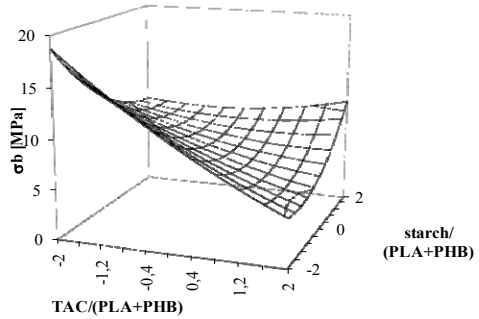

Fig. 1. **Response surface for dependency of tensile strength at break on the ratios starch / (PLA + PHB) (factor x2) and TAC / (PLA + PHB) (factor x4) at a constant level factors x3 = 0 (the ratio GL / starch) and x1 = 0 (ratio of PLA / PHB)**

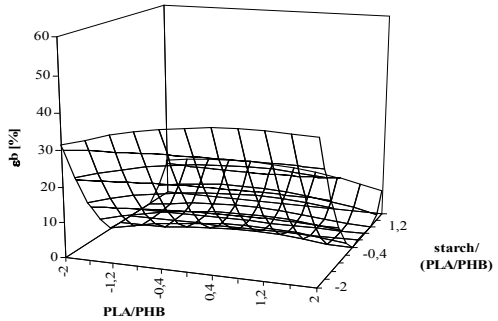

Fig. 2. **Response surface for dependency of elongation at break on the ratio of PLA / PHB (factor x1) and starch / (PLA / PHB) (factor x2), at constant levels of factors x3 = 0 (the ratio GL / starch) and x4 = 0 (the ratio of TAC / (PLA + PHB))**

In contrast to σb, εb is influenced by all four factors. The strongest effect on εb exhibit factor x2 (starch content), which logically reduce this property (Fig. 2). Significancy of others factors on εb is not clearly visible on response surface because the effect of x2 factor is several times stronger than others.

It is necessary to say that the absolute values of mechanical properties were much lower as it could be assumed on the basis of the values of mixtures of PLA / PHB / TAC without starch. Based on our previous experiences as well as based on literature, the glycerol in TPS was identified as a substance which causes deterioration of properties of PLA/ PHB/TPS blends. It was assumed that glycerol causes degradation of PHB in the blend and degraded PHB causes decreasing of mechanical properties of the material. For confirmation of this assumption we tried to prepare four blends with composition according to Table I.

All dry blends of composition according to Table I were processed on twin screw extruder. Only blend 1 (glycerol free) was able to create strand at extruder die, the others blends had very low viscosity and after cooling down they were very brittle. Therefore no samples for mechanical properties measurements were prepared and only viscosity was measured using oscillation rheometer. Obtained results in form of flow curves are shown in Fig. 3.

Table I
Composition of PHB/TAC/GL blends

No.	PHB [wt.%]	TAC [wt.%]	GL [wt.%]
1	85	15	0
2	80	15	5
3	75	15	10
4	70	15	15

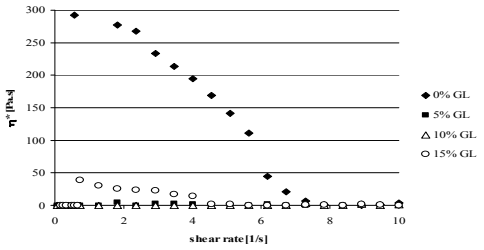

Fig. 3. **Dependency of viscosity of the mixture of PHB / TAC / GL on shear rate at different glycerol content**

The viscosity of PHB/TAC without GL is low in principle, but already addition of 5 % of glycerol reduces its viscosity practically to zero. Based on these results the glycerol was confirmed as substance which accelerates thermal degradation of PHB during its processing in the melt. Therefore the other plasticiser for starch has to be finding for application of TPS in the PLA/PHB blends.

Conclusion

The blends PLA/PHB/TAC/GL were prepared according to five level four factor experimental design. The absolute level of mechanical properties was very low. The accelerated degradation of PHB during blend processing in the melt was found as the main reason of this effect. Based on the rheological measurements it was confirmed that the presence of glycerol in TPS is the factor which accelerate thermal degradation of PHB. The other plasticiser for starch has to be used for application of TPS in the PLA/PHB blends.

This project is supported by Norwegian Financial Mechanism, Financial Mechanism of EEA and State budget of Slovakia – project No. SK 0094.

REFERENCE

1. Vogel Ch., Hoffmann G., Siesler H.: Vib. Spectrosc. *2009*, 284.

P-03
ABRASIVE RUBBERS WEAR DURING GRINDING

ONDŘEJ BÍLEK and DAVID SÁMEK

Tomas Bata University in Zlín, Faculty of Technology, DPE, nám. T. G. Masaryka 5555, 760 01 Zlín, Czech Republic
bilek@ft.utb.cz

Grinding historically belongs to the oldest machining methods. It is widely used whenever higher precision of size, shape or surface quality is demanded. Furthermore, the grinding is applied in machining of material that cannot be machined by other methods or the grinding is more profitable than other methods. The importance of the grinding has increased from the original field of finishing operations to the production machining field due to high-performance grinding tools development[5].

Grinding offers higher final precision of products while at the same time the surface is made up and the tools are sharpened. Grinding materials can be used either in the powder form or various wheels or bars. Separation of chips is similar to the chips separation during milling. Despite the milling cutter the edges of grinding wheel made of grains of grinding material. These grains are statistically dislocated around the tool circumference and they have unequal geometry of the edge. Cutting resistance during grinding is higher than during milling, because cross sections of the cut chips are small[3].

The main problem in understanding the friction properties of rubber materials in machining is the fact that there does not exist adequate, widely applicable and clearly expressed law of rubber friction. However, there are known models of the basic friction behavior and the basic process of abrasive wear of the tires[4]. Another problem is the inaccuracy of the terminology used to describe friction processes. This problem probably originated from a general tendency to denote all the ratios of the gearing force to the normal force as the friction of coefficients, no matter if there is a slip or not[2].

There is no rubber, which would show high friction on all surfaces in all conditions. The influence of the base polymer and additives on the friction properties depends on many factors determining the character of the process of sliding, such as the second surface material, type of lubricants and load.

Table I
Rubber compounds used for test samples

Rubber – recipe marking	Rubber type	Phr	Vulcanization conditions [°C min^{-1}]
275	SBR	100	150°C/20´
346	IIR	100	170°C/60´
733	CR	100	150°C/20´
T 317	NR+BR	85+15	160°C/16´
TP 44	SBR+IIR+BR	70+15+15	160°C/16´
9341-358	NBR+CIS+BR	50+10+7	160°C/10´

This paper focuses on the dynamic monitoring of machinability of rubber materials. There were investigated following parameters: the after grinding surface quality depending on cutting parameters and components of cutting forces during grinding. The experiment aims to determine the effect of cutting conditions during grinding on the investigated parameters, if it is assumed the reversed process of abrasive wear of rubber by analogy for example to prepare before the tire retreading.

Six rubber mixtures and pure rubber were used for the test samples preparation. They are all listed in the Table I. Then, these mixtures were processed by twin cylinder mixing mill. After that, required amount of mixture was prepared using blanker. This operation was followed by vulcanization in the mold under defined conditions, i.e. temperature and time. The clamping force of the press was 120 MPa.

Fig. 1–2 describe the surface quality after the grinding of the given rubber materials both in the longitudinal direction (Fig. 1), consistent with the traverse velocity vector, and in the transverse direction (Fig. 2), perpendicular to the traverse velocity vector. To emphasize the differences in the behavior of different rubber compounds the results are given for a maximum speed of the traverse and maximum cutting depth, i.e. a_e = 0,04 mm, v_f = 23 m min^{-1}. The experiment shows that the surface roughness using 30P 8V 99A wheel reaches lower values of roughness parameters in the transverse direction than the longitudinal direction. What is more, in all cases the material 9341-358 has the lowest surface roughness of all used materials. When using a wheel of a type 49C 120J 12V, we can state the lowest values of surface roughness in the transverse direction of all the types of wheels, which could be caused by grain fineness of wheel.

During the cutting forces evaluation, when the feed rate was raised and depth of cut remained constant a_e = 0,01 mm, the continuous rise of cutting forces (both the component *Ff* and *Fp)* was observed. The increasing cutting depth caused non-uniform rise of the cutting forces. However, as can be seen in Figure 3, the components of cutting forces due to hyperelastic behavior of materials are decreasing for certain rubber materials. Growth in components of cutting forces can be observed with increasing depth for the types of wheels 30P 8V 99A, 99A and 49C 80i 8V 12V 120J.

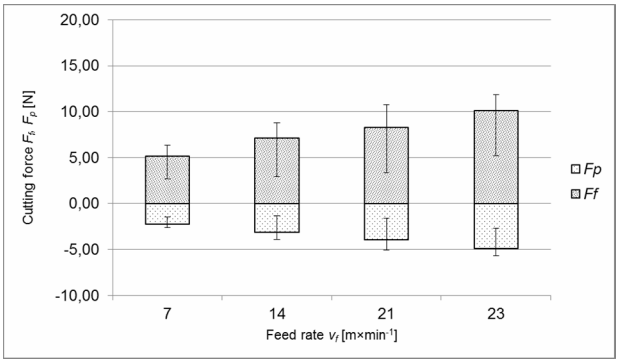

Fig. 1. **The dependence of components of cutting forces on the feed rate, material TP44, grinding wheel 49C 120J 12V**

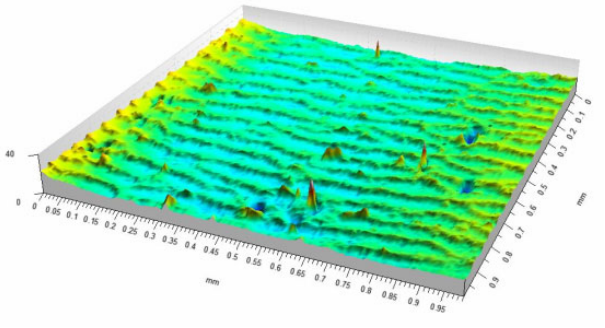

Fig. 2. **Spatial surface quality evaluation of material 9341-358, grinding wheel 49C 60K 9V, a_e= 0,04 mm, v_f = 7 m min^{-1}**

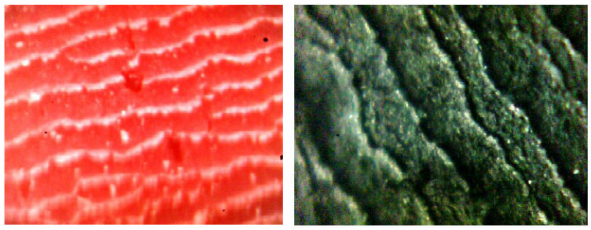

Fig. 3. **Microscopic observation (50x) of the surface waves for materials 9341-358 and 733**

By the surface observation using digital microscope ProScope HR there was found for some types of materials formation of the characteristic waves that may be considered Schallamach waves. This characteristic shape is due to the friction surface of a soft elastomer on solid surface. The interface is often dominated by the occurrence and distribution of elastic instabilities in the form of surface waves. The presence of these waves can lead to significant changes in friction characteristics. The Schallamach waves are composed of small regular fractures (layers) across the direction of feed[1]. The Schallamach waves are formed on the elastomer, when the hard body, or in this case the grinding tool, moves across the surface of the elastomer by critical speed.

This work was supported by the Ministry of Education, Youth and Sports of the Czech Republic under the grant MSM 7088352102. This support is gratefully acknowledged.

REFERENCES

1. Barquins M.: Wear *1993*, 160.
2. Matula L.: *Dynamic machinability of rubber materials using grinding*, UTB Zlín, (2010).
3. Kundrák J., Zebala W., Bana V.: Manuf. Technol. *2003*, 3.
4. Lukovics I., Sýkorová L.: *Determination of grinding wheels cutting property for high performance grinding*. Tools 99, Zlín 1999.
5. Madl J., Jersak J.; Holesovsky F.: *Quality of machined surfaces*. UJEP Ústí n. Labem 2003.

P-04
MANUFACTURING OF THERMOPLASTICS AND CHIP FORMATION

ONDŘEJ BÍLEK, IMRICH LUKOVICS, and LUBOŠ ROKYTA

Tomas Bata University in Zlín, Faculty of Technology, DPE, nám. T. G. Masaryka 5555, 760 01 Zlín, Czech Republic
bilek@ft.utb.cz

Separation of chips in chip working methods is a very complicated process; its course depends on many factors, especially on the physical properties of the machined material and its dependence on plastic deformation conditions. It is characterized by a high local shear stress in the order of 10^5 MPa, a high speed of shearing deformation (10^3–10^5 s^{-1}), interaction of the tool with the newly created surface that is chemically active; comparatively high number of tool and geometry parameters, which can significantly change the cutting process; structurally metallurgical parameters of the machined surface that can influence its behaviour against material of the cutting tool[2].

The cutting process is realized in a machine-workpiece-tool system with the machined surface parameters being the most important output. From this point of view, problems of identified chip formation and its technological characteristics plays an important role. Theoretical and experimental studies of these materials are usually done for a case of orthogonal cutting. Elastic and plastic deformations in the take-off layer result at the point of cutting; there is primary plastic deformation in front of the tool edge and secondary plastic deformation occurs in surface layer of the chip in connection with the tool face[3]. There is an outer load that affects the take-off layer and causes tension in this layer at relative motion of the tool against the workpiece. A field of deformation narrows with the increase of the cutting speed. As a result, angle of plastic and elastic deformation plane grows. At high cutting speed the mentioned angles virtually coincide and it can be thought that the chip is formed by plastic slip in the shear plane of which position is defined by the shear plane angle ϕ.

It is desirable to achieve a continuous chip flow while machining to prevent the generation of heat and deformation of the workpiece. To achieve this it is necessary to machine by tool with critical or a large rake angle, which ensures that

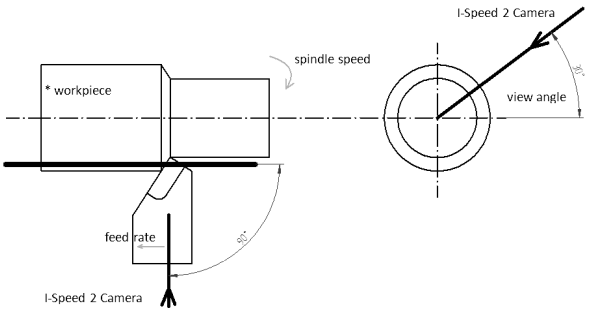

Fig. 1. **Simplified model of chip formation in the take-off layer at orthogonal cutting – view into the work plane**

the chip will generate a continuous chip with minimal surface distortion[4]. Selection of cutting conditions is also very important. In particular, the size of the chip per tooth is determined by the feed rate. Cutting conditions, allowing the increase of depth of cut should be chosen on the ground to reduce heat generation in the material.

An example of turning PA6 material is set in Fig. 1. Conditions of experiment were: workpiece diameter 44 mm, revolutions per minute 630 min^{-1}, feed rate 0,2 mm, depth of cut 1 mm a geometry of cutting tool (SCLCR1616H09) κ_r = 45°, γ_o = 0°, λ_s = 0°. Chip formation was recorded highspeed camera Olympus I-Speed2 with recording rate 5000 frames per second. At the beginning of the experiment, the chip starts to break after a while. It might be explained by low temperature at the point of cutting. In the next phase (Fig. 2), the chip is long and turns into a regular spiral.

Grinding thermoplastics is difficult because of their low melting temperature, resulting in the clogging of surface grinding wheel. It is recommended to use a grinding wheel with more open spaces between the grains and a low level, together with the excessive amount of coolant to prevent overheating and clogging the grinding wheel[1].

For example, Kobayashi[5] recommends grinding wheel 38A46F12V for grinding polystyrene. Generally, materials hard to grind are grinded by finer grit wheels and a soft materials are grinded by coarse grained grit wheels. The author recommends usage of wheels with a grain size 54 for thermosets and 46 for thermoplastics. Cutting speed has strong influence on the selection of a suitable grinding wheel degree. It is known that the cutting speed is higher, the finer the grinding wheel should be. In the case of thermosets should be chosen the "F" degree of hardness and the "G" degree of hardness for thermoplastic. The reason is the relationship between a higher ratio of peripheral speed and cutting speed during grinding thermoplastics than thermosets.

Most of the machined technological materials are crystallic materials, especially metals, due to their chemical composition, mechanical and physical properties, method of production (thermal or mechanical machining) and structure. Literature describes theory of metal machining in details; on the other hand, machining of plastics is partly neglected despite having several specialties. Plastics have small values of cutting resistance that decrease with a heat generating at machining. Next, they are characterized by low thermal conductivity. Therefore the heat is not conducted by the machined material or the chip but almost fully absorbed by the tool that is significantly heat loaded. This causes rapid tool wear at

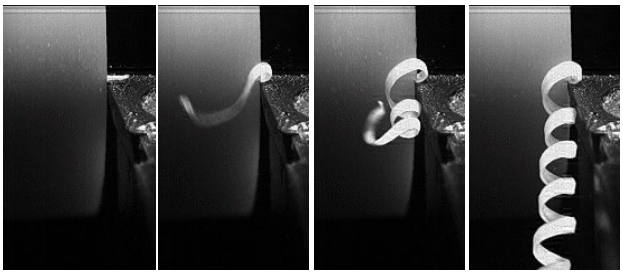

Fig. 2. **Stages of chip formation by turning of PA6**

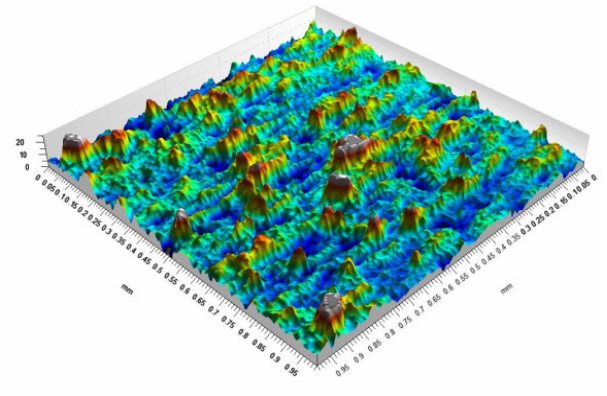

Fig. 3. **Spatial analysis of grinded surface, grinding wheel A99 60J 12V V, PP material**

machining of soft plastics. In comparison to steel, multiple thermal expansion of plastics induces considerable changes of part dimensions during or just after machining. Very hard plastics (phenols, polyesters and plastics with fillers) substantially wear out the tool by abrasion so that it is necessary to machine them by tools with sintered carbides. Plastics without mineral fillers can be machined by tools made of high-speed steel.

Evaluation of 3D structure of grinded surface of samples using Talysurf CLI 500 was carried out under the cutting conditions a_e = 0.01 mm, steel a_e = 0.04 mm and feed rate v_f = 7 m min^{-1}. The size of the investigated area was 1 × 1 mm.

Fig. 3 can identify cut tops for PP material caused by the poor reflectivity of the material. Comparison of 2D microsurfaces for material PP and steel shows Fig. 4.

Based on measured data statistical model of behavior was developed. As dependent variables were chosen depth of cut a_e, feed rate v_f and grain type of grinding wheel. Obtained results from the software STATISTICA7 show that: feed rate at least affects roughness parameters, the correlation coefficient between *Ra* and *Rz* is statistically significant at $p<10^{-3}$, the correlation coefficient r = 0.97.

Roughness parameter *Ra* does not significantly affect these parameters and combinations: feed rate; material (only PA6GF30); type of grain * material (only PA6GF30).

Roughness parameter *Ra* significantly affects these parameters and combinations: depth of cut; type of grain; mate-

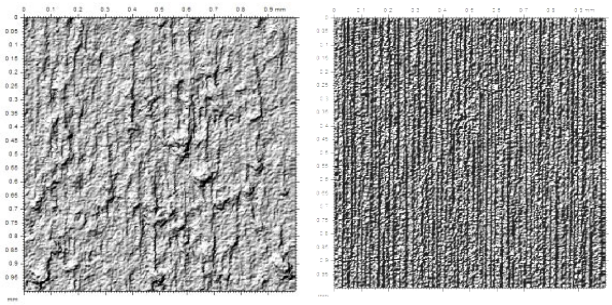

Fig. 4. **2D surface cutout, grinded material PP -left and steel 1.0060 (E335) -right, grinding wheel A99 60J 12V**

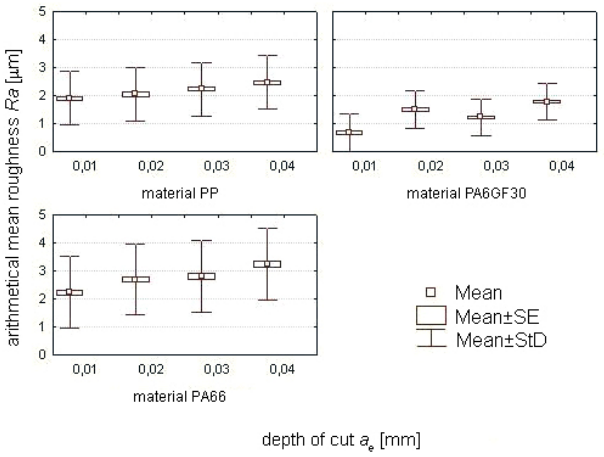

Fig. 5. **The dependence of roughness parameter *Ra* at a depth of cut during grinding of thermoplastics**

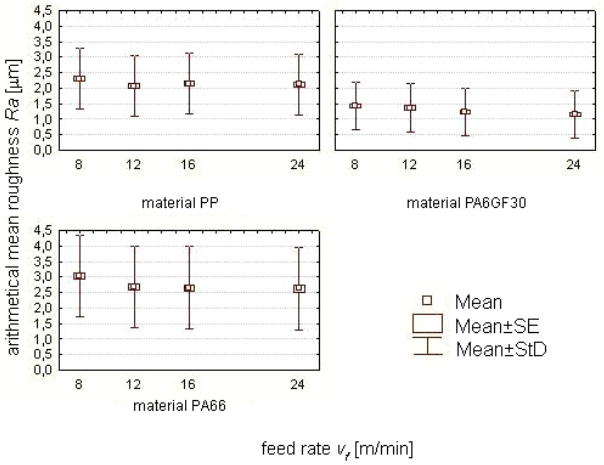

Fig. 6. **The dependence of roughness parameter *Ra* at a feed rate during grinding of thermoplastics**

rial; type of grain * material.

The results are presented in the box plots, Fig. 5 to 6.

This work was supported by the Ministry of Education and Youth of the Czech Republic under grant MSM 7088352102.

REFERENCES

1. Kolář D.: *Correlation between grinding wheel topography and surface quality*, UTB Zlín, 2010.
2. Kocman K., Prokop J.: *Special technology – Machining*. Učební texty Vysokých škol, VUT Brno, 2003.
3. Neslušan M., et. al.: *Experimental Methods in Chip Working Methods*. Žilinská univerzita v Žiline, 2007.
4. König W.: *Fertigungsverfahren*, Band 2. VDI-Verlag, Düsseldorf 1980.
5. Alauddin M., Choudhury I. A., et al.: *Plastics and their machining: a review*. JMPT, 5, 40–46, 1995.

P-05

IMPROVEMENT OF HOMOGENEITY OF NR/NBR RUBBER BLENDS

S. H. BOTROS*, A. F. MOUSTAFA, and S. A. IBRAHIM

National Research Center, Polymers Department, Dokki-12622, Cairo, Egypt
botros-1@hotmail.com

Abstract

The graft copolymerization of acrylonitrile (AN) onto natural rubber (NR) was carried out in toluene at 80 °C, using dibenzoyl peroxide (BPO) as initiator. The synthesized acrylonitrile-grafted-natural rubber (NR-g-AN) was characterized by FT-IR/Raman spectroscopy and N % elemental analysis. The NR-g-AN was incorporated into natural rubber/ butadiene acrylonitrile rubber (NR/NBR) blend with different ratios, where the homogeneity of such blends was examined with scanning electron microscopy (SEM) and differential scanning calorimetry (DSC). The scanning electron micrographs illustrate improvement of the morphology of NR/NBR rubber blend as a result of the incorporation of NR-g-AN onto that blend. DSC traces exhibits $T_{g's}$ transitions shift of NR and NBR in their blend indicating some degree of compatibility. Thermal stability of the homogeneous and inhomogeneous rubber blend vulcanizates was investigated by determination of the physico-mechanical properties after and before accelerated thermal aging. NR/NBR (50/50) blend possesses the best thermal stability.

Introduction

Blending of two incompatible polymers yields a material with poor mechanical properties. The physico-mechanical properties of such blends can be significantly improved by the addition of suitable compatibilizing agent. The degree of compatibility of the two individual components plays an essential role in the applicability of the final product in industry. Acrylonitrile–butadiene rubber (NBR) has a very good resistance to hydrocarbon oil. High degree of hydrogen bonding and polarity of NBR can be adjusted, depending on acrylonitrile content, to suit the applications of final rubber products; the greater the acrylonitrile content the higher the oil resistance[1–3]. Due to molecular restriction, the glass transition temperature (T_g) of NBR shifts to higher temperature when AN content is increased. Due to the absence of strain-induced crystallization, unfilled NBR vulcanizate suffers from its low mechanical properties. In contrast, natural rubber (NR) is a non-polar rubber which has very good mechanical properties as a result of formation of strain-induced crystallization at high deformation strains. Compared to NBR, NR is less expensive and, therefore, a blending of NR with NBR is usually carried out for cost reduction of the final products requiring inherent NBR properties[4,5]. According to the solubility parameters values of NR and NBR obtained using Joel Hildebrand equation[6,7].

$$\partial = \sqrt{C} = \sqrt{(\Delta H - \frac{RT}{Vm})}$$

Where C is the cohesive energy density, ΔH is the heat of vaporization, Vm is the molar volume, R gas constant and T is the temperature in Kelvin; NR and NBR are immiscible at all blend ratios because they are 10 units apart in the ∂ scale. The way to overcome this miscibility problem is either to chemically bond the two phases which will hinder the elasticity of the system or by using a compatibilizing agent, which can stabilize one phase into the other by lowering the interfacial tension. Many authors[8–12] have used grafted rubber to ease the blending of other rubbers. Poly (acrylonitrile-co-methyl methacrylate-co-styrene) has successfully been used as compatibilizer for NBR rubber blend[13]. From our previous work[14] non-polar rubber (EPDM) grafted with poly (acrylonitrile) and/or poly (acrylic acid) were proven to act as good compatibilizers for NBR rubber blends. Also, EPDM has been grafted with maleic anhydride (MAH) by mechanical method. The resulted MAH-g-EPDM has successfully been used in our laboratories[15] as compatibilizer for NR blend. In the present article, grafting AN onto NR was carried out to obtain a system of two far distinct solubility parameters; NR (∂=8.5) which is identical to NR and the other AN (∂= 21.5) is close to NBR (∂ = 18.5).

The application of NR-g-AN as a compatibilizer for NR/NBR blend is discussed. The Physico-mechanical properties of the blends are evaluated after and before accelerated thermal aging.

Experimental

Materials

Acrylonitrile monomer a product of Merck, Darmstadt, Germany, was purified with vacuum distillation. Benzoyl peroxide, a product of Acros, New Jersey, USA, was re-precipitated from chrorofrom twice. Toluene, chloroform and methanol products of El Nasr Chemical Company, Cairo, Egypt, were used as received. Dimethylsulfoxide, acetone, anhydrous sodium sulfate products of Riedel de Haën, Seelze, Germany, were of analytical grade and used as received. Natural rubber (smoked sheets) of 48 Mooney viscosity [ML (1+4) 100 °C] is a product of Malaysia. NBR (Krynac 3450) of 34 % acrylonitrile content and 50 Mooney viscosity [ML (1+4) 100 °C] is a product of Bayer Company, Leverkosen, Germany.

Techniques

SYNTHESIS OF NR-g-AN Grafting of AN onto NR was carried out in 2L nitrogen flushed three-neck round bottom flask, using a mechanical stirrer at 500 rpm. One liter NR/toluene solution (10 g L^{-1}) was introduced into the reaction vessel and heated up to 70 °C, then BPO (2.06 mmol) was added. Forty mL AN (603 mmol) was added to the reaction medium within 60 minutes in a step-wise manner; in order to avoid crosslinking. The copolymerization reaction mixture was stirred for 330 min. The reaction product was precipitated overnight in methanol, decanted and washed several times with methanol. NR-g-AN was purified from poly acrylonitrile homopolymer by being dissolved in THF and precipitated in DMSO twice. The precipitate then rinsed with water as well as methanol several times and finally dried in vacuum oven at 40 °C for 7 days.

Characterization

NR-g-AN was characterized by means of the following techniques:

1. FT-IR Spectrophotometer (Nicolet, Nexus 821, Madison, USA) was used in order to assign the characteristic peaks. The grafted rubber sample, for this test, was prepared by swelling followed by dissolution of 2 g NR-g-AN in 20 mL toluene. One drop of the concentrated solution resulted was spread over the KBr disc.
2. DSC (Shimadzu, DSC-50, Foster City, CA, USA), was used to determine the glass transition temperatures. The T_{gs} are kept from second scan.
3. Elemental Analyzer (Perkins-Elmer, Elementar, Hanau, Germany) was used to determine the nitrogen content in the grafted rubber prepared.

Scanning electron microscopy

Scanning microscopy was conducted in order to investigate the morphology of NR/NBR rubber blends in presence and absence of SBR-g-AA, with the aid of scanning electron microscope, Model JSM-T20, JEOL, Technics Co. Ltd., Tokyo, Japan, at magnification M=500X.

Mixing and vulcanization

NR, NBR and NR/NBR rubber blend mixes with different blend ratios (75/25, 50/50, 25/75) were prepared in presence and absence of SBR-g-AA on an open two roll-mill of 170 mm diameter and 300 mm working distance at 24 rpm speed of slow roll and gear ratio of 1:1.25 at 70 °C. NR-g-AN was first mixed with NR then NBR was added onto the mill followed by the rubber compounding ingredients. The rheometric characteristics were assessed with a Monsanto Oscillating Disc Rheometer R-100 at 152 ± 1 °C according to ASTM D 2084-95 (1998). The formulations and the rheological properties of rubber mixes are listed in Tables I and II. The rubber mixes were then cured in a hydraulic press at the same temperature.

Rubber testing

The physico-mechanical properties of rubber vulcanizates were determined with a Zwick-1425 tensile tester according to ASTM D412-98a (1998). Accelerated thermal aging of rubber vulcanizates was carried out in an air circulated electric oven at 90 °C according to ASTM D573-88 (1994). It should be noted that the results are taken in five replicates.

Results and discussion

Inhomogeneous NR/NBR blends

It is obvious from Table I that the minimum torque increased as the NBR content increased. Also, NBR and NBR rich blend possess longer cure time ($tc90^{o}$) and lower cure rate index; this can be attributed to acrylonitrile plastic portion of NBR. The rubber mixes were then vulcanized at their cure

times. Physico-mechanical properties of NR, NBR and their blends with different blend ratios were measured and listed in Fig. 1. Tensile strength and elongation at break of NR are the highest and those of NBR are the least. However tensile strengths and elongation at break of the blends show irregular pattern as NBR content increases in the blends; this can be attributed to the incompatibility of NR and NBR. The rubber vulcanizates under investigation were subjected to thermal aging accelerated. The physico-mechanical properties were determined after thermal aging for different periods up to 7 days. Fig. 2 illustrates that tensile strengths of NR and NR rich blend decrease dramatically upon thermal aging whereas NBR shows thermally stable tensile strength but with low values. NBR rich blend possesses high tensile strength values with thermal stability up to 4 days of aging; thereafter it shows low values indicating low thermal stability. However, NR/NBR (50/50) rubber blend shows good thermally stable tensile strength with good values. Elongation at break (Fig. 3) of NR and NR rich blend shows dramatic decrease upon thermal aging. However NBR and NBR rich blends show thermally stable elongation at break up to 4 days of aging, thereafter they show low thermal stability. On the other hand NR/NBR (50/50) blend shows thermally stable elongation at break over the whole range of aging periods. Tensile strength and elongation at break of the rubber vulcanizates, obtained after 7 days of aging, are plotted vs. NBR content in the blend (Fig. 4). Tensile strengths and elongation at break of the blends show irregular pattern for all rubber vulcanizates as NBR content increases in the blends It is clear that the best tensile strength together with good elongation at break are shown with NR/NBR (50/50) blend after aging for 7 days.

Table I
Formulations and rheological properties of NR/NBR rubber blends with different blend ratios

Ingredients, phr.	S1	S2	S3	S4	S5
NR	100	75	50	25	0
NBR	0	25	50	75	100
Zinc oxide	5	5	5	5	5
Stearic acid	2	2	2	2	2
Silica	20	20	20	20	20
Carbon black	20	20	20	20	20
Processing oil	5	5	5	5	5
*CBS	1	1	1	1	1
Sulfur	2	2	2	2	2
Rheological properties					
Minimum torque, Nm.	1	3	3.5	4	5
Maximum torque, Nm.	48	56	56	59	55
Scorch time (ts**2**), min.	4.5	3.75	4	4.25	4.75
Cure time (tc**90**), min.	10	10	10	13	18
Cure rate index, min^{-1}.	2.1	1.9	1.9	1.8	2

**N*-cyclohexyl-2-benzothiazole sulfenamide

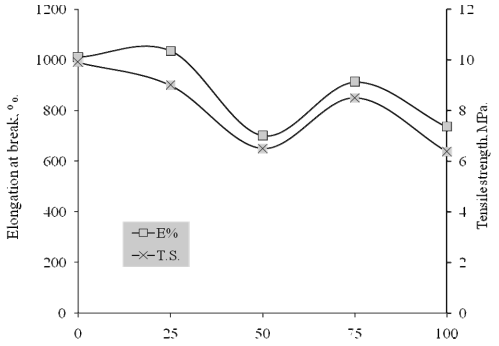

Fig. 1. **Tensile strength and elongation at break of NR/NBR blend vulcanizates vs NBR content in the blend**

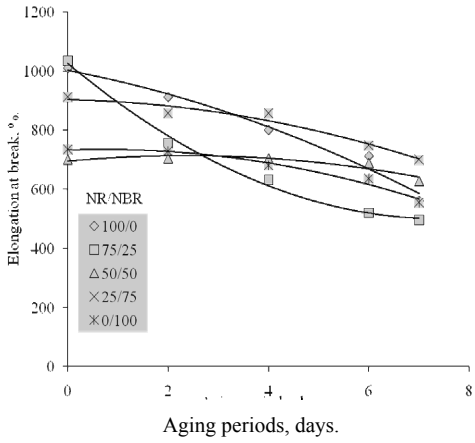

Fig. 2. **Tensile strength of NR/NBR blend vulcanizates vs aging periods, at 90 °C**

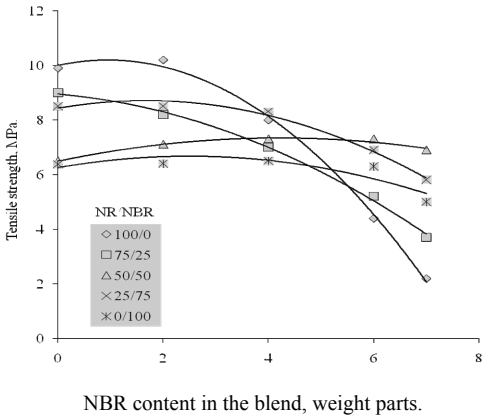

Fig. 3. **Elongation at break of NR/NBR blend vulcanizates vs aging periods, at 90 °C**

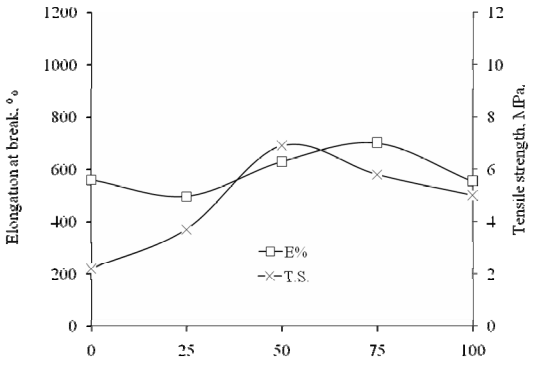

Fig. 4. **Tensile strength and elongation at break of NR/NBR blend vulcanizates vs NBR content in the blend after aging for 7 days at 90 °C**

Grafting of acrylonitrile onto NR

Fig. 5 shows the graft copolymerization of AN onto NR conversion- time curve as a function of N %. The induction period of the graft copolymerization is quite low ~ 30 minutes. The conversion to NR-g-AN increases with time without any aspect of leveling off (plateau) up to 6 hrs; this can be explained in terms of the high concentration of AN (603 mmol L^{-1}) and the huge number of double bonds in the high NR molecular weight chains. The probability of achieving high molecular weight of grafted polyacrylonitrile segment is quite sure very low; due to solubility problems of NR-g-AN obtained[14].

Elucidation of NR-g-AN structure

Fig. 6 shows the FT-IR spectrum of AN-g-NR. The spectrum shows the characteristic groups (CH_3, CH_2, C=C) of NR at 1376, 1452 and 1666 cm^{-1} respectively, and the characteristic (-C°N) group of NR-g-AN at 2240 cm^{-1}. The peak at 1715 cm^{-1} is attributed to the carbonyl group of the BPO initiator. The peak at 1770 cm^{-1} is attributed to (C=N) group which results from the interaction of benzoate group with the cyanide group[14]. The weak intensity of the nitrile group is attributed to the low concentration of NR-g-AN subjected to IR beam.

Homogeneity of NR/NBR blend

Uncured NR/NBR (50/50) blends with and without NR-g-AN (10 phr) were prepared. The micrograph (Fig. 7a) of the blend, without NR-g-AN, illustrates two different phases for the individual rubbers indicating phase separation and inhomogeneity of NR/NBR blend. However, the micrograph (Fig. 7b) of NR/NBR blend containing NR-g-AN shows one phase and no phase separation takes place indicating a change in morphology and enhancement of homogeneity of NR/NBR blend. This can be a result of co-continuous phases where both NR and NBR form continuous phase after addition of NR-g-AN. DSC technique was used to detect qualitatively the homogeneity of NR/NBR blends. Figure 8 a, b illustrates the DSC traces of NR/NBR (50/50) blends with and without NR-g-AN. The $T_{g's}$ of NR and NBR in their blend appear at −76.2 °C and −39.9 °C respectively with T_g difference of 36.3 °C. However, the $T_{g's}$ of NR and NBR in their blend with NR-g-AN appear at −75.3 °C and −42.6 °C respectively with T_g difference of 32.7 °C. These data illustrate that $T_{g's}$ of NR and NBR became closer to each other upon incorporation of NR-g-AN. This can be attributed to the reduction of interfacial energy and to the increase of adhesion between phases. Therefore, NR-g-AN succeeds to improve homogeneity of NR/NBR blend.

Homogeneous NR/NBR blends containing NR-g-AN

Physico-mechanical properties of the rubber vulcanizates (formulations and rheological properties are listed in Table II) were measured and plotted vs. NBR content in the blend as shown in Fig. 9. It is obvious that tensile strength and elongation at break of the rubber vulcanizates lie on straight lines upon incorporation of the NR-g-AN indicating that those values follow the linear relation of additive rule. The rubber vulcanizates were then subjected to thermal aging accelerated. Physico-mechanical properties of the rubber vulcanizates were measured and plotted vs. aging periods. Fig. 10 illustrates that the tensile strengths of the NR and NR rich blend decrease dramatically upon thermal aging. NBR and NBR rich blend possess thermally stable tensile strength with moderate values. However, NR/NBR (50/50) blend possesses excellent tensile strength values but with low thermal stability. Also, the elongation at break (Fig. 11) of NR and NR rich blend decreases dramatically with aging periods and possesses the least values. The elongation at break of NBR and NBR rich blend decreases with aging periods but with higher values. However, NR/NBR (50/50) blend shows good elongation at break values with low thermal stability. The elongation at break and the tensile strength results confirm one another. The tensile strength and the elongation at break of NR/NBR blend vulcanizates containing NR-g-AN were plotted vs. NBR content in the blend after aging for 7 days at 90 °C, as shown in Fig. 12. It is clear that the tensile strength and the elongation at break values show straight lines and follow the additive rule (desirable phenomenon); this behavior can be attributed to the improvement in the

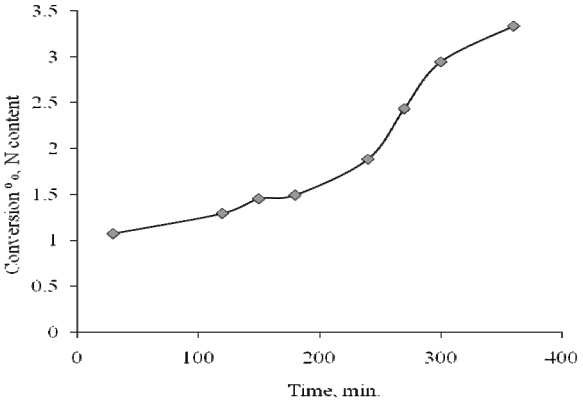

Figure 5. Conversion-time curve of graft copolymerization of acrylonitrile onto natural rubber.

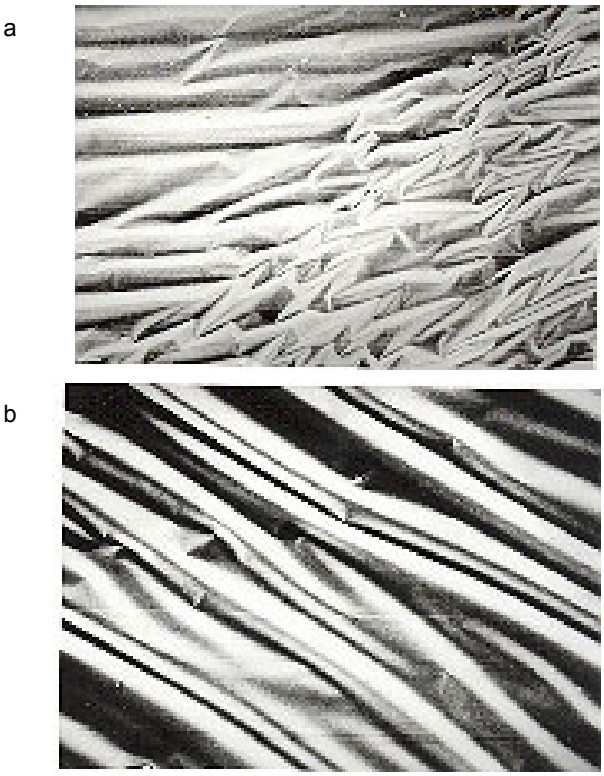

Fig. 7. **SEM micrographs of NR/NBR blend;** (a) Uncompatibilized, (b) Compatibilized with AN-g-NR, M=500X

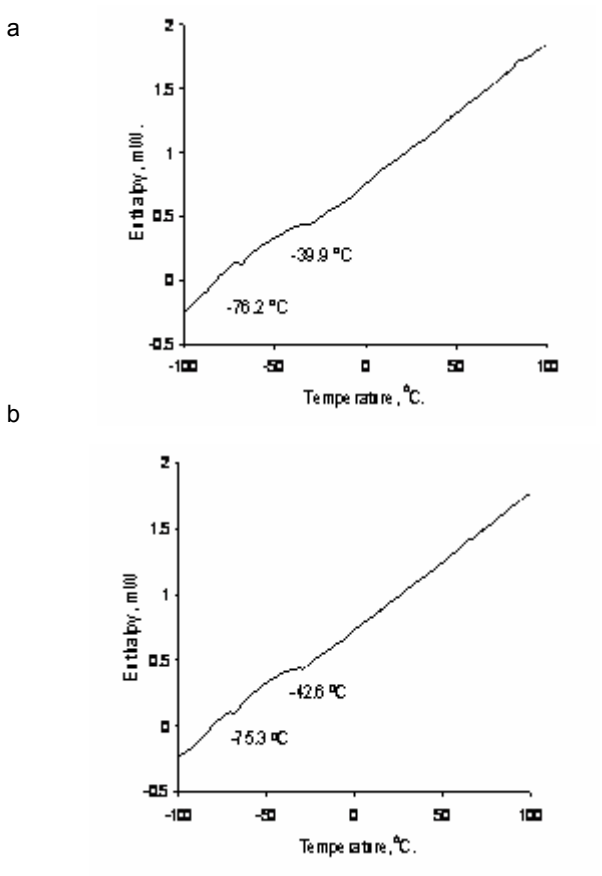

Fig. 8. **DSC traces of NR/NBR rubber blends,** (a) Compatibilized blend, (b) Uncompatibilized blend.

homogeneity of NR/NBR blends upon incorporation of NR-g-AN. In addition the best mechanical properties are possessed with NR/NBR (25/75) blend, after thermal aging.

Conclusions

1. The percentage grafting of AN onto NR continuously increase with time without any aspect of leveling off.
2. Incorporation of NR-g-AN into NR/NBR blend improves the blend morphology as shown from SEM micrographs.
3. $T_{g's}$ shifts of NR and NBR in their blend confirm some degree of NR/NBR homogeneity as seen from the DSC traces.
4. Of the entire blend ratios examined NR/NBR (25/75) rubber blend containing NR-g-AN possesses the best thermal stability together with good physico-mechanical properties.
5. The physico-mechanical properties of NR/NBR homogeneous blends follow the additive rule, after and before thermal aging for 7 days at 90 °C.

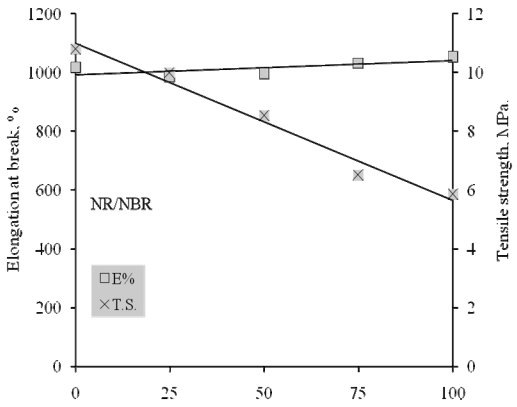

Fig. 9. **Tensile strength and elongation at break of NR/NBR blend vulcanizates compatibilized with AN-g-NR vs NBR content in the blend**

Table II
Formulations and rheological properties of NR/NBR rubber blends compatibilized with AN-g-NR

Ingredients, phr.	S6	S7	S8	S9	S10
NR	100	75	50	25	0
NBR	0	25	50	75	100
AN-g-NR	10	10	10	10	10
Zinc oxide	5	5	5	5	5
Stearic acid	2	2	2	2	2
Silica	20	20	20	20	20
Carbon black	20	20	20	20	20
Processing oil	5	5	5	5	5
*CBS	1	1	1	1	1
Sulfur	2	2	2	2	2
Rheological properties					
Minimum torque, Nm.	2	3.5	4	4.6	6
Maximum torque, Nm.	50	58	58	61	57
Scorch time (ts2), min.	3.75	3.5	3	4	4.75
Cure time (tc90), min.	9	8	8	11.5	22
Cure rate index, min^{-1}.	2.1	1.8	1.85	1.8	2

**N*-cyclohexyl-2-benzothiazole sulfenamide

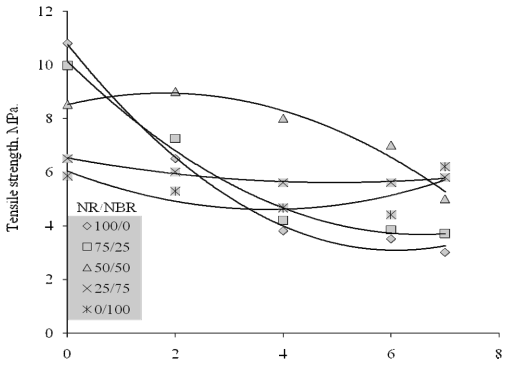

Fig. 10. **Tensile strength of NR/NBR blend vulcanizates compatibilized with AN-g-NR vs aging periods, at 90 °C**

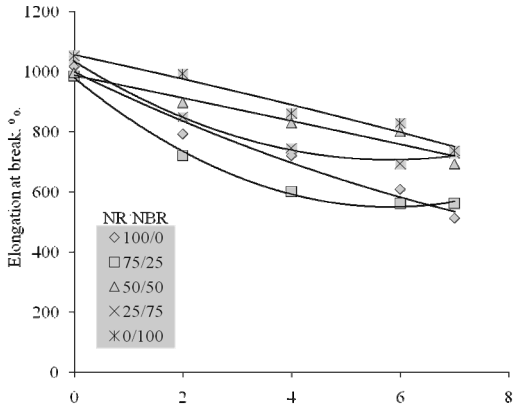

Fig. 11. **Elongation at break of NR/NBR blend vulcanizates compatibilized with AN-g-NR vs aging periods, at 90 °C**

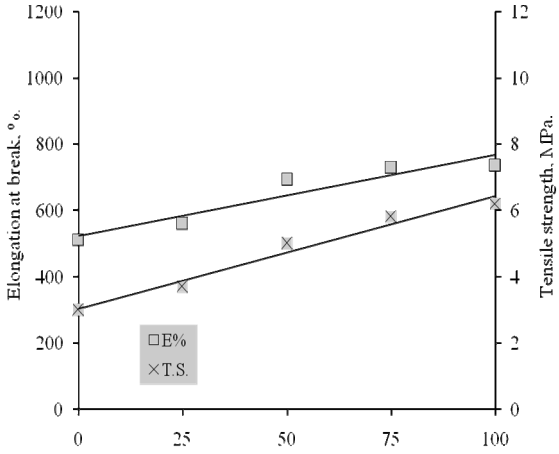

Fig. 12. **Tensile strength and elongation at break of NR/NBR blend vulcanizates compatibilized with AN-g-NR vs NBR content in the blend after aging for 7 day at 90 °C**

REFERENCES
1. Kantalaa C., Wimolmala E., Sirisinha C., Sombatsompop N.: Polym. Adv. Technol. *20*, 448 (2009).
2. Sirisinha C., Baulek-Limcharoen S., Thunyarittikorn J.: J. Appl. Polym. Sci. *82,* 1232 (2001).
3. Sirisinha C., Limcharoen S., Thunyarittikorn J.: J. Appl. Polym. Sci. *89*, 1156 (2003).
4. Tinker A. J.: *Blends of Natural Rubber with Specialty Synthetic Rubbers, in Industrial Composites Based on Natural Rubber*. Malaysian Rubber and Development Board, Kuala Lumpur, 1998, 103–113.
5. Sirisinha C., Sae-oui P., Guaysomboon J.: J. Appl. Polym. Sci. *90*, 4038 (2003).
6. Brandrup J., Immergut E. H.: *Polym Handboo*k 3rd Ed., 1989. Wiley Interscience Publication copyright by John wiley & Sons Inc.
7. Barton A. F. M.: in *Handbook of Solubility Parameters and Other Cohesion Parameters*, 2nd Ed., 1983 chapter 13, 14, CRC Press, Boca Raton 1983.
8. Ao Y., Tang K., Xu N., Yang H., Zhang H.: Polymer Bulletin *59*, 279 (2007).
9. Nakason C., Pechurai W., Sahakaro K., Kaesaman A.: Polym. Adv. Technol. 16, 592 (2005).
10. Derouet D., Tran Q. N., Leblanc J. L.: J. Appl. Polym. Sci. *112*, 788 (2009).
11. Brosse J. C., Campistron I., Derouet D. : J. Appl. Polym. Sci. *7*8, 1461 (2000).
12. Chuayjuljit S., Moolsin S., Potiyaraj P.: J. Appl. Polym. Sci. *95*, 826 (2005).
13. Botros S. H, Moustafa A. F.: J. Appl. Polym. Sci. *89,* 3143 (2003).
14. Botros S. H., Moustafa A. F.: J. Elastomers Plastics *34*, 15 (2002).
15. Botros S. H.: Polym-Plast Technol. Eng.41, 341 (2002).
16. Moustafa A. F., Fang Z., Kennedy J. P.: Polymer Bulletin *48*, 225 (2002).

P-06
POLYMER-BASED COMPOSITES FOR MINIMIZATION OF EMI IN AUTOMOBILE ELECTRONIC SYSTEMS

RASTISLAV DOSOUDIL*, MARIANNA UŠÁKOVÁ, and JOZEF SLÁMA

Slovak University of Technology, Faculty of Electrical Engineering and Information Technology, Department of Electromagnetic Theory, Ilkovičova 3, 812 19 Bratislava, Slovakia
rastislav.dosoudil@stuba.sk

Abstract

FeSi/PVC composite materials with different filler concentrations (10, 20, 30, 40, 50 and 60 vol.%) were prepared using a dry low-temperature hot-pressing process (at 135 °C and 5 Pa) and the electromagnetic wave (EM-wave) absorption properties have been investigated by means of a oaxial S-parameter method in the frequency range from 1 to 3000 MHz. The return loss (RL), matching frequency (fm), matching thickness (dm), and the bandwidth (_f) for RL ≤ −20 dB were numerically simulated by a simple program. Decreasing the FeSi content in the composite, the matching frequency increases, the matching thickness decreases and the band width enlarges. Compared with spinel ferrite/polymer absorbers, the absorbers with conductive magnetic filler have better absorbing properties, such as a thinner matching thickness and a wider EM-wave bandwidth.

P-07
PLASTICIZERS INFLUENCE ON PHYSICAL-MECHANICAL PROPERTIES AND DMTA OF RUBBER MIXTURES – PART A

JANA ĎURFINOVÁ[a] IGNÁC CAPEK[b] IVAN CHODÁK[b], AREK LIŠKA[c] PAVEL KOŠTIAL[d] MÁRIA CHROMČÍKOVÁ[c], PETER POČAROVSKÝ[a], JANKA JURČIOVÁ[e], MARTINA ŠARLAJOVÁ[a], IVAN RUŽIAK[d], ZORA JANČÍKOVÁ[d], MILADA GAJTANSKA[f], andMICHAL LACKO[a]

[a]Slovak university of technology in Bratislava, The Faculty of Chemical and Food technology,Radlinskeho 9, Bratislava 812 37, [b] Slovak Academy of Sciences, Institute of Polymers, Bratislava 812 37, [c] Vitrum Laugaricio – Glass competency center - ÚACh SAV, TnU AD, FChPT STU, RONA, a.s., Študentská 2, 911 50 Trenčín, Slovak Republic, [d] VŠB-Technical university of Ostrava, Faculty of Metallurgy and Material Engineering, 17. listopadu 15/2172, 70833 Ostrava-Poruba, Czech Republic, Department of Materials Engineering, [e] Saar Gummi Slovakia spol. s r.o., Gumárenska 397/21, Dolne Vestenice 972 23, Slovak Republic, [f] Department of Physics, Electrical Engineering and Applied Mechanics, Faculty of Wood Science and Technology, Technical University in Zvolen T.G.Masaryka 24, 960 53 Zvolen, Slovak Republik
pavel.kostial@vsb.cz

Abstract

Present trend in the field of chemistry technology is to replace plasticizers based on high-aromatic oils for other type of plasticizers, because high-aromatic oil contains polycyclic aromatics which are carcinogen. This replacements are mainly because of ecological and economical reason.

The use of plasticizers in rubber is very old. They are added into the rubber mixtures to reduce the friction at the system or improve other characteristics like adhesiveness, elasticity, resistance of ozone, frost and flammability resistance. The oleic acid and oleylamine are useful as potentional plasticizers for rubber mixtures. To improve observed mainly physic-mechanical properties of cured rubber mixtures we also used these plasticizers in combination with emulgators Triton 405, Tween 40 and Etoxon AF5. We compared changes in cured butadiene styrene rubber (SBR) mixture properties with basic plasticizers and plasticizers with emulgators by using the dynamic mechanical thermal analysis DMTA.

TMA measures material deformation changes under controlled conditions of force, atmosphere, time and temperature. The Q400 features the standard mode, offers all the major TMA deformation modes necessary to characterize a wide range of materials such as solids, foams, films and fibers. These include expansion, penetration, compression, tension and three point bending, while the Q400EM additionally offers stress /strain, creep, stress relaxation, dynamic TMA and modulated TMA modes. We used TMA for characterization of fillers influence on thermal and physical properties.

1. Introduction

Knowledge of the chemical resistance of materials to their environment is critical as their failure leads to downtime for the system and increased maintenance costs, as well as fire and safety hazards. The changes in weight, hardness, mechanical properties and glass transition temperature Tg are used to assess and understand the effect of plasticizers on the properties of the elastomers[1].

The aim of this work is to produce a rubber mixture with optimized plasticizer composition. Since the usage of plasticizers is improving the mechanical and physical properties of composites it is expected that the ideal composite will obtain maximum E' in the dynamic mechanical testing[2].

Thus, it is felt important to look into the composites performances related to their dynamic mechanical thermal properties that can be studied via dynamic mechanical testing. This test measure the response of a material to a sinusoidal stress which posses valuable structural information of the plasticizers alone and plasticizers with emulgators systems when they are subjected to dynamic load over a wide range of temperature and frequency[3,4].

The practical importance of the material parameters improvement in post-curing process scenarios must be tested in connection with the complex demands of the customers but DMTA can help to find out optimal post-curing conditions in a short time[5].

The ability to measure both of these moduli enables the full characterization of a viscoelastic material. Increases of tan delta can be due to microscopic factors such as molecular relaxations or macroscopic factors such as phase boundary motion, interfacial failure. It has far greater sensitivity to both macroscopic and molecular relaxation processes than thermal analysis techniques based upon a temperature probe alone[6].

The term "thermal analysis" meant simply heating a sample in a capillary melting point tube to measure the melting point, or incinerating it to measure its ash content[7].

2. Experimental part

Mixtures were prepared by mixing in a two Brabender mixer with chamber of volume 70 cm^3.

Triton, Tween, Etoxon are emulgators. Finally was mixed activator ZnO. Mixtures have been prepared with the standard, which doesn´t contains the oils. Other components in the first instance were constant. In the second mixing step we added curing agent (sulfur) and accelerator to the compound[8, 9].

Measurement of dynamical mechanical properties device for TMA Q400 EM (TA Instruments) were performed on samples with dimensions (30 × 3 × 0.3) mm^3 and over a range of temperature from –60 to 12 °C at frequency 0.5Hz. Prepared samples were measured at heating rate (3 °C min^{-1}) and then at cooling rate (−5 °C min^{-1}). In order to attach the vertical sample during measurement to avoid significant application of viscose flow, were chosen 100 mN static force and dynamic force of 60 mN. Heating rate (3 °C min^{-1}) showed better reproducibility of measurements (in the frequency used), therefore it was applied to other measurements.

Table I
Formulation of the mixture

I. step	dsk
Styrene Butediene Rubber	100
Filler – Starch	40
ZnO	2
Plasticizer	1 and 4 dsk
II. Step	
Sulphur	2
CBS	1,5

3. Results and discussion

3.1 Physical-mechanical properties

Mechanical properties of rubber blends plasticized with the two plasticizers and three emulgators were obtained by tensile test. Mixtures of softened oleic acid achieved comparable strength values of mixtures using oleylamine. The use of ecologic plasticizers showed some changes of physical and

Table II
Mechanical properties for oleic acid blends and standard

	R_m [MPa]	A[%]	Dl[mm]	E_s[MPa]	E_l[MPa]
Oleic acid 4 dsk+1 dsk TWEEN (A4 Tw)	22,64	203	142	2468	480
Oleic acid 4 dsk+1 dsk ETOXON (A4 Et)	21,3	263	149	2437	460
Oleic acid 4 dsk+1 dsk TRITON (A4 Tr)	20	263	183	2156	420
Oleic acid 4 dsk	19,8	272	216	1937	370
Standard	18,7	354	248	312	230
				T_{max}=55	T_{max}=55

Table III
Mechanical properties for oleylamine blends and standard

	R_m [MPa]	A[%]	Dl[mm]	E_s[MPa]	E_l[MPa]
Oleylamin 4 dsk+1 dsk TWEEN (B4 Tw)	22,64	316	148	1812	359
Oleylamin 4 dsk+1 dsk ETOXON (B4 Et)	21,9	324	219	1375	275
Oleylamin 4 dsk+1 dsk TRITON (B4 Tr)	20,7	328	222	1314	265
Oleylamin 4 dsk	20,5	340	238	1312	218
Standard	18,7	354	248	312	230
				T_{max}=55	T_{max}=55

mechanical properties as shown in Tables II and III.

REFERENCES

1. Hiltz J. A., Morchat R. M., Keough I. A., *Defence Research Establishment Atlantic/Dockyard Laboratory, Building D-17*, FMO Halifax, 2001.
2. Gokturk H. S., Fiske G.: IEEE Trans. Mag. *29*, 4170 (1991).
3. Nielsen L. E., Landel R. F.: *Mechanical Properties of Polymers and Composites*. Marcel Dekker, New York 1994.
4. Hamdan S., Hashim D. M. A., Yusop M.: *Dynamic mechanical thermal analysis (DMTA) of thermoplastic natural rubber (TPNR) barium ferrite (BaFe12O19) composites*, 2004.
5. Stark W., Goering H., Michel U., Bayerl H.: *Online monitoring of thermoset post-curing by dynamic mechanical thermal analysis DMTA*, University of Applied Science Aalen, 2009.
6. Wetton R. E., Marsh R. D. L., Van-de-Velde J. G.: *Theory and application of dynamic mechanical thermal analysis*, 2001.
7. Thakhiew W., Devahastin S., Soponronnarit S.: *Effects of drying methods and plasticizer concentration on some physical and mechanical properties of edible chitosan films,* 2010.
8. Kovářová M.: *Pomocné zpracovatelské přísady v gumárenském průmyslu-using processing additives in rubber chemistry*, SPUR a.s. Zlín, 1999.
9. Gonhard N., Guilbert S. and Cuq J. L.: J. Food Sci. *58*, 206 (1993).
10. Cherian G., Gennadios A., Weller C., Chinachoti P.. *Cereal Chem*, 72, 1 (1995), p. 1–6.
11. Pouplin M., Redl A., Gontard N.: J. Agric. Food Chem. 47, 538 (1999).

P-08

PLASTICIZERS INFLUENCE ON PHYSICAL-MECHANICAL PROPERTIES AND DMTA OF RUBBER MIXTURES – PART B

JANA ĎURFINOVÁ[a], IGNÁC CAPEK[b], IVAN CHODÁK[b], MAREK LIŠKA[c], PAVEL KOŠTIAL[d], MÁRIA CHROMČÍKOVÁ[c], PETER POČAROVSKÝ[a], JANKA JURČIOVÁ[e], MARTINA ŠARLAJOVÁ[a], IVAN RUŽIAK[d], ZORA JANČÍKOVÁ[d], PAVOL ŠVEC[f], and MICHAL LACKO[a]

[a] Slovak University of technology in Bratislava, The Faculty of Chemical and Food technology,Radlinskeho 9, Bratisava 812 37, [b] Slovak Academy of Sciences, Institute of Polymers, Bratislava 812 37, [c] Vitrum Laugaricio – Glass competency center - ÚACh SAV, TnU AD, FChPT STU, RONA, a.s., Študentská 2,SK - 911 50 Trenčín, Slovak Republic, [d] VŠB-Technical university of Ostrava, Faculty of Metallurgy and Material Engineering, 17. listopadu 15/2172, 70833 Ostrava-Poruba, Czech Republic, Department of Materials Engineering, [e] Saar Gummi Slovakia spol. s r.o., Gumárenska 397/21, Dolne Vestenice 972 23, Slovak Republic, [f] Department of Physics, Electrical Engineering and Applied Mechanics, Faculty of Wood Science and Technology, Technical University in Zvolen T.G.Masaryka 24, 960 53 Zvolen, Slovak Republik
pavel.kostial@vsb.cz

Dynamic mechanical thermal analysis

The properties obtained from the dynamic mechanical thermal analysis are the storage modulus (E'), loss modulus (E˝) and tan delta (tan delta) that is recorded as a function of temperature in range between (−60 °C) and 12 °C. Temperature dependences of storage modulus are shown in Fig. 1,2.

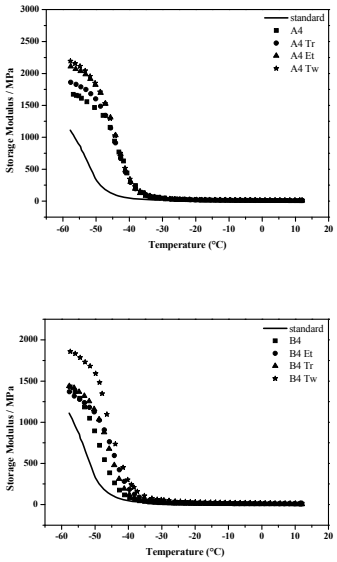

Fig. 1,2. **Temperature dependence of storage modulus for oleic acid and oleylamine blends**

These measurements have been confirmed and the results for storage modulus E´ of blends containing plasticizer oleic acid 4dsk, oleic acid with triton, tween, etoxon and standard are shown in Table II. In Table III are shown results for storage modulus E´ of blends containing plasticizer oleylamine 4 dsk, oleylamine with triton, tween, etoxon and standard.

Isochronal loss curves at a frequency of 0,5 Hz are shown in Fig. 3,4 for blends with oleic acid and oleylamine. The curve clearly shows maximal peak at temperature of glass transition.

The behavior of an amorphous polymer, since the decrease in the storage modulus and the peak in the tanδ corresponds to a typical transition from a glassy to a rubbery state[11, 12].

According to the tanδ plot, the Tg of plasticizers of first part in figure 5 can be estimated at –37,5 °C for A4 Tr and A4 Tw; –37 °C for A4 Et and –35,5 °C for A4.

Values of Tg for oleylamine blends are –41 °C for B4; –39,5 °C for B4 Et and B4 Tw and (–39 °C) for B4 Tr. Thus, there are few differences between these two plasticizers alone and with emulgators at the same weight concentration.

The highest values of Storage and Loss of modules were obtained in the chronological order (see Tables II, III). From results can be seen that for both types of plasticizers used, we reached the same sequence. For increasing storage and loss modules, we noticed increase in tensile strength. The results show that storage modulus increased significantly in mixtures prepared with emulgators, Tween especially reached the highest values for both types of plasticizers.

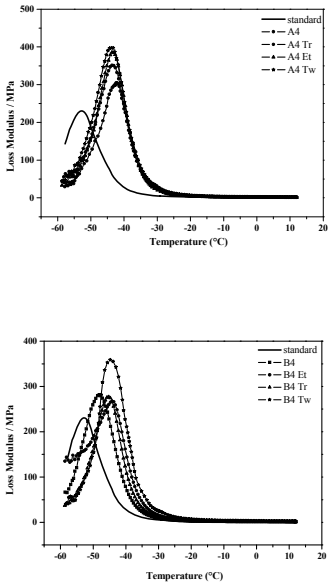

Fig. 3, 4. **Temperature dependence of loss modulus for oleic acid and oleylamin blends**

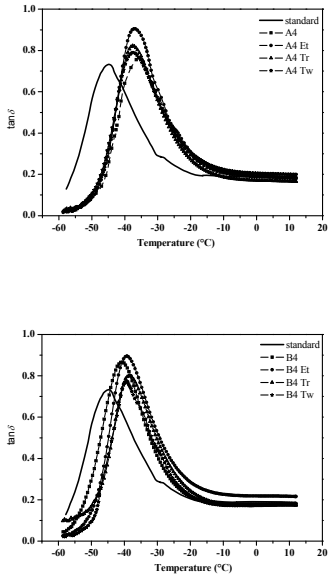

Fig. 5,6. **Temperature dependence of tanδ for oleic acid and oleylamin blends**

Table IV
Determination of the dynamic loss - tangent delta

	T (max tgδ)	max tgδ	Tgδ (-25 °C)	Tgδ (0 °C)	Tgδ (60 °C)
A4	–35,50	0,76	0,40	0,19	0,11
A4 Tr	–37,50	0,81	0,38	0,17	0,10
A4 Et	–37	0,91	0,43	0,19	0,11
A4 Tw	–37,50	0,79	0,44	0,22	0,14
B4	–41	0,87	0,26	0,18	0,12
B4 Tr	–39	0,80	0,31	0,16	0,10
B4 Et	–39,50	0,90	0,36	0,22	0,15
B4 Tw	–39,50	0,77	0,29	0,17	0,11
Standard	–45	0,73	0,25	0,20	0,13

Samples denomination:
Standard – mixture without plasticizer A4 – 4 dsk oleic acid
A4 Et – 4 dsk oleic acid + 1 dsk Etoxon
A4 Tr – 4 dsk oleic acid + 1 dsk Triton
A4 Tw – 4dsk oleic acid + 1 dsk Tween
B4 – 4dsk oleylamin
B4 Et – 4dsk oleylamin+ 1dsk Etoxon
B4 Tr – 4dsk oleylamin + 1dsk Triton
B4 Tw – 4dsk oleylaminu + 1dsk Tween

Tan delta at –25 °C is characterized by traction on snow and ice. It is required that the value of tan delta was high. We

may say that higher values are noticed for mixtures with application of organic plasticizer which is oleic acid. From this we can conclude that oleic acid as organic plasticizer could be a substitute for winter tread compound.

Tan delta at 0 °C is characterized by wet traction. It is required that the value of tan delta is high. The highest values were achieved with a mixture of A4 Tw application of oleic acid with Tween surfactants and B4 with Et application with oleylamine surfactant Etoxon. All other mixtures have lower values of tan delta. The lowest value was achieved with a mixture of B4 Tr application with oleylamine surfactant Triton.

Tan delta at 60 °C is characterized by rolling resistance. It is required that the value of tan delta is low. Mixture reached relatively low values. However, the lowest value reached mixture A4 Tr (oleic acid with surfactant Triton) and B4 Tr (oleylamine with surfactant Triton).

Finally, we can say that the mixture that have better values of traction in wet adhesion (A4 Tw and B4 Et) achieve a higher rolling resistance. Lower rolling resistance achieved contrast mixture, which have higher levels of traction on snow and ice. In Figures 5, 6 are the comparison curves of the loss-tangent delta temperature of mixtures.

REFERENCES

1. Hiltz J. A., Morchat R. M., Keough I. A.: *Defence Research Establishment Atlantic/Dockyard Laboratory, Building D-17*, FMO Halifax, 2001.
2. Gokturk H. S., Fiske G.: IEEE Trans. Mag. *29*, 4170 (1991).
3. Nielsen L. E., Landel R. F.: *Mechanical Properties of Polymers and Composites*. Marcel Dekker, New York 1994.
4. Hamdan S., Hashim D.M.A., Yusop M.: *Dynamic mechanical thermal analysis (DMTA) of thermoplastic natural rubber (TPNR) barium ferrite (BaFe12O19) composites*, 2004.
5. Stark W., Goering H., Michel U., Bayerl H.: *Online monitoring of thermoset post-curing by dynamic mechanical thermal analysis DMTA*, University of Applied Science Aalen, 2009.
6. Wetton R. E., Marsh R. D. L., Van-de-Velde J. G.: *Theory and application of dynamic mechanical thermal analysis*, 2001.
7. Thakhiew W., Devahastin S., Soponronnarit S.: *Effects of drying methods and plasticizer concentration on some physical and mechanical properties of edible chitosan films,* 2010.
8. Kovářová M.: *Pomocné zpracovatelské přísady v gumárenském průmyslu - using processing additives in rubber chemistry*, SPUR a.s. Zlín, 1999.
9. Gonhard N., Guilbert S., Cuq J. L.: J. Food Sci. *58*, 206 (1993).
10. Cherian G., Gennadios A., Weller C., Chinachoti P.: Cereal Chem. *72*, 1 (1995).
11. Pouplin M., Redl A., Gontard N.: J. Agric. Food Chem. *47*, 538 (1999).

P-09

EXPERIMENTAL TIRE TEMPERATURE-PRESURE MEASUREMENTS IN REAL DRIVING CONDITIONS- PART A

JANA ĎURFINOVÁ[a], PAVEL KOŠTIAL[b], IVAN RUŽIAK[b], ZORA JANČÍKOVÁ[b], MARTINA FARKAŠOVÁ[b], LUBOŠ KRIŠŤÁK[c], JANKA JURČIOVÁ[d], SOŇA RUSNÁKOVÁ[e], and IVAN LETKO[e]

[a] Slovak University of Technology in Bratislava, The Faculty of Chemical and Food Technology,Radlinskeho 9, Bratisava 912 37, [b] VŠB-Technical university of Ostrava, Faculty of Metallurgy and Material Engineering, 17. listopadu 15/2172, 70833 Ostrava-Poruba, Czech Republic, Department of Materials Engineering, [c] Technical University in Zvolen, Faculty of Wood Science and Technology, T.G.Masaryka 24, 960 53 Zvolen, Slovak Republic, [d] Saar Gummi Slovakia spol. s r.o., Gumárenska 397/21, Dolné Vestenice 972 23, Slovak Republic, [e] Tomas Bata University in Zlín, Faculty of Technology, T. G. Masaryka 275, 762 72 Zlín, Czech Republic
pavel.kostial@vsb.cz

Abstract

In this contribution we present measurements of external and internal tire temperature as well as the internal tire pressure by complex system for the simultaneous contact less measurement of these values (CTPA). The measurement is fully automatic, controlled by a personal computer and installed "*in situ*" on the car. The global position system, which is connected to a *PC*, further allows us to measure also the car speed in synchronized regime with other measured parameters. All external temperatures under investigation were independently tested by other contact thermometers.

Introduction

The measurements of thermal conductivity, heat capacity and thermal diffusivity play an important role in rubber industry, mainly in tire construction, because these values and their changes directly influence the instantaneous value of viscosity, loss factor $tg\delta$ and by means of that the adhesion of tire to a road surface.

Tire is a product constructed from composite material consisting of rubber, textile and metal. Tire deformation (accompanied by hysteresis) and friction create a heat in a tire and its amount depends on many factors such as material properties, pressure and construction, etc.

Smart Tire's light vehicle products[1] are designed to provide accurate and up-to-date tire information at the driver's fingertips and activate an alert or warning when the tire pressure or temperature irregularities are detected.

Another one is the Performance Calculator Tire Temperature Analysis, which provides a handy way to get a quick analysis of the tire temperatures measured from a vehicle[2].

TireChek, a tire pressure monitor is a unique new invention that affords a low cost system for monitoring vehicle tire pressures. If any of the vehicle's tires loses a small amount of

air so that its pressure becomes THREE PSI low, that tire's appropriate under-dashboard mounted red indicator light will flash a warning. The drawing below shows a Deluxe version that includes yellow indicators for ONE PSI low earlier warning[3].

One of the features of "Tire Temperature Analyzer", the software, which uses artificial intelligence to evaluate a large quantity of information and decide what should be changed on the race car to improve the tire temperatures[4].

First, an input of lap times, track surface temperature and air temperature is needed. This allows the software to see if the resulting tire temperatures will be valid representations of the car's performance. You also enter wheel temperatures, hot and cold air pressure and tire circumferences, number of heat cycles, and weight on each tire, which are also evaluated by the software's artificial intelligence[5].

The CTPA measuring system (Complex Temperature – Pressure Analyzer) described in this chapter enables simultaneous measuring of the internal temperature and pressure in a passenger or sports tires. The development of this system was subsequently described in works[6–8].

This system offers the tire constructors "in situ" and "just in time" testing of personal tires in the point of view of real heat generation in a tested tire. In the paper are presented time –pressure – temperature – car velocity results obtained on tires of different producers.

Experimental equipment

Electronic and control system of CTPA consists of three independent measuring loops of measurement (see Fig. 1). First measuring loop represents contact less measurement of the external temperature by sixth pyrosensor type Raytek THERMALERT MID 02. Three sensors are located near each front tire (see Fig. 1a and 1b). Two are close to the tire borders and second one at its centre. The fundamental characteristic of sensors is as follows. Temperature range form –40 to 600 °C, spectral response from8 to 14 μm, response time 150 ms (95 % response), accuracy ±1 % or ±1 °C (±2 °F) whichever is greater.

The internal temperature – pressure sensors serve as tire valves.

Second one is for measuring of internal tire pressure and temperature MTPM-200 (TPMS, Magic Control) with radio frequency data transport from four sensors (MTPM-TX4) located inside each tire. Transmitter frequency is 433.92 MHz, 32-bit ID-code, operating voltage 3 V and operating temperature from –40 to +120 °C.

Third one is a global position system located on the top of the car, which permits the measurement of car velocity and gives thus possibility to create pressure – temperature – velocity dependences. Block schema of whole CTPA is in the Fig. 3.

A notebook, using an assistant hardware and software, does collecting of the measured data from all sensors and GPS, which enable it to gain data and graphic outputs of the dependence of the external and internal temperatures and pressure in dependence on time or on the speed of the car. The measuring is fully automated, without an operator's interference. The computer is supplied with the energy from the car battery through an additional source, which is protected against potential over poling of the source during assembling. Practical testing of CTPA installed on car shown high reproducibility and precision of obtained data tested also by independent contact thermometers.

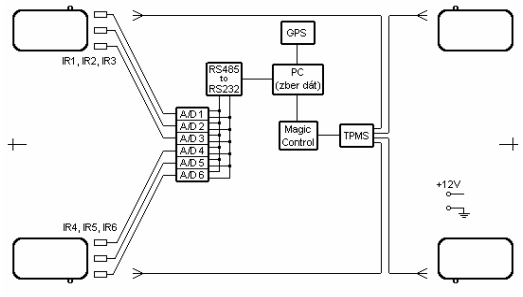

Fig. 3. **The block schema of CTPA**

Results and discussion – part A

External temperature was measured on left and right wheel. Denomination of sensors valid for all measure cases is shown in the Fig. 4.

First interesting information for tire constructors offers Fig. 5. For the sample *A* we can see the overheating of shoulder area (sensors 1-blue and 3-yellow) which signals the imperfect tire-road contact. In other words the lateral parts of tire are overheated and the central part of the tire has worse tread-road contact.

The explanation of such behavior is possible to find in following experimental and simulation findings[9].

It is well known that a breaker angle (or steel wires angle of belts, which are placed under a tire tread) influences the security of a tire as well as the driving comfort and stiffness of a tire. The driving properties of the tire as a whole could be substantially improved by optimizing such angle of steel wires of the breaker.

Increasing of the breaker angle changes the shape of the tread deformation from convex to concave. For instance in the case of the 20° angle it leads to high overloading of the rolling resistance, heat generation and quick damage of the tire because the tire rolls at the edge of the tread and sidewall[9].

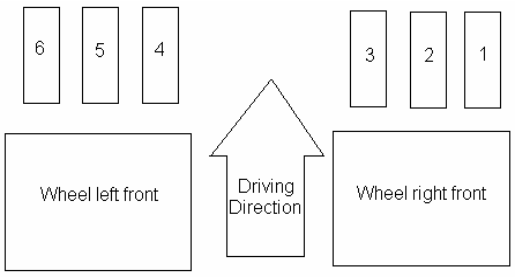

Fig. 4. **Denomination of sensors**

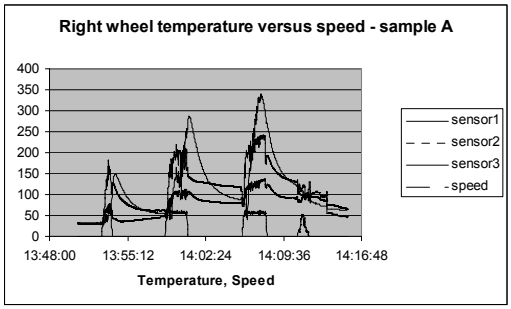

Fig. 5. **Right wheel time-temperature-speed curves for sample A**

It has been also shown that the higher the breaker angle the higher the displacement is in both axial and radial directions. In other words, the tire "grows" with rising of the breaker angle). These results support the highest values of elongation and a relatively high value of strength and elasticity which provide also the so called driving comfort.

In the other words, the tire "grows" with rising of the breaker angle. These results support the highest values of elongation and a relatively high value of strength and elasticity, which provide also the so called driving comfort[9].

The best solution (concerning the tread-road contact) at one from investigated tires was obtained when the breaker angle equals 27°, where practically the full profile of the tread is in contact with the road. It is nevertheless specific for every tire type[9].

After this analysis we can expect caved-in tire profile for the case presented in Fig. 5.

REFERENCES

1. Smartire 2010. *SmarTire for Commercial Vehicles*, http://www.smartire.com/cv.
2. SPEED-WIZ 2010. *Chassis Calculations*, http://www.speed-wiz.com/calculations/ chassis/index.htm.
3. TireChek 1999. *TireChek Tire Pressure Monitor*, http://mb-soft.com/tirechek/.
4. Autoware Inc. 2009. *Tire Temperature Analyzer*, http://www.auto-ware.com/ software/ tta/tta.htm.
5. BorgWarner BERU Systems GmbH 2010. *Tire Safety Systems TSS – The Tire Pressure Control System*, http://www.beru.com/english/produkte/tss.php.
6. Koštial P., Hutyra J., Kopal I., Mokryšová M.: *10th International Conference: Progress in materials engineering*. 2005, 29.
7. Koštial P., Hutyra J., Kopal I., Mokryšová M., Klabník M., Žiačik P.: Chem. Listy *99*, 23 (2005).
8. Koštial P., Mokryšová M., Šišáková J., Mošková Z., Rusnáková S.: Int. J. Thermophysics *30*, 334 (2009).
9. Mokryšová M., Koštial P., Kučerová J., Mošková Z.: Exp. Techniques *33*, 33 (2009).

P-10

A NEW FATIGUE TEST MACHINE FOR ACCURATE CRACK GROWTH ANALYSIS IN RUBBER COMPOUNDS

ARNAUD FAVIER

01dB-Metravib 200 chemin des Ormeaux 69760 Limonest-France
arnaud.favier@areva.com
www.dma-instruments.com

Resistance to tearing is a key factor for elastomer in many applications: (tire tread, dampers, seals, …).

01dB-Metravib (DMA manufacturer), enlarges its range of elastomer testing products by introducing a brand new machine: DMA+300.

This instrument is specifically designed for fatigue and crack growth tests analysis on elastomers.

The principle of the crack growth test consists in initiating a crack on an elastomer film and following up the growth of the crack while applying on the specimen some excitation.

A new algorithm, controlling simultaneously multiple harmonics, applies various waveforms like sine, pulse, triangle and even customized waveforms. It also gives important information about non linearity of material.

DMA+300 includes a thermal chamber operating in a temperature range covering completely the requirements for elastomer, (–150 °C to 500 °C).

The test can be carried out by controlling a specific oxygen rate in the chamber. (Oxygen is a key parameter for crack growth).

A dedicated cutting system integrated inside the front door of the thermal chamber, initiates a crack, precisely and repeatedly.

In front of the chamber the motorized binocular microscope follow up the crack growth with a unique accuracy.

P-11
UV CURING OF INORGANIC-ORGANIC HYBRID POLYMERS

VIERA JANČOVIČOVÁ*, PAVOL GEMEINER, and BOHUSLAVA HAVLÍNOVÁ

Department of Printing Arts Technology and Photochemistry IPM, Faculty of Chemical and Food Technology SUT, Radlinského 9, 812 37 Bratislava, Slovak Republic viera.jancovicova@stuba.sk

Introduction

The hybrid (inorganic-organic) polymers are synthetized via the sol-gel process from organoalkoxysilanes, and they have strong covalent or ionic-covalent bonds between the inorganic and organic components. These materials combine the properties of their constituents, such as low processing temperatures, high optical transparency, chemical and thermal stability and hardness. Due to the wide variation in chemical structure that is possible for hybrid polymers, their properties can be adjusted in a wide range[1–4]. Inorganic-organic composite materials (ORMOCER®s: Trademark of the Fraunhofer Gesellschaft zur Förderung der angewandten Forschung e. V., Munich) are well-suited for the specific functionalization of different polymer and paper surfaces. These materials are water-based or dispersed in nontoxic solvents. Curing is performed photochemically or thermally at relatively low temperatures. Resulting layers are transparent, sturdy and chemically stable. The gas permeability of coated papers is significantly reduced and barrier properties to water vapour and odours are enhanced[5,6]. Multilayer, flexible and transparent high-barrier system based on flexible plastic foils, polyethyleneterephthalate (PET) and ethylene-tetrafluoroethylene-copolymer (EFTE) combined with vacuum-deposited, inorganic SiOx layers and hybrid ORMOCER® varnish layer were prepared in different orders on a semiproduction level[7].

Experimental

Materials

ORMOCER® (Fraunhofer Gesellschaft zur Forderung der angewandten Forschung, Munich, Germany), 1-[4-(2-hydroxyethoxy)-phenyl]-2-hydroxy-2-methyl-1-propane-1-one (Irgacure®2959, Ciba, Switzerland), 1-hydroxy-cyclohexyl-phenyl-ketone (Irgacure®184, Ciba, Switzerland), bis(2,4,6-trimethylbenzoyl)-phenylphosphineoxide (Irgacure®819, Ciba, Switzerland) were used.

Preparation of films

The samples were applied immediately after preparation. Various types and amounts of initiator (from 0.5 to 5 wt.%) were added to ORMOCER®, mechanically mixed and stored in opaque bottle. Photocuring reactions were realized on aluminium plates. The defined sample volume (according to layer thickness) was spread on the plate by spin coating and the layer thickness was determined gravimetrically. The layer thicknesses of our samples were 10 μm.

UV curing of coatings

The samples coated on the aluminum plates were irradiated by a medium pressure mercury lamp 250W (RVC, Czech Republic) built into an UV-cure device constructed in our laboratory. The intensity of incident light was changed with the varying distance of the light source from the sample (5 cm = 28 mW cm^{-2}, 12 cm = 12 mW cm^{-2}). The curing process was monitored by ATR-IR spectroscopy (FTIR spectrophotometer EXCALIBUR SERIES Digilab FTS 3000 NX, USA). The degree of conversion of the cured film was determined based on the abosrption of acrylate double bond (twisting vibration at 810 cm^{-1}, stretching vibration at 1630–1640 cm^{-1}) by a baseline method. The degree of conversion X and relative polymerization rate R_p were calculated from well-known equations[8,9]

$$X = 1 - \frac{[A_\lambda]_0}{[A_\lambda]_t} \qquad (1)$$

where $A_{0(\lambda)}$ and $A_{t(\lambda)}$ are the absorbances of monomers C=C bounds measured at chosen wavelength (810 and 1635 cm^{-1}) before and after the exposure to UV light for the time t or exposition dosage, respectively.
The relative polymerization rate R_p was calculated from the equation

$$R_p = (\Delta X/\Delta t) \qquad (2)$$

where X is the conversion degree of monomer's C=C bounds, at the exposure time t. The values of maximum conversion X_{max} and maximum polymerization rate $R_{p,max}$ were obtained from the plots of X and R_p vs. time.

Results

In order to optimize the coating compositions samples of ORMOCER®s containing 0.5, 1, 3 and 5 wt.% of three radical type initiators (Irgacure®184, Irgacure®2595 and Irgacure®819) were prepared. As shown in Fig. 1, during the curing process, a decrease of absorbance can be observed of the bands characteristic for carbon-carbon double bond (810 and 1635 cm^{-1}).

The functional and handling properties of UV cured layers strongly depend on the conversion of the double bond achieved during irradiation. It is obvious that concentration and type of used photoinitiator markedly affects the values of maximum conversion (X_{max}) and maximum rate of polymerisation (Rp_{max}) parameters.

The initial rate of curing at the light intensity 28 mW cm^{-2} for the composition containg Irgacure®184 is the fastest for 5 wt.% content of photoinitiator, where 70 % conversion is achieved within 10 s. The curing of samples with smaller initiator content is slower. However, in the case of all

three samples the curing process was completed and the conversion reached 88–90 % (ref.[5]). At the light intensity 12 mW cm^{-2} (Fig. 2) we observed that the Rp_{max} and X_{max} was reached at the initiator concentration of 1 wt.% (X_{max} 93 %). In the experiment with the increase of the amount of photoinitiator from 1 to 5 wt.%, decreased the double bond conversion as well as the rate of polymerization were observed. The higher concentration of Irgacure®184 probably provides high absorption, and the initiator acts as internal filter.

The results obtained for UV curing of ORMOCER®s with photoinitiator Irgacure®2959 (Fig. 3) at the light intensity 12 mW cm^{-2} are in a good agreement with the results obtained with Irgacure®184.

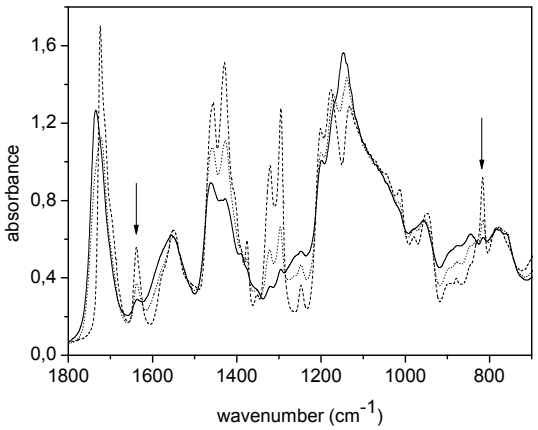

Fig. 1. **Changes in FTIR spectra of ORMOCER®s with 1 % of initiator Irgacure®184 during UV curing** (curing time 0 s – solid line, 70 s – dot line, 900 s – dash line) at the light intensity 12 mW cm^{-2}

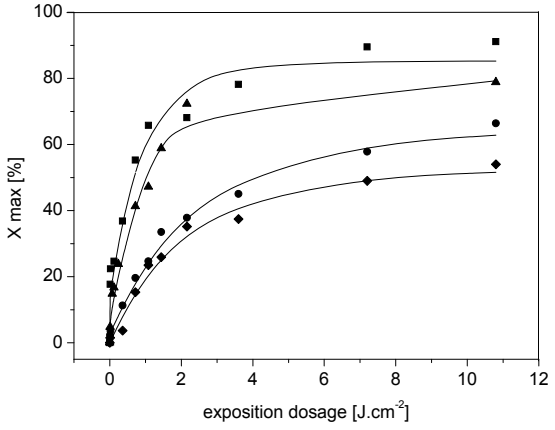

Fig. 2. **Influence of exposition dosage on the UV curing of ORMOCER®s at various Irgacure®184 concentrations** (0.5 % ●, 1 % ■, 2 % ▲ and 5 % ♦; layer thickness 10 μm) at the light intensity 12 mW cm^{-2}

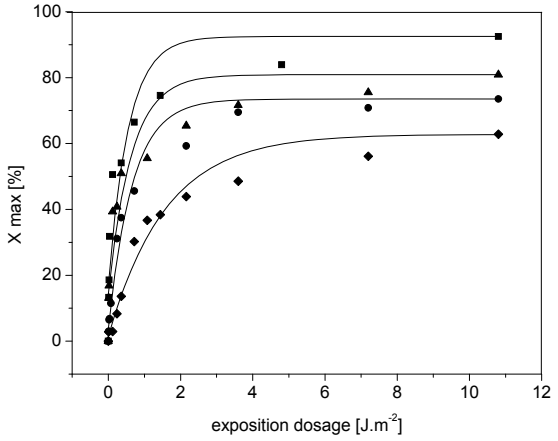

Fig. 3. **Influence of exposition dosage on the UV curing of ORMOCER®s at various Irgacure®2959 concentrations** (0.5 % ●, 1 % ■, 2 % ▲ and 5 % ♦; layer thickness 10 μm) at the light intensity 12 mW cm^{-2}

UV curing of ORMOCER®s was studied also in the presence of the photoinitiator Irgacure®819 at the same light intensity. In this case the photopolymerization didn´t occur effectivelly. Even the high exposition dosage (20 J cm^{-2}) was not enough to cure the coating. The samples were tacky, smelling and cracked. The maximal conversion degrees X_{max} achieved by using each of these three initiators are presented in Fig. 4.

The highest values of X_{max} (around 90 %) were achieved for systems containing Irgacure®184 (1 wt.%) and Irgacure®2959 (1 wt.%). These systems were cured by sunlight (2 hours at noon) and the achieved conversion values were similar for compositions with both initiator (X_{max} 78 % for Irgacure®184 and 72 % for Irgacure®2959). The both composition were sufficiently cured.

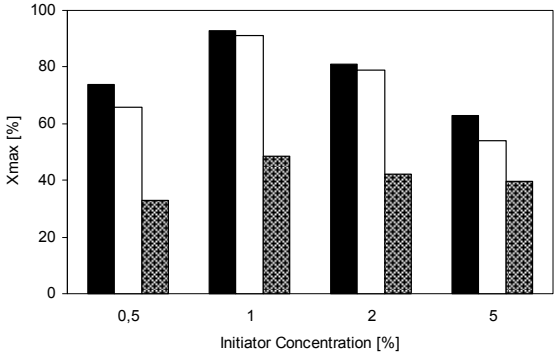

Fig. 4. **The influence of initiator** (Irgacure®184 ■, Irgacure®2595□ and Irgacure®819 ▒) on the maximal degree of conversion at the light intensity 12 mW cm^{-2}

Conclusions

UV curing of compositions containing the hybrid (inorganic-organic) polymers ORMOCER®s and radical photoinitiator type I was monitored by FTIR spectroscopy. The properties of UV cured coatings depend on their compositions (type and concentration of used initiator) as well as on the curing conditions. The highest conversion was achieved for initiators Irgacure®184 and Irgacure®2959 at the initiator concentration 1 wt.%. Both systems were effectivelly cured also by sunlight.

The authors thank the Slovak Grant Agency for the financial support (project VEGA 1/1006/11).

REFERENCES

1. Laskarakis A., Georgiou D., Logothetidis S., Amberg-Schwab S., Weber U.: Mater. Chem. Phys. *115*, 269 (2009).
2. Amberg-Schwab S., Weber U., Burger A., Nique S., Xalter R.: Monatsh. Chem. *137*, 657 (2006).
3. Haas K., Amberg-Schwab S., Rose K., Schottner G.: Surf. Coat. Technol. *111*, 72 (1999).
4. Amberg-Schwab S., Katschorek H., Weber U., Hoffmann M., Burger A.: J. Sol-Gel Sci. Technol. *19*, 125 (2000).
5. Jančovičová V., Amberg-Schwab S., Dzik P., Mikula M.: Chem. Pap. *102*, 1051 (2008).
6. Amberg-Schwab S.: PTS *Symposium Innovative Packaging*, p. C02 Munich (2005).
7. Vaško K., Noller K., Mikula M., Amberg-Schwab S., Weber U.: Central Eur. J. Phys. *7*, 371 (2009).
8. Müller U.: J.M.S.-Pure Appl. Chem. *A33*, 33 (1996).
9. Müller U.: J. Photochem. Photobiol. A: Chem. *239*, 237 (1997).

P-12
PLASMA TREATED THIN TiO_2 SOL-GEL LAYERS ON PLASTIC FOILS

MICHAL ŠANDREJ, MILAN MIKULA*, and PAVOL GEMEINER

Department of Printing Arts Technology and Photochemistry IPM, Faculty of Chemical and Food Technology SUT, Radlinského 9, 812 37 Bratislava, Slovak Republic
milan.mikula@stuba.sk

Abstract

TiO_2 xerogel layers prepared by sol-gel techniques ought to be sintered to more dense, anatase structure, in order to use them in photocatalysis or photovoltaics. Desired sintering temperatures exceed considerably allowable temperature for polymer substrates like PET or PP supposed for printed electronic application. Lower-temperature sintering and reconstruction of xerogel layers could be very beneficial for cheap production of photoactive layers on flexible substrates. Successful sintering of ink-jet printed nano-silver ink by low-pressure plasma was already published. Thin dip coated TiO_2 sol-gel layers (50 nm) deposited on PP, glass and Si-plate were treated in dielectric barrier discharge (DBD) plasma (standard volume and coplanar) in air at atmospheric pressure to study the level of reconstruction of the xerogel layers using FTIR spectroscopy, atomic force microscopy (AFM) and conductivity measurements.

Introduction

Titanium dioxide (TiO_2), well known due to photocatalysis effect, belongs to the most popular materials of present days. It is used in heterogenous catalysis as a photocatalyst, in solar cells for the production of hydrogen and electric energy, as gas sensor, as white pigment, as corrosion protective coating, as an optical coating, in ceramics and in electric devices[1].

With the invention of Dye Sensitized Solar Cell (DSSC) in 1991 (ref.[2]), the new materials get into the interest. Non toxicity, prompt availability and low cost of production process are the most required properties. The synergy of these conditions is found in conventional printing techniques such flexo printing, ofset printing, screen printing and ink-jet, which provides high variability in deposited solutions. The nanostructure layer of TiO_2 is key element in the structure of DSSC and preparation, deposition and modification are frequently investigated.

Preparation of nanostructured TiO_2 layers is based on Sol-Gel method invented around 1880 by investigation of hydrolysis of tetraoxosilicates in acid environment[3]. Sol-gel process is based on chemical reaction of hydrolysis and polycondensation of titania alcoxides, with formation of oxopolymers. These are transformed into oxide network. Condensation continues with gel formation. After evaporation of solution the xerogel is built and the calcination step continues[4,5].

Low-temperature plasma is a technology used for treatment and modifying thin films under low temperature, including inorganic materials. In this technique, nitrogen plasma, oxygen plasma, and argon plasma are typically used reaction sources. Recently, plasma treatments have been used as a calcination step for removal of organic additives and generation of mesoporous films with sol–gel precursors[6].

In this paper attention has been devoted to deposition of thin film TiO_2 layers by dip coating onto PP, glass and Si-plate and additional atmospheric plasma treatment of the xerogel layer. The influence of plasma parameters and exposition time on the layer properties was determined by UV-Vis and FTIR spectral methods and conductivity measurement. The results were compared with results obtained by conventional thermal annealing.

Experimental

Three types of substrates, polypropylene foil (PP, 40 μm, Chemosvit, Slovakia), microscopy slide glass (1.1 mm thick) and Si plate with epitaxial Si layer (111) were coated by 3 % TiO_2 sol, Ti-tetrabuthoxide in waterfree ethanol (stabilized by HNO_3) by simple dip coating (the draw up rate was 10 cm min^{-1}). After 1 day in Lab, the layers prepared on glass and Si substrates were calcinated at different temperatures up

to 400 °C. The layers prepared on PP substrates were treated in atm. pressure plasmas of standard volume DBD (5 kHz, 30 W) and coplanar surface DBD (8 kHz, 300 W) in different exposition times. Afterwards, the layers were characterized by UV-Vis. and FTIR spectroscopy, using diffuse reflectance (CECIL 550) and diamond ATR technique (Excalibur Digi-lab, FTS 3000), respectively. DC and AC conductivities of layers were measured using multimeters Keithley 2000 and Metex M-3650D, and LCR Digibridge Quadtech 1715.

Results

The prepared xerogel layers were free of cracks and precipitates, stable in time and also stable on the flexible PP foil. Plasma treated layers have generally larger scale texture, Fig. 1 (tapping mode AFM, Veeco, CP II).

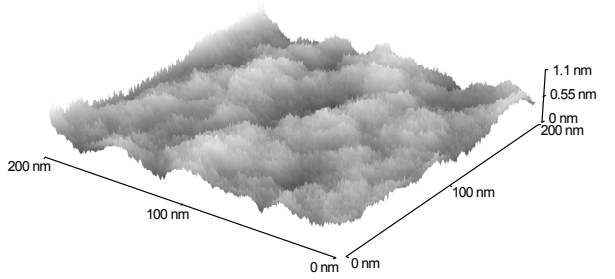

Treated, 10 s, CS DBD

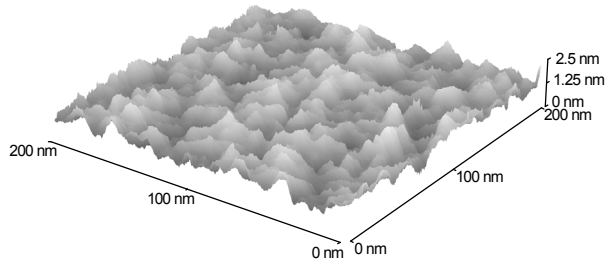

Non-treated

Fig. 1. **Topography of plasma treated and non-treated layers on PP**

Fig. 2. **The xerogel layer on glass with the scratch (50 μm wide) and with the AFM cantilever above the measured edge**

The layer thickness was measured by AFM, scanning the layer scratch on the glass substrate, made by a sharp knife, Fig. 2. The thickness of layers were round 50 nm, while after sintering at 300 °C were reduced to about 35 nm.

UV-Vis. spectra of layers on PP and glass substrates were measured with diffuse reflectance technique to suppress the interference. Al mirror was used as a background also when measured a foil. The layers on Al metalized glass substrates were calcinated up to 400 °C. Some decrease of formal absorbance has occurred mainly for thermal treated samples. The influence of plasma treatment is very small (Fig. 3).

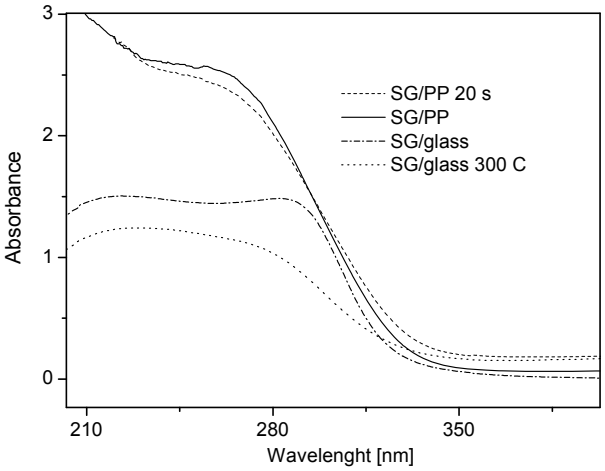

Fig. 3. **Optical density of remission (formal absorbance) in UV spectral region for sol-gel layers on PP (as prepared "SG/PP" and plasma treated 20 s by CSDBD) and on the glass (as prepared "SG/glass" and calcinated at 300 °C**

Measuring FTIR spectra, diamond ATR for glass substrates and (horizontal) HATR techniques for PP substrates were used. However, the difference spectra had to be used because the sol-gel layers were very thin compared with the depth of evanescent wave penetration (Fig. 4).

Conductivity was measured for the layers prepared on Si and Al coated glass substrates, in capacitor like geometry. Most of the samples were not measurable and the rest had a very high dispersion of data. So the error was higher than the mean value itself. However, the evident increase with the plasma treatment, namely for CS DBD was observed.

Conclusions

The dip coated TiO_2 sol-gel layers on PP, glass and Si substrates were plasma treated to achieve reorganization of the xerogel and to increase the electrical conductivity as well. Simultaneously, the xerogel layers on Si and glass substrates were calcinated to find and study the changes in layer structure measuring the FTIR, UV and Vis. spectra and electric conductivity.

Coplanar DBD discharge was more effective than standard volume DBD, regarding conductivity measurements and spectral changes, due to its better discharge homogeneity.

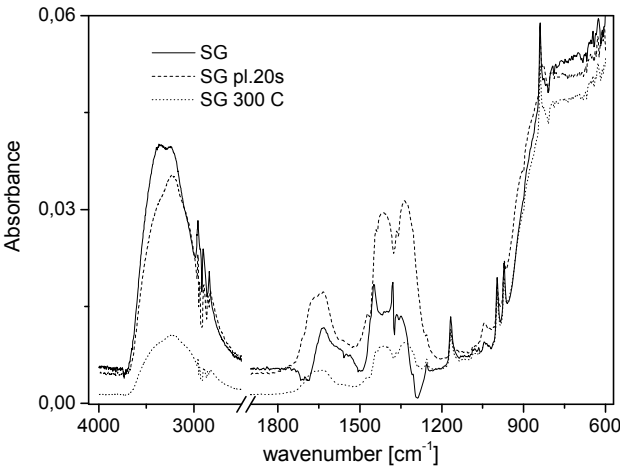

Fig. 4. **Difference FTIR spectra of sol-gel layers on PP (as prepared "SG" and plasma treated 20 s by CSDBD) and on the glass calcinated at 300 °C**

However, the spectral changes with plasma treatment were small comparing with those of thermal treated (that were also small due to very thin layers). Spectral changes have correlated mainly with the water and alcohol removing. The conductivity changes were the most readable, however, the error of measurement was too big and the reproducibility was very pure. If it will enhanced, the electric conductivity would be the most sensitive parameter to structural changes of thin layers, caused by plasma treatment.

The authors thank the Slovak Grant Agency for the financial support (project VEGA 1/1006/11).

REFERENCES

1. Diebold U.: *PhD Thesis*, Department of Physics, Tulane University, 2002.
2. Regan B., Grätzel M., Nature *353*, 737 (1991).
3. Brinker C. J., Scherer G. W.: *The Physics and Chemistry of Sol-Gel Processing, in Sol-Gel Science*, Acad. Press 1990.
4. Suzuki Y., Yoshikawa S.: J. Mater. Res. *19*, 982 (2004).
5. Ruzycki N., Herman G. S., Boatner L. A, Diebold U.: Surf. Sci. Lett. *529*, L239 (2003).
6. Huang J., Ichinose I., Kunitake T., Nakao A.: Langmuir *18*, 9048 (2002).

P-13

DIRECT ADHESION OF RUBBERS TO VARIOUS RESINS DURING CURING USING MOLECULAR ADHESIVES

HIDETOSHI HIRAHARA, KATSUHITO MORI, EIICHI NARITA, YOSHIYUKI OISHI, SUMIO AISAWA, and KUNIO MORI

Graduate School of Engineering, IWATE UNIVERSITY, 4-3-5 Ueda Morioka IWATE, Japan
hiraha@iwate-u.ac.jp

In studying the direct adhesion of rubbers to various resins using molecular adhesives, we investigated 6-triethoxy silyl propylamino-1,3,5-triazine-2,4-dithiols (TES) for the linking of –OH groups on resin surfaces, the TES linking conditions, curing conditions of rubbers, material dependence of the resins, relationship between linked TES concentration and peel strength, and failure behavior. The –OH groups were generated on resin surfaces using an atmosphere corona discharge apparatus. The –OH group-linked resins were heated with TES adsorbed on the resin surfaces, and TES was chemically linked to the resin surfaces to yield TES-linked resins. We heated TES-linked resins with halogen-containing rubber compounds to obtain resin/rubber adherends. Peel strength was influenced by the TES treatment conditions, namely, TES concentration in an ethanol solution and reaction temperatures between the adsorbed TES and the –OH groups on the resin surfaces. The concentration and reactivity of curing agents as well as rubbers had an effect on peel strength. Many resins, except for PP, adhered to rubbers during curing. The results indicated a low material dependence of resins for adhesion. The low adhesion properties for PP were due to the low –OH group concentration, which was obtained by the corona discharge treatment. The linked TES concentration dominated peel strength, rubber coverage, and failure behavior in the peeling test.

In the molecular adhesion technique, it is extremely important that functional groups, which react at interfaces during the adhesion of materials, are present on the surfaces to reduce the material dependence. To introduce functional groups onto many material surfaces, –OH groups must first be present. Metals and ceramics inherently have –OH groups on their surfaces. Using atmosphere corona discharge treatment, it is possible to add –OH groups to the surfaces of organic materials such as resins and vulcanizates[1,2] . The –OH groups widely react with alcoxysilyl groups to yield ether linkages[3] (Fig. 1). Fig. 2 shows C1s components in the XPS analyses of nylon 6 (PA6) surfaces before and after corona discharge treatment. On the PA6 surfaces before corona discharge treatment, C1s peaks assigned to $=CH_2$, C=O, and C–NH groups appeared. Further, after corona discharge treatment, C1s peaks assigned to new –OH and –COOH groups appeared. Fig. 3 shows the effects of 1,3,5-triazine-2,4,6-trithiol (TT), concentration and torque on peel strength of adherents between ECOG and PA6 resin using the molecular adhesive TES. Here, the TES concentration and the linked TES concentration were always constant. We estimated that the interfacial bond concentration remained constant regardless of the TT concentration. Peel strength decreased with an increase in the TT concentration and torque.

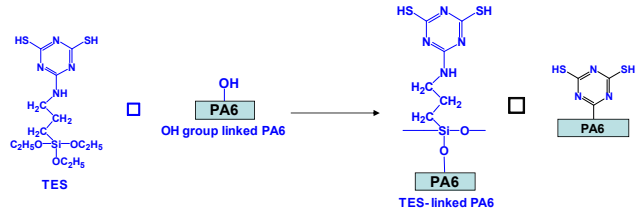

Fig. 1. **Reaction of OH-linked PA6 with TES**

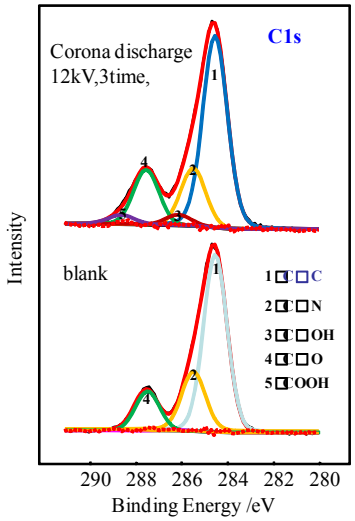

Fig. 2. **C1s components in the XPS analysis of resin surfaces before and after corona discharge**

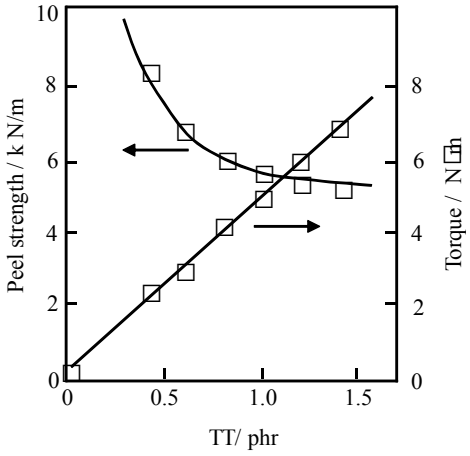

Fig. 3. **The effects of TT concentration and torque on peel strength of adherents between ECOG and PA6 resin using the molecular adhesive TES. Curing conditions: 160 °C × 20 min, 10 MPa**

The increase in the TT concentration and torque brought an increase in the modulus of ECOG vulcanizates. The increase of the modulus decreased peel strength in a 90° peeling test for two reasons. One was a decrease in the tearing strength of ECOG vulcanizates[12,13] and the other was a decrease in the interfacial area between ECOG and PA6 on which stress was applied during the peel testing. Fig. 3 the effects of TT concentration and torque on peel strength of adherents between ECOG and PA6 resin using the molecular adhesive TES. Curing conditions: 160 °C × 20 min, 10 MPa.

We investigated the effects of TES concentration on peel strength in the adherends between ECOG and PA6 resin using the molecular adhesive TES and on the linked-TES concentration ($C_{L\text{-}TES}$) of the PA-6 surface as shown in Fig. 4. TES concentrations in TES ethanol solutions most likely affected peel strengths and the related interfacial bond concentrations. Peel strength increased with an increase in the TES concentration and then reached a plateau. $C_{L\text{-}TES}$ values increased with an increase in the TES concentration and then reached a plateau. The two results indicated a relationship among peel strength, TES concentration, and $C_{L\text{-}TES}$ values. The relationship suggested that peel strength was exhibited by interfacial bonds, which increased with the TES concentration. The TES concentration at both plateaus was different from peel strength and $C_{L\text{-}TES}$. The former was an issue related to interfacial strength and ECOG strength. Fig. 5 shows the failure patterns and types in the peeling test of ECOG and TES-linked PA6 adherends. When the $C_{L\text{-}TES}$ value was zero, we only observed interfacial failure (see Fig. 5(1)) in the peeling test because no interfacial bonds formed in the molecular adhesion technique. In this case, we did observe even small pieces of cured ECOG on the PA6 surfaces because the Ra on the PA6 surfaces after the peeling test was in the range of 40 to 50 nm (38 nm before adhesion). When $C_{L\text{-}TES}$ was in the range of 0.003 to 0.012, small pieces of cured ECOG on PA6

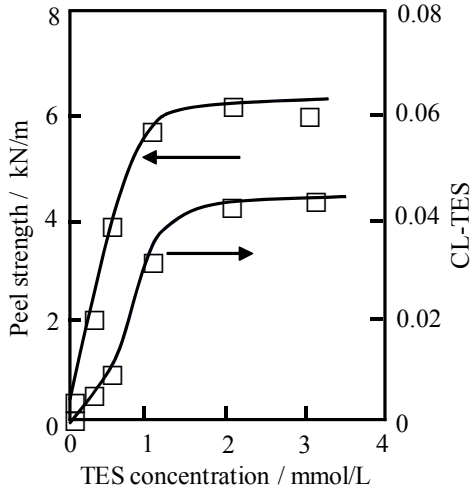

Fig. 4. **Effect of TES concentration on peel strength of adherends between ECOG and PA6 resin using the molecular adhesive TES and on the linked-TES concentration (CL-TES) of the PA-6 surface Corona discharge:** 10.6 kV (59 W), 3.3 mm/s, 2 mm gap. TES treatment: 0–3 mmol/L alcohol solution. 20 °C × 10 min dipping time, 120 °C × 10 min heating. Curing conditions: 160 °C × 20 min, 10 MPa

surfaces were invisible to the eye. However, Ra on the PA6 surfaces after the peeling test increased in the range of 0.1 to 5 μm, meaning that the presence of small pieces of cured ECOG on PA6 surfaces indicated the practical cohesive failure of cured ECOG although it appeared similar to interfacial failure (see Fig. 5(2)). In this case, the failure occurred on the ECOG side because the failure energy of ECOG is considerably smaller than that of PA6. When $C_{L\text{-}TES}$ increased to the range of 0.013 to 0.028, the pieces of cured ECOG on the PA6 surfaces were visible to the eye. We observed peeling surfaces as sea island patterns (see Fig. 5(3)), which consisted of both cohesive and apparent interfacial failures.

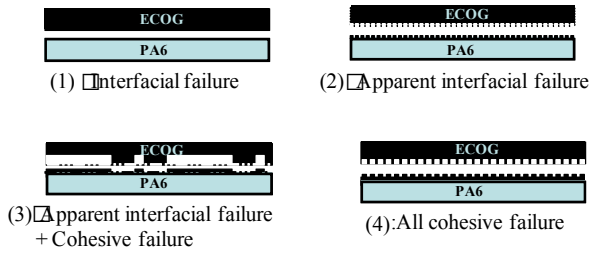

Fig. 5. **Failure patterns and types in the peeling test of CHR and TES-linked PA6 adherends**

REFERENCES
1. Mitsuya T.: Sei Denki Gakkaishi *13*, 17 (1993).
2. Ogawa T.: Nippon Secchaku Gakkaishi *36*, 126 (2000).
3. Nakamura Y., Nagata K.: Sci. Technol., Tokyo (2006).
4. van Ooij W. J.: Rubber Chem. Technol. *51*, 52 (1978).
5. Gent A. N., Kinlok A. J.: J. Polym. Sci., A-2, 9, 659 (1971).

P-14
THERMAL STABILITY OF MODIFIED NANOCOMPOSITE PP FIBERS FOR SILICATE COMPOSITES

ĽUBA HORBANOVÁ[a], JANA VNENČÁKOVÁ[b], ANNA UJHELYIOVÁ[a], and JOZEF RYBA[a]

[a]Department of Fibers and Textile Chemistry, Institute of Polymer Materials, Faculty of Chemical and Foot Technology, Slovak University of Technology in Bratislava, Radlinského 9, 812 37 Bratislava, [b]Research Institute for Man-Made Fibers, a.s., Štúrova 2, 059 21 Svit, Slovakia
luba.horbanova@stuba.sk

Introduction

Fiber reinforced concrete is in the present firmly established as worldwide most commonly used construction material. The term fiber-reinforced concrete is defined as concrete containing dispersed randomly oriented fibers[1−3]. The 3D reinforcement of the concrete results in post-elastic property changes that range from subtle to substantial, depending upon a number of factors, including matrix strength, fiber type, fiber aspect ratio, fiber strength, fiber surface bonding characteristics, fiber content, fiber orientation, aggregate size effects, and the like[4].

Practical function of fibers is to protect composite against sudden failure at the crack initiation in matrix. The tension is transferred to the fibers until the ultimate strength of fibers is reached[5,6]. The enhanced properties include also tensile strength, compressive strength, elastic modulus, crack resistance, crack control, durability, fatigue life, resistance to impact and abrasion, shrinkage, expansion, thermal characteristics, and fire resistance[4].

The basic kinds of large-tonnage fiber-forming polymers and the fibers made from them include polypropylene (PP) and PP fibers. PP fibers are used as reinforcement in construction applications for many years. There is a wide variety of applications of PP fibers in concrete including general constructions and specifically in ground-floor slabs. PP fibers are easy and inexpensive to prepare, easy to disperse and confer advantageous reinforcing properties to the composite materials[7,8].

However, PP fibers also have their specific features which do not always allow arriving at the optimum consumer properties for the fiber materials and articles made from them[7]. This insufficiency is possible to eliminate with fiber modification. More intense anchoring of polypropylene fibers in cement matrix is reached by physical and chemical modification. Addition of sufficient additive ensures that fibers are consistently fixed in matrix. This leads to expressive improve of functional of PP fibers in relation to transmission and absorption of deformation energy to form and load silica composites.

By the addition of additives the structure of polypropylene fibers and by this the properties of fibers may be changed. In this work the thermomechanical and mechanical properties of standard PP fibers and PP fibers modified by inorganic additives with content 2 wt.% and 4 wt.%, before and after stabilization were studied. Information about fiber structure was obtained from TMA scans showing shrinkage behavior before melting. The extent of shrinkage and the temperature at which shrinkage takes place depend on the orientation and crystallinity of the samples[9].

Mechanical properties of fibers were study by investigation of characteristics as tenacity at the break, Young's module and elongation of PP fibers with and without stabilization.

Experimental

Material used

In this study polypropylene (PP) TATREN HT 1810 with MFI = 20.9 g min^{-1} produced by Slovnaft a.s., Bratislava (SK) was used for the preparation of concentrates and fibers modified by inorganic additives. The PP with different content of inorganic additive has been mechanically mixed and melted using the two screw extruder. The obtained PP/ nanoadditive concentrates have been used at the preparation of PP composite fibers by continual technology. PP fibers were used in a form of standard fiber (PP/S) and composite PP fibers. Content of inorganic additive in composite PP fi-

bers was 2 wt.% (PP/C2) or 4 wt.% (PP/C4).

PP/S and PP/C fibers were drawn on the different draw ratios (λ) in the range 2.0–4.0. Samples were exposed the stabilization. Stabilization of PP fibers was carried out at 95 °C for 1 minute.

Methods used

Thermomechanical properties of PP/S and PP/C fibers were performed using Shimadzu Thermomechanical Analyzer TMA-50. TMA dependences were used for determine temperature (T_D) at which the fiber is deformed as well as total deformation – shrinkage (l_D) of fiber at 90 °C. Measurement were carried out at following conditions: heat from room temperature to 90 °C at the heating rate 5 °C min^{-1}, and fiber length 9.8 mm.

Mechanical properties (tenacity at the break, Young's modulus, elongation) were measured by Instron 3343 device and evaluated using Instron program. Tensile test was done in order to measure the tension of fiber to tensile stress until the interruption of fiber. Fibers are straining continuously. Maximum tensile tenacity at the break and corresponding extension is measured at the rupture of fiber. Measuring conditions were the length of fiber 125 mm and rate of clamp 500 mm min^{-1}.

Results and discussion

Thermomechanical properties of PP/S and PP/C fibers with drawing ratio of 2.0–4.0 were evaluated by TMA. Dimensional stability was measured in dependence on temperature growth from room temperature to 90 °C at rate 5 °C min^{-1}. Shrinkage temperatures and total shrinkages of PP fibers with and without stabilization at 90 °C were obtained from experimental dependencies. The results are shown in Tabs. I and II.

From obtained results it is obvious that shrinkage takes place at all measured PP fibers. At both, stabilized PP fibers and PP fibers without stabilization the values of shrinkage were measured higher after addition of inorganic additives. However, increase of content of inorganic additives in PP fibers to 4 wt.% does not lead to growth of shrinkage, but obviously, the shrinkages decrease. The increase of draw ratio of fibers causes decrease of shrinkage.

These results are confirmed by values of temperature at which the fiber deforms. After stabilization the values of deformation temperatures of fibers with addition of inorganic additives are more comparable to standard fibers. At higher draw ratio the influence of modification with inorganic additives on dimensional stability of PP fibers decreases.

In this part mechanical properties of standard and composite PP fibers were evaluated. Tenacity at the brake (σ), Young's module (E) and elongation (ε) of standard and composite PP fibers were measured without and after stabilization (at 95 °C for 1 min, Figs. 1, 2 and Tab. III).

Tenacity at the break and elongation of composite PP fibers without stabilization are decreasing with rising content of inorganic additives and in compare to standard fiber. At higher draw ratio values of tenacity at the break are growing while elongation decreases. After the stabilization tenacity at the break and elongation were found to be comparable to fibers without stabilization.

Table I
Temperature (T_D) of standard PP fibers and composite PP fibers with 2 wt.% and 4 wt.% content of inorganic additives without stabilization (ws) and after stabilization (as)

	T_D[°C]					
λ	PP/S ws	PP/C2 ws	PP/C4 ws	PP/S as	PP/C2 as	PP/C4 as
2.0	52.4	47.1	48.3	50.4	49.7	48.8
2.5	55.5	50.9	49.6	50.8	49.0	51.5
3.0	54.9	50.4	55.4	53.0	52.9	52.1
3.5	56.8	51.3	57.2	55.7	54.3	56.0
4.0	57.4	57.2	54.6	54.5	54.2	54.3

Table II
Shrinkage (l_D) of standard PP fibers and composite PP fibers with 2 wt.% and 4 wt.% content of inorganic additives without stabilization (ws) and after stabilization (as)

	l_D[%]					
λ	PP/S ws	PP/C2 ws	PP/C4 ws	PP/S as	PP/C2 as	PP/C4 as
2.0	–6,5	–12,2	–9,5	–6.5	–10,6	–10.7
2.5	–5,9	–11,1	–8,4	–6.9	–10,0	–7.9
3.0	–6,0	–9,9	–7,6	–7.4	–9,1	–7.4
3.5	–4,1	–6,7	–4,2	–3.8	–4,3	–4.3
4.0	–3,7	–3,7	–5,7	–4.1	–6,0	–5.7

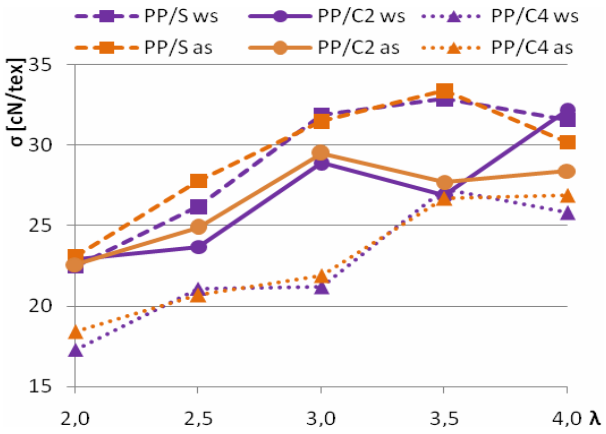

Fig. 1. **Tenacity at the break (σ) of standard and composite PP fibers with different concentration of inorganic additives stabilized at 95 °C during 1 minute (as) and without stabilization (ws)**

By measuring Young's module it was detected, that attributes of standard and composites fibers are comparable and growing with increasing of draw ratio. After the stabilization was at standard PP fibers detected lower Young's module

Table III
Elongation (ε) of standard and composite PP fibers with different concentration of inorganic fillers without stabilization (ws) and after stabilization (as)

	ε [%]					
λ	PP/S ws	PP/C2 ws	PP/C4 ws	PP/S as	PP/C2 as	PP/C4 as
2.0	191	187	168	203	187	172
2.5	144	134	127	154	135	129
3.0	112	105	106	113	99	107
3.5	97	86	75	95	82	74
4.0	74	81	82	74	72	85

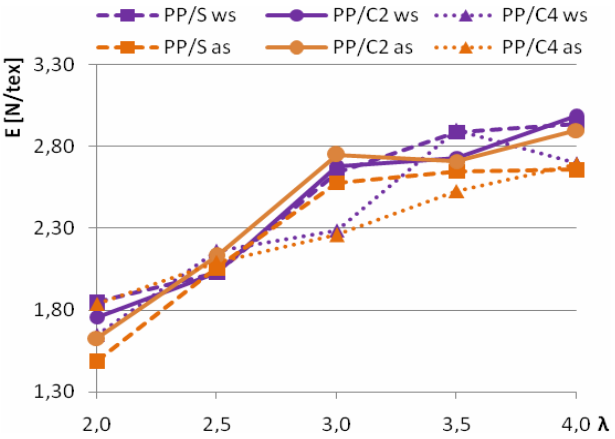

Fig. 2. **Young's module (E) of standard and composite PP fibers with different concentration of inorganic additives stabilized at 95 °C during 1 minute (as) and without stabilization (ws)**

than at samples without stabilization. By addition of inorganic additives are values of Young's modulus approaching to samples without stabilization.

Conclusions

This work was aimed on evaluation of thermomechanical and mechanical properties of standard and composite PP fibers drawn on the different draw ratio. Measurements were realized without and after stabilization of PP fibers.

Thermal stability of PP fibers with addition of inorganic additives was achieved higher at PP/C4 fibers with draw ratio 3.5.

Also at measurements of mechanical properties higher tenacity at the break and Young's module was found at higher draw ratio of PP standard and composite fibers. However, elongation with growth of values of draw ratio decreases.

This work was supported by the Slovak Research and Development Agency under the contract VMSP-P-0007-09 and VEGA 1/0444/09.

REFERENCES

1. Sideris K. K., et al.: Construction and Building Materials *23*, 1232 (2009).
2. Zollo R. F.: Cem. Concr. Compositer *19*, 107 (1997).
3. Banfill P. F. G.: Cem. Concr. Composites *28*, 773 (2006).
4. Trottier J. F., Mahoney M.: Fiber reinforced building materials, US Patent No.: 6,423,134, (2002).
5. Noumowe A.: Cem. Concr. Res. *35*, 2192 (2005).
6. Singh, S., et al: Cem. Concr. Res. *34*, 1919 (2004).
7. Perepelkin K. E.: Fibre Chem. *37*, 2 (2005).
8. Hansen A. S.: Patent number 5,330,827; Date of patent 19.jul 1994.
9. Chand S., Bhat G. S., Spruiell J. E., Malkan S.: Thermomechanical Acta *367-368*, 155 (2001).

P-15
ELECTRON MICROSCOPE, MORPHOLOGY AND STRUCTURE DETERMINATION OF POLYMERS BY CONFINED THIN FILM TECHNIQUES

MARTINA HŘIBOVA and FRANTIŠEK RYBNIKÁŘ*

Tomas Bata University in Zlin, Department of Production Engineering, Czech Republic
rybnikar@ft.utb.cz

Abstract

Advantages of the confined thin film polymerization and crystallization technique are shown on some examples of various polymers. The method requires only a very small amount of sample for crystallization, orientation and additional transformation studies. The effects of various substrate modifications on the polymer structure and morphology are illustrated.

Introduction

Besides crosslinked and very high molecular weight materials stiff and high crystalline aromatic polyesters and polyamides belong to this group also. A big problem, however, is the study of the detailed morphology and crystal structure of such intractable materials by electron microscopy and electron diffraction. These methods demand samples of a suitable thickness and orientation which are not easily attained, e.g., by ultrasectioning. For this reason we have developed a special technique which is based on simultaneous monomer polymerization and crystallization in a confined thin narrow space between two flat solid surfaces (CFTP) resulting in a polymer sample of suitable thickness, structure and orientation[2]. The CTFP method could be used for polymers normally prepared by melt, solution or gas phase polymerization. The aim of this article is to show some typical examples which illustrate the advantage of using the CTFP method.

Experimental

Substrates: As substrates, mostly flat, clean or surface modified glass cover slips or freshly cleaved mica (muscovite) sheets were used.
Samples: For illustration, mainly the laboratory prepared samples of aromatic polyesters and polyamides such as poly-*p*-oxybenzoate (pOB), poly-2,6-oxynaphtoate (pON) and poly-*p*-benzamide (pBA) were used.

Results and discussion

The CTFP technique is a simple, versatile and low cost method accessible in every laboratory with many advantages for polymer research:

1. Sample thickness.
The main advantage is an easy preparation of samples ideally suited for EM and ED examination with a minimum amount of polymer material. The sample thickness can be adapted by the amount of monomer used: a few drops of 0,1−0,5 % monomer solution in a suitable solvent (acetone e.g.).

2. Polymerization mechanism and rate.
We have established with aromatic polyesters and polyamides that in CTFP the polycondensation reaction proceeds much faster than in bulk melt or solution polymerization due to the catalytic effect of the large solid surface[1].

3. Sample crystallization and orientation.
Due to capillary and surface adhesion forces in the closely spaced solid surfaces the polymer tends to polymerize and crystallize in a highly regular conformation e.g. monolayered single crystals or their multilamellar aggregates with a regular crystallographic orientation[3,4].

4. Epitaxial crystallization.
Many crystalline polymers tend to epitaxial crystallization on crystal surfaces of other compounds[5]. In CTFP this tendency is even enhanced. The epitaxial overgrowth is highly crystalline and preferentially oriented in some principal crystallographic directions. Example of P-4-OB and PONA are shown in Figs. 1c,d.

5. Effects of substrate modifications.
For selecting a suitable solid substrate many possibilities are available. Basically, one can select either an amorphous (glass) or crystalline (mica, silica, NaCl), an inorganic or organic, low molecular or high molecular weight substrate. With a given substrate there still are additional possibilities. The substrate can be modified physically or chemically.

Conclusions

The CTFP technique proved useful in the research in a broad range of structure and morphology characterization of various tractable and intractable polymers.

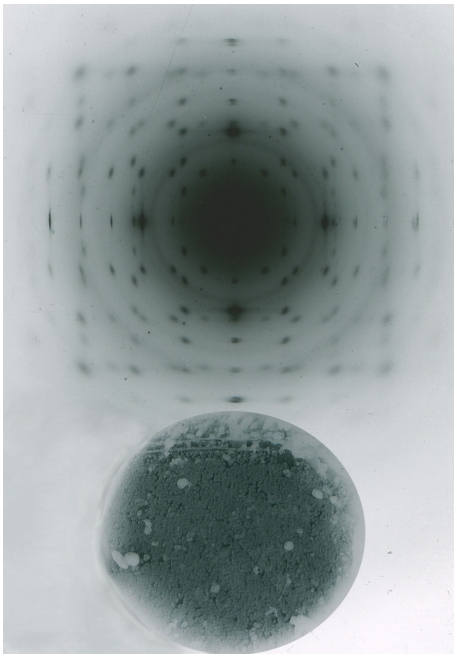

Fig. 1a. **Electron diffraction pattern of POB epitaxially crystallized between mica sheets. Insert is EM bright field of the same sample area**

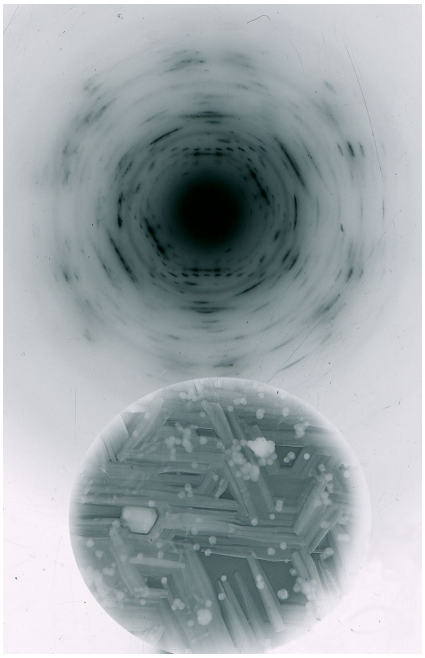

Fig. 1b. **Electron diffraction pattern of PON epitaxially crystallized between mica sheets. Insert is EM bright field of the same sample area**

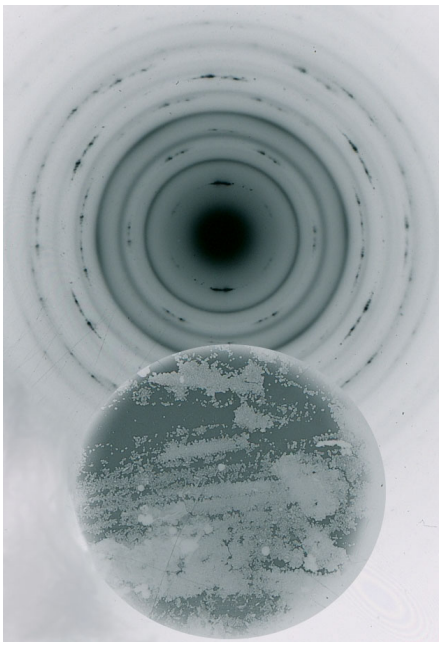

Fig. 1c. **Electron diffraction pattern of PBA epitaxially crystallized between mica sheets. Insert is EM bright field of the same sample area**

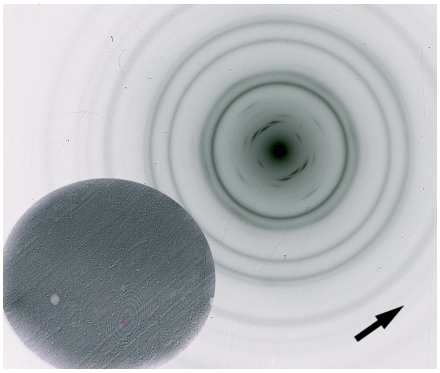

Fig. 2. **Oriented electron diffraction pattern of polyterephthanhydride prepared by shearing monomer polyterephthaloychloride at 200 °C. Arrow indicates the deformation direction**

REFERENCES

1. Liu J., et al. : Polymer 38, vol. 24, 6031 (1997).
2. Rybnikar F., et al. : J. Polymer Sci. Pol. Phys. *37*, 3520 (1999).
3. Rybnikar F., et al. : Macromol. Chem. Phys. *195*, 81 (1994).
4. Rybnikar F., et al.: Polymer *35*, 183 (1994).
5. Wang J., et al.: Macromolecules *29*, 8271 (1996).
6. Manas, M. et al.: Chem. Listy *103*, (2009).
7. Stanek, M. et al.: Chem. Listy *103*, (2009).
8. Manas D. et al. : Chem. Listy *103*, (2009).

P-16
RHEOLOGICAL PROPERTIES OF POLYPROPYLENE COMPOSITES

MARCELA HRICOVÁ[a], ĽUBA HORBANOVÁ[a], ANTON MARCINČIN[a], ŠTEFAN KRIVOŠ[b], and ANNA UJHELYIOVÁ[a]

[a] Slovak University of Technology in Bratislava, FCHFT, IPM, Department of Fibres and Textile Chemistry, Radlinského 9, 812 37 Bratislava, [b] Research Institute for Man-Made Fibers, a.s., Štúrova 2, 059 21 Svit, Slovak Republic
marcela.hricova@stuba.sk

Polypropylene fibres are often used as a reinforcing material in construction applications. Special polypropylene fibres show poor adhesion with cement matrix due to their hydrophobic character and smooth surfaces[1]. Desired fixation of PP fibres in cement matrix can be achieved by physical and chemical modification of PP. Addition of suitable additive insures that fibres are consistently fixed in matrix.
Fibers as a reinforcing material in cement matrix can improve both tension and compression mechanical resistance, improve impact resistance, control cracking and kind of fracture by means of improved ductility after cracking as well as modify rheology and material flow[2].

The effect of the silica and selected organic additives as dispersants on the rheological properties of polypropylene (PP) composite melt is discussed in this paper. Rheological parameters such as apparent viscosity and deviation from the Newtonian flow, expressed by exponent of the Oswald-de Vaele equation, as well as activation energy of melt flow were used for estimation of the melt processing of the PP/SiO_2 composites at melt spinning and preparation of the PP composite fibres used as fibrous filler for construction of composites with inorganic e.g. cement concrete matrix.

The mixture of inorganic additives and PP was processed using twin-screw extrude (Φ 28 mm). The composites containing 8 or 10 wt.% of inorganic additives (S) and 2 wt.% of dispersants (A, B, C, D, E and F) were prepared.

The rheological properties of the PP composites were measured using a capillary extrusiometer Göttfert N 6967 (ϕ = 20 mm).

The viscosity of PP composites increases with content of additives and decreases with temperature. Deviation from the Newtonian behaviour, expressed by power law exponent n, is the highest for pure polypropylene. In addition, the melt viscosity for PP is the lowest. The presence of silica solid particles in PP composites decreases the deviation from Newtonian behaviour but at the same time increases the melt viscosity (Table I). The values of melt viscosity are very similar for PP/S composites regardless of type of used dispersants.

The dispersants A, B and C show slightly positive effect on melt viscosity of PP/S composites, mainly at higher temperatures and lower shear rate. The higher values of power law exponent of PP/S composites with dispersants reveal the decrease of the melt elasticity and give an assumption of improved processability of these polymer materials at fibres preparation.

Table I
Power law exponent n and viscosity η of the PP/S composites

PP/S composites	T [°C]	n	η [Pa.s]		
			γ=300 s^{-1}	γ=500 s^{-1}	γ=1000 s^{-1}
PP	240°C	0.38	185	135	87
	260°C	0.44	147	111	76
	280°C	0.46	129	97	66
PP + 8% S + A	240°C	0.45	197	148	101
	260°C	0.49	165	127	89
	280°C	0.54	140	110	80
PP + 8% S + B	240°C	0.42	202	150	100
	260°C	0.47	168	128	88
	280°C	0.53	139	109	79
PP + 8% S + C	240°C	0.43	198	148	99
	260°C	0.47	166	127	88
	280°C	0.51	139	109	77
PP + 8% S + D	240°C	0.43	207	155	104
	260°C	0.47	174	133	92
	280°C	0.51	146	114	82
PP + 10% S + E	240°C	0.42	225	168	112
	260°C	0.45	194	147	101
	280°C	0.47	169	129	89
PP + 10% S + F	240°C	0.39	208	152	100
	260°C	0.43	177	132	89
	280°C	0.46	151	115	79

Table II
Activation energy of polymer melt flow at assigned shear rate γ

PP/S composites	ΔE [kJ/mol]		
	γ=300 s^{-1}	γ=500 s^{-1}	γ=1000 s^{-1}
PP	21.4	19.2	16.1
PP + 8 % S + A	20.2	17.5	13.9
PP + 8 % S + B	22.3	18.9	14.2
PP + 8 % S + C	20.7	18.2	14.7
PP + 8 % S + D	20.5	17.9	14.2
PP + 10 % S + E	16.8	15.4	13.6
PP + 10 % S + F	18.8	16.6	13.7

Additives and dispersants decrease the activation energy of melt flow of PP/S composites in temperature range 240–280 °C (Table II). It means that the presence of solid particles in PP composites has a positive effect on activate transitions of "independent" segments of polymer chains and facilitate flow of composite melt at spinning.

This work was supported by the Slovak Research and Development Agency under contract No. VMSP-P-0007-09 and VEGA agency No. 1/0444/09.

REFERENCES

1. Lee S. D., Sarmadi M., Denes E., Shohet J. L.: Plasmas Polym. *2*, 177 (1997).
2. Hannant D. J. :*Fibre cement and fibre concrete*, 1st ed. John Wiley & Sons, 1978.

P-17
OPTICAL AND ATOMIC FORCE MICROSCOPY ON FILLED RUBBER COMPOUNDS

SYBILL ILISCH, HAI HONG LE, KATRIN REINCKE, and HANS-JOACHIM RADUSCH

Martin Luther University Halle-Wittenberg, Center of Engineering Sciences D-06099 Halle (Saale), Germany
sybill.ilisch@iw.uni-halle.de

Introduction

The quality of rubber mixtures is strongly dependent on the effective dispersion and uniform distribution of the filler throughout the polymer matrix. Therefore different test procedures have been developed for the characterization of filler dispersion. Microscopical methods on different length scales are an indispensable tool for the characterization of filler dispersion, phase selective filler distribution and phase morphology.

From the beginning of rubber processing, the compounder has used some procedures to determine the quality of mixing. Especially surface inspection of stretched or cutted samples was utilized. In 1956 Leigh-Dugmore[1] quantified the optical microscope analytical procedure to determine the percentage of carbon black dispersed below a certain agglomerate size (6 μm). His method was adopted by ASTM and is still widely used today (Dispersion Index). Stumpe and Railsback[2] used photographic technique in connection with a rating system for the characterization of the carbon black dispersion (Dispersion Degree).

After the invention of the atomic force microscope (AFM) this technique was also applied for the investigation of filled rubber blends [3–9].

Experimental

Optical Microscopy

The comparison between estimated dispersion index and dispersion degree as measure of the filler macro dispersion was conducted for industrial mixed samples (75/25 NR/E-SBR blend with 50 phr N 330, Banbury Pomini 3.5 l, fill factor 0.7, n=80 rpm, T_A=70 °C, T_D= 140 °C). The values show a similar trend: with increasing mixing time the dispersion index and the dispersion degree increase (Fig. 1).

For the calculation of dispersion index gloss cuts were produced by cutting thin, stretched samples by a razor blade at room temperature. If the surface of the cut contents filler agglomerates or aggregates, the light is scattered and its area

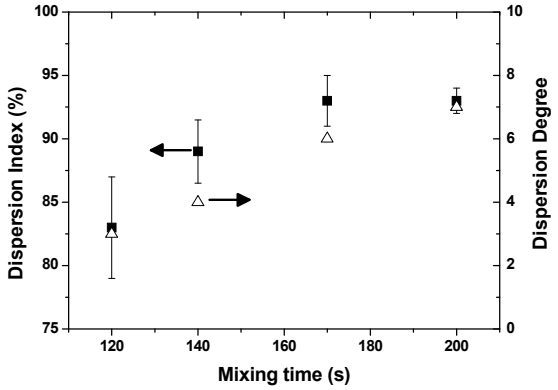

Fig. 1. **Dispersion index and dispersion degree versus mixing time for CB filled NR/SBR blend**

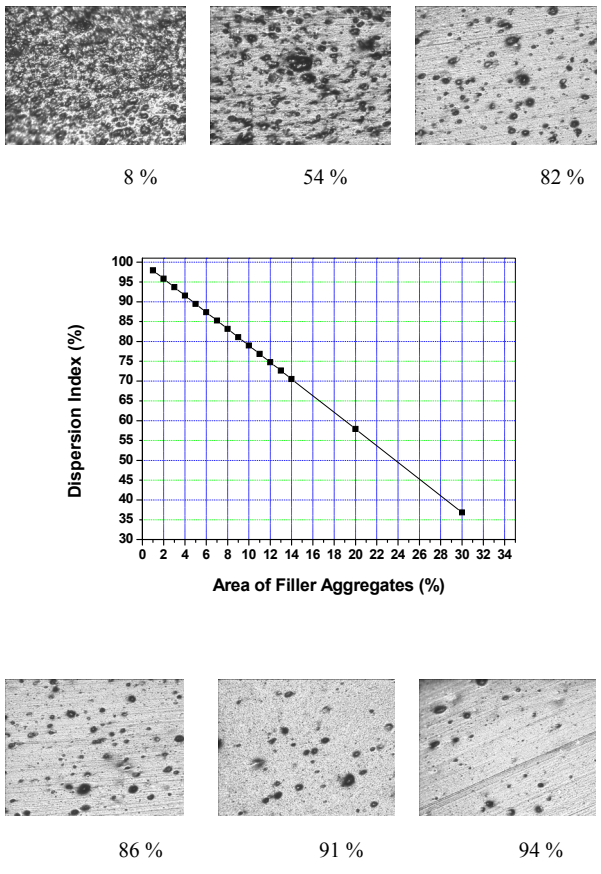

Fig. 2. **Dispersion index versus area of filler aggregates and optical micrographs for different dispersion states**

appears dark. With a Leica image analysis program the area of larger filler regions was calculated (Fig. 2). The dispersion degree was assessed as the amount of the non-dispersed agglomerates with an average diameter larger than 6 μm. After processing microscopic visualization image analysis was used to quantify the degree of filler dispersion. A dispersion index of 100 % means that no aggregate size larger than 6 μm could be found in the cut surface. From each sample 6 pictures were made and from each picture 6 image analyses were taken.

$$D = (1 - \frac{\frac{1}{n}\sum_{i}^{n}(A \cdot \phi_{Med})}{\phi \cdot A_0}) \cdot 100\ \% \qquad (1)$$

The macro dispersion index D (Eq. *1*)[10] is assumed to be the ratio of the sum of the surfaces, which can be assigned to non-dispersed filler clusters and exhibit a diameter larger than 6 μm (A) with respect to the whole viewed surface (A_0). φ is the volume fraction of the filler and φ_{MED} the Medalia[11] factor, which is linked with the effective volume of the filler, in case of carbon black 0.4.

Atomic Force Microscopy

For the creation of AFM phase images a very smooth sample surface is essential. We cut the samples in frozen state in a cryo-chamber by diamond knife in microtom. Fig. 3 shows the filler dispersion for 75/25 NR/E-SBR blends with 50 phr N 330 mixed in Banbury Pomini 270 l, n=40 rpm, T_A=120 °C, T_D= 165 °C, t=190 s for variable fill factors (Table I).

Table I and Fig. 3 show the correlation between macro and micro dispersion: with increasing macro dispersion also the micro dispersion of filler increases. The bright areas in the

Table I
Sample names, fill factors and dispersion index

Sample	F1	F3	F5
Fill Factor	0.64	0.70	0.775
Dispersion Index, %	94.2 +/– 2.3	95.4 +/– 2.1	97.6 +/– 0.9

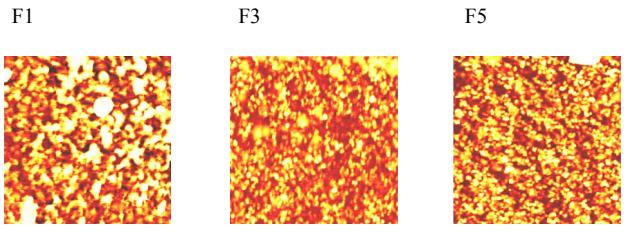

Fig. 3. **AFM images (5 × 5 μm), made in intermittend mode on diamond knife cutted samples (–100 °C) according Table I**

Table II
Results of dimensional analysis of different carbon black types in an E-SBR matrix (50 phr CB, Brabender Plasticorder N 50, n=50 rpm, T_A=50 °C, T_D= 85 °C, t=20 min, fill factor

Carbon Black	N 220	N 330	N 550	N 772	N 990
Particle Size, nm	20-25	26-30	40-48	61-100	201-500
Size of largest Aggregate, nm	440	510	725	572	827
Size of smallest Aggregate, nm	290	220	128	151	186

shown pictures are filler aggregates, the darker areas rubber regions of different hardness.

The quantitative dimensional analysis of CB aggregates of different CB types shows an increasing number of particles included in the aggregates with decreasing dimension of CB primary particles (Table II).

Recently a correlation between the fracture surface roughness and the toughness[12] could be shown (Fig. 4).

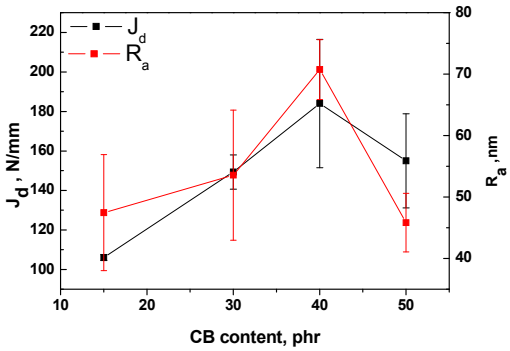

Fig. 4. **Fracture toughness J_d and roughness R_a versus carbon black content (E-SBR, N330)**

Conclusions

Optical microscopy and AFM are suitable tools for the visualization and quantification of filler dispersion in the scale of 500 μm to 50 nm. AFM images can also be used to show the roughness of sample surfaces. In case of blends with high filler content similar dimensions of filler aggregates and polymer phases hinder the quantification of filler localization in different blend phases.

The authors thank the German Research Foundation (DFG) for the financial support of this work.

REFERENCES

1. Leigh-Dugmore C. H.: Rubber Chem. Technol. *29*, 1303 (1956).
2. Stumpe N. A. Jr., Railsback H. E.: Rubber World *151*, 41 (1964).
3. Galuska A. A., Poulter R. R., Mc Elrath K.O.: Surf. Interface Anal. *25*, 418 *(*1997).
4. Ganter M., Brandsch R., Thomann Y., Malner T., Bar G.: KGK, Kautsch. Gummi Kunstst. *52*, 717 (1999).
5. Herrmann V., Unseld K., Fuchs H. B.: KGK, Kautsch. Gummi Kunstst. *54*, 453 *(*2001).
6. Jeon I. H., Kim H., Kim S. G.: Rubber Chem. Technol. *76*, 1 *(*2003).
7. Wang C. C., Donnet J. B., Wang T. K.: Rubber Chem. Technol. *78*, 17 (2005).
8. Bielinski D.M.: Kautsch. Gummi Kunstst. *58*, 239 (2005).
9. Johnson L. L.: Rubber Chem. Technol. *81*, 359 (2008).
10. Radusch H.-J., Androsch R., Ilisch S.: Practical Metallography *48*, 29 (2011).
11. Boonstra B. B., Medalia A. I.: Rubber Chem. Technol. *36*, 115 (1963).
12. Horst T., Reincke K., Ilisch S., Heinrich G., Grellmann W.: Phys. Rev. E80, 046120 (2009).

P-18
PREPARATION AND CHARACTERIZATION OF POLYMER BLENDS OF POLYETHYLENE WITH GALACTOMANNAN-PART II

PETRA SKALKOVÁ[a], ZUZANA JAKUBÍKOVÁ[b], and DANIELA JOCHEC-MOŠKOVÁ[c]

[a] Faculty of Industrial Technologies, Trenčín University of A. Dubček, I. Krasku 491/30, 020 32 Púchov, [b] Vitrum Laugaricio – Joint Glass Center of IIC SAS, TnU AD, FCHPT STU and RONA, j.s.c., Študentská 2, 911 50 Trenčín, [c] Polymer Institute, Slovak Academy of Sciences, Dúbravská cesta 9, 842 36 Bratislava, Slovak Republic
skalkova@fpt.tnuni.sk

Abstract

This work deals with blends preparation low density polyethylene and locust bean gum (LBG) with degree of substitution DS 0,28 in four different amounts (0, 5, 10, 25 wt.%) with and without compatibilizer EAA in three different amounts: 10, 25 and 50 wt.% in respect of polysaccharide. The presence of filler LBG and the effect of compatibilizer have been studied through the mechanical properties (tensile strength, elongation at break and Young`s Modulus) of blends. TGA, DMA and REM were employed to determine the structure and properties of the blends. Increasing amount of LBG and presence of compatibilizer had positive effect on thermal stability of LDPE/LBG blends.

Using of polyolefins and polysaccharides and their relative compatibility

Polyolefins are very important and useful synthetic polymers because they posses good properties, well-known technology of production and low cost. A representative polyolefins used as packaging materials are high density polyethylene (HDPE), low density polyethylene (LDPE) and polypropylene (PP). Since the use of these plastics is continuously increasing, the problem of post-consumer recycling of these materials has become an important issue for economic and environmental reasons[1,2]. An increasing interest in the recycling and the use of biodegradable materials, with the aim of improving thermo-mechanical properties of polymer blends, has lead to the use of polysaccharides as biodegradable filler. The greatest application of polysaccharides, especially starch, cellulose, xylans and their derivatives in the polymers field are as a component in various polymer formulations[3]. Most of the applications are focused on polyethylene, which is widely used as packaging material and in automotive. Polysaccharides are hydrophilic macromolecules, while polyethylene is hydrophobic. The difference in their properties results in poor compatibility of polysaccharide/polyethylene blends. One approach in achieving miscibility and improving adhesion of phases is to replace the hydrophilic OH groups of polysaccharide with hydrophobic groups through esterification. Another way to increase compatibility, and thus the incorporated amount of polysaccharide in polyethylene blends, is to use a compatibilizer containing groups capable of hydrogen bonding with polysaccharide hydroxyls. The most frequently used compatibilizer is ethylene/acrylic acid copolymer (EAA)[4].

Galactomannan specification

Locust bean gum (LBG) is a polysaccharide built up of a main chain of mannose units with short branches of single galactose units. The molecular weight of locust bean gum is 310 000 g mol^{-1}. An average quality locust bean gum contains 12 % moisture, 0,7 to 1,5 % acid insoluble ash, and 6 % protein[6]. Locust bean gum is compatible with other hydrocolloids as well as carbohydrates and proteins. LBG is extremely versatile as thickener or viscosity modifier, binder of free water, suspending agent and stabilizer[5,6].

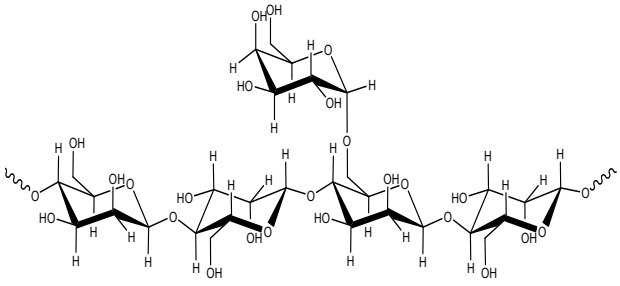

Scheme 1. **Structural unit of locust bean gum**

This work was supported by the Slovak Grant Agency for Science under the grant No. VEGA 1/0330/09 and by the Agency for Promotion Research and Development under the contract No. APVV LPP-1-0156-09.

REFERENCES

1. Pracella M., Pazzagli F., Galeski A.: Polymer Bulletin, *48*, 67 (2002).
2. Ishiaku U. S., Pang K. W., Lee W. S., Ishak Z. A.: Eur. Polymer J. *38*, 393 (2002).
3. Heyde M.: Polym. Degrad. Stab. *59*, 3 (1998).
4. Willett J. L.: J. Appl. Polym. Sci. *54*, 1685 (1994).
5. Smith J., Hong-Shum L.: *Food Additives data book:* Part X. Polysacharides: Locust Bean Gum, 2003.
6. Wang J., Somasundaran P.: J. Colloid Interface Sci. *309*, 373 (2007).
7. Koštial P., Ružiak I., Jonšta Z., Tvrdý M.: Defect and Diffusion Forum *297*, 30 (2010).

P-19

REMOVAL OF RESORCINOL FROM WATER SOLUTION BY USING M-EXCHANGED MONTMORILLONITE (M = Co, Ni)

RÓBERT JANÍK, EUGEN JÓNA, SOŇA ŠNIRCOVÁ, DARINA ONDRUŠOVÁ, and MARIANA PAJTÁŠOVÁ

Department of Chemical Technologies and Environment, Faculty of Industrial Technologies, University of Trenčín, 020 32 Púchov, Slovakia
janik @fpt.tnuni.sk

Phenol and its derivatives (especially resorcinol) are the priority pollutants since they are toxic and harmful to organism even at low concentrations. Surface and ground waters are contaminated by resorcinol as a result of the release of these compounds from rubber, petrochemical and other phenol producing industries[1].

The immobilization and detoxification of hazardous substances with clay minerals represents a vital area for research. Smectites (especially montmorillonite) have a layered structure and adsorb the organic pollutants and also can catalyze their chemical transformation[2–4]. In this paper x-ray diffraction and infrared absorption spectra have been used to study the removal of resorcinol (3-hydroxy phenol) from water solutions by using Co- and Ni- exchanged montmorillonite. It was found, that resorcinol was successfully intercalated into interlayer spaces of Co- and Ni- exchanged montmorillonite. Resorcinol may form a hydrogen bond with the water molecule and accept a proton from this acid species. The absorption of resorcinol depends on the experimental conditions (the concentration of resorcinol, time of interactions).

REFERENCES

1. Yapar S., Yilmaz. M.: Adsorption *10*, 287 (2004).
2. Yariv S.: Thermochem. Acta *274*, 1 (1996).
3. Ovadyahu D., Yariv S., Lapides I., Deutsch Y.: J. Therm. Anal. *51*, 431 (1998).
4. Šnircová S., Jóna E., Lajdová Ľ., Jorík V., Drábik M., Pajtášová M., Ondrušová D., Mojumdar S. C.: J. Therm. Anal. Cal. *96*, 63 (2009).

P-20
METHODS FOR EVALUATION OF SLOVNAFT′S PETROCHEMICALS IMPACT AND TERMOPLASTIC PP COPOLYMER GRADES PROPERTIES ATTRACTIVE TO THE AUTOMOTIVE INDUSTRY

EVA KAMESCHOVÁ

Slovnaft Petrochemicals, s.r.o., Product and Application Development, Vlčie Hrdlo 4846, 824 12 Bratislava, Slovak Republic
eva.kameschova@petchem.sk

Slovnaft Petrochemicals, s.r.o., the member of MOL Group, is producer of two different polyolefines. LDPE – registered trademark Bralen and PP (homopolymers, ethylene /propylene random and impact (block) copolymers) – registered trademark Tatren.

Impact copolymers (IM) and thermoplastic copolymers (TPO) were tailored for automotive industry demands. IM copolymers, with broad range of MFR (from 6 to 100 g/10 min), have very good balance between the toughness and stiffness and due to these excellent properties have very broad utilization in injection moulding of rigid packaging, storage, medical and transport boxes and containers, household appliances, garden furniture, auto battery cases and other technical items. TPO copolymers are, due to excellent impact properties, suitable for compounding, automotive applications and bumpers.

There is variety of properties which can be determined but each has not equal importance for different usage area. For example as regards automotive industry the most crucial are content of C – emissions, Ethylene Content, impact properties (such as Izod Impact vs. Gardner), Modulus of Elasticity in Flexure (bidirectional), Shrinkage, Demoulding Force and Cycle Time (checked by thermal properties).

C – emissions are evaluated from final pellets by method designed for GC/Static Headspace with Flame Ionization Detector (FID). Exact amount of sample is preheated in glass vials for specific time and temperature. Organic compounds are evaporated from the heated sample and released into the space above pellets. When equilibrium is reached, the concentration of the volatiles in the headspace is at its maximum and it is injected onto the analytical column for separation Then the C – emissions potential is measured on the basis of the sum of all values provided by the emitted substances after gas chromatography analysis and flame ionization detection[1].

Ethylene Content is evaluated by infrared spectroscopy. The point of Ethylene Content evaluation is in monitoring of intensity of recurrented methylene group peak in infrared spectra of samples. We can determine Et (total content of ethylene in copolymer), Ec (content of ethylene in rubber phase) and Fc (content of rubber phase in copolymer) as well.

Impact properties can be measured by Izod Impact or Gardner Impact equipment. Gardner Impact is for American method and it describes the real impact properties better then Izod, because in Izod we use notched samples and hammer is moving from side to side. In case of Gadner Impact weight is falling down onto injection molded sample without notch, so it simulates the real situation for example in car bumpers better[2].

Modulus of Elasticity in Flexure can be interpreted as one-directional or bidirectional mechanical property of material. In the first case sample has rectangular shape and the crosshead is applying the load perpendicular to the flow. In the second case sample has squared shape and crosshead is applying the load perpendicular and parallel to the flow as well. Comparing one-directional and bidirectional testing, the latter announces the isotropy of material in addition to the Flexural Modulus and it fits to the reality better[3].

As regards isotropy of material another very reliable property is Shrinkage. Samples are squared shaped plates prepared by injection molding. Shrinkage is calculated from changing dimensions of plates. First dimensions are determined by dimensions of mold and the second dimensions of plates are measured by calipers after the certain time of conditioning[4].

One option how to influence demoulding of injection molded products is to add appropriate nucleation agents. Reduction of the demoulding time we can measure indirectly through thermal properties determined by Differential Scanning Calorimetry (DSC) such as Temperature of Crystallization (T_c) and Half Time of Crystallization ($t_{1/2}$)[5].

REFERENCES

1. VDA 277, Determination of emission of organic compounds, 1995.
2. ISO 180, Determination of Izod impact strength, 2000 and STN EN ISO 294-1Injection moulding of test specimens of thermoplastic materials, 1996.
3. ISO 179, Determination of flexural properties, 2000.
4. ISO 294 – 4, Injection moulding of test specimens of thermoplastic materials -- Part 4: Determination of moulding shrinkage, 2001.
5. ISO 11357, Differential scanning calorimetry (DSC), 2009.

P-21
INFILTRATION BEHAVIOR OF RUBBER IN SILICA COMPOUNDS

M. KELLER, H. H. LE, S. ILISCH, and H.-J. RADUSCH

Martin Luther University Halle-Wittenberg, Center of Engineering Sciences, D-06099 Halle (Saale), Germany
melanie.keller@iw.uni-halle.de

Abstract

The wetting behavior as pre-step of the infiltration and dispersion of silica by different rubbers during the mixing process in an internal mixer was investigated by extraction experiments and discussed by a new developed model. Compared to the wetting in a stationary state the wetting process in the in-stationary state in internal mixer takes place very fast due to the effect of shear stress and pressure. Addition of silane and curing additives leads to a large change of the wetting behavior of silica.

Introduction

Since the 1990s carbon black is more and more substituted by silica/silan systems as reinforcing filler in rubber compounds for tire applications. The dispersion of filler both silica and carbon black is the key for achieving good quality and consistent product performance of rubber compounds. After incorporation of filler into polymer matrix the polymer molecules start to infiltrate into the pores of the filler agglomerates. The presence of infiltrated polymer within the agglomerate introduce additional forces which have a direct effect on the dispersion ability of filler[1–3]. The rheological behavior of the penetrating polymer is an influencing factor to overcome the cohesive forces of the agglomerates, and consequently on the type of dispersion mechanism rupture or erosion. Astruc et al.[3] recently showed that the more entropy-elastic the matrix, the larger the stress required to erode agglomerates and the slower the erosion proceeds. This was observed in the case where the matrix infiltrated the agglomerates and the more difficult erosion was explained by an increase of the agglomerate cohesiveness due to the elastic character of the penetrated fluid. The knowledge of infiltration kinetics of the polymer inside the filler agglomerate is necessary to understand the dispersion of porous filler during mixing operations. Basis knowledge on the penetration kinetics has been gained in the last decade for CB and silica in Newtonian liquids using a transparent counter-rotating plate-and-plate shear cell coupled with an optical device. Fluid infiltration into agglomerates is driven by capillary pressure, which depends on, amongst other factors, the characteristic pore size and the interfacial tension between fluid and particle surface. Bohin et al.[4] studied the kinetics of the penetration of a Newtonian silicon oil into silica agglomerates in a stationary state. They proposed a model based on the capillary forces driving the penetration and viscous effects resisting it.

In the present work we characterized the infiltration kinetics of rubbers into silica during the real mixing process by means of the rubber-layer *L*, which is determined from the development of the bonded rubber on the silica surface. Effect of rubber viscosity, polarity, and addition of additives as well as mixing conditions on the infiltration process will be discussed by taking into consideration the known theories.

Experimental

The used materials are listed in Table I (ref.[5]). The compounding of the material was carried out in a laboratory internal mixer (Plasticorder PL2000).

To characterize the wetting behaviour of filler by the rubber molecules the rubber-layer *L* was determined by means of the extraction experiment[6] according to eq. (*1*).

$$L = \frac{m_2 - m_1 \cdot c_S}{m_2} \qquad (1)$$

The mass m_1 corresponds to the rubber compound before extraction; it is the sum of the mass of the undissolvable rubber, the mass of the soluble rubber and of silica. m_2 is the mass of the rubber-filler gel, which is the sum of the undissolvable rubber and the mass of silica. c_S is the mass concentration of silica in the mixture.

Table I
Used materials

Name	Trade Name, Supplier	Remarks
BR	Buna® cis 132-Schkopau, Styron Deutschland GmbH	95 % cis-1,4
S-SBR	Sprintan® SLR 4602-Schkopau, Styron Deutschland GmbH	21 % styrene, 63 % vinyl
Silane	NXT Silane, Momentive Performance Materials	3-Octanoylthio-1-propyltriethoxysilane
Silica	Ultrasil 7000 GR, Evonik Europe GmbH	
ZnO	Zinc oxide	
StA	Stearic Acid	
CBS	Vulkacit CZ/EG-C, Rhein Chemie Rheinau GmbH	N-Cyclohexyl-2-benzothiazole sulfenamide
DPG	Vulkacit D/EG-C, Rhein Chemie Rheinau GmbH	Diphenylguanidine

By taking into consideration the eq. 1 the rubber-layer *L* can also be expressed by eq. (*2*):

$$L = \frac{hbt^{1/2}}{hbt^{1/2} + \rho_F(1-\varepsilon)} \qquad (2)$$

The wetting rate *b* is given by eq. (*3*), ref.[7]:

$$b = (2A + 2B)^{1/2} \qquad (3)$$

with $A = \frac{S\gamma_R \cos\theta}{6\eta_R}$; $B = \frac{S^2 \Delta P}{12\eta_R}$ and $S \approx \frac{D_p \varepsilon^2}{2(1-\varepsilon)}$

where *t* is the mixing time, ΔP is the pressure in the internal mixer. D_P, ρ_F and ε are the primary particle diameter, density and porosity of the filler, respectively. γ_R and η_R are the surface tension and viscosity of the rubber, respectively. $cos\theta$ is the contact angle between rubber and filler. The correlation between the plateau value L_P and the factor *h* is described as followed:

$$L_P = \frac{\varepsilon h}{\varepsilon h + \rho_F(1-\varepsilon)} \qquad (4)$$

Results

Wetting of silica by SBR in a stationary state

The infiltration experiment in stationary state was carried out according to the work of Astruct[3]. Two thin films of S-SBR containing a few agglomerates of silica randomly

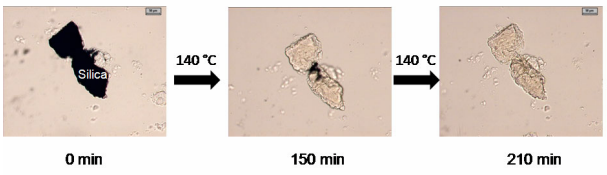

Fig. 1. **Infiltration of silica by S-SBR in a stationary state at 140 °C**

placed in between two glass plates and its thickness is controlled. The infiltration was characterized by optical microscopy by following the change of the dry part of the silica agglomerates vs. time. Non-infiltrated parts of the agglomerates appear black (due to the large difference of refractive index between air and silica), whereas, the infiltrated parts are transparent (small difference of refractive indices between silica and the fluid). It is clear to see from Fig. 1 that a silica agglomerate needs about 150 min to be fully infiltrated.

Effect of additive addition on the wetting behavior at 50 °C

The addition of additives, i.e. ZnO, stearic acid and CBS/DPG, into the S-SBR and the BR mixture obviously elevate the development of *L*. As seen in Fig. 2 additives can fast diffuse into the silica agglomerates thanks its low molecular weight. If the additives get in contact with silica surface, they are able, dependent on type, to interact with silanol groups in various ways. Ramier et al.[8] showed that both CBS and DPG are able to interact with the silica surface whereupon DPG would adsorbed first, because of the stronger basicity. ZnO and stearic acid react via an ion exchange reaction with the silanol groups[9]. The presence of additives on the silica surface changes the filler-filler- and filler-matrix-interaction and thereby the physisorption of rubber molecules to the silica that elevates the formation of the rubber-layer *L*.

Effect of mixing temperature and silane on the wetting behaviour

For BR a significant change of the wetting rate due to mixing temperature or silane is unverifiable as seen in Fig. 3. The calculated wetting rate for all three mixture is b = 0.2.

Conclusions

The wetting behavior of silica by different rubbers during the mixing process in an internal mixer was investigated by extraction experiments and discussed by a new developed model. The Addition of additives leads to a significant change of the wetting behavior of silica. For BR an influence of temperature or silane was not detectable under the chosen conditions.

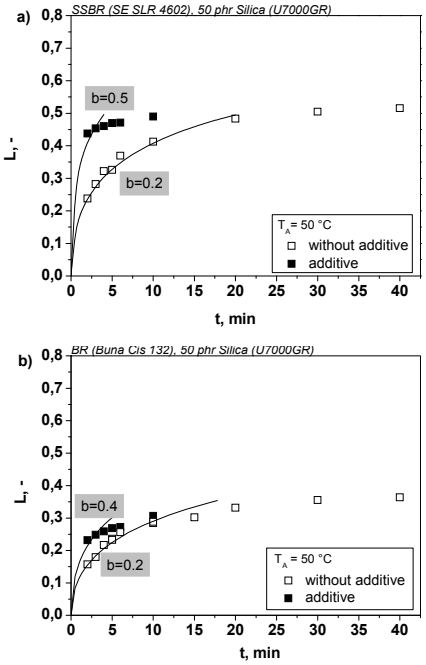

Fig. 2. **Wetting behaviour of silica by S-SBR (a) and BR (b) under influence of additives addition**

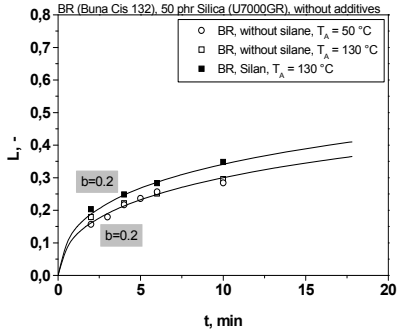

Fig. 3. **Wetting behaviour of silica by BR under influence of temperature and silane**

REFERENCES

1. Levresse P., Feke D. L., Manas-Zloczower I.: Chem. Eng. Sci. *56*, 3211 (2001).
2. Gopalkrishnan P.: *PhD thesis*, Case Western Reserve University Cleveland/USA, 2004.
3. Astruc M., Collin V., Rusch S., Navard P., Peuvrel-Disdier E.: J. Appl. Polym. Sci. *91*, 3292 (2004).
4. Bohin F., Manas-Zloczower I., Feke D. L.: Rubber Chem. Technol. *67*, 602 (1994).
5. Thiele S., Bellgardt D., Holzleg M.: Kautsch. Gummi Kunstst. *5*, 244 (2008).
6. Le H. H., Kasaliwal G., Ilisch S., Radusch H.-J.: Kautsch. Gummi Kunstst. *5*, 241 (2007).
7. Lin C. M., Chang W. J., Fang T. H.: J. Electronic Packaging *129*, 48 (2007).
8. Ramier J., Chauzeau L., Gauthier C.: Rubber Chem. Technol. *80*, 183 (2007).
9. Hewitt N.: *Compounding Precipitated Silica in Elastomers*, William Andrew Publishing, Norwich/USA (2007).

P-22
DEGRADATION OF GROUND RUBBER FROM WASTE TYRES STUDIED BY SOLID STATE NMR

MÁRIA KOVAĽAKOVÁ*[a], OĽGA FRIČOVÁ[a], VIKTOR HRONSKÝ[a], DUŠAN OLČÁK[a], JÁN MANDULA[b], BRIGITA SALAIOVÁ[b], and MARIYA HOLUBKA[b]

[a] Department of Physics, Faculty of Electrical Engineering and Informatics, Technical University of Košice, Park Komenského 2, 042 00 Košice, [b] Department of Geotechnics and Traffic Engineering, Institute of Structural Engineering, Civil Engineering Faculty, Technical University of Košice, Vysokoškolská 4, 042 00 Košice, Slovakia
Maria.Kovalakova@tuke.sk

Introduction

Disposal of waste tyres is a serious environmental problem since tyre rubber as other polymeric materials does not decompose easily. Two major approaches to solve this problem are the recycling and reclaiming of waste rubber[1]. Tyre rubber is a complex material consisting of natural rubber (NR), styrene-butadiene rubber (SBR), polybutadiene rubber (BR) and several additives whose purpose is to improve physical properties of the final product[2]. The average composition of tyre rubber varies with the type of tyres[3]. The mechanical recycling of waste tyres consists in their shredding, grinding and removing steel cords and textile parts and gives ground rubber. This material can be used e.g., in road construction[4] as additive in hot mix asphalt[3] and the rate of degradation of this material can significantly influence the performance and service life of road surface.

Mobility of polymer chains in rubber is restricted by crosslinks. The optimum cross-linking gives rubber good flexibility and elasticity. The ageing processes in rubber lead to chain scission and/or increased cross-linking giving weaker, brittle polymer[5]. Information about the segmental motion in rubber can be obtained from the measurements of temperature dependence of NMR spin-lattice relaxation time T_1 of protons in polymer chains. At the temperature minimum of the relaxation time T_1 the condition $\omega\tau_s = 0.62$ is fulfilled, where ω is the Larmor frequency and τ_s is an average (local) segment reorientation time. With increasing degree of cross-linking τ_s increases and T_1 minimum shifts to higher temperature[6]. Information about the molecular motion can be also obtained from the proton spin-spin relaxation time which is related to elasticity and flexibility of material[7]. The more restricted a molecules motion is, the faster the system will return to its initial condition after being excited, so the shorter is T_2[5].

The aim of this study is to quantify the degradation of ground rubber from waste tyres by means of NMR spin-lattice relaxation time T_1 and spin-spin relaxation time T_2 determined for protons in methylene groups of rubber chains.

Experimental

The ^{1}H and ^{13}C NMR experiments were performed in the temperature range 22–100 °C on Varian NMR spectrometer operating at 400 and 100 MHz, respectively, using 4 mm rotor and a magic angle spinning (MAS) rate of 6 kHz and 10 kHz. ^{13}C NMR spectra were obtained with 90° pulse (1.9 μs), a high power proton decoupling of 92.6 kHz, a recycle delay of 6 s, and averaging over 4000–6000 scans. ^{1}H MAS NMR spectra of sufficient resolution were obtained with 90° pulse (4.75 ms), using a recycle delay of 4 s and averaging 20 scans. An inversion recovery pulse sequence was used for T_1 measurements. T_2 was obtained from the experiments using MAS rate of 10 kHz and 90-τ-180 sequence in which spin-echo was detected after a delay time τ. The spectra measured for τ from the range 100 μs – 40 ms were deconvoluted using MestReNova software and the areas under the peak given by methylene protons were plotted versus the delay time $t_d = 2\tau$. The curve fitting was performed in SciDavis programme using scaled Levenberg-Manguardt algorithm.

The samples of ground rubber were supplied by V.O.D.S, Kechnec, Slovakia. The material underwent a standard recycling procedure. Prior to NMR measurements the traces of metallic parts in the samples were removed using permanent magnet. The measurements were carried out on the as-supplied sample (GR-0) and the samples GR-3 and GR-8 which were thermally treated at 85 °C for 3, and 8 days, respectively, in Ecocell oven with natural convection. The spectra were recorded also for new tyre rubber (TR).

Results and discussion

The ^{13}C MAS NMR spectra of ground rubber are qualitatively the same (spectrum of GR-0 is shown in Fig. 1) and consist of lines with chemical shifts of 134.8, 125.3, 32.5, 26.7, and 23.6 ppm assigned to C_1, C_2, C_3, C_4 and C_5 carbons in cis-1,4-isoprene units of NR and lines with chemical shifts of 129.6, 30.4 and 27.6 ppm assigned to SBR carbons.

The chemical shift pattern is in accordance with the tyre rubber ^{13}C NMR chemical shifts[8].

The ^{1}H NMR spectra of ground rubber samples display three dominant lines with chemical shifts of 1.6, 2.0 and 5.1 ppm assigned to the methyl, methylene and unsaturated methine protons of cis-1,4-isoprene units of natural rubber, the ^{1}H lines of aromatic and methine protons in SBR are visi-

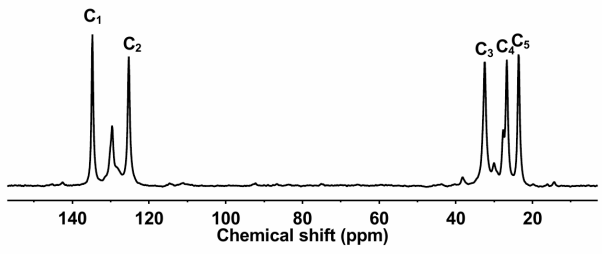

Fig. 1. **^{13}C MAS NMR spectrum of GR-0 sample recorded at room temperature**

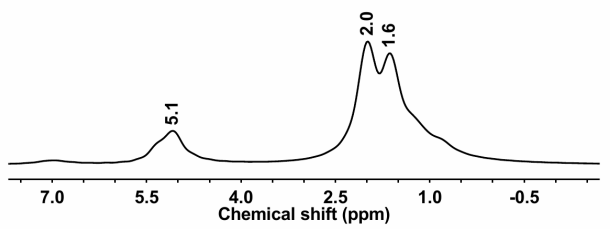

Fig. 2. **^{1}H MAS NMR spectrum of GR-0 sample recorded at room temperature**

ble in the spectra of these samples as a broad line at 7 ppm, and a shoulder at 5.3 ppm, the line of methylene protons has the shift of 2.0 ppm so it overlaps with the line of NR methylene protons (spectrum of GR-0 sample is shown in Fig. 2).

The values of spin-lattice relaxation time T_1 for protons in methylene groups versus 1/T are plotted in Fig. 3. The T_1 minimum of new tyre rubber (TR) is below room temperature. The shift of T_1 minima to higher temperatures for GR samples indicates the increase of cross-linking in these samples since higher temperature is required to achieve the τ_s value fulfilling the condition for T_1 minimum. The minima of thermally treated samples show a slight tendency to move to higher temperature and longer T_1 values with longer thermal treatment and hence higher degradation of the polymer structure.

The values of spin-spin relaxation time of methylene protons were determined from the deconvoluted ^{1}H MAS NMR spectra recorded with increasing delay time. The plots of the areas under the peaks given by methylene protons versus t_d time are shown in Fig. 4. The curve fitting required the sum of two exponential decay functions:

$$M(t)/M(0) = \mathrm{A}\exp(-t_\mathrm{d}/T_{2\mathrm{A}}) + \mathrm{B}\exp(-t_\mathrm{d}/T_{2\mathrm{B}})$$

The values of function parameters are listed in Table I. The parameters A and B are proportional to the fractions of samples with different degree of cross-linking. The T_2 values in both fractions decrease with longer thermal treatment inducing further rubber degradation. The fitting of transverse mag-

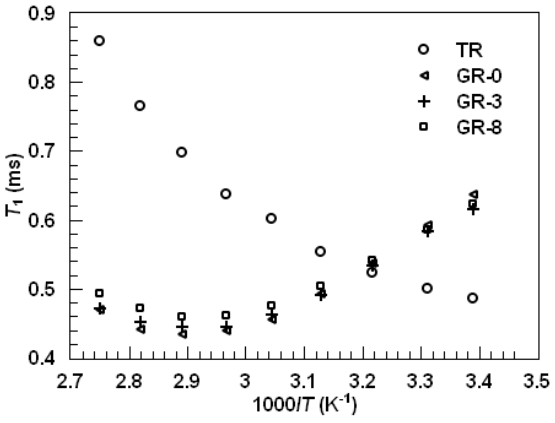

Fig. 3. **Temperature dependence of spin-lattice relaxation time of methylene protons of ground rubber sample and new tyre rubber**

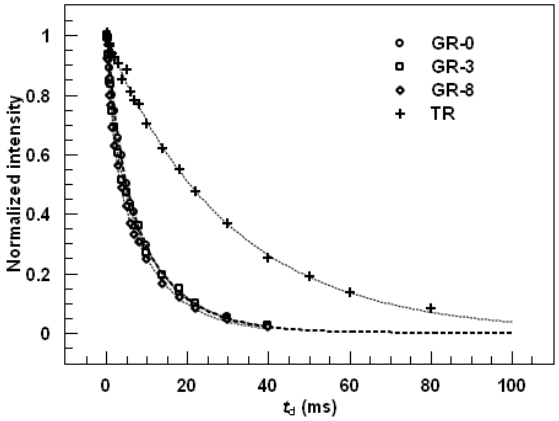

Fig. 4. **Plots of normalized transverse magnetization and fitting functions for all studied samples**

Table I
The parameters of fitted curves $M(t)/M(0)=f(t_d)$

	A	T_{2A} (ms)	B	T_{2B} (ms)
GR-0	0.39	2.96	0.67	11.3
GR-3	0.39	1.79	0.68	11.4
GR-8	0.41	1.50	0.65	10.4
TR			1	29.9

netization of new tyre rubber (TR sample) was successful with one exponential function providing as expected a long T_2 value characteristic for highly elastic and flexible materials.

The spin-lattice and spin-spin relaxation times reflect the changes in the structure of ground rubber induced by even a short thermal treatment at relatively low temperatures and can be used for quantifying the ground rubber degradation.

This study was supported by funding from the Project of the State Program of Research and Development No. 2003SP200280203, Slovakia. The paper presents results of the research activities of the Centre „Progressive Constructions and Technologies in Transportation Engineering". The Centre was supported by the Slovak Research and Development Agency under the contract No. SUSPP-0013-09 and the companies Inžinierske stavby and EUROVIA SK .

REFERENCES

1. Adhikari B., De D., Maiti S.: Prog. Polym. Sci. *25*, 909 (2000).
2. Williams P. T., Besler S.: Fuel *74*, 1277 (1995).
3. Roberts F. L., Kandhal P. S., Brown E. R., Dunning R. L.: *Investigation and evaluation of ground tire rubber in hot mix asphalt*, NCAT Report No.89-3 (1989)
4. Kudrna J.: Využití ojetých pneumatik ve stavbě PK, *Sbornik Recyklace a využití druhotných surovin při stavbě a opravě pozemních komunikací*, VUT FAST, Brno, Czech Republic (2006).
5. Somers A. E., Burgar T. J,, Forsyth M., Hill A. J.: Polym. Degrad. Stab. *70*, 31 (2000).
6. Stapf S., Kariyo S.: Acta Physica Polonica A *108*, 247 (2005).

7. Alexandre J., Feio G., Marvao M. R., Figueredo J.: Mater. Sci. Forum *455−456*, 459 (2004).
8. Nielsen N. Ch., Bildsoe H., Jakobsen H. J: Macromolecules *25*, 2847 (1992).

P-23
ELECTRICAL CONDUCTIVITY OF COMPOSITES DURING MECHANICAL DEFORMATION

JURAJ KRAJČI and IVAN CHODÁK

Slovak academy of sciences, Dúbravská street 9, 845 41 Bratislava, Slovakia
juraj.krajci@savba.sk

Eletroconductive composites are formed by mixing electroinsulating polymeric, mainly thermoplastic and rubber matrix with electroconductive filler[1,2]. In this work we investigated the composite styrene-butadiene rubber filled with carbon blacks N 234. The influence of mechanical deformation on changes of electrical conductivity and current was investigated on line during mechanical deformation of the composite. Changes in electrical conductivity of composite were observed in dependence on mechanical deformation in process of simple uniaxial tensile deformation, followed by stress relaxation and recovering after the release of tension[3,4]. This process is not simple, but we observed interesting changes of current during mechanical deformation, relaxation and recovery. The results were considered taking into account the destruction of conductive paths as a result of small movement of styrene-butadiene rubber chains and possible recovery of the paths during deformation, relaxation and recovery. Changes of electrical conductivity were markedly dependent on degree of deformation. The shape of the curves were not monotonous but exhibited maxima and minima which correspond to certain patterns on the stress-strain curves. Reseach of this changes conductive paths can lead to produce electrically conductive composites, which are sensitive towards changes of mechanical deformation.

This work was supported by projects APVV 51-010405 and VEGA 2/0185/10.

REFERENCES
1. Feller J. F., Langevin D., Marais S.: Synt. Met. *144*, 81 (2004).
2. Omastová M., Košina S., Pionteck J., Janke A., Pavlinec J.: Synthetic Metals *81*, 49 (1996).
3. Flandin L., Chang A., Nazarenko S., Hiltner A., Baer E.: J. Appl. Polym. Sci. *76*, 894 (2000).
4. Flandin L., et al.: Polymer *42*, 827 (2001).

P-24
MECHANICAL AND ELECTRICAL PROPERTIES OF COMPOSITES BASED ON LOW DENSITY POLYETHYLENE AND EXPANDED GRAPHITE

JÁN KRATOCHVÍLA[a], IGOR KRUPA[a]*, ZDENKO ŠPITÁLSKÝ[a], and JAN PROKEŠ[b]

[a] Polymer Institute, Slovak Academy of Sciences, Dúbravská cesta 9, 84541 Bratislava, Slovakia, [b] Charles University Prague, Faculty of Mathematics and Physics, V Holešovičkách 2, 182 00 Prague 8, Czech Republic
upolkrup@savba.sk
jan.kratochvila@savba.sk

Over the last years, the conducting polymer/graphite composites and nanocomposites have attracted considerable interests because of their exceptional properties. Polymer micro and nanocomposites prepared from high aspect ratio layered graphite nanofillers achieve significant improvements in mechanical, thermal, electrical and barrier properties at very low filler concentrations[1], compared to conventional composites, without a significant increase in density.

Here we discuss various aspects of electrical and mechanical behavior of composites based on the low density polyethylene (LDPE) matrix filled with various grades of expanded graphite having an average size 5, 50 and 500 μm. The aspect ratio of the fillers varies dependently on degree of exfoliation. We also compare the influence of various routes of preparation on the final mechanical and electrical properties.

The research was supported by the Scientific Grant Agency of the Ministry of Education of Slovak Republic and the Slovak Academy of Sciences (project No. 2/6114/26) and by Science and Technology Assistance Agency under the contract No. APVV-0478-07. This work is a part of the research plan MSM0021620834 that is financed by the Ministry of Education, Youth and Sports of the Czech Republic.

REFERENCE
1. Kalaitzidou K., Fukushima H., Drzal L. T.: Carbon *45*, 1446 (2007).

P-25
APPLICATION OF LIGNIN IN NATURAL RUBBER- BASED BLENDS

JANKA KUBAČKOVÁ*, IVAN HUDEC, and JOZEF FERANC

Slovak University of Technology in Bratislava, Faculty of Chemical and Food Technology, Institute of Polymer Materials, Department of Plastics and Rubber, Radlinského 9, 812 37 Bratislava, Slovakia
janka.kubackova@stuba.sk

Introduction

It is well known that lignin is a polydisperse natural amorphous polymer consisting of phenylpropane (C_6-C_3)

units and that some differences in its molecular mass and type of funcional groups exist dependent on the genetic origin of the wood and the method of isolation[1]. Lignin is readily available and relatively inexpensive material due to the fact its obtained as by-product of pulp production during delignification, which presents environmental problems and give altered lignin. Nevertheless, another important source of lignin exists, straw, a very diffuse and very low cost agricultural residue, which allow to obtain a less altered lignin.

Lignin has many functions in wood, but its commercial utilization is relatively low, usually it is burnt as an energy source. However, various properties of lignin designate it for different technical purposes. Lignin can be utilised as stabilizer (antioxidant) for plastics and rubber, the modified lignins have been used in crosslinked polyurethanes or phenolic resin or as a mechanical properties modifier for rubber mixtures[2,3]. Most studies of lignin as an additive to rubber compounds have investigated carbon black replacement in order to achieve similar reinforcement of rubber composites, but important problem is producing rubber composites with sufficient stability. Lignin, as the most stable cell-wall polymer of wood, may have great potential to be a filler with a stabilizing effect[4].

The present work deals with the possibility of application of commercially available lignins in rubber blends. There was studied influence of different types of lignin in natural rubber-based model blends on cure characteristics and mechanical properties.

Experimental

The formulation used in this study is given in Table I.

Rubber blends were prepared by mixing dry lignin powder and other ingredients with natural rubber. Six types of lignin (Table II) were used in range from 0 to 30 phr.

Results and discussion

Influence of lignin on cure characteristics – scorch time t_{s1} and optimum cure time t_{C90} were studied. Fig. 1 shows that the increasing of lignin content causes a decrease of scorch time t_{s1} for every type of lignin.

The same trend it is seen from Fig. 2 where optimum cure time t_{C90} decreases as well. The t_{C90} of maximum filled rubber blend with Li-Ca lignin decreased in about 35 % and the t_{s1} in about 42 % in comparison with unfilled blend.

More significant decrease of the t_{s1} in about 53 % was observed in case of rubber blend filled with 30 phr of DP 991 lignin. This results indicate that lignin may affect the curing behavior, probably due to the interaction of lignin with vulcanization system.

The effect of lignin on the mechanical properties of the prepared vulcanizates is illustrated in Fig. 3 and 4.

The properties such as tensile strength at break (Fig. 3) and elongation at break (Fig. 4) improved remarkably with the increasing amount of lignin from 10 phr in case of vulcani-

Table I
Formulation of NR rubber model blends

Ingredient	phr
SMR 20	100
Lignin	0, 5, 10, 15, 20, 25, 30
Zinc Oxide	5
Stearic Acid	2
Sulfur	3.5
CBS	3.5

Table II
Lignins properties

Lignin		Ca content %	pH of 10% sol.
Li-Ca	Calcium lignosulfonate	5	4.5
DP 624	Calcium lignosulfonate	5	4.2
DP 625	Calcium lignosulfonate	5	7.4
DP 850	Calcium lignosulfonate	1.8	7
DP 990	Calcium lignosulfonate		7.5-9
DP 991	Natrium lignosulfonate		7.9-10.5

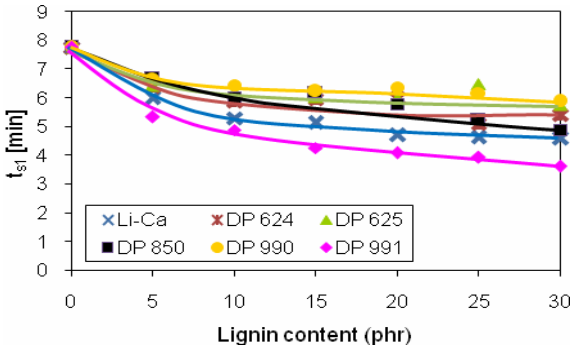

Fig. 1. **Effect of lignin content on scorch time t_{S1} of rubber blends**

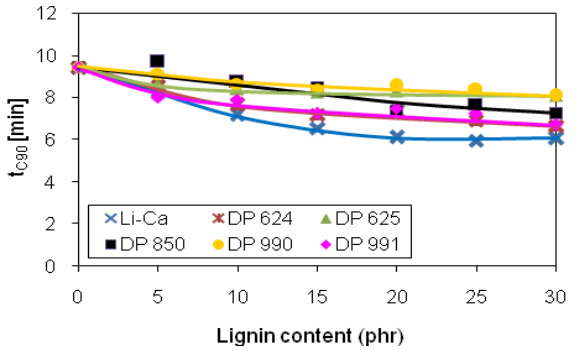

Fig. 2. **Effect of lignin content on optimum cure time t_{C90} of rubber blends**

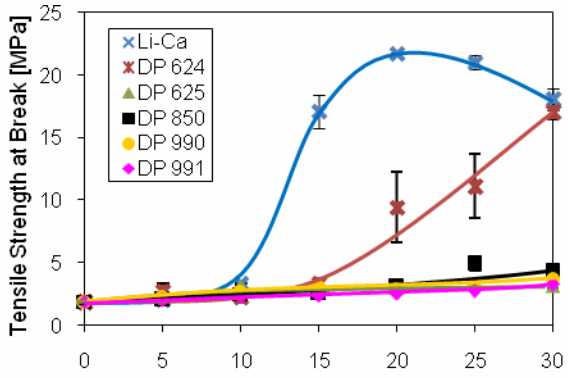

Fig. 3. **Effect of lignin content on tensile strength at break of vulcanizates**

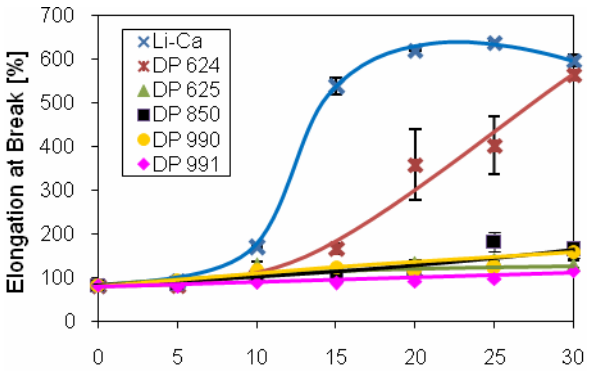

Fig. 4. **Effect of lignin content on elongation at break of vulcanizates**

zates filled Li-Ca and DP 624 lignins. The tensile strength at break and elongation at break of vulcanizates filled with lignin up to 10 phr were comparable or increased moderately in comparison with lignin free vulcanizates. The addition of other types of lignin had only very slight effect on an increase of evaluated properties. The values illustrated in Fig. 3–4 indicate that optimum lignin concentration for maximum reinforcement is about 20 phr for Li-Ca and 30 phr for DP 624 lignin.

Conclusion

The obtained results show that lignin has significant influence on cure characteristics as well as mechanical properties. The final results indicate a great potential for the use of Li-Ca lignin as a filler for NR rubber blends.

This work was supported by Ministry of Education of Slovak Republic project No. 26220220091 by the Research & Development Operational Programe funded by the ERDF.

REFERENCES

1. Košíková B., Gregorová A.: J. Appl. Polym. Sci. *97*, 924 (2005).
2. Alexy P., Košíková B., Podstránska G.: Polymer *41*, 4901 (1999).
3. Alexy P., Feranc J., Kramárová Z., Hajšová M., Ilisch S., Ďuračka M., Mošková D., Chodák I.: KGK, Kautsch. Gummi Kunstst. *61*, 26 (2008).
4. Košíková B., Gregorová A., Osvald A., Krajčovičová J.: J. Appl. Polym. Sci. *103*, 1226 (2007).

P-26
SIMULATION OF RUBBER INJECTION MOLDING PROCESS

KAMIL KYAS, MICHAL STANĚK, MIROSLAV MAŇAS, DAVID MAŇAS, MARTIN KŘŮMAL, and ZDENĚK HOLÍK

Tomas Bata University in Zlin, Department of Production Engineering, Nam. T.G.Masaryka 275, 762 72 Zlin, Czech Republic
kyas@ft.utb.cz

Abstract

Simulation analysis of injection moulding are a good tool for improving the quality of polymeric products and manufacturing equipment, an instrument to reduce the time to prepare new products for market. The poster point out that in terms of computational resources, nothing precludes the injection of the rubber compounds could be analyzed already in the design development stage of production and were thus achieved positive gains, which have been applied to thermoplastic parts. Reliable tool for analyzing injection moulding of rubber compounds is software Cadmould Rubber, a product developed by German company Simcon GmbH.

1. Introduction

Injection moulding is now a well-established fabrication process in environmental industry. It has more advantages in most situations over the older processes of compression and transfer moulding. These advantages comprise reduced labour cost, better dimensional control and shorter cure times for injection moulding process. This process is still improved and other materials (not only thermoplastic) are used for example elastomeric compound.

The injection moulding process is a cyclical process, each cycle comprises several operations: feeding, melting and homogenization of polymer grains inside the plasticizing cylinder mould closing, injection under pressure of melt in mould's cavities and cooling or heating of polymer inside the mould, mould opening and ejection of moulded piece. In figure 1 there is shown time influence for each parts of cycle. It is necessary to realize, that rubber injection moulding cycle is several times longer than for thermoplastics. It is evocated by long time period of heating (curing) of a compound.

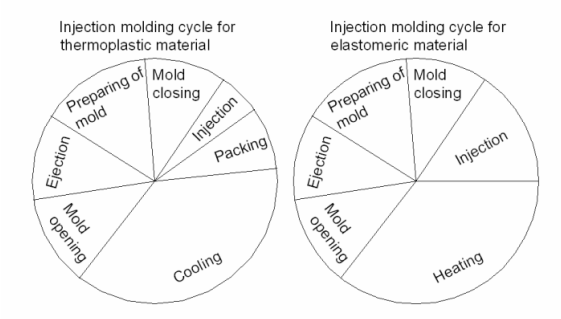

Fig. 1. **Moulding cycles**

During injection moulding process, melt is subjected to more severe processing conditions than during compression or transfer moulding. Values of temperatures, pressures, and shear stresses are higher, though cure times are shorter in rubber compound. Control over process variables can be more precise.

The cycle time can be minimized by independently controlling barrel temperature, screw speed, mould temperature and injection pressure. That is the reason why the analysis of injection moulding process should be improved and understood.

2. Experiment

As it was told, elastomeric mixtures consist of different additives and different quantities, therefore each compound is the "original" and they have differences at flow characteristics. These properties can be measured by Rubber Process Analyzer (RPA 2000). The amount sample of mixtures should be approximately 100 g. These prepared samples of rubber compound which weighs about 5 g is placed into the measuring device and is closed by force 15 kN. Top and bottom of the mould are heated with accuracy ± 0.3 °C.

Rubber compound with vulcanization system is used for measuring the curing characteristics (Fig. 2) and without the vulcanization system is used for measuring the complex dynamic viscosity (Fig. 3).

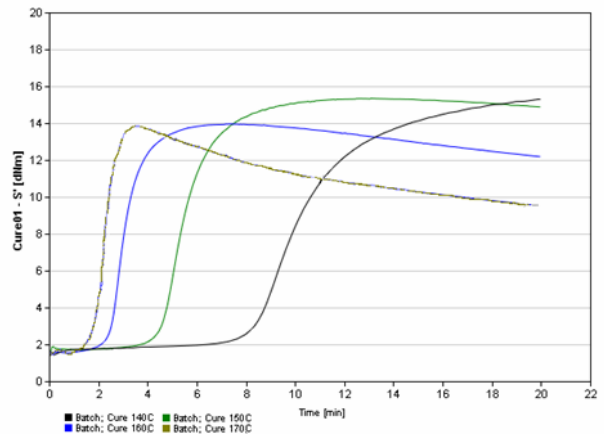

Fig. 2. **Cure rate for different temperatures**

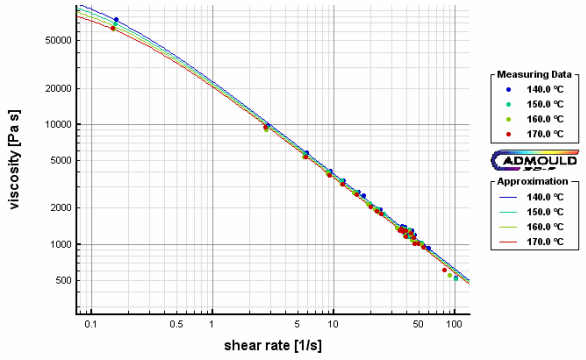

Fig. 3. **Viscosity for different temperatures**

Table I
Process parameters

Filling time	30	s
Pressure – controlled filling	99	%
Mass temperature	100	˚C
Uniform wall temperature	160	˚C
Heating time	600	s
Post curing	200	s

These Data are processed and imported to Cadmould Rubber programme, where analysis of injection moulding process can be done now.

The basic input format for importing components is STL. Before setting up process parameters is necessary to create a computational network and assign the measured material characteristics. These simulations of injection moulding process were optimized to finally form several times. Profitable last setting is shown in Table I.

3. Results and discusion

With using the colour spectrum is filling time displayed in Fig. 5. According to these results weld lines and air traps can be predicted. But software Cadmould Rubber displays these results automatically. It is easier and more comfortable especially for analyses of products with difficult shape.

Temperature and curing closely related together and it is important to know these values during injection moulding process of elastomeric compound. Program Cadmould Rubber has great advantage that it can show the temperature and percentage of crossed-links in each moment during injection moulding cycle and in the individual layers of the product. It is necessary to consider how many layers use before setting analyse. With large number of layers time of computing increase rapidly on the other hand the results are more accurate.

On a Fig. 5 there is shown a detail of part. For the better understanding of injection moulding process is necessary to

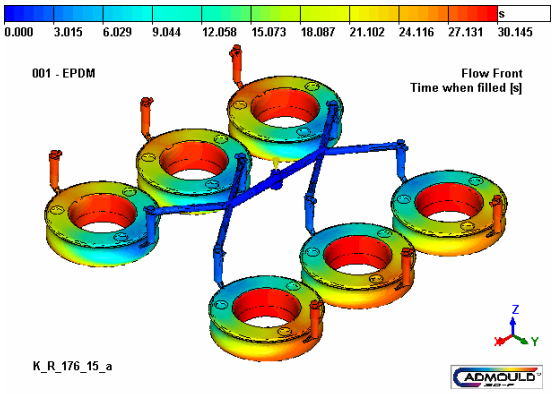

Fig. 4. **Filling time**

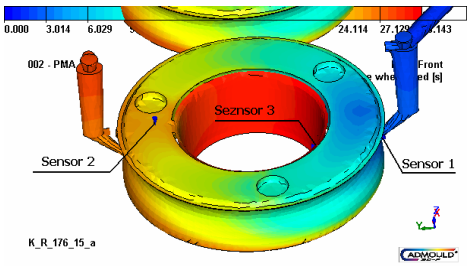

Fig. 5. **Places of sensors**

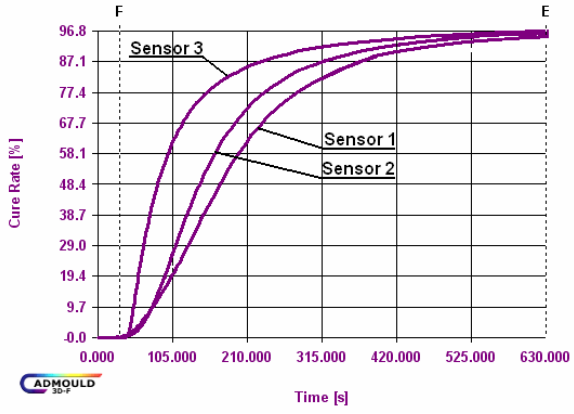

Fig. 6. **Cure rate for each sensor**

know how elastomeric compound behave in each places of part and sensors are right tools to show behaviour of material. It can rendered results of pressure, temperature, viscosity, shear rate and in Fig. 6 there are rendered curves of cure rate for each of used sensors.

These results can help to set up injection moulding cycles of injection moulding machine. Especially cure rate is necessary for setting of the longest and most energy-consuming cycles and it is heating time.

4. Conclusion

Software Cadmould Rubber can show more important and interesting result of analyse. Results show very similar tendency as in real process. It can be told that Cadmould Rubber is good and helpful computational tool for injection moulding process of elastomeric compound.

This article is financially supported by the Czech Ministry of Education, Youth and Sports in the R&D projects under the titles 'Modelling and Control of Processing Procedures of Natural and Synthetic Polymers', No. MSM 7088352102 and 'CEBIA Tech', No. CZ.1.05/2.1.00/03.008.

REFERENCES

1. Manas D., Stanek M., Manas M., Pata V., Javorik J.: KGK, Kautsch. Gummi Kunstst. *62*, 240 (2009).
2. Maňas M., Staněk M., Maňas D., Daněk M., Holík Z.: Chem. Listy *103*, 24 (2009).
3. Kyas K., Stanek M., Manas M., Manas D., Krumal M., Cerny J.: *21st International DAAAM Symposium, 2010, Zadar*, Croatia, p. 1081.

P-27
PROPERTIES OF COMPOSITES OF LOW DENSITY POLYETHYLENE FILLED WITH MAGNESIUM HYDROXIDE

ZUZANA NÓGELLOVÁ and IVAN CHODÁK

Polymer Institute, Slovak Academy of Sciences, Dúbravská cesta 9, 845 41 Bratislava, Slovakia
zuzana.nogellova@savba.sk

Several types of magnesium hydroxide in composites with low density polyethylene matrix were tested. Three types of magnesium hydroxide were modified with various agents. These experimentally prepared fillers were compared with two commercial types of this filler. Moreover, an attempt was done to increase rather low toughness of the composites by crosslinking initiated by thermal decomposition of organic peroxide. This would be beneficial also if considering possible application for fire-resistant cables. 2,5-dimethyl-2,5-di (tert-butylperoxy)hexyne(3) was used as the initiator of crosslinking.

Mechanical properties of composites filled with experimental types of magnesium hydroxide show only marginal differences. The differences are more remarkable for composites containing commercial fillers.

Crosslinking leads to a significant increase of tensile strength and elongation at break indicating improving the interactions between polymeric matrix and filler. Young's modulus is lower in this case, in accordance with lower crystallinity caused by restriction of macromolecules mobility in crosslinked matrix. Effectivity of crosslinking was determined from values of insoluble portion. Insoluble portion of uncrosslinked samples is increasing with concentration of filler in composites only slightly and it is related to formation of physically bonded polymer. In crosslinked samples the increase of insoluble portion with a filler content was substan-

tial and it reached almost 100 wt.% of insoluble portion at the highest concentration of a filler (70 wt.%).

The research was supported by project APVV 0203-07.

P-28
POLYETHYLENE MEMBRANES HYDROPHILIZATION BY ATMOSPHERIC LOW-TEMPERATURE PLASMA

IGOR NOVÁK*[a], IVAN CHODÁK[a], MILENA ŠPÍRKOVÁ[c], GALINA ELYASHEVICH[b], ALEXEJ OLIFIRENKO[b], ANTON POPELKA[a], ANGELA KLEINOVÁ[a], and VLADIMÍR POLLÁK[a]

[a] *Polymer Institute, Slovak Academy of Sciences, 845 41 Bratislava 45, Slovakia,* [b] *Institute of Macromolecular Compounds, Russian Academy of Sciences, Saint Petersburg, Russian Federation,* [c] *Institute of Macromolecular Chemistry, Academy of Sciences of the Czech Republic, v. v. i., Praha, Czech Republic*
Igor.Novak@savba.sk

Abstract

The contribution deals with surface modification of high density polyethylene (HDPE) porous film by surface barrier discharge plasma in nitrogen and oxygen. It was observed that the surface energy of HDPE porous film modified by diffuse surface barrier discharge plasma increased even for short time of modification.

Introduction

The hydrophobicity of polyethylene represents a permanent problem which cannot be solved without modification of polymer. The securing of good adhesion of more polar liquids to HDPE porous film surface necessitates increasing its surface energy by convenient modification methods. The most advanced method of modification of HDPE porous film surface, due to its practical usability, suitability to continuous modification processes, and efficiency the modification, is based on modification by electric discharge plasma[1–4]. The aim of the paper is presentation of research results relating to the change in surface and adhesive properties of HDPE porous film modified by diffuse surface barrier discharge plasma in the medium of N_2 or O_2 at atmospheric pressure.

Experimental

The experiments were carried out with HDPE porous film (Stavrolen, Russia) prepared by melt extrusion process with subsequent annealing and uniaxial extension. The thickness of HDPE porous film was 14 μm and it contained through channels 100−300 nm in size.

The modification of HDPE porous film was performed in static conditions by diffuse surface barrier discharge (DSBD) plasma. The modification of polymer was realized at atmospheric pressure in N_2 or O_2 of a technical purity.

Measurement of the surface energy of polymer was carried out by direct measurements of contact angles of testing liquids set (re-distilled water, ethylene glycol, formamide, methylene iodide, and α-bromo naphthalene) using Surface Energy Evaluation System (Advex, Czech Republic). The surface energy and its polar component were evaluated by Owens-Wendt-Rable-Kaelble (OWRK) modified by method of least squares[3].

Results and discussion

The surface properties of HDPE porous film modified by DSBD plasma in O_2 and N_2 are shown in Fig. 1. The surface energy of HDPE porous film traeted by DSBD increased markedly after a short treatment time (5 s) in comparison with unmodified polymer. The total surface energy of SBD plasma modified HDPE porous film increased from 33.2 mJ m^{-2} (unmodified sample) up to 51.8 mJ m^{-2} (DSBD, O_2,10 s) and 53.9 mJ m^{-2} (DSBD, O_2, 20 s), or 48.9 mJ m^{-2} (DSBD, N_2, 10 s) and 51.3 mJ m^{-2} (DSBD, N_2, 20 s), respectively. The degree of modification of HDPE porous film by DSBD discharge plasma was more pronounced with longer time of modification.

Conclusions

The significant increase of the surface energy and its polar component of HDPE porous film modified by DSBD plasma in O_2 and N_2 at atmospheric pressure was observed. This increase was important even for short times of polymeric porous film modification by DSBD plasma, and for longer times of modification was more pronounced.

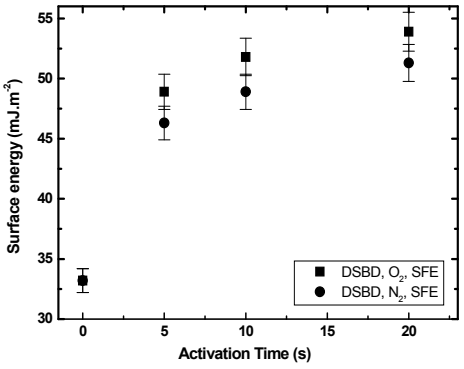

Fig. 1. **Surface energy of HDPE porous film modified by DSBD (50 W) plasma in O_2 and N_2 vs. time of activation**

The research was supported by the Slovak Scientific Agency project VEGA, No.2/0185/10, by the Slovak Research and Development Agency, project VSMP-P-0023-09, by the Grant Agency of the Academy of Sciences of the Czech Republic (grant A 400500505), and the Russian Foundation for Basic Research (Grant No. 07-03-00177).

REFERENCES

1. Mikula M., Jakubíková Z., Záhoranová A.: J. Adhes. Sci. Technol. *17*, 2097 (2003).
2. Ráhel J., Šimor M., Černák M., Štefečka M., Imahori Y., Kando M.: Surf. Coat. Technol. *604*, 169 (2003).
3. Novák I., Števiar M., Chodák I., Krupa I., Nedelčev T., Špírková M., Chehimi M. M., Mosnáček J., Kleinová A.: Polym. Adv. Technol. *18*, 97 (2007).
4. Novák I., Pollák V., Chodák I.: Plasma Process. Polymers *3*, 355 (2006).

P-29

ANTIBACTERIAL MODIFICATION OF MEDICAL/ GRADE PVC BY ATMOSPHERIC PLASMA AND POLYSACCHARIDES

IGOR NOVÁK*[a], MARIÁN LEHOCKÝ[b], IVAN CHODÁK[a], ANTON POPELKA[a], ITA JUNKAR[c], ALENKA VESEL[c], and IVICA JANIGOVÁ[a]

[a] Polymer Institute, Slovak Academy of Sciences, 845 41 Bratislava 45, Slovakia, [b] Tomas Bata University in Zlín, T.G.M. Sq. 5555, 760 01 Zlín, Czech Republic, [c] Department of Surface Engineering, Plasma Laboratory, Jožef Stefan Institute, Jamova cesta 39, SI-1000 Ljubljana, Slovenia
Igor.Novak@savba.sk

Abstract

Medical-grade polyvinyl chloride was coated by polysaccharides through a novel physicochemical approach. An initial surface activation was performed foremost via diffuse coplanar surface barrier discharge plasma in air at ambient temperature and pressure. Radical graft copolymerization of acrylic acid through grafting-from pathway was directed to render a well-defined brush, and finally chitosan monolayer and chitosan/pectin alternating multilayer were bound onto the functionalized surfaces.

Introduction

A multistep physicochemical approach making use of plasma technology combined with wet chemistry has fueled considerable interest in delivery of surface-active anti-adherence materials[1–3]. In the first step of the approach, concerning an inherent lack of befitting functional groups on pristine substrate, plasma treatment at low temperature and atmospheric pressure has been substantiated to be productive in yielding reactive entities on the surface[1]. In the second phase of the approach, an end-functionalized polymer brush is synthesized on the surface via surface-initiated polymerization (SIP). SIP encourages the formation of surface-confined thick brush layers of high grafting density on the surface using generation of appropriate initiators anchored to substrate in which monomers are able to easily make their way through already-grafted layer and contribute to the chain growth. In the final step, biomolecular species are immobilized onto this platform to bear sought after biological activity.

Experimental

General

PVC pellets, extrusion medical-grade RB1/T3M of 1.25 g cm^{-3} density, were obtained from ModenPlast (Italy) and used as received. Pectin from apple, (BioChemika, with esterification of 70–75 %), acrylic acid (99.0 %, anhydrous), and *N*-(3-dimethyl aminopropyl)-*N′*-ethyl carbodiimide hydrochloride (EDAC, 98.0 %) were supplied by Fluka (USA). Chitosan from crab shells with medium molecular weight and deacetylation degree of 75–85 %.

Plasma activation, PAA grafting and polysaccharides immobilization

Plasma treatment was implemented in static conditions by DCSBD technology with air as the gaseous medium at atmospheric pressure and room temperature. All samples were treated on both sides with plasma power of 200 W for 15 sec. PVC substrates, upon treatment with plasma, were immersed into spacer solutions containing 10 vol.% AA aq. solution. The reaction was allowed to proceed for 24 h at 30 ºC. The samples were taken out, washed with 0.05 vol.% Triton X-100 aq. solution, and also deionized water for 5 min at 30 ºC in an ultrasonic bath to remove any unbound PAA species on the surface. Drying was done in an air-circulating oven under 30 ºC for 24 h. PAA grafted PVC samples were dipped into 1 w/v % glutaraldehyde aq. solution at 4 ºC overnight which acted as an amine-reactive homobifunctional fixative to immobilize chitosan species onto the surface via crosslinking.

Results and discussion

A highly surface sensitive technique is contact angle analysis which enables a convenient assessment of the surface wettability. PVC exhibits a hydrophobic characteristic (θ_w = 85.9°), which after being treated by plasma, an evident change in θ_w = 64.9° arises, and hydrophilicity ascends as anticipated. This trend continues in the case when polyacrylic acid (PAA) chains are grafted where more hydrophilic propensity is shown inferred from θ_w = 46.5°. The elevated hydrophilicity upon multistep modifications is assumed to come from the inclusion of superficial hydrophilic entities. The hydrophilicity then decreases as polysaccharides are coated onto the investigated polymer (θ_w = 50.5°).

Conclusions

DSBD plasma is capable of raising surface energy of PVC, and introducing oxygen-containing functionalities anchored onto the polymeric surface. A structured PAA brush of high graft density is synthesized using surface-initiated approach to further improve hydrophilicity and develop a stable brush-like assembly to yield a platform for biomolecular binding. Surface-sensitive analyses evidence the presence of chitosan and chitosan/pectin multilayer.

Financial supports by the Slovak Academy of Sciences (Grant VEGA 2/0185/10),by Slovak Research and Development Agency, project VSMP-P-0023-09, the Ministry of Education, Youth, and Sports of the Czech Republic (Grant VZ MSM 7088352101 as well as Grant MPO 2A-1TP1/126), and the Slovenia Ministry of Higher Education, Science, and Technology (Program P2-0082-2)are gratefully acknowledged.

REFERENCES

1. Desmet T., Morent R., Geyter N. D., Leys C., Schacht E., Dubruel P.: Biomacromol. *10*, 2351 (2009).
2. Speranza G., Gottardi G., Pederzolli C., Lunelli L., Canteri R., Pasquardini L., Carli E., Lui A., Maniglio D., Brugnara M., Anderle M.: Biomater. *25*, 2029 (2004).
3. Kenawy E. R., Worley S. D., Broughton R.: Biomacromol. *8*, 1359 (2007).

P-30
THE INCREASE IN EFFICIENCY OF CURING SYSTEMS VULCANIZED AT LOW TEMPERATURES

DARINA ONDRUŠOVÁ*, MARIANA PAJTÁŠOVÁ, TATIANA BAZYLÁKOVÁ, MÁRIA KOPCOVÁ, MICHAELA ĎURČEKOVÁ, MARTINA ČECHOVÁ, and EUGEN JÓNA

Faculty of Industrial Technologies, TnU AD, I. Krasku 491/30, 020 01 Púchov, Slovakia
ondrusova@fpt.tnuni.sk

Increasing the efficiency of rubber compounds curing systems and effect of application new types of accelerators, or their combinations, has been intensively studied. Dithiocarbamates used in the curing process of rubber compounds form a group of ultra-accelerators[1]. Several new metal *N*-ethyl-*N*-phenyldithiocarbamates have been prepared recently, their structural properties and influence on the kinetics of cure were studied[2]. The kinetically most active Co(III) *N*-ethyl-*N*-phenyldithiocarbamate (Fig. 1) ($Co(epdtc)_3$) was mixed into commercial rubber compound – coupler, especially used for cold tire retreading, which is vulcanized at lower temperatures of 95−100°C.

Four new curing systems of rubber compound named with the addition of new dithiocarbamate accelerator Co $(epdtc)_3$ were prepared. Their efficiency was evaluated testing the vulcanization characteristics and physical and mechanical properties of vulcanizates before and after accelerated thermal aging in air. The optimal values of characteristics tested showed vulcanization system containing of 1,67 phr Co

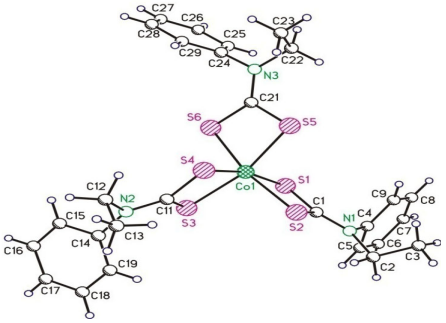

Fig. 1. **Crystal structure of $Co(epdtc)_3$** (ref.[3])

$(epdtc)_3$, specifically slightly decreased but comparable values of modulus 300 % and hardness in comparison with original vulcanization system, increased and thus better elongation value, tesile strength and elasticity. Obtained results are clearly positive for the possibility of increasing the efficiency of vulcanization systems by addition of $Co(epdtc)_3$.

REFERENCES

1. Debnah S. Ch. and Basu D. K.: KGK, Kautsch. Gummi Kunstst. *48*, 111 (1995).
2. Ondrušová D., Jóna E. and Šimon P.: J. Thermal Anal. Calorimetry *67*, 147 (2002).
3. Ondrušová D., Koman M., Jóna E., Pajtášová M., Glowiak T.: Acta Cryst. *E57*, 172 (2001).

P-31
THE ATMOSPHERIC PLASMA TREATMENT OF THE POLYMER FILMS

ANDREA ORAVCOVA* and IVAN HUDEC

Slovak University of Technology in Bratislava, Faculty of Chemical and Food Technology, Institute of Polymer Materials, Department of Plastics and Rubber, Radlinského 9, 812 37 Bratislava, Slovakia

The purpose of this work was to improve surface energy and wettability of the films before printing by plasma treatment. The printability of polymer materials is dependent upon the chemical and physical properties of the polymers. The surface of polypropylene consists solely of carbon and hydrogen. Using appropriate plasma treatment, the surface of the non-polar polymer material may be activated to contain the variety of functional groups including oxygen-based functionalities (carbonyl, carboxyl, ether, peroxide etc.) or nitrogen-based groups resulting in modification of the surface properties. Low-functionality polypropylene surfaces become more reactive by enhancing the concentration of polar groups on the surface.

The result of plasma modification of the polymer film is the increase of the surface energy of the polymer and the improvement of surface wetting by liquids. The minimum value of the surface free energy of the material being printed using the solvent-based inks is 38 mJ m^{-2}.

The advantage of the plasma treatment is the ability to change the surface properties of the most external layers of the material without modifying its bulk characteristics[1].

The transparent PP film (monoaxially oriented polypropylene, 30 μm thickness, CHEMOSVIT FOLIE, a.s. Svit) determined for packaging various products was studied. The films were activated by atmospheric pressure plasma treatment by the diffuse coplanar surface barrier discharge DCSBD (350W imput) using ambient air and nitrogen. The treatment time varied from 1 s to 5 s.

Surface properties were characterized by the contact angle measurement of sessile drop (4 μl, liquids; water, glycerol, α-bromonaphthalene, formamide, ethylene glycol) using CCD camera (SEE software 6.1, MU Brno, Czech.Rep.).

As it can be seen in the Fig. 1a, polar liquids, such water, do not wet the surface of the untreated hydrophobic PP film in comparison with the treated film sample (Fig. 1b).

1a 1b

Fig. 1. **A drop of water on the PP film before (1a) and after (1b) plasma treatment**

The dyne test pen Quick Test 38 was used to confirm changes in wetting of the films,too. In the Fig. 2 there are shown an untreated and a wettable 5s-plasma treated film.

The contact angles of testing liquids with different polarity and PP films largely decreased with increasing treatment time. The values of total surface energy, calculated by Owens-Wendt regression method, were increased, as shown in Fig. 3 and Fig. 4.

There was a significant increase in the polar (AB) component of the surface energy after the treatment.

untreated 5s plasma treated film

Fig. 2. **Test by Quick Test 38**

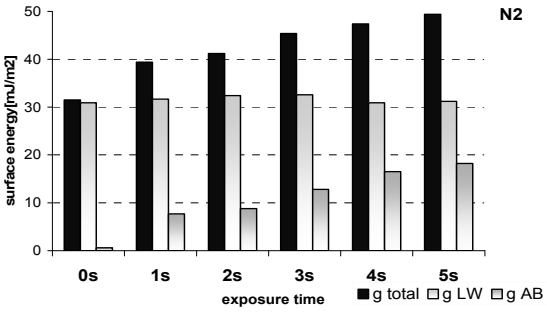

Fig. 3. **Influence of the time of plasma treatment on the surface energy of the polymer surface using nitrogene as a workink gas**

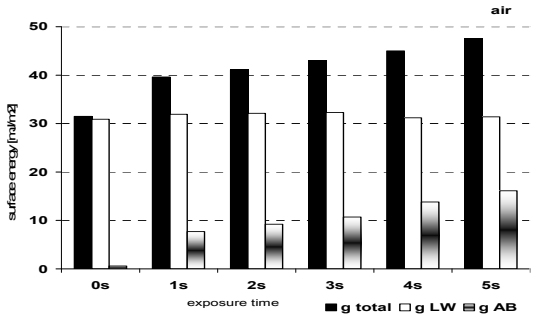

Fig. 4. **Influence of the time of plasma treatment on the surface energy of the polymer surface using ambient air as a working gas**

The required surface energy for printing using solvent-based inks (38 mJ m^{-2}) was detected by all the investigated samples.

The surface functionalities were also detected by attenuated total reflection (ATR) technique of FTIR spectroscopy. Fig. 5 shows the influence of plasma discharge on chemical composition of the surface of polypropylene films.

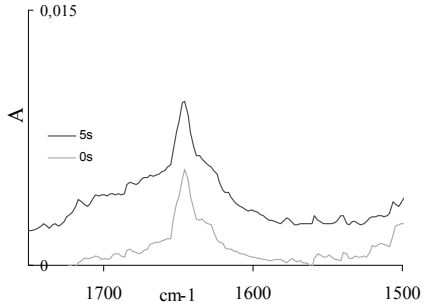

Fig. 5. **FT IR spectra of treated (5 s, air) and untreated PP films**

Fig. 5 shows the influence of plasma discharge on chemical composition of the surface of polypropylene films.

There are some small surface changes of PP films, before and after plasma treatment, in the region of carbonyl and carboxyl groups (1520–1750 cm^{-1}). It confirms creation of small amount of polar functional groups on the film.

AFM technique was used to study changes in morphology of PP films as it can be seen in Fig. 6b and Fig. 6c in comparison with untreated sample in Fig. 6a. There are changes in roughness, the value of middle roughness (RSM) increased.

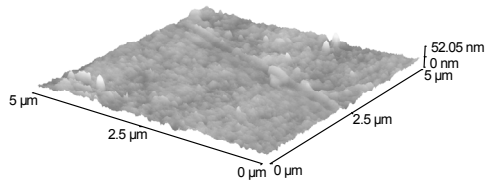

Fig. 6a. **AFM image of untreated PP, RSM= 3.1 nm**

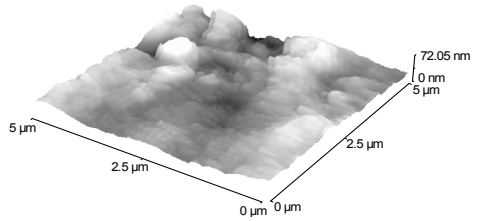

Fig. 6b. **AFM image of untreated PP in N_2, RSM=10 nm**

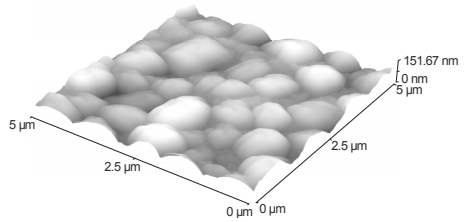

Fig. 6c. **AFM image of untreated PP in air, RSM=24 nm**

As it was expected, plasma treatment has no significant influence on mechanical properties ("bulk properties"). The values of tensile strength at break varied from 21.9 (3 s) to 23 MPa (1 s), the value for untreated sample was 23 MPa.

Based on obtained results it is possible to note that the plasma treatment at atmospheric pressure by diffuse coplanar surface barrier discharge seems to be a successful technique for improving wettability of hydrophobic polymer film materials.

As performed experiments showed, the contact angle of the treated polypropylene films decreased and the surface energy of the samples increased in comparison with the plasma untreated samples. Improved wettability of the samples was also obtained by using the dyne test pen. The proper surface energy for printing using solvent-based inks (38 mJm^{-2}) was detected by all the investigated samples after plasma treatment in ambient air. It was confirmed that plasma treatment has no significant influence on mechanical properties of polypropylene films.

REFERENCE

1. Inagaki N.: *Plasma Surface Modification and Plasma Polymerization*, CRCPress, London 1996.

P-32

SILICA LOCALIZATION IN NBR/SBR AND NBR/NR COMPOUNDS

KATJA OSSWALD[a], HAI HONG LE[b], SYBILL ILISCH[b], HANS-JOACHIM RADUSCH[b], and JÖRG KIRBS[a]

[a] University of Applied Science, D-06217 Merseburg, [b] Martin Luther University Halle-Wittenberg, Center of Engineering Sciences, D-06099 Halle (Saale), Germany
katja.osswald@hs-merseburg.de

Introduction

A multitude of rubber composites, especially in technical applications, are based on filler containing rubber blends. Effective dispersion and distribution as well as optimized phase selective filler localization in rubber blends has been recognized as one of the most important facts for achieving high quality and consistent product performance. Rubber type, rubber-filler interaction and also technological parameters during the mixing process control the filler distribution in the different blend phases[1–4]. The local filler distribution in vulcanized blends can be characterized by means of different direct and indirect methods. Transmission electron microscopy (TEM) was used by Sahakaro[5] and Suzuki[6]. Sircar[7] analyzed the filler migration in S-SBR/BR, NR/BR and CIIR/BR blends by atomic force microscopy (AFM). Nuclear magnetic resonance (NMR) and differential scanning calorimetry (DSC) in combination with bound rubber measurements were used by Massie[8] for BR/NR blends. Dynamic mechanical analysis (DMA) was used by Meier[9] and Sirisinha[10] to analyze the filler distribution in different rubber blends.

Experimental

The selective extraction in connection with thermogravimetric analysis (TGA) is presented in this work as new method for the characterization of the phase selective silica distribution in low filled S-SBR/NBR and NBR/NR blends. For the quantification of the different wetting behavior of the used rubber types, the so called rubber layer *L* was estimated by means of solubility measurements[11,12]. The effect of the mixing regime on the phase selective silica distribution was investigated by the methods described above and checked by atomic force microscopy for the S-SBR/NBR blends. For the NBR/NR blends, the effect of the viscosity of the NR phase and the effect of the polarity of the NBR phase on the filler localization were investigated. The infiltration rate *b* and the wetting parameter ω_S were used for the prognosis of the phase selective filler distribution in binary blends.

The wetting parameter ω_S was calculated by the Young equation[13] (Eq.*1*).

$$\omega_s = \frac{\gamma_{silica-rubber\ 1} - \gamma_{silica-rubber\ 2}}{\gamma_{rubber\ 1-rubber\ 2}} \qquad (1)$$

By application of eq. (*1*) the following cases could occur:

$\omega_s < -1$: silica is concentrated in the phase of rubber 2,
$\omega_s > 1$: silica is concentrated in the phase of rubber 1,
$-1 < \omega_s > 1$: silica is concentrated in the interface of both phases.

The interfacial tension between two phases was calculated by the Girifalco-Good equation (Eq. *2*)

$$\gamma_{12} = \gamma_1 + \gamma_2 - 2\sqrt{\gamma_1}\gamma_2 \qquad (2)$$

For the selective extraction 0.2 g uncured blend material were dissolved in 100 ml cyclohexane at 70 °C for 12 h in laboratory oven. The S-SBR respectively the NR phase of the blends are in solution. The gel of NBR phase was analyzed by TGA with regard to the residual filler. The investigations on S-SBR/NBR blend show a silica localization in the NBR phase already after short mixing time (Fig. 1). The S-SBR phase was free of silica. The reason is the high affinity of the acrylonitrile groups to the silica surface.

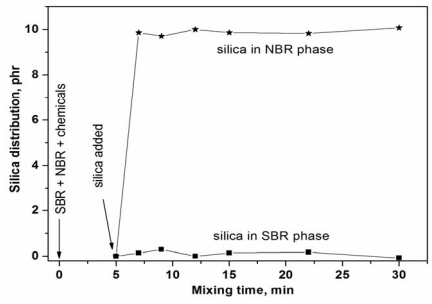

Fig. 1. **Silica localization for the S-SBR/NBR blend versus mixing time**

Furthermore, no effect of the viscosity of the NR phase and the polarity of the NBR phase was found on the silica localization in the binary blends. In addition, silica was determined in the NBR phase after short mixing time. The prognosis of the phase selective filler distribution by infiltration rate and wetting parameter[14] were confirmed by experimental values by the selective extraction.

REFERENCES

1. Le H. H., Ilisch S., Heidenreich D., Wutzler A., Radusch H.-J.: Polymer Composites *31*, 1701 (2010).
2. Ziegler J., Schuster R. H.: KGK, Kautsch. Gummi Kunstst. *56*, 159 (2003).
3. Hess W. M., Swor R. A., Micek E. J.: Rubber Chem. Technol. *57*, 959 (1984).
4. Natchimuthu N.: Rubber Chem. Technol. *83*, 123 (2010).
5. Sahakaro K., Naskar N., Datta R. N., Noordermeer J. W. M.: Rubber Chem. Technol. *80*, 115 (2007).
6. Suzuki N., Ito M., Ono S.: KGK, Kautsch. Gummi Kunstst. *57*, 303 (2004).
7. Sircar A. K., Lamond T. G., Pinter P. E.: Rubber Chem. Technol. *46*, 178 (1973).
8. Massie J. M., Hirst R. C., Halasa A. F.: Rubber Chem. Technol. *66*, 276 (1993).
9. Meier J. G., Klüppel M., Geisler H., Schuster R. H.: KGK, Kautsch. Gummi Kunstst. *58*, 587 (2005).
10. Sirisinha C., Prayoonchatphan N.: J. Appl. Polym. Sci. *81*, 3198 (2001).
11. Le H. H., Ilisch S., Kasaliwal G. R., Radusch, H.-J.: KGK, Kautsch. Gummi Kunstst. *60*, 241 (2007).
12. Le H. H., Ilisch S., Kasaliwal G. R., Radusch H.-J.: Rubber Chem. Technol. *81*, 767 (2008).
13. Wu S.: *Polymer Interface and Adhesion*, Marcel Dekker, New York 1982.
14. Le H. H., Osswald K., Ilisch S., Radusch H.-J.: Rubber Chem. Technol., submitted.

P-33
THE POSSIBILITY OF USING NON-AROMATIC OILS AND DITHIOPHOSPHATES IN RUBBER COMPOUNDS

MARIANA PAJTÁŠOVÁ*, DARINA ONDRUŠOVÁ, JANA PALIESKOVÁ, SLÁVKA ĽALÍKOVÁ, ZUZANA JANKUROVÁ, and ANDREA FERIANCOVÁ

Faculty of Industrial Technologies, TnU AD, I. Krasku 491/30, 020 01 Púchov, Slovakia
pajtasova@fpt.tnuni.sk

The ecological requirements are closely linked to the issue of environmental protection and human health, which is attaches currently the greatest importance. One of a number of measures is to use products that are not harmful to health. Using high-aromatic oils in the rubber industry is increasingly criticized, especially because of health risks, because these oils contain polycyclic aromatics (PCA), most of which are carcinogenic. The subject of the introduced work is to investigate the effects of non-aromatic oils of the type (TDAE – modified aromatic oils distilled, MES – Extract refined oils, RAE – residual aromatic oils) on the processing properties, physico-mechanical, dynamic-mechanical properties and vulcanization characteristics of the tread compound designed for winter use.

The measured results showed improvement of some observed properties of the compound with application of organic and commercially produced plasticizers.

The creation of Nitrosamine-free vulcanization systems is one of the importent environmental problems in the car tyres production. Present work deals with ecologisation of vulcanization system of rubber compond for passenger car tyres. The formation of Nitrosamine-free vulcanization system was providet by the way of substitution of commercially used benzothiazolic accelerator (Vulkacit DZ) with some new accelerators on the base of Dithiophosphates, that do not form dangerous Nitrosoamines.

Dithiophosphates tend to form monosulfidic or disulfidic crosslinks which, because of their higher bond energies, are much more resistant to reversion, so they added to enhance heat stability. The results of measurements show in

majority of studied properties the synergistic effects of combination Zn-dithiophosphate with Vulkacit DZ. On the base of evaluated results two optimal synergistic vulcanization systems were selected.

REFERENCES
1. Pimblott I. G., et al.: J. Appl. Polym. Sci. *23,* 3621 (1979).
2. Issel H.-M., Steger L., Bischoff A.: Application of Dithiophosphates in Silica Reinforced Elastomer Compounds, *6th Fall Rubber Colloquium, November 11th, 2004, Hannover, Germany*.
3. Graf H.-J.: Nitrosamine-free Vulcanization Systems, New Thiophosphate Generation - Advantages in Nitrosamine-free Vulcanization Systems, *IRC ´93, October 1993, Orlando*, USA.

P-34
MODIFICATION OF PROCESSING AND MECHANICAL PROPERTIES OF POLYLACTID ACID/POLYHYDROXYBUTYRATE BLENDS

MIROSLAVA PAVLAČKOVÁ, KATARÍNA TOMANOVÁ, FRANTIŠEK BENOVIČ, RODERIK PLAVEC, and PAVOL ALEXY

Institute of Polymer Materials, Faculty of Chemical and Food Technology, Slovak University of Technology, Radlinského 9, 812 37 Bratislava, Slovak Republic
miroslava.pavlackova@stuba.sk

Introduction

Plastic materials have found wide range of applications in different aspects of life and industries. However, most conventional plastics such as polyetylene, polypropylene, poly (vinyl chloride), polystyrene, poly (ethylene terepthalate) etc. are non biodegradable, and their increasing accumulation in the environment has been a threat to the planet[1]. One possibility how to solve this problem can be production of biodegradable polymers. On the other hand, these materials usually exhibit problematic processing properties following partially sensitive to thermal degradation as well as lower mechanical properties. These problems can be reduced by blending of two or more polymers as well as by addition of modifiers.

In our work PLA/PHB and PLA/PHB/TAC blends were studied. Styrene-acrylate copolymer containing epoxy groups was used as modifier. The aim of our work was study of influence of modifier on rheological and mechanical properties of PLA/PHB blends.

Materials and methods

PLA 4042D from NatureWorks, LLC, USA was used as polylactide acid, PHB from Biomer, Germany was used as polyhydroxybutyrate, Triacetine was used as plasticizer and Joncryl ADR-4368 from BASF, Asia was used as modifier (styrene-acrylate copolymer containing epoxy groups).

Preparation of blends

The blends of polylactide acid/polyhydroxybutyrate and polylactide acid/polyhydroxybutyrate/triacetine with content of polyhydroxybutyrate 5, 10, 15, 30 and 50 wt.% were prepared using twin screw extruder with screw diameter 16 mm, L/D = 40 with three kneading zones. The content of triacetine was 10 wt.% These blends were modified by addition of Joncryl ADR-4368 (2 wt.%) as well.

Rheological measurements

Rheological parameters of blends were measured using oscillation rheometer RPA 2000 from Alpha Technologies. Two types of tests were used in our work – strain sweep and timed test. Frequency was set up to 50 cpm during the strain sweep, while angle of strain varied from 0–60°. Timed test was done at constant angle of strain 30° and constant frequency 60 cpm. Time period of test was 20 min. Temperature of measurement for all prepared blends was 200 °C.

Mechanical properties measurement

For tensile test according to ISO 527 the Zwick machine was used at cross-head speed 1mm/min while deformation range was of 0–3 % and after this value of deformation the speed increased up to 50 mm min^{-1}. The tensile strength of break (σb), elongation at break (εb) and tensile strength at yield (σy) were determined based on recorded tensile curves.

Results and discussion

The dependencies of mechanical properties on PHB content in the blends of PLA/PHB, PLA/PHB/J 4368, PLA/PHB/TAC and PLA/PHB/TAC/J 4368 are shown in Fig. 1–3.

Tensile strength at yield (Fig. 1) of pure PLA is near to 60 MPa. After addition of 5 % of PHB, yield point disappear

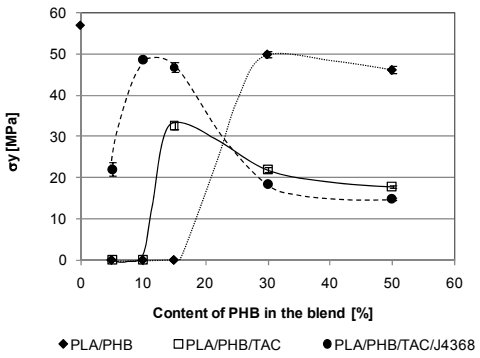

Fig. 1. **The dependency of tensile strength at yield on PHB content** *PLA/PHB/J4368 blends exhibit no yield point. Zero values mean that samples exhibit no yield points.

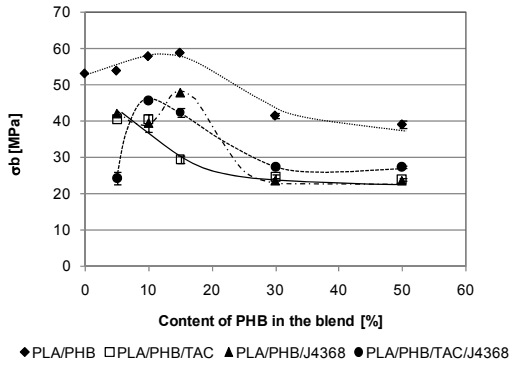

Fig. 2. **The dependency of tensile strength of break on PHB content**

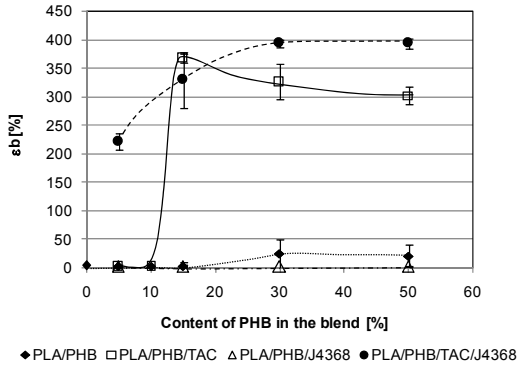

Fig. 3. **The dependency of elongation at break on PHB content**

from tensile curve of PLA/PHB blends. The PLA/PHB blends exhibit no yield point up to 30 wt.% of PHB content in the blends. Value of tensile strength at yield is about 50 MPa if concentration of PHB is from 30 to 50 wt.% Addition of plasticizer TAC shift the concentration of PHB to 15 wt.% where the yield point appears on tensile curve and its value is about 35 MPa, e.g. logically lower than in case of blends without plasticizer. Considerable improvement was obtained after application of Joncryl 4368. Dependency of σy on PHB content exhibit strong maximum around 10 % of PHB in the blend and value of maximum is about 50 MPa. If concentration of PHB is over 15 wt.%, σy again falls down to approx. 15 MPa. It can be assumed that position of maximum can be influenced by concentration of modifier Joncryl 4368. Similar dependencies were obtained also in case of tensile strength at break (Fig. 2). Addition of PHB to PLA without plasticizer causes increasing of σb up to 60 MPa at 15 wt.% of PHB. Application of TAC also causes decreasing of σb. Addition of modifier do not improve absolute values of σb, but similarly like in case of σy it shift position of maximum to lower concentration of PHB. Most significant improvement was observed in case of elongation of break if both additives (TAC as well as Joncryl) were applied in the PLA/PHB blends. While PLA/PHB blends exhibit in whole studied range of concentration practically 0 or very low values of εb, application of TAC logically causes increasing of it. Improving of εb in case of PLA/PHB/TAC blends starts from 15 wt.% of PHB if no Joncryl 4368 was used. Addition of Joncryl 4368 (2 wt.%) gives blends with εb more than 200 % already at concentration of PHB 5 wt.% and at higher concentration of PHB elongation at break is constant and higher in comparison with blends without Joncryl.

Discussed effects of Joncryl on mechanical properties of PLA/PHB and PLA/PHB/TAC blends are probably cause by chain extending of degrading polymer, preferably PHB, during its thermal processing. This assumption was confirmed also by rheological measurements.

The flow curves of blend containing 30 wt.% of PHB are shown on Fig. 4 and results of degradation (timed) tests in form of dependency of relative complex viscosity on time are shown on Fig. 5. Both figures show that the viscosity of blend

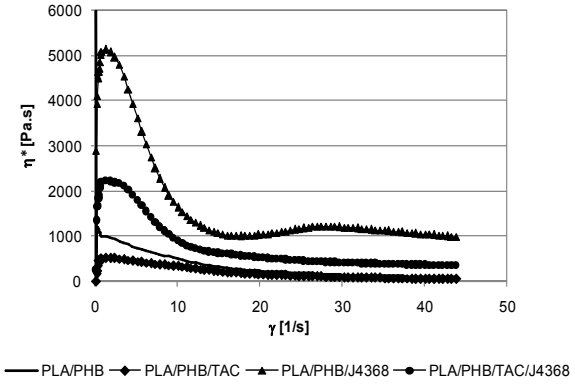

Fig. 4. **The dependency of complex viscosity on shear rate**

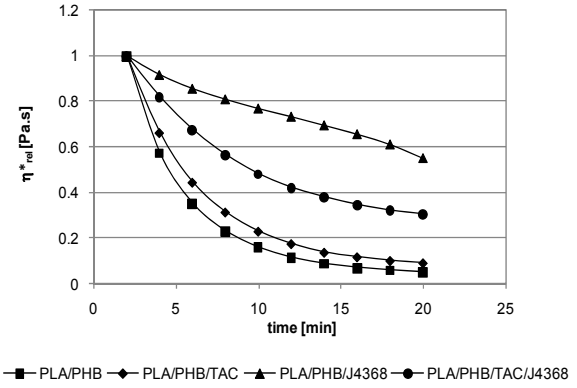

Fig. 5. **The dependency of complex viscosity on time during oscillation test**

containing 30 wt.% of PHB quickly decreases with shear rate as well as with time of thermal loading. Addition of TAC has only marginal effect on both characteristics. Addition of Joncryl markedly inhibits degradation process of the blends (see Fig. 5) and also it is able to keep higher viscosity of the blends at low shear rates (see Fig. 4). Application of TAC in PLA/PHB/Joncryl composition logically reduces viscosity as well as it decreases effect of Joncryl as processing stabilizer.

Conclusion

High sensitivity of PHB during its thermal processing was confirmed in our work. The negative effect of degradation of PHB which causes decreasing of mechanical properties of PLA/PHB blends can be significantly reduced by application of plasticizer and/or by application of chain extenders. Mainly epoxyded styrene-acrylate copolymer (Joncryl 4368) increases viscosity of the melt as well as mechanical properties. The best results in mechanical properties were achieved if both additives were applied in the PLA/PHB blends. Combination of plasticizer TAC and chain extender Joncryl 4368 give a good chance to prepare PLA/PHB blends with properties suitable for practical use of such materials in packaging for example.

This work is supported by Norwegian Financial Mechanism, Financial Mechanism of EEA and State budget of Slovakia - project No. SK 0094.

REFERENCE

1. Tokiwa Y., Calabia B. P., Ugvu. Ch. U., Aiba S.: Int. J. Mol. Sci. 10 (2009).

P-35

THE INFLUENCE OF SURFACE-ACTIVE CHEMICALS ON PHYSICO- MECANICAL PROPERTIES OF ELASOMERIC MIXTURE WITH UTILIZATION OF LIGNIN AS BIO-FILLER

PETER POČAROVSKÝ[a], IGNÁC CAPEK[b], IVAN CHODÁK[b], PAVEL KOŠTIAL[d], JANA ĎURFINOVÁ[a], LUBOŠ KRIŠŤÁK[c], SILVIA KOIŠOVÁ[f], JANKA JURČIOVÁ[e], ROMAN BREŠER[a], and MARTINA ŠARLAJOVÁ[a]

[a] Slovak university of technology in Bratislava, The Faculty of Chemical and Food technology,Radlinskeho 9,Bratislava 812 37, [b] Slovak Academy of Sciences, Institute of Polymers, Bratislava 812 37, [c] Technical University in Zvolen, Faculty of Wood Science and Technology, T.G.Masaryka 24, 960 53 Zvolen, Slovak Republic, [d] VŠB-Technical university of Ostrava, Faculty of Metallurgy and Material Engineering, 17. listopadu 15/2172, 70833 Ostrava-Poruba, Czech Republic, Department of Materials Engineering, [e] Saar Gummi Slovakia spol. s r.o., Gumárenska 397/21, Dolne Vestenice 972 23, Slovak Republic, [f] Department of Inorganic Materials and Environmental Engineering, Faculty of Industrial Technologies, University of Trenčín, 02001 Púchov, Slovakia
peter.pocarovsky@stuba.sk

Abstract

The given work is focused on the influence of surface-active chemicals on vulcanization characteristics and physico-mechanical properties of rubber mixtures where the natural rubber was used as a matrix and Lignin was used as an alternative bio-filler. Ethoxone AF5, Lauryl sulfate sodium salt and Cetyltrimetylamonium bromide are the tensides which were chosen by us. During the process of preparation of samples for infrared spectroscopy, the emulsion of Ethoxone AF5 and rubber SMR20 got blue after the heating (aging process) to temperature 140 °C and it means that there was the chemical reaction. We were adding the tensides which are mentioned hereinbefore and the adding of these tensides was from 0.5 to 4 hm.%. This mentioned weight was the weight from the total weight of prepared mixture and we were observing the changes of resultant properties of final vulcanizates.

1. Experimental work

Materials

Natural rubber of type SMR-20, which was used as the elastomeric matrix, was obtained from Malaysia. The natural Lignín, which was used in a function of reinforcement biofiller is a commercial product of global company firm Boregaard Lignotech.. The powder of pale brown colour Calcium, lignosulfonate is derived from eucalyptus wood, pH in solution was 7.4 and molecular weight was 1500 g mol^{-1}. Ethoxone AF 5 – anionic tenside $C_{12}H_{25} - OCH_2\ CH_2 - OCH_2\ CH_2 - OSO_3Na$, Cetyltrimetylamonium bromide – cationic

surfactant, white powder with the molecular weight p364, 45 g mol^{-1} were used as the surface-active chemicals. Lauryl sulfate sodium salt $C_{12}H_{25}OSO_2ONa$, anionic tenside with the molecular weight 288.37 g mol^{-1} was used as last one surface –active chemical. All agents were used directly without any further purification and modification.

The preparation of samples for investigation by IR spectroscopy

The preparation of the sample (SMR 20 + surface – active chemicals) before the aging: 1 g of natural rubber and 25 ml of toluene (used as a solvent) were mixed together and the given mixture was left for two days because of its swelling (imbibition). The 2 % of surface-active investigated substance were added into the mixture. Then, the thin film (layer) of this solution was deposited on KBr tablet which was placed into the dryer at temperature 100 °C for 2 minutes. After this process, the given KBr tablet was taken from the dryer and it meant that the sample was prepared for investigation and testing with help of IR spectroscopy. The mentioned testing of given sample had to be done until the KBr tablet absorbed the humidity from the air.

Preparation of sample (SMR 20 + surface – active chemicals) after the aging : 1 g of natural rubber and 25 ml of toluene (used as a solvent) were mixed together and the given mixture was left for two days because of its swelling (imbibition). The 2 % of investigated substance were added into the mixture after the two-day process of swelling of mentioned mixture. Then the all volume of the solution was poured into Petri dish and it was being observed during the process of evaporating or vaporizing of toluene at laboratory temperature. After the evaporation of solvent, the given matter was put into the beaker which was placed into the dryer where the temperature was 140 °C during the two-hour process of reaction – process of aging. Then the given sample was taken from the dryer and 25 ml of toluene was added there and then the sample was left for two days because of its swelling (imbibition). The process of swelling (imbibition) was followed by depositing of the thin film (layer) of the given solution on KBr tablet which was placed into the dryer at temperature 100 °C for 2 minutes. After this process, the given KBr tablet was taken from the dryer and it meant that the sample was prepared for investigation and testing with help of IR spectroscopy. The mentioned testing of given sample had to be done until the KBr tablet absorbed the humidity from the air.

2. Results and discussion

Characterization of infrared spectroscopy for natural rubber with Ethoxone AF 5

The process of preparation of sample is concerned with heating (aging process) at which the temperature was 140 °C and the given heating process took two hours. During this process of preparation for IR spectroscopy, the emulsion of Etoxone AF5 together with the rubber SMR 20 became blue and it means that there was chemical reaction.

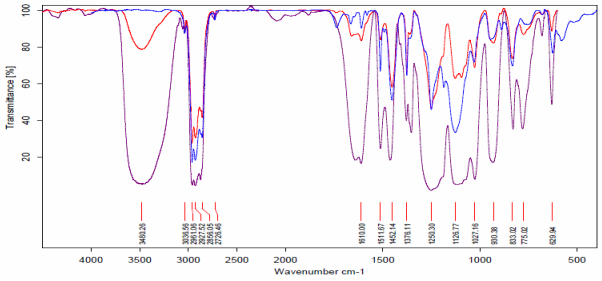

Fig. 1. **The violet colour shows IR spectrum of Etoxone as a pure substance.** The red colour is IR spectrum of the natural rubber together with Etoxone – it is before the process of aging. Blue colour represents IR spectrum of natural rubber together with Etoxone – it is after the process of aging which was at temperature 140 °C and it took two hours

Characterization of rubber compounds with surface – active chemicals

The results of measured cure characteristics (M_L, M_H, t_s, t_{90}, R_V) of prepared rubber compounds with lignin as bio-filer and surface-active chemicals are present in Table I.

According to the obtained values in Table I, it can be seen, that the selected type of filler acts as an reinforcing filler in prepared rubber compounds. The shown values confirm that there is the fluctuation of viscosity because of different types of surface-active chemicals which were added to the mixture (increase of values M_L and decrease of values M_H) and moreover, there is the change of the optimal time of vulcanization (t_{90}) – the highest value was obtained after the adding of Lauryl sulfate sodium salt. The values of rate coefficients of vulcanization (R_v), which characterize"activity"of ingredients in rubber compounds with lignin and surface-active chemicals are also markedly lower.

The results of measured physico-mechanical properties of prepared rubber compounds with surface-active chemicals and lignin are presented in Table II.

Table I
Cure characteristics of prepared rubber compounds

Variable	A	B	C	D
M_L [N m]	5,5	17	4	9
M_H [N m]	32	24	24	31
t_S [min]	7	4,5	7	1
t_{90} [min]	9	11	25	7,5
R_V [min^{-1}]	50	15,38	5,5	15,38

A – standard rubber compounds
B – rubber compounds with Ethoxone AF 5
C – rubber compounds with Lauryl sulfate sodium salt
D – rubber compounds with Cetyltrimetylamonium bromide

Table II
Physical – mechanical properties of prepared rubber compounds

Variable	A	B	C	D
Tensile strength [MPa]	11,95	10,05	10,8	13,87
Tensibility [%]	877	850	1044	720
Hardness [IRHD]	36	39	32	40
Modulus 300 [MPa]	4,09	3,55	3,2	5,78

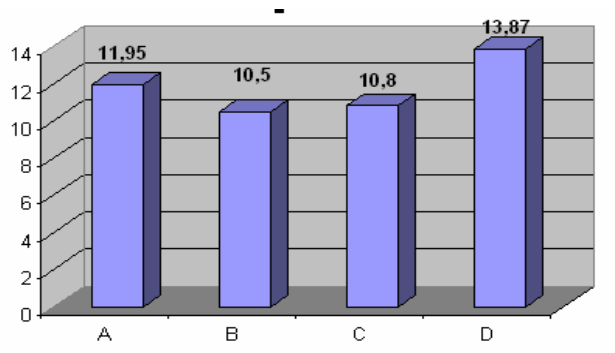

Fig. 2. **Tensile strength [MPa],** A – standard rubber compounds, B – rubber compounds with Ethoxone AF 5, C – rubber compounds with Lauryl sulfate sodium salt, D – rubber compounds with Cetyltrimetylamonium bromide

The mixtures on the basis of lignin together with Etoxone and Lauryl sulfate sodium salt have almost the same values and it was found according to the measured values of physico-mechanical parameters (see Table II). In comparison to standard, much higher value was found out in the case of mixture where the additive agent was Cetyltrimetylamonium bromide and this fact can be closely connected with positively charged particles of mentioned additive agent and there is the reaction of these particles with the matrix. The highest tensibility was obtained at mixture with Lauryl sulfate sodium salt and it means that it can be understood as a softener. On the other side, the values of hardness were quite low at the mixture with Lauryl sulfate sodium salt and it means that there less interaction between the polymer and filler. The comparison of the other two additives with the standards, there was the increase of values characterizing the hardness.

4. Conclusion

The analysis of results, which were obtained during the measuring of rubber mixtures, showed that Lignin with its interaction with surface-active chemicals can not be used as reinforcement filler. It also changes the course of vulcanization and it changes the physico-mechanical properties of vulcanizates after adding of surface-active chemicals. The physico-mechanical properties of vulcanizates are mainly changed because of composition of mentioned substances.

REFERENCES

1. Bech F. D., Boyd R., Uri N. D.: The Science of the total Enviroment 175, 219 (1995).
2. Prekop Š.,Várkoly L., Ďuriš Š., Fedorová E., Matuščinová A., Michálek J.: Gumárenská technológia I, 69-72 (1998).
3. Fredhaim G. E., Christensen B. E.: Biomacromolecules *4*, 232 (2003).
4. Košíková B., Gregorová A., Oswald A., Krajčovičová J.: J. Appl. Polymer Sci. *103*, 1226 (2007).
5. Alexy P., Feranc J., Kramárová Z., Hajšová M., Ďuračka M., Mošková D., Chodák I., Ilisch S.: KGK, Kautsch. Gummi Kunstst. *61*, 26 (2008).

P-36
MODIFICATION OF LDPE SURFACE BY POLY(2-ETHYL-2-OXAZOLINE) USING LOW-TEMPERATURE PLASMA

ANTON POPELKA, JURAJ KRONEK, IGOR NOVÁK, MATEJ MIČUŠÍK, and IVAN CHODÁK

Polymer Institute, Slovak Academy of Sciences, Dubravska cesta 9, 845 41 Bratislava 45, Slovakia
anton.popelka@savba.sk

Abstract

Modification of polyolefins by a low-temperature discharge plasma is very frequently used in automotive industry, for upholstery production, bumpers covering by varnishes as well as in the production of plastics elements for car interiors. The worldwide production of low-density polyethylene (LDPE) reaches the highest value among the polymers produced for many industrial applications including the automotive industry (bumpers or steering wheels manufacture). However, it is polymer with chemically inert and hydrophobic character, what is limiting to the further processing. This lack of LDPE properties can be removed by the surface modification of LDPE by the low-temperature plasma. Moreover, the plasma discharge can be used for surface treatment by biocompatible materials such as poly(oxazoline) to improve the adhesion of the laminating materials.

Introduction

Polyethylene (PE) belongs among important materials using in the many technological sectors. PE is often used in the automotive, medical, aerospace, electronics industry[1]. PE is often used for automotive applications. In this work, surface and adhesion properties of LDPE foil were studied. Although the LDPE excels by volume properties an inert and hydrophobic character, that relevant with lower surface energy, there can be problem in bonding, printing and laminating processes[2].

The surface changes of LDPE films can be achieved by various methods of surface modification, such as by low-temperature discharge plasma, and by substances containing polar functional groups, such as 2-oxazoline polymers. Thus surface of LDPE treated by discharge plasma is homogenous without the bulk changes. As working gases for plasma treatment can be used oxygen, nitrogen, argon, and carbon dioxide[3]. Polymers poly(2-ethyl-2-oxazoline) (PETOX) (Scheme 1) containing polar amide groups on the backbone were prepared by cationic polymerization of 2-ethyl-2-oxazoline[4] and it belongs to biocompatible materials[5].

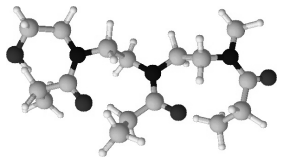

Scheme 1. **PETOX structure**

Experimental

Following materials and treatment conditions were used in our experiment:

Foil of LDPE BRALEN FB 2-17 (Slovnaft MOL, Slovakia) containing no additives. The thickness of LDPE film was 20 μm. PETOX with the degree of polymerization equals 100 was prepared by cationic polymerization 2-ethyl-2-oxazoline, which was iniciated by methyl-*p*-benzenesulfonate at 110 degrees Celsius, and 24 hours in *N*,*N*-dimetylacetimide with molar concentration equals 4 mol per liter.

The LDPE foil modification were carried out by DCSBD equipment (made in Comenius University, Bratislava, Slovakia) under dynamic conditions, power supply = 200 W, treatment time = 20 s, in oxygen atmosphere. The surface properties of modified LDPE were carried out by the measurements of contact angles of testing liquids set, such as water, ethylene glycol, glycerol, formamide, and methylene iodide by Surface Energy Evaluation System (See system, Advex Instruments, Czech Republic). The surface energy was calculated by Owens-Wendt-Rabel-Kaelble model. The structure changes of the modified surface were monitored by X-ray photoelectron spectroscopy (XPS) (model K-Alpha, monochromated high-performance XPS spectrometer, Thermo Fisher Scientific).

The adhesive properties, namely peel force and peel strength (force per unit width) of adhesive joint of modified LDPE by PETOX using DCSBD to poly(2-ethylhexyl acrylate) deposited onto polypropylene foil (with 15 mm width), were carried out by measurements of 90° peel test using Instron 4301 (England).

Results and discussion

The water contact angle changes of LDPE treated by DCSBD plasma, and subsequently modified by PETOX before and after washing in H_2O are shown in Fig. 1. The water contact angle of modified LDPE surface by PETOX using discharge plasma significantly decreased in comparison with unmodified polymer. The treated samples were washed in H_2O to remove weakly bounded PETOX from LDPE surface. The water contact angles of LDPE treated by PETOX after washing were higher than before washing in H_2O, what is causing by removal non-covalently bounding chemical substances from LDPE surface. Analogously, the surface energy significantly increased with PETOX content increasing from 1 % w/v up to 10 % w/v before washing in H_2O, but after washing was independent on content of PETOX, such as shown in Fig. 2.

This decrease of the water contact angle and increase of the surface energy of LDPE modified by PETOX is caused by the increase of hydrophilic character after this surface treatment, which is caused by the presence of polar functional groups in PETOX.

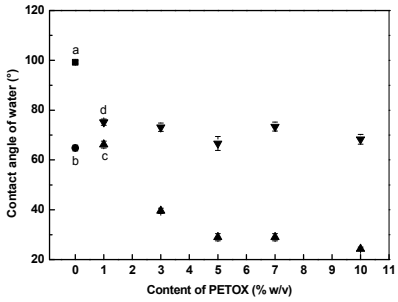

Fig. 1. **Contact angle of water: a) LDPE untreated, b) LDPE plasma treated, c) LDPE treated by PETOX via plasma before washing, d) LDPE treated by PETOX via plasma after washing vs. PETOX content in dichloromethane solution**

The modification of LDPE by PETOX via plasma discharge resulted in an increased adhesion to more polar polymer, specifically to poly(2-ethylhexyl acrylate) deposited onto polypropylene foil, when peel force and peel strength significantly increased (Fig. 3). It is also obvious that peel force and peel strength negligible decreased after samples washing in H_2O, as a result of chemically and structure changes in the surface layers.

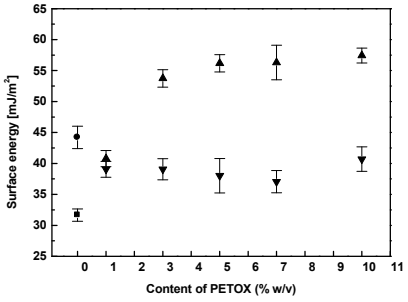

Fig. 2. **Surface energy vs. PETOX content in dichlormethane solution (description see Fig. 1)**

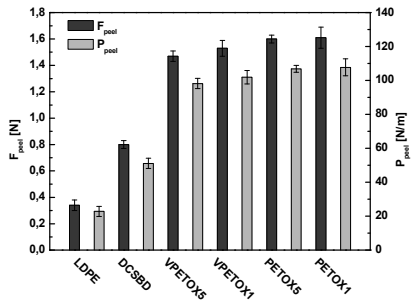

Fig. 3. **Peel force (F_{peel})** and peel strength (P_{peel}) of adhesive joint LDPE modified by PETOX via discharge plasma-poly(2-ethylhexyl acrylate); V – means after washing in H_2O, number means content of PETOX in dichlormethane solution

The survey spectra from XPS measurements with the corresponding surface atomic compositions of LDPE treated by plasma and by PETOX are provided in Fig. 4. Carbon spectrum of untreated LDPE has only one peak due to C-C bonds. After plasma treatment of LDPE foil, new peaks due to different carbon-oxygen bonds appear. Also the small amount of silicon was found supposedly coming from plasma parts as a pollutant. Moreover**,** after PETOX bounded on LDPE surface via plasma discharge, some carbon-nitrogen bonds were found. Also the presence of carbon-nitrogen bonds was apparent for LDPE treated by PETOX after washing in H_2O, which corresponds with amide´s group of PETOX.

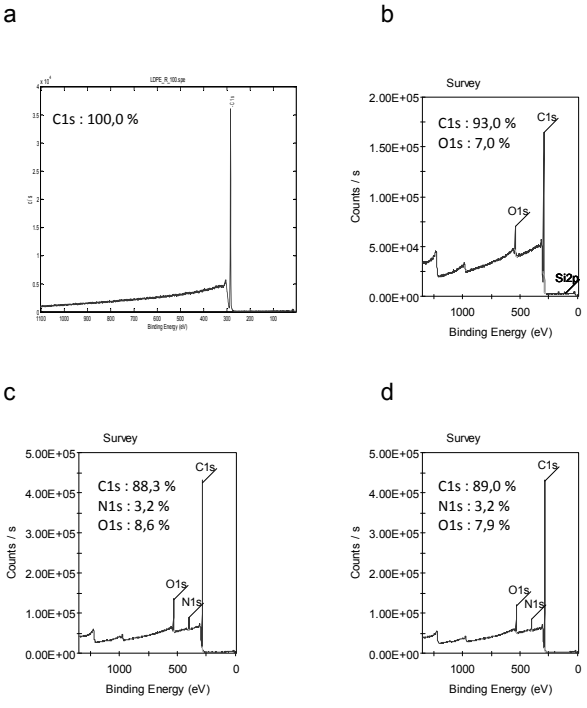

Fig. 4. **XPS survey-scan spectra: a) LDPE untreated, c) LDPE plasma treated, c) LDPE treated by PETOX via plasma before washing d) LDPE treated by PETOX via plasma after washing**

Conclusions

The significant decrease of the water contact angle as well as an increase of surface energy of LDPE foil grafted by PETOX via DCSBD plasma in O_2 at atmospheric pressure were observed. The hydrophilicity of LDPE after surface treatment significantly increased. The PETOX remaining onto LDPE surface after washing was covalently-bonded. The presence of amide group in PETOX introduced onto surface of LDPE using DCSBD plasma was verified by XPS measurements. The presence of polar functional groups of PETOX grafted onto LDPE surface has been confirmed, because peel strength of adhesive joint modified LDPE-polyacrylate due to introduction of polar PETOX groups onto polymer surface markedly increased.

Authors are grateful to Scientific Grant Agency of the Ministry of Education and Slovak Academy of Sciences (Grant VEGA 2/0185/10) and No. 2/0157/09), and Slovak Research and Development Agency – APVV (grants No. 0044-07, and 0023-09).

REFERENCES

1. Sanchis R., Fenollar O., Garcı´a D., Sa´nchez L., Balart R.: Int. J. Adhes. Adhes. *28*, 445 (2008).
2. Novák I., Chodák I.: Makromol. Chem. *260*, 47 (1998).
3. Novák I., Pollák V., Chodák I.: Plasma Proc. Polyms. *3*, 355 (2006).
4. Kobayashi S.: Prog. Polym. Sci. *15*, 751 (1990).
5. Adams N., Schubert U. S.: Adv. Drug Delivery Rev. *59*, 1504 (2007).

P-37
ECOLOGICAL ASPECTS OF USED SOFTENERS FOR RUBBER COMPOUNDS

JOZEF PRETO*, JAN ORAVEC, and JAN HRONKOVIC

VIPO a.s.,958 01 Partizanske, Slovakia
jpreto@stonline.sk

The European directive 2005/69/EC restricts the use of certain Polycyclic aromatic Hydrocarbons in oils used in tyre production. The directive was applied to tyres produced after January 1st 2010. Extender and processing oils may not be used for production of tyres if they contain more then 1 mg kg^{-1} of benzo(a)pyrene (BaP) and /or more than 10 mg of the sum of all listed Polycyclic Aromatic Hydrocarbons (PAHs). Many authors deal with replacement of aromatic oils with oils having low content of harmful components[1,2], or look for application of different, environmentally friendly softeners[3,4].

Several types of oils with low content of PAHs in various rubber blends (e.g. apex blend, inner liner blend) were tested for purpose to replace highly aromatic processing oils.

The oils were selected with respect to the viscosity gravity constant (VGC) value and to the aromatic extract PAHs value.

The physical and mechanical properties of tested blends are in correlation with values of VGC. A higher VGC value means a higher content of naphthenic and aromatic structures and relatively higher polarity in comparison with paraffinic oils, what is beneficial to the oil-elastomer compatibility. It means, that compound consisting of SBR containing oil with higher value of VGC gains higher physical properties.

The tensile strength gradually decreases with lower VGC values, only one blend with higher sulfur content in used oil. reached higher tensile strength values probably affected with this extra content of sulfur

The experimental results showed that tested physical properties of evaluated rubber blends after replacement of usually used aromatic oil are:

- in correlation with VGC values of used oils,
- affected with residual sulfur content also and,
- mostly reached the required physical parameters.

This publication was prepared as part of the project MŠSR-3933/2010-11 „Application of Knowledge-based Methods in Designing Manufacturing Systems and Materials – MANUSMAT" co-funded by the Ministry of Education, Science, Research and Sport of the Slovak Republic within the scheme constituted by Act No. 185/2009 Coll. "Research and Development Incentives".

REFERENCES

1. Durfinova J., Capek I., Novak J., Jurciova J., Lacko M., Jurik R.: Chem. Listy *104*, 513 (2010).
2. Joona M.: Rubber World *235*, 15 (2007).
3. Plasty a Kaucuk *40*, 374 (2003).
4. US patent 5 252 649.

P-38
EMISSION TESTING OF NON-METAL VEHICLE MATERIAL ACCORDING TO VDA 278

FRANKY PUYPE and JIŘÍ SAMSONEK

Institute for Testing and Certification – Zlín, testing division - laboratory of analytical chemistry, Třida T. Bati 299,764 21 Zlín-Louky, Czech Republic
fpuype@itczlin.cz

Introduction

VDA (Verband der Automobilindustrie) is the German quality management system for the automobile industry which is concerned about the passengers` health, comfort and protection. To monitor the emissions from the non-metallic parts of car interior on passengers` health, all car interior material needs to be tested under conditions that simulate real conditions in the vehicle.

The standard VDA 278 requires emission testing from non-metal materials intended for use in automotive industry and is based on analytical thermal desorption by a semi-quantitative method. This test is based on dynamic desorption of analytes from the solid phase (sample) to a vapor phase (emissions)[1].

Thermal desorption is a sampling technique that utilizes heat to increase the volatility of analytes so they can be removed (separated) from the solid matrix (plastics, rubber, wood, textile, extracts, foam, hair, gel, paint, etc.). Analytical thermal desorption connected to gas chromatography with mass spectrometry detection (TD-GC-MS) is a highly developing sampling technique in modern chromatography.

Thermal desorption allows analysis of almost all sorts of materials including insoluble and complex materials. No solvent extraction or other pre-treatment is needed and a small amount of sample is required (approx. 20 mg).

The analytes/emissions are trapped in the GC injector on Peltier-cooled sorbent trap (filled by Tenax TA sorbent). After trapping emissions (concentrating), analytes are transferred from the injector towards the analytical column of the gas chromatograph by quickly heating of this trap (12 K/sec.). After chromatographic separation mass spectrometry detects the compounds and helps to identify them.

Typical emissions from automotive parts are firstly the oligomers or matrix related compounds and secondarily the additives and their degradation products.

Technical parameters

The principle of VDA 278 can be divided into two parts. Both parts are applied on the same sample.

The first part describes the volatile organic compound analysis (VOC) with thermal desorption of the sample at 90 ºC for 30 minutes. The peaks are quantified on toluene equivalent and integrated from *n*-hexane till *n*-eicosane. This is the total VOC region (tVOC) and partly the semi-VOC region (SVOC). The VOC unit is expressed as $\mu g\ g^{-1}$ of toluene equivalent.

The second part describes the semi-volatile organic compound analysis (SVOC/FOG) with thermal desorption of the sample at 120 ºC for 60 minutes. The peaks are calibrated with a *n*-hexadecane standard and integrated from *n*-hexadecane till *n*-dotriacosane. The FOG unit is expressed as $\mu g\ g^{-1}$ *n*-hexadecane equivalent.

The thermal desorption parameters defined in VDA 278 do not intend a full thermal extraction, these smooth parameters are limited in thermal desorption time and temperature. VDA 278 is intended to compare samples and to simulate the emissions of non-metal compounds during their life-time.

For measurement of VDA 278, a TD-20 thermal desorber unit coupled to a GC-MS 2010 (Shimadzu, Kyoto, Japan) was used. This system is fully automatized and its performance is screened regularly by inter-laboratory testing.

Expected values and trends

It is logical that the emission behavior of the material is different for each type of sample. Purity of the polymer (recycled polymer!), quality of additives, amount of additives, reactivity and stability of additives (UV), thermal stability during desorption, presence of brominated flame retardants and impact of plasticizers are only a few impact factors on the

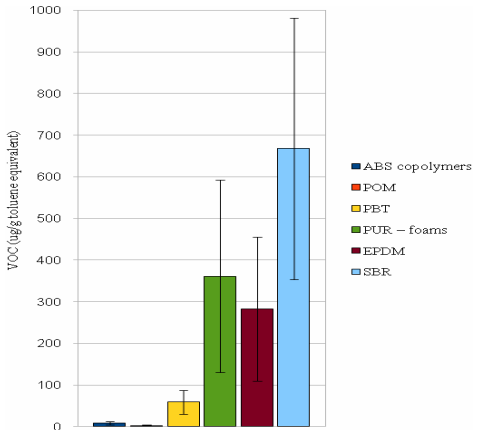

Fig. 1. **VOC results sorted according to matrix**

final VOC/FOG value.

In Fig. 1 is shown an overview of VOC values sorted by matrix. The standard deviation ($\sigma_{n-1}/\sqrt{n}$) of the matrix is given just to show the expected range of test results. In first view there is a difference between the VOC emissions from the hard polymers (ABS, POM and PBT) and softer polymers (PU and rubbers).

Harder matrixes have more ability to retain emissions (low emission rate) and usually contain fewer components. The softer matrixes are mostly loaded with more components and generally have a higher diffusion rate through the polymer matrix.

Defect analysis - smell characterization

However the VDA 278 is initially developed to screen emissions from non-metallic material to assure the passengers` health, this method is also useful for defect analysis. Due to the long sampling time and low emission temperature, defects like smell and blooming can be fully characterized.

It is recommended for defect analysis to compare a reference sample with the defect sample. The VDA 278 is used as a screening method, making an “emission fingerprint” of the material, in most cases it helps to get to know the reason of a defect and the answer for further defect prevention. This method can save the manufacturer lots of money, if the results are properly interpreted.

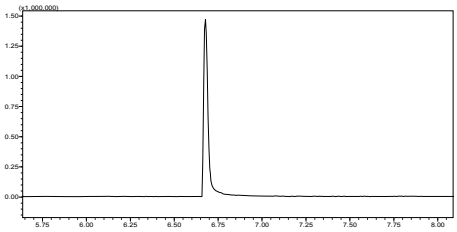

Fig. 2. **VOC emisions from PU sealing contaminating other car parts**

Firstly a description of the smell can help the analyst to get to know the type or target analyte. Further identification of the emissions can be done by mass spectrometry. In Fig. 2 is shown a chromatogram of a PU foam sample with a slight “amine” smell causing fogging on the car parts around. After analysis in VOC there was detected the amine catalyst triethylenediamine (TEDA).

Emission equivalents - another approach

For homogenous matrixes, a model based on emission equivalents can be used to predict the emission value of individual compounds. For a certain amount of compound (ng) there is a corresponding maximum VOC value (ng of toluene). The use of emission equivalents can help to ban additives for ``risky`` formulations or optimize a mixture to ensure that the VOC value is lower than a fixed limit.

The VDA 278 measurement is performed by electron impact ionization mode (70 eV) and all compounds are compared relatively to one chemical. The electron impact fragmentation mechanism of alkanes is completely different from the electron impact fragmentation of aromatic amines. According to the type of fragmentation for a same amount of compound the signal, and so VOC/FOG value, might be completely different.

In Table I are given some VOC emission equivalent values. 2-ethyl-1-hexanol, a typical hydrolysis product from di-ethylhexylphtalate has a lower impact on the final VOC value than *n*-decane. Aniline, a degradation product from phenylamine antidegradants or thiazole accelerators in rubber has the lowest impact on the VOC value. It is up to the operator to make decisions but the use of these VOC emission equivalent values can help in case of looking for better replacements of additives. Using emission equivalents might be very practical in use to check if the replacement gives a higher VOC value.

Table I
VOC emission equivalent values for some typical emissions

Chemical	VOC emission equivalent (ng toluene/ng compound)	% RSD (*n*=3)
Aniline	1,6	5
n-Decane	4,3	6
2-Ethylhexanol	2,8	8

Many problems with high VOC values in polyurethanes might be related to the choice of amine catalysts. For rubbers the VOC emissions are mainly depended on the choice of accelerators and low MW anti-degradants.

Emissions from degradation products

By use of VDA 278 a comparison of additives and their VOC values can lead to important decisions to choose for a certain type of additive. Also the degradation products from

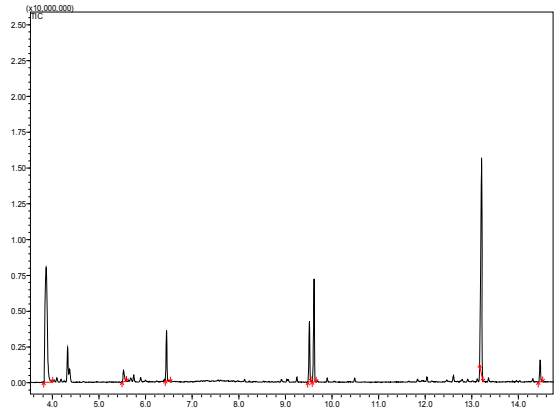

Fig. 3. **VOC emisions from SBR showing mainly degradation products**

original substances can have a high impact on the VOC value. This is the case for many rubber applications.

In the Fig. 3 is shown a typical VOC chromatogram of SBR (VOC 667 μg g^{-1} toluene equivalent). The emissions seen in the VOC fraction are mainly based on degradation products from rubber accelerators used for vulcanization.

2,2`-Dibenzothiazoledisulfide (MBTS) creates after thermal breakdown products like aniline, benzothiazole and 2-(methylthio)-benzothiazole (Fig. 4). The high peaks of cyclohexane and isothiocyanatocyclohexane are typical fragmentation products from cyclohexyl-dithiocarbamate based accelerators (Fig. 5). These accelerators give generally high emissions. Not the substance itself but the degradation products give high VOC values. The VOC emissions and area % value of these degradation products are given in Table II. In many cases a trace of the original substance is visible in the FOG analysis due to its higher boiling point.

As aniline (mutagene/carcinogene class 3) is limited till a VOC level of 1 μg g^{-1} toluene equivalent, the dosage of 2,2`-dibenzothiazole disulfide in the rubber mixture is critical. The operator should be aware of this potential risk that the automotive will not accept the final product due to fact that a mutagenic compound has been detected after VOC analysis despite the fact that no CRM substances are in the recepy!

Table II
VOC emission values from accelerator degradation products in SBR as shown in Fig. 3

t_R (min.)	ID	VOC value (μg g^{-1} toluene equivalent)	VOC % (area %)
3,9	cyclohexylamine	169,0	24
5,6	aniline	1,1	0,2
9,5	benzothiazole	36,4	5,2
9,6	Isothiocyanato-cyclohexane	65,0	9,6
14,5	2-(methylthio)-benzothiazole	13,7	2,0

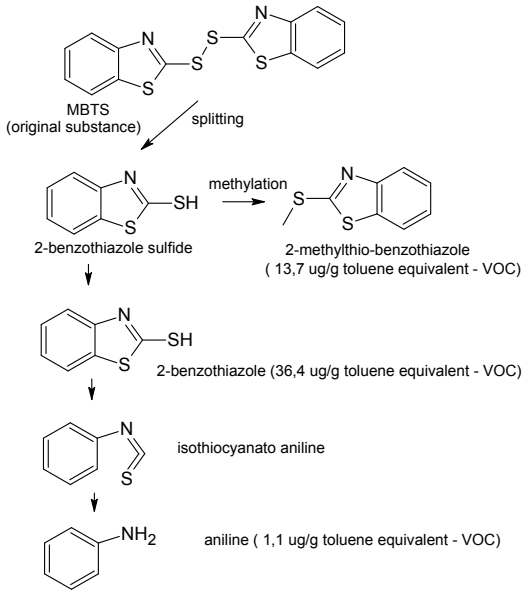

Fig. 4. **Thermal breakdown of 2,2`-dibenzothiazoledisulfide (MBTS accelrator) making high VOC emissions**

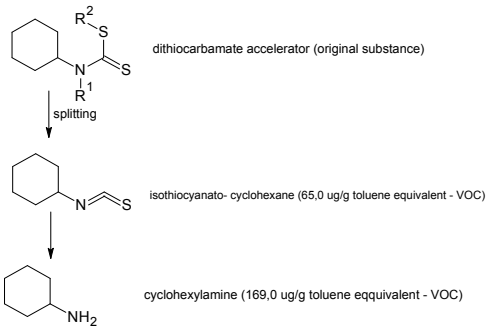

Fig. 5. **Thermal breakdown of a dithiocarbamate acclerator making high VOC emissions**

Target values; Limiting values for individual substances

The VDA 278 is for many years already a reference for the European automotive industry. It requires a limit of 100 μg g^{-1} toluene equivalents for VOCs on test parts and a limit of 250 μg g^{-1} *n*-hexadecane equivalents for FOG. For some matrixes (rubbers) these limits are difficult to reach. Some concerns have even lower limits in their specification list. But it is more than VOC and FOG values.

Other criteria based on this analysis like limit values and targets for individual substances like carcinogens, reprotoxics or mutagens (CRM) are set from 1 μg g^{-1} till 8 μg g^{-1} toluene equivalent. The sum of phtalate esters which are toxic for reproduction are limited till 20 μg g^{-1} toluene equivalent. Regarding the formation of nitrosoamines the sum of selected

secondary aliphatic amines should not be higher than 3 μg g^{-1} toluene equivalent. These limits are depending on demand of the car producer[2].

Conclusion

New trends in modern analytical chemistry are based on quickness, trueness and quality. The sampling and quantification of the VOC and FOG values are relatively quick and easy. However the interpretation and information which this semi-quantitative method gives is in many cases underestimated. Its broad application range from quality control to defect analysis makes this method a nice source of information for material engineers dealing with automotive.

REFERENCES
1. VDA 278 (2000).
2. DBL8585, Suply Specification, (2008).

P-39
COMPOSITE MATERIALS WITH MAGNETIC FILLERS AND ELASTOMERIC MATRIX FOR CONSTRUCTION OF INTELLIGENT TYRES

JANA REKOŠOVÁ[a], IVAN HUDEC[a], JÁN KRUŽELÁK[a], and RASTISLAV DOSOUDIL[b]

[a] *Slovak University of Technology in Bratislava, Fakulty of Chemical and Food Technology, Institute of Polymer Materials, Radlinského 9, 812 37, Bratislava,* [b] *Slovak University of Technology in Bratislava, Facutly of Electrical Engineering and Information Technology, Ilkovičova 3, 812 19 Bratislava, Slovak Republic*
jana.rekosova@stuba.sk

Introduction

The influence of preparation of magnetic hard ferrite fillers on the properties of filled mixtures used in construction of tyre sidewall was studied.

The advantage of elastomeric magnetic composites are possibility of modification their properties for the requirements of specific applications. Rubber magnets can be applied in intelligent tyres, in microwave and radar technology, also in other technological applications. As a sensors of intelligent tyres are able to take of tyre deformation, resp. side forces directly in the tyre and to transfer them directly to electronic equipment of the vehicle and like this obtain information on the adhesion of tyres to the ground, about the forces acting on the tyre or about the deformation of the tyre respectively. They inform the driver of changes while driving, able of the feedback reaction to optimize the movement of the vehicle on the road[1].

Experimental

For preparation of composites commercially produced sidewall rubber mixture made by Continental Matador Rubber s.r.o . Puchov base on butadiene rubber BR SKD 2 and natural rubber was used Two types of rubber mixture were prepared – mixtures I. – ferrite filler and vulcanization system were added into first grade of sidewall rubber mixture and mixing in laboratory mixer (chamber of Brabender mixer), mixtures II. – magnetic filler was added into second grades of sidewall rubber mixture and mixing in laboratory mixer (chamber of Brabender mixer).

Anisotropic magnetically hard strontium ferrite FD 8/24 made by ceramic technology of wet grinding with addition of poly vinyl alcohol, dried by spraying was used in this work as magnetic filler.

Results and discussion

From physical – mechanical properties of vulcanizates tensile strength at break, elongation at break , hardness and modulus M300 were evaluated.

As it can be seen from Fig. 1 modulus M300 with the increasing content of ferrite filler in elastomeric mixtures decreased slightly.

In the mixture type II., where the magnetic filler was added into second grade of sidewall rubber mixture, the influence of the filling on module M300 was observable only very little.

In the case of tensile strength, which dependence on the filler content is showed on Fig. 2, is clear that with increasing of content of ferrite filler tensile strength slightly decreased and the differences between the vulcanizates I and II are minimal.

From the dependence of the elongation at break of vulcanizates on the magnetic filler content (Fig. 3) is clear that in the case of vulcanizates I elongation not changes with increasing of contents of ferrite filler, but in the case of vulcanizates II with the increasing of content of ferrite the elongation slightly decreased.

From the determination of hardness IRHD (Fig. 4) is shown that the hardness of vulcanizates increasing by the increasing content of magnetic filler in the mixture.

Magnetic propeties of the vulcanizates were evaluated on a vibrating magnetometer TVM- 1, at a laboratory temperature and maximum coercivity $H_m = 750$ kA m^{-1}.

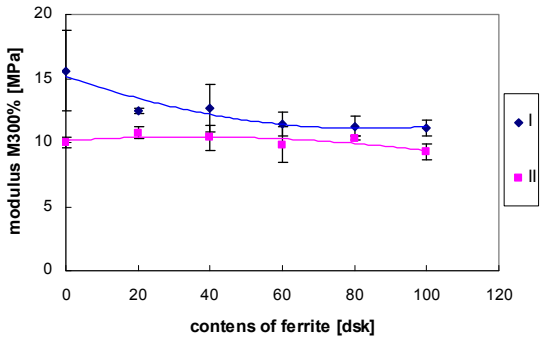

Fig. 1. **Influence of content of ferrite on rubber modulus M300 vulcanizates I, II**

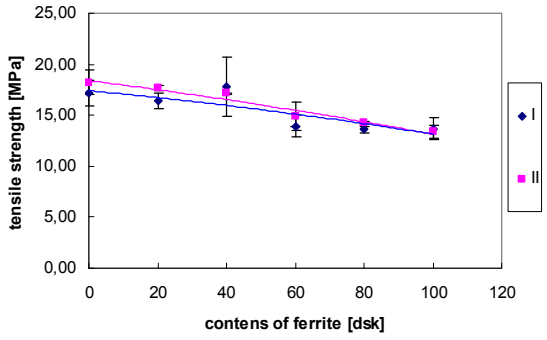

Fig. 2. **Influence of content of ferrite on tensile strength of vulcanizates I, II**

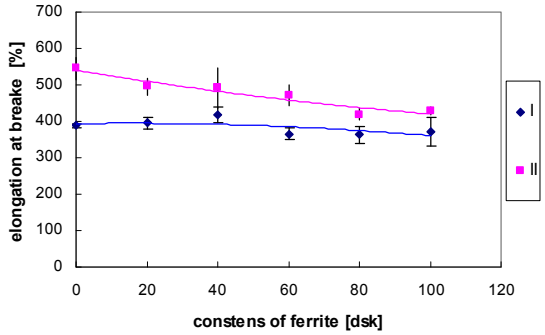

Fig. 3. **Influence of content of ferrite on elongation at break of vulcanizates I, II**

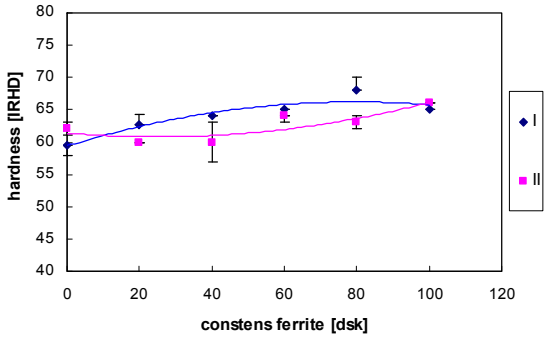

Fig. 4. **Influence of content of ferrite on hardness of vulcanizates I, II**

The coercivity H_c, which specifies the level of energy necessary for cancellation of residual magnetism, maximum magnetic flux Φ_m and remanent magnetic flux Φ_r were subtracted from hysteresis loops.

Maximum magnetic polarization J_m (in saturation) and remanent magnetic polarization J_r were calculated by following equations:

$$J_m = \frac{\Phi_r}{S}.D \quad [T] \qquad (1)$$

$$J_r = \frac{\Phi_m}{S}.D \quad [T] \qquad (2)$$

where S – surface of a sample $S = 3{,}2.10^{-5}\ m^2$
D – constant factor of the equipment TVM- 1 characterizing its demagnetizing effects.
Maximum magnetic induction B_m and remanent magnetic induction B_r was calculated using the following equations[2]:

$B_m = \mu_o H_m + J_m$ [T] (3)

$B_r = \mu_o H + Jr$ ak H=0 => $B_r = Jr$ [T] (4)

where: μ_o – permeability of vakuum [N A^{-1}], H_m – maximum intensity of magnetic field [kA m^{-1}], H – intensity of magnetic field [kA m^{-1}].

From dependence expressing the influence of contents of ferrite filler on maximum magnetic induction B_m (Fig. 5) and remanent magnetic induction B_r (Fig. 6) come through that in the case of remanent magnetic induction and maximum magnetic induction there is a big rise of its values with the increasing content of ferrite filler in the elastomeric composities.

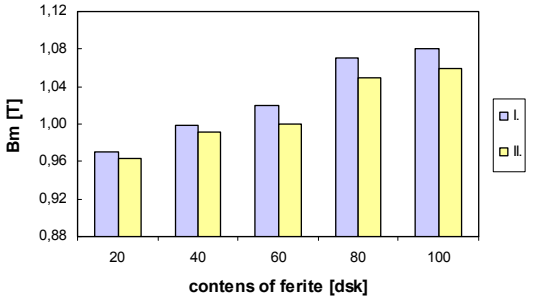

Fig. 5. **Influence of content of ferrite on maximum magnetic induction B_m vulcanizates I, II**

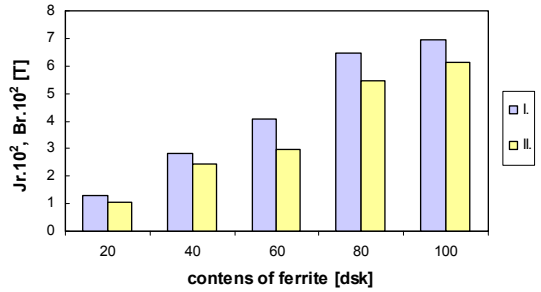

Fig. 6. **Influence of content of ferrite on remanent magnetic induction B_r and remanent magnetic polarization J_r vulcanizates I, II**

Higher values were reached in the case of adding the filler into the first grades (vulcanizates I) in comparison with the magnetic characteristics of composites in which the filler was added into second grade, what is apparently related to the process of dispersion of the filler and uniformity of its distribution in the branched matrix of vulcanizates.

Conclusion

From the evaluation of the physical – mechanical properties, tensil strength at break and rubber modulus M300, has been concluded that by increasing the contents of ferrite FD 8/24 are all these parameters decreasing, but hardness with increasing of content of ferrite increasing slightly. Bigger differences in physical – mechanical characteristics show, that the addition of magnetic active filler into the first grade sidewall tyre mixture is preferable, what is connected with a better dispersion of the filler in the non cross-linked elastomeric matrix.

Magnetic characteristics has markedly rising with the increasing ratio of ferrite filler. This shows, that materials filled with magnetic hard ferrite potentially can be used for valuation of the tyre deformation by building it into the tyre sidewall.

The obtained results are showing the possibility to prepare elastomeric magnetic composite materials to be used as a sensor in intelligent tyres.

This work was supported by grant agency VEGA, project No.1/0575/09.

REFERENCES

1. Ürögiová E.: *PhD Thesis*, FCHPT STU Bratislava, 2006 122 s.
2. Kruželák J., Szabová R., Bellušová D., Kyselá G., Hudec I.: KGK, Kautsch. Gummi Kunstst. *63*, 20 (2010).

P-40
STUDY OF THERMOELASTIC PROPERTIES OF ACRYLATE COMPOSITES IN AUTOMOTIVE INDUSTRY – PART II

BRANISLAV JURAČKA[a], SOŇA RUSNÁKOVÁ*[b], IVAN LETKO[b], PAVEL KOŠTIAL[c], IVAN RUŽIAK[c], and JANKA JURČIOVÁ[d]

[a] VACUUMSCHMELZE, s.r.o., 916 24 Horná Streda 1325/14, Slovak Republic, [b] Tomas Bata University in Zlín, Faculty of Technology, T. G. Masaryka 275, 762 72 Zlín, Czech Republic, [c] VŠB-Technical university of Ostrava, Faculty of Metallurgy and Material Engineering, 17. listopadu 15/2172, 708 33 Ostrava-Poruba, Department of Materials Engineering, Czech Republic, [d] Saar Gummi Slovakia spol. s r.o., Gumárenská 397/21, Dolné Vestenice 972 23, Slovak Republic
rusnakova@ft.utb.cz

Abstract

The wide spectrum of composite materials application in automotive, aerospace and military industry, heterogeneous and their large –scale utilization requires necessary demanding accurate knowledge of material parameters those materials.

The thermal expansion behaviour and elastic properties of acrylate resin MODAR reinforced by glass fibre are studied. MODAR − Modified Acrylic Resins offers a series of unique thermoset polymers used in many markets such as automotive, mass transit, railways, building, rods for optical cable, structural parts and profiles and optical fire retardant / low smoke / low toxicity composite parts. MODAR resins offers: low viscosity, rapid cure, fast cycle times, superior physical properties, and resistance to cracking, long shelf-life and stability (valuable for hot climate countries).

Results and discussion - Part B

The diagrams of work for the sample B are described on the schemes 6–9.

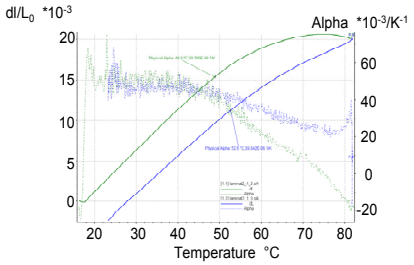

Scheme 7**. Behaviour dependency T to α, sample B, measurement 1**

Sample B: measurement 2,
Mode of heating, T=50,2 °C, $\alpha_f = 29{,}035.10^{-6}$ K^{-1}
Mode of cooling T = 52,7 °C $\alpha_f = 42{,}558.10^{-6}$ K^{-1}.

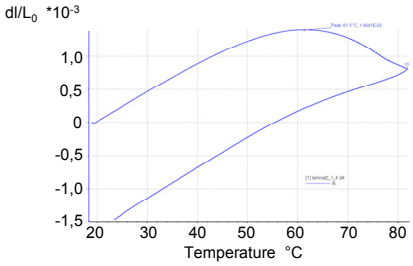

Scheme 8. **Behaviour dependency ε to T, sample B, measurement 2**

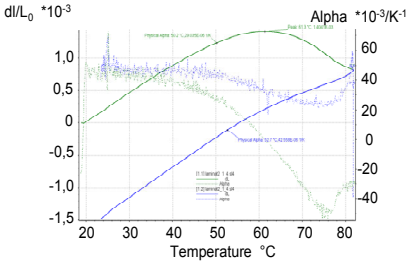

Scheme 9. **Behaviour dependency T to α, sample B, measurement 2**

Table I
The average values for the sample A

	sampleA	
	measurement Nb. 1	measurement Nb. 2
T_1(°C)	32,55800	47,08400
T_2(°C)	35,60300	49,28800
α x 10^{-5} 1/K	6,35170	6,73320
$\alpha_{hister.}$ x 10^{-5} 1/K	6,85770	1,78310
ε_{hister} (°C)	0,00186	0,00136

T_1 – beginning of the linear part, $\alpha_{hister.}$ – hysteresis between curves of coefficient of thermal expansion, T_2 – finish the linear part, $\varepsilon_{hister.}$ – hysteresis between curves of specific elongation, α – coefficient of thermal linear expansion.

Table II
The average values for the sample B

	sample B	
	measurement Nb. 1	measurement Nb. 2
T_1(°C)	23,27600	26,56700
T_2(°C)	27,37300	29,95400
α x 10^{-5} 1/K	5,03910	4,46770
$\alpha_{hister.}$ x 10^{-5} 1/K	2,60440	4,71610
ε_{hister} (°C)	0,00094	0,00112

T_1 – beginning of the linear part, $\alpha_{hister.}$ – hysteresis between curves of coefficient of thermal expansion, T_2 – finish the linear part, $\varepsilon_{hister.}$ – hysteresis between curves of specific elongation, α – coefficient of thermal linear expansion

The primary field of application for fibre reinforced polymer composites is the aerospace industry. For several years, however, composite materials have been increasingly used for various other technical tasks, where it is beneficial to apply lightweight construction materials which have high strength and stiffness characteristics. The favourable specific properties of fibre reinforced polymer composites are based on the low density of the matrix resins used, and the high strength of the embedded fibres[5].

Composites are unconventional material with those we have only short-term experiences with their using resulting in new methods their testing. These results to bad reproducibility of tests and comparison materials suitable to the same standard in various countries can offer very different values. Gradually unification testing methods is performing by patronage ISO (International Standards Organization). In term of reinforcement it can testing methods distributes to the group conversant in composites with unidirectional fibres (lamina, pole-stage stand) and the group conversant in composites with woven and unwoven mat. The outline the standards being used to testing and quality evaluation of composite materials is mentioned in the literature[6].

Shortly, for measurement materials characteristic materials reinforced with continuous glass fibres are used those standards:

- Young's modulus of elasticity, strength, maximal deformation – tensile test ISO 3268, ISO 527, ASTM 3039,
- tensile strength ASTM D 638,
- coefficient of thermal expansion ASTM D 696, DIN 51005, DIN 52612.

On the basic of results tensile strength between samples A and B we can constant, that composite material B is firmer like sample A. During classification influence of reinforced compound to properties of unreinforced acrylate resin Modar (the solid stage), which has tensile strength 56 MPa we constant, that none reinforcement do not improve strength of MODAR. Vice-versa strength of reinforced acrylate resin is lower (strength of sample A is 21, 42 MPa a strength of sample B is 36,90 MPa. Actual tensile strength samples A and b are lower compared to value Rm, reinforced laminate with reinforcement UNIFILO, Rm = 93 MPa, mentioned in material paper of the producer Ashland[3]. Relative elongation unreinforced acrylate resin MODAR is 6,5 % and reinforced acrylate resin with reinforcement UNIFILO is 1,4, what are higher values like mentioned the producer Ashland[3]. From the measured values by bursting test with extensometer located on investigated samples we obtained Young's modulus of elasticity to samples A and B. The values are to the sample A E = 5,861 GPa and to the sample B E = 7,106 GPa. The calculated values E on the basic measurements of flexure rod are to the sample A E = 4,907 GPa a to the sample B E = 5,977 GPa. As we compare with values mentioned in material list of the producer to reinforced laminate with fabric UNIFILO E = 10,4 GPa we found, that Young's modulus of elasticity of the samples A and B is lower.

To the achieving same deformation those composite materials we need lower strain like is mentioned in materials list of the producer. By the comparison E of the samples A and B unreinforced resin MODAR (E = 2,2 GPa) we can constant, that the application of reinforcement increase Young's modulus of elasticity and so on the same deformation we need higher strain.

The aim of this paper was obtain by experimental measurement thermoelastic properties of acrylate composite MODAR reinforced with continuous glass fibres.The seriousness of determination of materials parameters of composite materials was confirmed as well as experimental results because they are distinctive diversity from physical values in material parameters of producer. In generic term some experimental studies consider reinforced composite materials like isotropic if reinforcement meets the criteria is very simplifying fact.

Consequently in other measurements of composite materials we should have in mind anisotropy the properties of composite materials and the samples should be prepared to the testing method in various directions to the reinforcement orientation. During measurement of deformation (elastic and plastic) and the relative extension of samples and subsequent calculating of Young's modulus of elasticity it could think of application biaxial extensometer, which provide simultaneously measurement the changes of sample size upon loading in longitudinal and transverse direction with regard to loading direction. For a consideration results of experimental measurements and diagrams of work on Dilatometer DIL 402 PC realized on the same samples predicate, that the thermal ex-

pansion our investigated material is change in dependence on number of temperature cycles of loading. At the same time the measurement demonstrate, that dependency of change size to the temperature and dependency of thermal expansion coefficient to temperature is characteristic by sizeable nonlinearity and so coefficient of thermal expansion is not constant, it changes in dependence on the applied thermal cycle.

So for objective evaluation of thermal expansion acrylate resin MODAR reinforced by continuous glass fibres is necessary realized a series another measurement with repeated thermal loading the same samples and simultaneously with monitoring influence of reinforcement orientation to thermal expansion.

REFERENCES

1. Koštial, P. and all: *Využitie statických metód a kmitov v diagnostike materiálov*: Diagnostické metódy v materiálovom inžinierstve. UKC ZSVTS, Púchov 2009.
2. Daw J. E., Rempe J. L., Knudson D. L., Condie K. G., Crepeau J. C.: *Viability of Pushrod Dilatometry Techniques for High Temperature In-Pile Measurements.* Idaho National Laboratory, 2008.
3. ASHLAND, Composite polymer division MODAR 835 SCS [online]. http://www.ashchem.com
4. Dasgupta A., Agarwal R. K., Bhandarkar S. M.: Compos. Sci. Technol. *56*, 209 (1996).
5. Manfredi L. B., Rodríguez E. S., Maria Wladyka-Przybylak M. W., Vázquez A.: Polymer Degrad. Stab. *91*, 255 (2006).
6. Geier M. H.: *Quality Handbook for Composite Material*. ASM International, 1999.

P-41
EXPERIMENTAL TIRE TEMPERATURE-PRESSURE MEASUREMENTS IN REAL DRIVING CONDITIONS - PART B

JANA ĎURFINOVÁ[a], PAVEL KOŠTIAL[b], IVAN RUŽIAK[b], ZORA JANČÍKOVÁ[b], MARTINA FARKAŠOVÁ[b], LUBOŠ KRIŠŤÁK[c], JANKA JURČIOVÁ[d], SOŇA RUSNÁKOVÁ[e], and IVAN LETKO[e]

[a] Slovak University of Ttechnology in Bratislava, The Faculty of Chemical and Food Technology,Radlinskeho 9, Bratisava 912 37, [b] VŠB-Technical University of Ostrava, Faculty of Metallurgy and Material Engineering, 17. listopadu 15/2172, 70833 Ostrava-Poruba, Czech Republic, Department of Materials Engineering, [c] Technical University in Zvolen, Faculty of Wood Science and Technology, T.G.Masaryka 24, 960 53 Zvolen, Slovak Republic, [d] Saar Gummi Slovakia spol. s r.o., Gumárenska 397/21, Dolné Vestenice 972 23, Slovak Republic, [e] Tomas Bata University in Zlín, Faculty of Technology, T. G. Masaryka 275, 762 72 Zlín, Czech Republic
pavel.kostial@vsb.cz

Abstract

In this contribution we present measurements of external and internal tire temperature as well as the internal tire pressure by complex system for the simultaneous contact less measurement of these values (CTPA). The measurement is fully automatic, controlled by a personal computer and installed "in situ" on the car. The global position system, which is connected to a *PC*, further allows us to measure also the car speed in synchronized regime with other measured parameters. All external temperatures under investigation were independently tested by other contact thermometers.

Results and discussion - Part B

The same kind of dependence for the left wheel (sample A) is in the Fig. 5, to demonstrate decrease of measured outdoor temperature in this case caused by left tire release. In the Fig. 6 (B) and 7(C) are right wheel temperature-speed dependences for tires of other producers. On the Fig. 8 is a dependence of internal tire temperature versus time. Due to relatively small pressure changes we don't present the pressure/speed changes which are also registered by the *CTPA* system.

The results of "peak" outdoor (T_{ext}.Max) right wheel temperature as well as the onset time of internal temperature (t_{onset}) increase are in Table I (see also the Fig. 9). This Table also contains fitted value of experimental relaxation time $\tau_{exp.}$ Values of τ_{exp} are mean values of fitted data.

From experimental outdoor temperature decay curves we can determine the experimental "relaxation time". In every case it depends on the heat capacity and sample density as material constants (for convective heat transport characterized by constant *h* relaxation time is possible to express in the form $\tau=\rho.c_p.V/h.S$). The slowest tire temperature decay is observed for sample *A* ($\tau_{exp}=76,2$), which is accompanied by tire overheating ($T_{ext}.Max=338,8\ °C$). The onset time ($t_{onset}=60s$) signals quick energy transfer (also through tire sidewall) from rubber composite to the air inside a tire. As we said this fact is probably caused by improper breaker angle.

Different situation is for samples *B* and *C* .The smallest value of relaxation time ($\tau_{exp}=53,8$) was observed for the sample *B* and a $\tau_{exp}=65,6$ for the sample *C*. In both cases the tire overheating is sufficiently smaller than in the case *A* which is seen on values of $T_{ext}.Max=236,4$ for the sample *B* and *236,3* for the sample *C*.

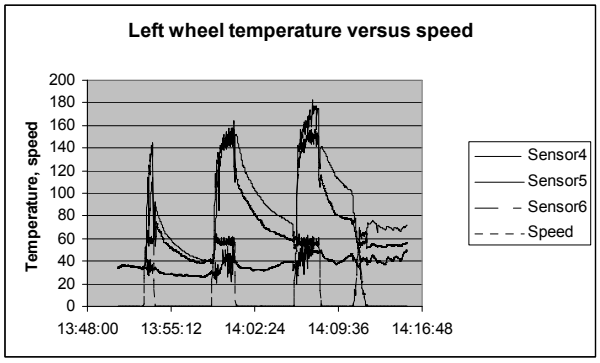

Fig. 5. **Left wheel time-temperature-speed curves for sample A**

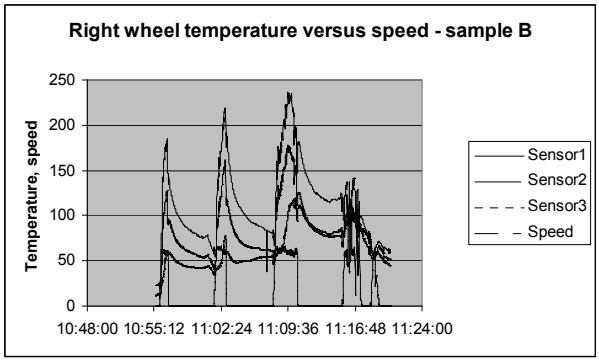

Fig. 6. **Right wheel time-temperature-speed curves for sample B**

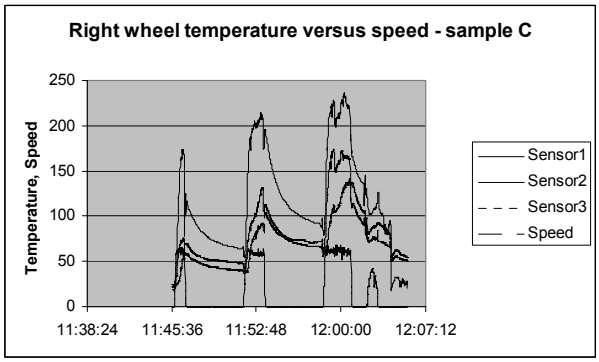

Fig. 7. **Right wheel time-temperature-speed curves for sample C**

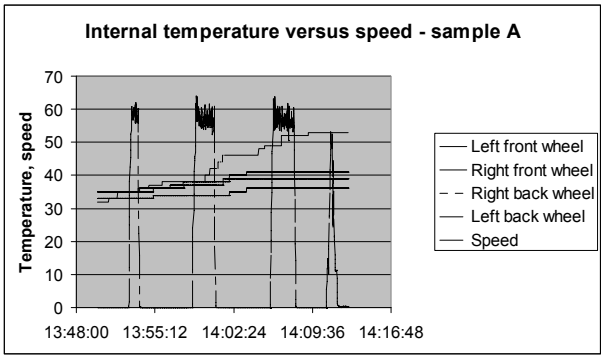

Fig. 8. **Internal temperature-speed curves for sample A**

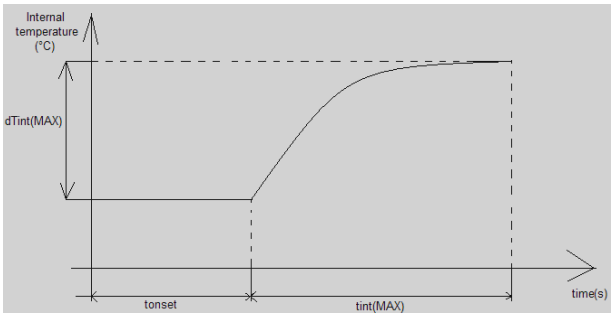

Fig. 9. **The internal temperature-time curve**

Table I
The data of maximum external tire temperatures, as well as the onset time of internal temperature increase t_{onset} and experimental relaxation time

Sample	A	B	C
T_{ext}(MAX)[°C]	338,8	236,4	236,3
t_{onset}[s]	60	289	1281
τ_{exp} [s]	76,2	53,8	65,6

Conclusion

CTPA is useful, fully automatic instrument for "*in situ*" monitoring of both internal and external tire temperatures and tire pressure. The CTPA system allowes the easy data matching and offer constructors interesting information about tire temperature trends in real driving conditions.

REFERENCES

1. Smartire 2010. *SmarTire for Commercial Vehicles*, http://www.smartire.com/cv.
2. SPEED-WIZ 2010. *Chassis Calculations*, http://www.speed-wiz.com/calculations/ chassis/index.htm.
3. TireChek 1999. *TireChek Tire Pressure Monitor*, http://mb-soft.com/tirechek/.
4. Autoware Inc. 2009. *Tire Temperature Analyzer*, http://www.auto-ware.com/ software/ tta/tta.htm.
5. BorgWarner BERU Systems GmbH 2010. *Tire Safety Systems TSS – The Tire Pressure Control System*, http://www.beru.com/english/produkte/tss.php.
6. Koštial P., Hutyra J., Kopal I., Mokryšová M.: *10th International Conference: Progress in materials engineering. 2005,* 29.
7. Koštial P., Hutyra J., Kopal I., Mokryšová M., Klabník M., Žiačik P.: Chem. Listy *23*, 99 (2005).
8. Koštial P., Mokryšová M., Šišáková J., Mošková Z., Rusnáková S.: Int. J. Thermophysics *30*, 334 (2009).
9. Mokryšová M., Koštial P., Kučerová J., Mošková Z.: Exp. Tech. *33*, 33 (2009).

P-42

INFLUENCE OF CROSS-SECTION MODIFICATION OF PP FIBRES ON THE END-USED PROPERTIES

JOZEF RYBA[a], ANNA UJHELYIOVÁ[a], ĽUBA HORBANOVÁ, and PETER MICHLÍK[b]

[a] Department of Fibres and Textile Chemistry, Institute of Polymer Materials, Faculty of Chemical and Food Technology, Slovak University of Technology in Bratislava, Radlinského 9, 812 37 Bratislava, Slovakia, [b] Research Institute for Man-Made Fibres, a.s., Štúrova 2, 059 21 Svit, Slovakia
jozef.ryba@stuba.sk

Abstract

Shape of cross-section of the fibres has significant influence on end-used properties of fibres which are used for textile or technical applications. This work is focused on an evaluation of the influence of this varied fibre geometry on different properties and characteristics of polypropylene (PP) fibres.

Introduction

Ones of the main end-used properties of textile materials are mechanical and transfer properties (heat, humidity and air).

The transfer properties of fibres correspond mainly with their surface properties. The transfer properties of fibres are mainly related to their geometry. The cross-section and longitudinal fibre geometry is defined by the following characteristics such as shape and size of fibre surface, volume of fibre, measuring surface of fibres and capillary system between the fibres and yarns. A great variety of fibre profiles with different surfaces and sur-face properties can be reached during the technological conditions of synthetic fibre spinning and drawing by profiling in cross-section and longitudinal direction[1-3].

Shaped fibres with special or strongly irregular profiles are very promising. They are manufactured with spinnerets with the appropriate profile of holes[4]. The shaped fibres can be used to develop new kinds of textiles and low-melting knits, since the irregular profile sharply increases the frictional forces between filaments. In addition, the high covering power of the shaped fibres reduces materials consumption for the articles.

For evaluation of shaped fibre characteristics are used following relations:

Degree of branching:	$R=P_N^2/S_N$	
Filling degree:	$Z=S_N/S_Y$	
Degree of segmentation:	$S_e=P_N/P_Y$	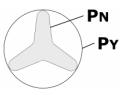
Degree of deformation:	$D=R/r$	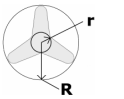
Coefficient of fullness (for hollow fibres):	$F_P=(1-A_D)/A_V$	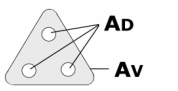

P_N – circumference of cross-section, S_N – surface of cross-section, S_Y – surface of circumscribed circle, P_Y – circumference of circumscribed circle, R – radius of circumscribed circle, r – radius of inscribed circle, A_D – surface of hollows, A_V – surface of fibre

Triangular and three-pronged — "trilobal" — are the most frequently encountered shape. Triangular fibres with a flat surface can be used to manufacture articles with a "luster effect" due to high light reflection by their individual segments. Fibres with a flat (more precisely, oval) section also have a luster effect. In addition, high flexibility is characteristic of these fibres due to the lower moment of inertia of the flat section in flexure in comparison to round sections[4].

This article deals about influence of the cross-section shape of the polypropylene fibres onto above mentioned end-used properties.

Experimental

Materials used

For the preparation of non-modified (nPP) and modified PP (mPP) fibres was used polypropylene Tatren HT 1810 with MFI = 20.9 g/10 min from Slovnaft a.s., Slovakia and micronized inorganic filler (6.4 wt.%). From these materials were prepared undrawn fibres with circle and five pointed star shape cross-section and modified by inorganic filler on the laboratory spinnig machine. Next, the undrawn PP fibres have been to drawn to the drawing ratios $\lambda = 3$ and 4.

Method used

Mechanical properties were measured on INSTRON 1122 and evaluated according to STN EN ISO 1973, 5079, 2062 – standard methods for evaluation of mechanical parameters.

For evaluation of shaped PP fibre characteristics was used optical microscope Olympus BX51 equipped with CCD camera and software analySIS FIVE version 5.0 (build 1120).

For evaluation of water vapour sorption of PP fibres was used gravimetric analysis. Samples were dryed at 80 °C for 1 hour in drying chamber. After that samples were puted into glass vessel with saturate solution of NH_4NO_3 (relative humidity over this solution is 65 % at 20 °C) for 96 hours. After this period the samples were weighing. In the next step samples were dryed in drying chamber at 105 °C for 3 hours and weigh again.

Content of water vapour (C_{WV}) sorption was calculated on the backround of this formula:

$$C_{WV} = \frac{m - m_0}{m_0} * 100\% \qquad (1)$$

were m – weight of the fibre with water vapour sorption in equilibrium state (after 96 hours), m_o – weight of the fibre after drying.

Results

Mechanical properties of non-modified and modified PP fibres are shown in Table I and Table II. Tenacity at the break of PP fibres modified by micronized inorganic filler is lower in comparison with non-modified PP fibres at both drawing ratios λ=3 and 4. This is caused by particle size of micronized inorganic filler, which decrease the sufficiency of drawing of polymer matrix. This type of inorganic filler has no reinforcement effect on PP fibre matrix. However tenacity at the break of non-modified and modified PP fibres with cross-section shape of five pointed star is higher than tenacity at the break of non-modified and modified PP fibres with circle shape cross-section. The micronized inorganic filler due to decrease of tenacity at the break of PP fibres with cross-section shape of five pointer star in comparison with the non-modified PP fibres with the same cross-section shape. This confirms the theoretical knowledge, that the addition of micronized filler to the oriented polymer matrix decreases their mechanical properties. These all statements are analogical for Young's modulus as well as elongation at the break.

Next part of end-used properties of non-modified and modified PP fibres is shown in Tables III and IV. Cross-section area (A) of circle shape cross-section of modified PP fibres is higher in comparison with cross-section area of non-modified PP fibres. This is caused by present of micronized inorganic filler (lower filament diameter homogenity). Cross-section area of the PP fibres with five pointed star cross-section shape is higher than cross-section area of the PP fibres with circle cross-section shape. This can cause the different cooling and crystallization of PP melt flow from various profiles of hole at the same conditions of preparation.

Table I
Fineness (T_d), tenacity (σ) and elongation (ε) at the break, Young's modulus (E) of the non-modified and modified PP fibres with drawing ratio λ=3

Sample	T_d [dtex]	σ [cN/dtex]	ε [%]	E [cN/dtex]
nPP-circle	6,0	2,8	155	24,8
mPP-circle	6,3	2,6	139	23,4
nPP-star	6,0	3,4	158	26,2
mPP-star	6,2	3,0	185	21,8

Table II
Fineness (T_d), tenacity (σ) and elongation (ε) at the break, Young's modulus (E) of the non-modified and modified PP fibres with drawing ratio λ=4

Sample	T_d [dtex]	σ [cN/dtex]	ε [%]	E [cN/dtex]
nPP-circle	6,1	3,4	117	35,3
mPP-circle	6,2	3,0	95	32,5
nPP-star	5,9	4,2	140	35,0
mPP-star	6,4	3,6	122	27,0

Table III
Cross-section area (A), degree of branching (R), filling degree (Z), degree of segmentation (S_e), content of water vapour (C_{WV}) of the non-modified and modified PP fibres with drawing ratio λ=3

Sample	A [μm^2]	R	Z	S_e	C_{WV} (wt.%)
nPP-circle	535	–	–	–	1,05
mPP-circle	670	–	–	–	1,15
nPP-star	604	24,8	0,63	1,09	1,21
mPP-star	940	20,9	0,67	1,05	1,30

Degree of branching (R) and degree of segmentation (S_e) of the non-modified and modified PP fibres with five pointed star cross-section shape decrease with increasing drawing ratio. Filling degree (Z) of the non-modified and modified PP fibres with five pointed star cross-section shape slightly encrease with higher drawing ratio.

All calculated parameters (R, Z, S_e) obtained by optical microscopy for fibres with circle cross-section shape are equal 1.

Table IV
Cross-section area (A), degree of branching (R), filling degree (Z), degree of segmentation (S_e), content of water vapour (C_{WV}) of the non-modified and modified PP fibres with drawing ratio λ=4

Sample	A [μm^2]	R	Z	S_e	C_{WV} (wt.%)
nPP-circle	560	–	–	–	0,61
mPP-circle	705	–	–	–	0,70
nPP-star	630	23,9	0,64	1,11	0,83
mPP-star	811	20,7	0,69	1,06	0,99

Content of water vapour sorption of modified PP fibres is higher than sorption of non-modified PP fibres. This is also caused by present of micronized inorganic filler which can invade surface homogenity of each filament of the fibre. These all statements are analogical for both types of cross-section shape of the fibres and drawing ratios.

The PP fibres with the circle shape cross-section as well as with five pointed star cross-section shape at the lower drawing ratio (λ=3) have higher segmentation of their profile and it provide the higher water vapour sorption of these fibres.

Conclusion

On the backround of experimentally obtained results it can be concluded that:

– change of cross-section geometry from circle to five pointed star have positive influence onto tenacity and Young's modulus of the non-modified and modified PP fibres,

− cross-section area of the fibres with five pointed stars cross-section shape is higher than cross-section area of circle cross-section shape fibres and have positive influence on content of water vapour sorption.

Modificated fibres like these are applicable for technical fabric and for improving of the other types of materials like concrete for example.

This work was supported by the VMSP-P-0007-09 and VEGA 1/0444/09.

REFERENCES

1. Jambrich M.: Fibres Text. East. Eur. *6*, 33 (1998).
2. Murárová A.: Chemical Papers. *47*, 356 (1993).
3. Murárová A.: Chimvolokno *3*, 56 (1993).
4. Perepelkin K. E.: Fibre Chem. *37*, 123 (2005).

P-43
COMPARISON OF INJECTION MOLD COOLING SYSTEMS

STEPAN SANDA, MIROSLAV MANAS, DAVID MANAS, MICHAL STANEK, and JIRI KNOT

Tomas Bata University in Zlín, nám. TGM 5555, 760 01 Zlín, Czech Republic
sanda@ft.utb.cz

Abstract

This article deals with a problem of the injection mold cooling. For the two cavities, injection mold was designed different cooling systems. The first system was made by drilling holes and the second cooling system was made by DMLS technology – rapid prototyping. Both systems were compared with the help of the CAE application.

Introduction

Cooling system of injection mold affects the quality of injected part and cycle time. The most common design of cooling system is in the form of drilled holes or milled channels. Machining of holes and channels is time consuming process and does not enable to set up steady temperature distribution inside the cavity mold. DMLS (Direct Metal Laser Sintering) is one of the Rapid Prototyping technologies that any geometry of cooling system makes possible.

Compared cooling system

Two-plate injection mold with cold runner system and cylindrical ejector pins has been chosen for comparison of conventional and new (generative) cooling systems. Design of the injection mold enables to change cavity only regardless of used cooling system.

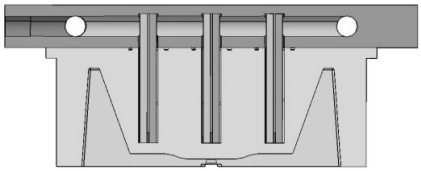

Fig. 1. **Cavity of classical cooling system**

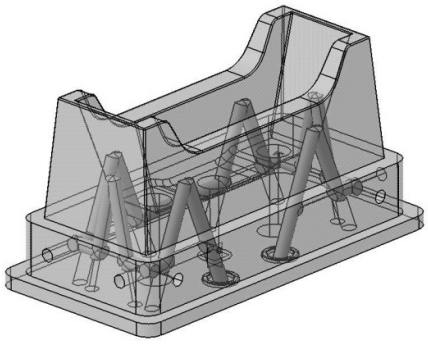

Fig. 2. **Core of classical cooling system**

The first of the cavity has conventional cooling system and another one is made by DMLS technology. The DMLS technology makes possible to create complicated holes with diameter of 4 to 5 millimetres, which more effectively cool down cavity and core.

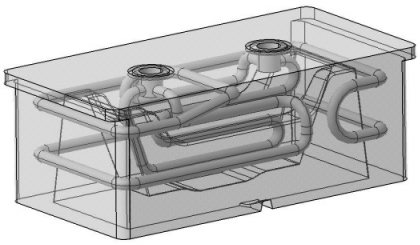

Fig. 3. **Cavity of DMLS cooling system**

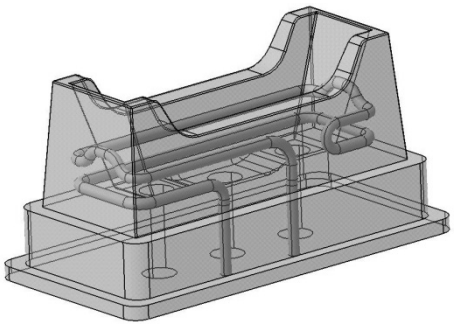

Fig. 4. **Core of DMLS cooling system**

CAE analyses

Comparison of both cooling systems was carried out with Autodesk Moldflow Insight 2010, where were defined cavity, gating and cooling system. The same process condition, 3D volume mesh and same analyses sequence has been used in all analyses.

DMLS technology

Direct Metal Laser Sintering (DMLS) rank among Rapid Prototyping (or Rapid Tooling) technologies. This technology enables production of part with very complicated geometry.

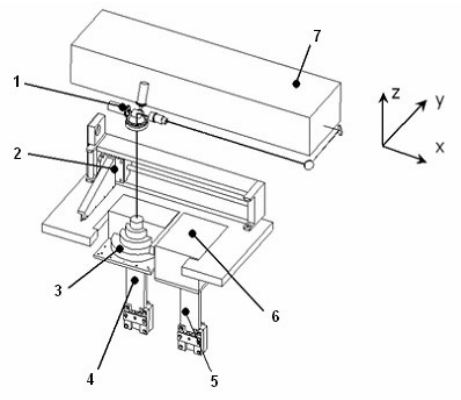

Fig. 5. **Principle of DMLS technology;** 1 – galvanometer-scanner with f-Theta lens; 2 – laminated system; 3 – product of DMLS; 4 – structural platform; 5 – storage bin platform; 6 – storage bin; 7 – laser.

Building of product is realized layer by layer (so called generative method). The laser beam melts metal powder in very thin layer. Suitable materials for DMLS technology are bronze, tool steel, stainless steel, titanium, Co-Cr alloys etc. The product is homogenous metal part with similar properties like the product made by the working.

The advantage of new technology for design of cooling system of injection mold lies in unlimited shapes of cooling channels, generation of turbulent flow coolant and uniform temperature distribution.

Discussion

Results confrontation of both cooling systems show the more uniform temperature distribution by the DMLS products. This fact is very clearly seen in the Fig. 6 and Fig. 7 describing efficiency of heat removal by the given circuit.

This efficiency depends on the shape of the cooling channel, the distance of cooling channel from the cavity wall, Reynolds number and type of coolant. The cooling channels made by the classical way are thermal overloaded inside of cavities. This problem does not appear by the DMLS parts where all parts of cooling systems have been thermal steady loaded.

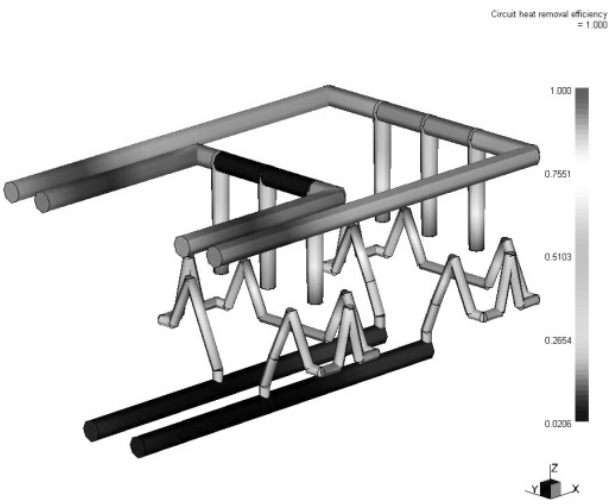

Fig. 6. **Circuit heat removal efficiency of classical cooling system**

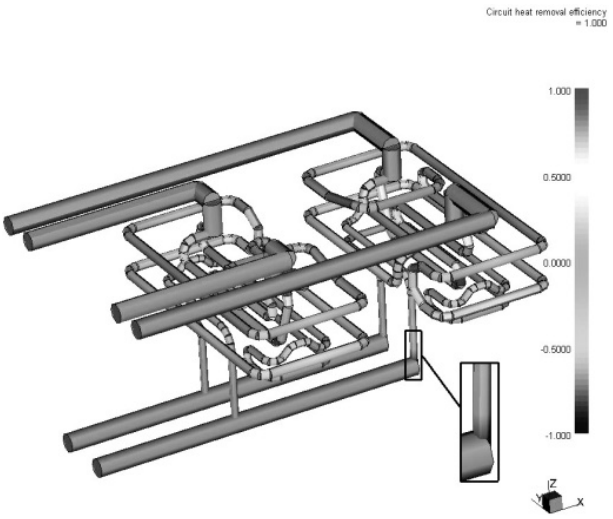

Fig. 7. **Circuit heat removal efficiency of DMLS cooling system**

Thanks to new design of cooling system made by DMLS technology the cycle time was of 10 seconds shorter in comparison with traditional one. Besides this, the dimensional stability of final part has been improvement.

Conclusion

DMLS as new technology in production of metal parts could be an alternative for production of parts with very complicated geometry, which cannot produce by traditional technology. New way in production of cooling systems of injection mold leads to improvement of part quality and reduce significantly cycle time mainly due to steady temperature distribution.

This article is financially supported by the Czech Ministry of Education, Youth and Sports in the R&D projects under the titles 'Modelling and Control of Processing Procedures of Natural and Synthetic Polymers', No. MSM 7088352102 and 'CEBIA Tech', No. CZ.1.05/2.1.00/03.0089.

REFERENCES

1. Knot J.: *Diplomová práce*. Univerzita Tomáše Bati ve Zlíně, Zlín 2010.
2. DMLS [online]. 2007 [cit. 2010-11-01]. DMLS - Direct Metal Laser Sintering, Kovové prototypy. Dostupné z http://www.dmls.cz.
3. Mayer S.: Conformal cooling: Why use it now?. Injection Molding [online]. December 8th, 2009, [cit. 2010-11-01]. Dostupný z http://www.plasticstoday.com/imm/articles/tooling-conformal-cooling-1209.
4. Šanda Š., Maňas M., Staněk M., Maňas D., Rozkošný L.: Chem. Listy *103* (S), 140 (2009).

P-44
CO_2 LASER MICROMACHINING AND PLASTICS PROPERTIES

LIBUŠE SÝKOROVÁ and OLDŘICH ŠUBA

Tomas Bata University in Zlín, Faculty of Technology, Department of Production Engineering, T. G. Masaryka 275, 762 72 Zlín, Czech Republic
sykorova@ft.utb.cz

Introduction

There are several types of plastics that have been processed by laser. They absorb electromagnetic energy at 10.6 micrometers – the wavelength of light emitted by CO_2 lasers.

The task of the laser micro-machining has very extensive usage in industrial applications. Production specifications trend to continual minimization of product's dimensions. The laser is optimal tool for its features in this development. Results of the laser micro-machining – surface quality of product and his utility in specific application – depend on the laser parameters and the polymer material type.

Experiment

From the obtained scientific knowledge it follows, that the character of surface machined by laser depends among others on the thermal conductivity of polymer. Therefore it was decided to test more kinds of polymers – ABS and PMMA. Commercial CO_2 laser Mercury L-30 by firm Laser-Pro, USA was used for cutting of specimens. Ray of laser could be focused on mark diameter d = 185 μm. The maximum value of density of energy flow is q = 1,1 GWm^{-2}.Desired symbol was created in program Corel Draw, the width of slot was 2 mm in all cases. Cutting parameters (output power and feed) were set and these were changed gradually. Values of power and feed are presented as percents from maximum power (P = 30 W) and maximum feed (fmax = 1066 mm s^{-1}) in charts of parameters combination and graphs. These specimens were prepared from this sheet (proportions 130 x 61 mm, thickness 10 mm). The edges were milled and grinded. Dependence of slot depth on the laser parameters – output power and feed – was measured. The dimension and profiles measuring of machined slots were realized on the optical microscope ZEISS 2772. Suitable microscope optics which ensured 117 x enlargements was set first of all. For the reason of statistical evaluation of measured values the measurement of depth was realized in all slots 5 times. Slot depth (d in μm) in dependence on laser parameters combination is presented in following results tables. Values of power and feed are presented as percents from maximum power (P = 30 W) and maximum feed (f_{max} = 1066 mm s^{-1}) in charts of parameters combination and graphs. Description 20/70 means 20 % value from power 30W and 70 % value from maximal feed 1066 mm s^{-1}.

Especially at short power slot values were very short and it was not possible to measure. These experimental results

Table I
Slot depth in μm for ABS

P [%] f [%]	10	20	30	40	50	60	70	80
50	–	10	75	90	105	118	162	206
70	–	–	10	54	68	75	102	127
100	–	–	–	20	31	65	75	101

Table II
Slot depth in μm for PMMA

P [%] f [%]	10	20	30	40	50	60	70	80
50	24	38	102	126	178	200	246	248
70	–	3	15	39	51	116	146	160
100	–	–	8	25	31	37	47	63

Table III
Regression equation of slot depth dependencies on laser parameters combination designated in program EXCEL

Feed f [%]	equation	correlation coeffic. R^2
	PMMA	
50	y = 3,5167x	0,9759
70	y = 2,8929x	0,9525
100	y = 0,9914x	0,9681
ABS		
50	y = 2,8214x	0,9432
70	y = 2,1029x	0,9536
100	y = 2,0600x	0,9735

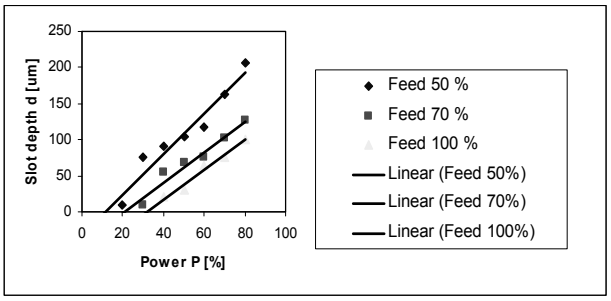

Fig. 1. **Slot depth linear dependence for ABS**

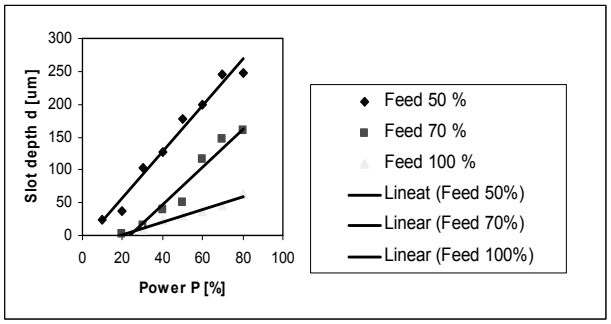

Fig. 2. **Slot depth linear dependence for PMMA**

were evaluated and depicted into the graphs. Approximating straight-line and their correlation coefficients were created for these dependencies.

Because of exact evaluation of machined groove profile cuts of specimen were made and then these ones were grinded. This exploration was realized on the optical microscope MU ZEISS. Suitable microscope optics which ensured 250 x enlargements was set first of all. Than digital camera was installed in microscope and it scanned photo of specimens. Photos of grooves and melted boundaries were made. (Fig. 3).You can see the photo of groove detail ABS, PMMA on the following picture.

Digital photos were modified with the help of software ADOBE PHOTOSHOP 6.0 and AUTOCAD 2002. Scales factor corresponding used optics of microscope were assigned at modified photos. Modified photos in JPG format were imported into software AUTOCAD 2002 for the purpose of profile groove digitalization of cut. Lower left corner was localised into coordinate global basic origin. Profile groove of cut was digitized by 30 pixels at coordinates [x, y]. These coordinates were multiplied by corresponding scale so that value corresponded to real values in mm (bitmap inserts into AUTOCAD 2002 is not in real scale). Subsequently the model was defined with the help of software DataFit V.8 :

$$h = A + B.e^{-(x-C)^2} \qquad (1)$$

and numerical values of coefficients A, B, C were itemized. Finally nonlinear regression was realized with the help of DATAFIT V.8. Results of these tests are presented thereinafter on the following figures.

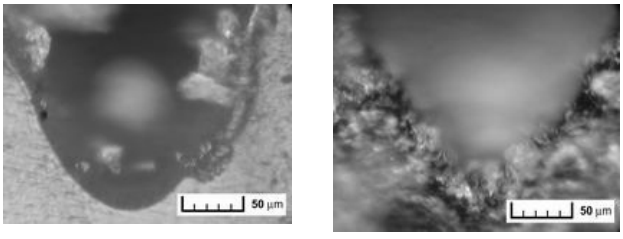

Fig. 3. **The illustration of groove 50/10 ABS and PMMA**

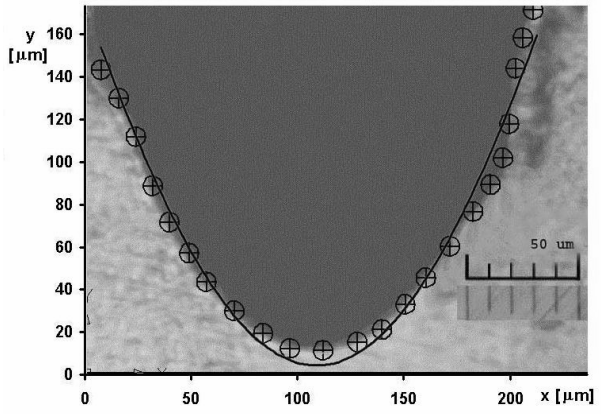

Fig. 4. **Gaussian density of laser beam energy for cutting parameters 50/10, material ABS**

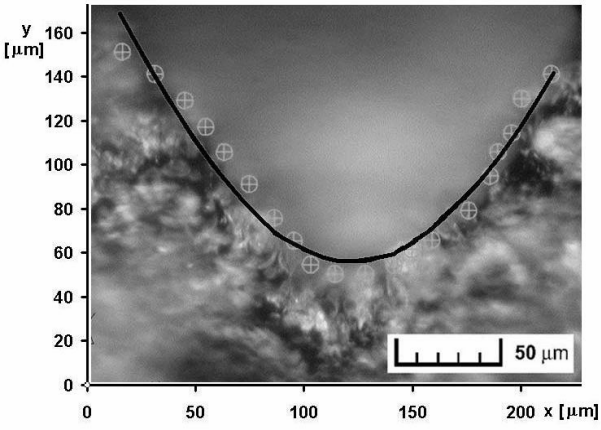

Fig. 5. **Gaussian density of laser beam energy for cutting parameters 50/10, material PMMA**

Conclusions and intentions

From this experiment it is evident the slot depth grows linear with increasing values of power at concrete adjusted value of feed. Biggest depth is at low values of feed. This phenomenon was observed at all materials. Biggest slot dept vas measured at PMMA material. Gradient of lines and corre-

lation coefficients offer information about dependence character of slot depth on adjusted power and feed at graphic presenting results. Value of gradient (k) is used for exact control of stock removal (slot depth). Gradient of line gives information about sloth depth at increasing of power about definite number of percents. Correlation coefficient gives approximate quality of linear dependence (compare with $R^2 = 1$).

Resulting structures can be very exact and with high quality of surface in dependence on laser parameters and on type of machining materials.

From results of experiment is evident that density distribution of used laser beam is Gaussian. The TEM $_{00}$ mode is ideal for most cutting, drilling, and welding applications because it produces a beam that can be focussed to a minimum spot size for very high power density. It is a Gaussian mode, with most of the energy in the centre.

This work was supported by the Ministry of Education and Youth of the Czech Republic under grant MSM 7088352102. This support is very gratefully acknowledged.

REFERENCES

1. Bílek O., Lukovics I. (2006). Manufacturing Technology, J. for Science, Res. and Production. December 2006, vol VI, Ústí nad Labem, p. 12–16.
2. Lukovics I., Bílek, O. In.: Acta Mechanica Slovaca, Košice, 2B/2006, Pro-tech-ma, ročník 10, Košice 2006.

P-45
RESEARCH OF THE LASER TECHNOLOGY

LIBUŠE SÝKOROVÁ and OLDŘICH ŠUBA

Tomas Bata University in Zlín, Faculty of Technology, Department of Production Engineering, T. G. Masaryka 275, 762 72 Zlín, Czech Republic
sykorova@ft.utb.cz

Abstract

The paper deals with possibilities of using the laser in technologies. It evaluates the influence of design and technological conditions on output parameters of cutting process, and also presents relative laser workability of some polymers. Finite element analyses of the transient nonlinear heat and mass transfer were simulated using of the two-dimensional model.

Introduction

The term „laser“ tells us that a simplified description of the lasing process could be „opposite of absorption”. At the heart of the lasing phenomenon is the ability of photons to stimulate the emission of other photons, each having the same wavelength and direction of travel as the original.

The photons oscillating from one end of the resonator to the other constitute electromagnetic energy which forms an intense electromagnetic field. The shape of this field is critically dependent not only on the photon wavelength, but also on the mirror alignment, curvature, and spacing, and on the bore diameter of the laser tube. This field can assume many different cross-sectional shapes, termed transverse electromagnetic modes (TEM), but only certain modes, or mixtures of them, are useful for processing materials. The TEM 00 mode is ideal for most cutting, drilling, and welding applications because it produces a beam that can be focussed to a minimum spot size for very high power density. It is a Gaussian mode, with most of the energy in the centre.

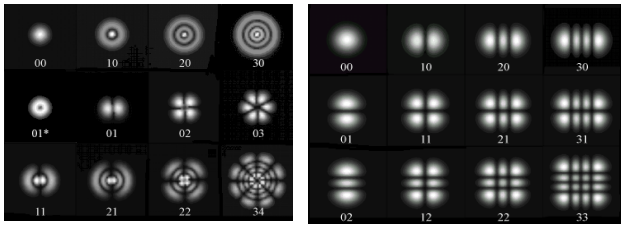

Fig. 1. **Selected Mode TEM**

This mode distributes the beam energy efficiently for other heat-treating and drilling applications. TEM01 also has its particular uses. But not the difference between the cross-sectional representation of the widely used TEM00 mode and that of mode called TEM11.It is evident that the distribution of power across the TEM00 beam, results in a more efficient tool for cutting than does the more fragmented power distribution of the divided TEM11.

Experiment

Absorption of luminous radiation and followed heating depend on thermal conductivity of material. Heat convection from the laser to the material is complicated effect. Today true theory for formulation of thermal conductivity and temperature calculation isn´t exist because heat transfer is very quick. The process propounded by Carslaw-Jaeger is used for formulation of heat transfer for mobile source with speed in (m s^{-1}). The process presents solution partial differential equation for heat convection from the source with dimension of focused beam to surface layer and in material at definite marginal conditions. It goes from simplified hypothesis that material of product is isotropic and heat transfer can describe by Fourier-Kirchhoff differential equation:

$$\frac{\partial T}{\partial t} = \alpha \nabla^2 T \quad , \qquad \alpha = \frac{\lambda}{\rho c} \tag{1}$$

where λ is thermal conductivity, ρ is density, c is heat capacity.

A PMMA side wall gradually cools after a laser light passed through in a specific cut. At the same time, the thermal flow is distributed from a cut plane to the internal dimension of the wall. Thermal conductivity of thermoplastic materials is (100–1000) times less then that of metals. As a result, plastics keep high differences of temperatures between external and internal layers. The physical characteristics of the thermo-

plastic materials were changed significantly in this temperature interval. Values λ, ρ, c were entered as the function of the temperature through the medium of the thermal curves. The heat flow values were entered as the variable parameters. Progressive ignition and extinction of the heat flow simulates the ray laser movement. The maximal temperature was regulated on the already alluded cracking temperature by repeated changes of the heat field value and following thermal field calculation. The time variable heat flow was entered into the particular flat elements (constituent the model half of cut) by time curves i=1,2,3. (Fig. 1).

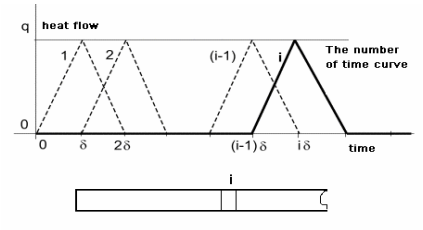

Fig. 2. **Scheme of boundary conditions of the movement ray laser**

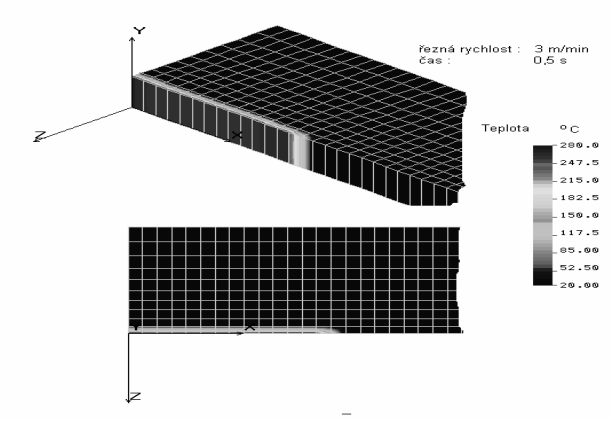

Fig. 3. **The thermal field for cutting speed $1{,}6\times10^{-3}$ ms^{-1} in time t=15 second**

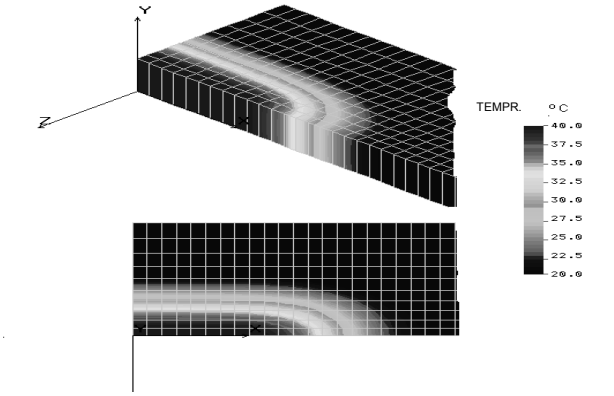

Fig. 4. **Simulation of the heat distribute at surrounds after 3 min**

The results are presented in the following pictures.

Defining and determining of laser workability is a big problem. More workplace for laser cutting determines possessiveness that 15 input variables, further on by time and space variable physically − mechanical and chemical properties of machined material, scoria and the fact, that during the cutting plasma arises. According to our experience it is the most advantageous to define the laser workability with the help of isometric h-v of P-v diagrams. They are describes dependence between depth of cut (h) on laser cutting speed for some metals for range of power (P). Dependencies of laser cutting speed on power for some materials are shown in Fig. 5. Relative laser workability has been defined. It is characterized with the depth of the depth of the cut related to the unit width of the cut and unit output.

The results of the experiments so show very good relative workability of materials and composites whose particles do not tend so separate during the process. If technological conditions (moving speed of the laser head, the beam output, mode parameters of the optics) are optimized, a good quality of the cut can be reached for both metals and plastics.

In case of polymers (plastics and rubber), the surface modification is completely different. During exposition of polymeric material (PP, PS, PE, PC, PVC, PA) samples to concentrated energy, the surface layer degrades and the strength of the samples derogate. On the other hand, PMMA and metal are influenced in a different way. When the output (and therefore heat) increases, the metal material surface is heated above modification temperature. It causes structural transformations in surface layer. The result is a hardened surface layer of the metal and improved strength of samples.

The effect of the laser beam upon PMMA is of interest, too. Due to the layer structure modifications, the surface hardness rises, flaws and creases are healed and as the result of this the sample strength increases. Due to the activity of high concentrate energy and at the same the high temperature, PMMA depolymerize and it rise an amount of radicals at the end of the polymer strings. Thanks to existing of radicals and minor amount of monomer, it raises a net structure here and so the layer strength increases. The strength of the machined layer depends on the time of interaction, too. Longer time of the laser beam contact to material imports better material

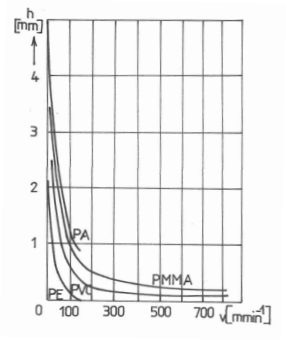

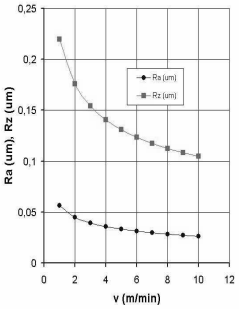

Fig. 5. **Results of laser cutting for some polymers**

strength and hardness. This phenomenon is typical for plastics and it can be useful in special tools manufacturing.

Conclusion

Laser beam is the tool of the future. It can cut without affecting the surrounding material. Its energy is clean, reliable and docile it's ready to be tamed and handled to give an unequalled quality to the process. Quality of cut depends from working parameters of laser cutting process (laser power, feed rate, material thickness.)

The results of the experiments so show very good relative workability of materials and composites whose particles do not tend so separate during the process. If technological conditions (moving speed of the laser head, the beam output, mode parameters of the optics) are optimized, a good quality of the cut can be reached for both metals and plastics.

The model LASER interaction with thermoplastic material is possible. The result area of the high temperature respectively its gradients are narrow after passing of through the LASER ray. The width of the thermal influence area is only a minimal depends on the cutting speed. The high temperature gradients induce both short time transient thermal stress values and residual tension at the cut proximity.

This work was supported by the Ministry of Education and Youth of the Czech Republic under grant MSM 7088352102. This support is very gratefully acknowledged.

REFERENCES

1. Lukovics I., Sýkorová L.: In.: WORKSHOP 97., 1996, p. 1433.
2. Varga V., Maňková I.: In.: Technologia 95 STU Bratislava, 1995.
3. Bílek O., Malachová M.: Academic Journal of Manufacturing Engineering. Politehnica University of Timisoara. 2007, no. 3, s. 16–20.
4. Mádl J., Jersák J., Holešovský F.: *Jakost obráběných povrchů.* UJEP, Ústí nad Labem 2003.

P-46
INFLUENCE OF TENSIDES ON PROPERTIES OF RUBBER BLENDS

MARTINA ŠARLAJOVÁ[a], PAVOL ALEXY[a], JANKA JURČIOVÁ[b], PETER POČAROVSKÝ[a], and JANA ĎURFÍNOVÁ[a]

[a] STU Bratislava, [b] Saar Gummi Slovakia, Dolné Vestenice, Slovakia
martina.sarlajova@stuba.sk, pavol.alexy@stuba.sk, jana.jurciova@saargummi.com, peter.pocarovsky@stuba.sk, jana.durfinova@stuba.sk

Introduction

Tensides are substances which are able to decrease the surface tension on interfaces. Tensides are utilised in polymer blend preparation process for modification of interface between polymeric matrix and particles of inorganic filler. They improve compatibility of polymeric matrix (usually with lower polarity) with surface of more polar filler. Simultaneously addition of tensides causes better properties of blends as an affect of better dispergation of filler in the matrix. Active and inactive fillers have significant influence on properties of vulcanisates. High degree of distribution and high degree of dispergation are necessary to achieve the optimal properties of filed vulcanisates.

In the present work, the influence of two types of tensides (Triton X 405, Tween 40) on properties of rubber blends was tested. Rubber blends based on natural rubber were used in combination with two types of fillers – silica (Perkasil KS 408 PD) and clay (clay KKA). Tensides were dosed at five concentration level from 0 to 5 phr. Influence of type of tenside as well as influence of its concentration on vulcanization parameters and mechanical properties were tested. Morphology of blends was observed using scanning electron microscopy (SEM). Fracture surfaces were prepared by breaking of samples at liquid nitrogen temperature.

Materials and methods

Two types of tensides were used in the work – Triton X 405 (nonionic tenside, octylphenol ethoxylate from Procter&Gamble) and Tween 40 (polyoxyethylen sorbitan monopalomitate from Procter&Gamble). Two types of filler were used as well – Perkasil KS 408 as silica from Werba-Chem GmbH Wien and clay from LB Minerals s r. o. Horní Bříza. Natural rubber SIR 10 was used as rubber matrix. Vulcanisation system consisted from sulphur, ZnO and strearic acid. Sulfenax CBS (sulphenamide) and diphenylguanidine were used as accelerators. All components of vulcanisation system were dosed at 4,5 phr. Paramo MES (mixture of residual and refined oil) was used as well. All mixtures were prepared using brabender chamber kneader, volume 75 ml. Cline loading was 10 kg. Blends were prepared in two stages. In the first stage rubber, oil, filler, tenside, ZnO and stearic acid was blended together during 9 minutes 30 seconds. Temperature of first stage was 90 °C and rotor speed was 50 rpm. Temperature in second stage was 80 °C, rotor speed was 50 rpm. Sulphur and accelerators were blended in this stage during 6 minutes. Final blend was calenderd on calender. Vulcanisation curves were measured at 150 °C using Rheometer Monsanto R100. Vulcanisation parameters were calculated based on recorded vulcanisation curves. Optimum of vulcanisatiom (t_{90}), torque increment (ΔM) and scorch time (t_{02}) were evaluated. Plates with dimension 150x150x2mm were pressed at temperature 150 °C and time of vulcanisation was according to optimum of vulcanisation. Tensile test according to standard ISO 37 was done and tensile strength at break as well as elongation at break were evaluated. Fracture surfaces of vulcanisates were prepared under liquid nitrogen for SEM measurements. Tesla BS 300 with Tescan interface was used for scanning electron microscopy. Relative values of measured properties were calculated for more objective evaluation and comparison of obtained results. Relative values were calculated according to the next formula:

$$P_{rel} = \frac{P}{P_0} - 1$$

where P_{rel} are relative properties, P are measured properties at given concentration of additive and P_0 are properties at zero concentration of additive. All graphs are drawn for relative values of measured properties.

Results and discussion

Both tensides were dosed into blends in concentration 1, 2, 3 and 5 phr while filler content was kept at constant concentration 40 phr. Filler free compounds were prepared for both tensides as well.

Tensides causes decreasing of t_{90} approx. about 20–25 % calculated from its value for blend without tensides (Fig. 1).

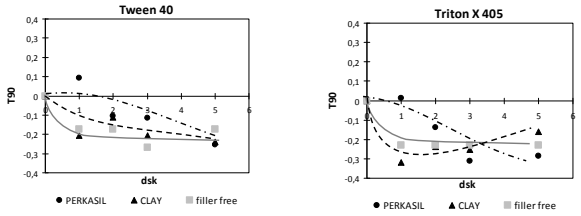

Fig. 1. **Dependency of t_{90} on concentration of tensides**

Decreasing is significant only after addition of 1 % of tensides. No other changes were observed above this concentration in case of filler free blends. Dependencies are slightly different if fillers are applied. In both cases t_{90} decrease, but at lower concentration of tensides decreasing of t_{90} is stronger in case of clay. At higher concentration of tensides decreasing of t_{90} is similar for both fillers.

Mechanical properties of prepared vulcanisates are representing by tensile strength at break (TSb) and elongation at break (Eb). Dependencies of these parameters on type and concentration of tenside are shown on Fig. 2 and 3. TSb slightly decreases (about 5–10 %) if only Triton X 405 is used at concentration up to 5 phr without fillers. In the opposite, if fillers are applied, TSb increases. Increasing of TSb in case of silica is more intensive (up to 15 %) in comparison to clay (up

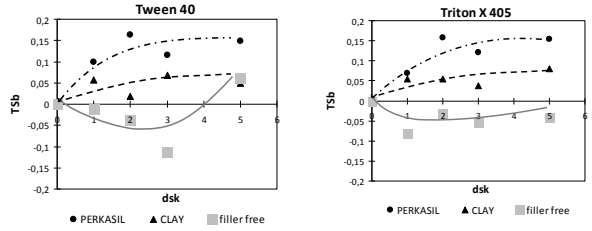

Fig. 2. **Dependency of TSb on concentration of tensides**

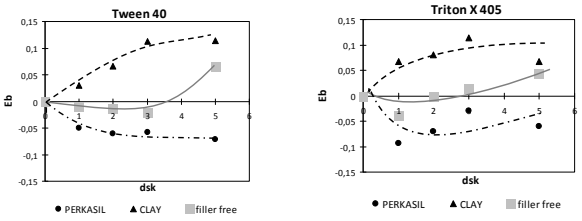

Fig. 3. **Dependency of Eb on concentration of tensides**

to 5 % only). Similar effect can be observed also in case of Tween 40 except dependency of TSb if only tenside was dosing. In such case TSb after very small decreasing significantly increase if concentration of Tween 40 is higher than 3 phr but this effect have no influence on dependency of TSb in case of filled blends.

Elongation at break (Eb) for both tested tensides exhibit practically no changes if tensides are used in unfilled blend up to 3 phr. Above this concentration of tensides Eb slightly increase (approx. up to 5 %). Effect of concentration of tensides on Eb is different for both fillers. Eb significantly increases if clay is used as filler and decreases in case of silica. Increasing respectively decreasing level is approximately the same for both types of tensides.

Based on results obtained from evaluation of mechanical properties, it can be said that applied tensides have positive effect on TSb. Application of tested tensides causes increasing of TSb for both fillers. Effect of tensides is higher in case of silica in comparison to clay. Eb increase or decrease with concentration of tenside in dependency on type of filler. Silica exhibit decreasing and clay exhibit increasing of Eb in dependency on tenside concentration.

Effect of tensides on morphology of vulcanisates was studied using the SEM method. SEM pictures of fracture surfaces are shown in Fig. 4. Differences in dispergation can be observed on SEM pictures in dependency on type of tenside as well as on type of filler. The pictures for blends without filler were done for background identification. Fracture surface shows relative good dispergation of Perkasil particles for both tested tensides. Agglomerates with dimension from approx. 100 nm up to approx. 1–2 μm can be observed on fracture surface for both types of tensides. This results can confirm that both types of tensides improve the dispergation ability of silica, but also it have to be said that the distributive part of mixing proces was not sufficient because described agglomerates create relatively large domains in rubber matrix. This effect is probably caused by insufficient homogenisation ability od Brabender laboratory kneader and the better distribution can be expected if industrial kneader will be used.

The different ability of tensides to satisfy dispergation of filler was observed if clay was used as filler. Better dispergation was observed if Tween 40 was applied. Clay was dispersed in this case into parts with thickness from approx. 400 nm to 700 nm and with longitude up to approx. 10 μm. Triton X 405 gives bigger domains of Clay with dimension in range of microns.

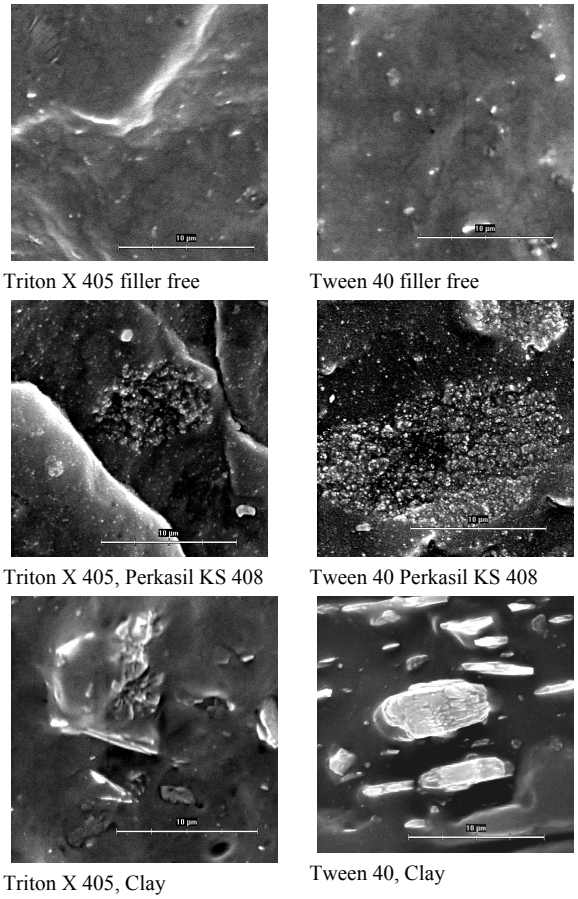

Fig. 4. **SEM pictures of fracture surfaces for samples with 5 phr of tenside**

Conclusion

Results presented in our work show that tested tensides have the significant influence on morphology of final vulcanisates as well as on mechanical properties and vulcanisation parameters of rubber blends. Effect of both tensides is similar if silica is used as filler, but in case of clay Tween shows better dispergation ability in comparison to Triton. Improvement in mechanical properties due to better dispergation of fillers was at level from 5 to 15 %. The higher improvement can be expected if industrial blender will be applied because of better homogenisation and dispergation ability in comparison to laboratory kneader.

REFERENCE

1. Blažej A., a kol.: *Tensidy*, ALFA, Bratislava 1977.

P-47
APPLICATION OF INTEGRATED TEXTILES IN THE AUTOMOTIVE INDUSTRY

KATARÍNA ŠČASNÍKOVÁ[a], JARMILA BALOGOVÁ[b], MARTIN JAMBRICH[c], JAROSLAV LUČIVJANSKÝ[b], and KATARÍNA ŠTEFÁNKOVÁ[c]

[a]Faculty of Chemical and Food Technology, STU Bratislava, [b] Chemosvit – Fibrochem, a.s. Svit, [c] Faculty of Industrial Technologies Púchov, Trenčín, University Alexander Dubček, Slovakia
scasnikova@tnuni.sk

Abstract

This paper deals with the preparation, structure and properties of integrated textiles from the mixture special of polypropylene (PP), elastane (El), polylactide (PLA), bamboo (Bs) and cotton (ba) fibres. The used fibres for the preparation of integrated textiles – fibrous materials, which are introducing raw base of synthetic, microbial and celullose polymers. These fibres are from conventional and from renewable sources of raw materials. Fibrous materials – textiles based on mentioned types fibres having good physiological, physical-mechanical and with wide scale utility properties.

Introduction

Current development fibers is directed towards the preparation new or innovative materials in all branches of industry. The main requirement is that these materials solely high user demand and were also environmentally friendly, ie readily biodegradable and recyclable[1,3]. The essence of the solutions which solely these trends are well integrated fibrous materials for clothing, furnishing and technical textiles on the basis of renewable fibers from biodegradable polymers and synthetic fibers[2].

Integrated fibrous materials prepared in the form of knits and woven fabrics usually contain structurally different types of chmical fibers from renewable, biodegradable, compatible and antimicrobial materials (bamboo, polylactide, cellulose) and synthetic fibers (polypropylene, elastane), or mixtures thereof in admixture with at least one auxiliary material[2].

Much attention has been devoted to preparing many-component fibers and fibrous materials for integrated textiles, mainly to increase physical activity. One approach to increase utility properties fibers is a modification of the transverse and longitudinal geometry fiber, but also change the surface properties of fiber by physical modification of suitable additives such as increasing. hydrophilicity of the material. Selection and application of appropriate modification process to improve the properties of PP fibers depends primarily on the requirements that are imposed on their use[4,5]. Modifications of polymer additives, nanoparticles, dendrimers, branched polymer, and polymers for the preparation of polymer blends counts among the most studied modifications to improve the properties of fibers in recent years[6]. Modifications of the PP fibers are primarily directed at the increasing hydrophilicity

PP. Among the modifications that have been studied at improving hydrophilicity PP fibers we can include: esc. grafting of a PP membrane surface with poly(*N*-vinyl-2-pyrrolidone) and PP hollow fibers membrane surface with *N*,*N*-dimetylaminoethyl metacrylate leads to the higher hydrophilicity of a PP surface[7].

Theme of our work is focused on preparation of integrated fabric of PP fibers 56/33x2 with a hydrophilic additive, PP 56/33x2 and PP 56/43x2 from hollow fibers that are combined together with El, PLA and Bs fibers. Creating space for expansion of knowledge in this area particularly in relation fiber type, its structure and utility properties of the product. This article is focused on the preparation and evaluation of physico-chemical, physiological and utility properties of integrated textiles – knitted fabrics with different composition of the fibers used.

Theoretical part

Preparation commercial types polypropylene fibers is based on the use of isotactic polymer chirality. The new generation of m-iPP polymers can be prepared fibers with lower weight and higher measuring physical – mechanical properties. Metallocene PP types of polymers are the real basis for qualitative progress in the assortment of PP fibers. Macromolecular chain iPP is characterized by recurring monomer unit. In fact, the influence of bulky isotactic chain – CH3 groups interested in a regular conformation (gauche), which is reflected in good crystallizable polymer, in its strength and stiffness. The only intermolecular forces are Van der Waals[8,9].

Polyurethane fibers are made of glycol and diisocyanate special spinning method. These fibers can also be manufactured from hexamethylene diisocyanate, but have less meaning[10].

Cotton fibers are the natural cellulose fibers, which is a constituent of cellulose fibers of plant origin. Macromolecules in the form of cellulose fiber axis elementary fibrils, which are linked to senior staff, protofibrils and microfibre, and these aggregate into fibrils. Layers of fibrils form lamellae, which form the cell walls of fiber[11].

Bamboo fiber belongs to the cellulose fibers of regenerated cellulose, which is made from bamboo pulp prepared from bamboo plants. Bamboo pulp is extracted from the bamboo and the process of hydrolysis alkalization and multi-phase bleaching. Process for the preparation of bamboo fibers is similar to the preparation process of viscose fibers. Bamboo is a typical natural composite material, which is the length reinforced by strong fibers. Fibers are densely distributed in the outer surface area and sparsely in the inner part. Bamboo fiber is biodegradable in soil microorganisms and sunlight. Folding process does not cause any pollution environment. This thread is considered natural and EKO – acceptable type of textile material[12].

Polylactide fibers are assigned to groups of microbial chemical fiber types. The favorable development of microbial polymers is due to the limited resources of fossil raw materials. Polylactides are produced from lactic acid. Fibers from polylactic acid are biodegradable and biokompaktibilný type, which represents the character of its properties of natural and synthetic fibers. PLA fibers are a new kind of biodegradable and biocompatible fiber type available source material. Properties of PLA fibers and renewable resource materials predispose them to be future fiber[4,12].

Experimental part

Our experimental work focused on the preparation of integrated fabric – knit of hydrophobic and hydrophilic fibers and evaluation of their structure, physico – mechanical, physiological andutility properties. The following types of fibres were selected for the preparation of integrated fibrous materials:

- polypropylene fibres with changed reluctant geometry (hollow) as hydrophobic unbiodegradable type,
- polypropylene fibres without changing reluctant geometry (full) as hydrophobic unbiodegradable type,
- polypropylene fibres with using of hydrophilic additive, unbiodegradable type,
- synthetic, hydrophobic, unbiodegradable elastane fibres,
- cellulose, hydrophilic, biodegradable type from the renewable resources of raw materials (bamboo) with antibacterial efficacy,
- cellulose, hydrophilic, biodegradable type – natural fibre – cotton,
- polyactid (PLA) – microbial, hydrophobic and biodegradable type with the changed reluctant geometry (hollow) from renewable resources of raw materials.

For fibers and yarns were evaluated:

- Physico-mechanical properties (determination of linear weights (fineness) fibers, fiber strength and elongation, the number of seats previre (PPM), the number of fibrils and the determination of fibers contraction (KK – value)).
- Evaluation parameters and structure of the fibers – yarns (transverse and longitudinal evaluation of the geometry of fibers, microscopic method, determine the speed of sound propagation in fibers, melting, crystallization and crystalline fibers share)

For fabric:

- Macromorfological structure and geometric properties.
- Physico – mechanical properties (determination of strength, ductility printed textiles, fabric areal weight).
- Physiological properties (determination of sorption, wetting contact angle, thermal – insulation thermocontact method for device ALAMBETA).

REFERENCES

1. Dirk De Saedeleir, Alain Goossens, The U.S. Manufactured Fiber and Textile Industry : Innovative applications of biopolymers, *48th International Man-Made Fibres Congress, Dornbirn, 16-18 September 2009*, Austria.
2. Jambrich M., Macho V., Olšovský M., Balogová J., Vnenčáková J., Sroková I., Benčíková E.: Vláknité materiály na ošatenie a/alebo bytové textílie. Úžitkový vzor - 5182, udelil Úrad priemyselného vlastníctva SR, Banská Bystrica 2.4. 2009.
Herben, P.-Lonardo, A.: Chemical Fibers International *59*, 125 (2009).

4. Jambrich M.: In.: Prednáška na medzinárodnej konferencii *59. Zjazd chemických spoločností, 2.-6. 9. 2007, Vysoké Tatry*.
5. Bolhová E., Ujhelyiová A., Marcinčin A.: Vlákna a textil *11*, 147 (2004).
6. Ujhelyiová A., Bolhová E., Vaľková K., Marcinčin A.: Vlákna a textil *12*, 48 (2005).
7. Krištifič M., Náčiniaková Z., Legéň J., Ryba J.: Vlákna a textil *12*, 104 (2005).
8. Michlík P., Brejka O., Ujhelyiová A., Vnenčáková J. : *7 th International conference Advantes in plastics technology, november 13.-15. 2007 Katovice*, PL, Conference Papers No. 5.
9. Jambrich M., Pikler A., Diačik I.: *Fyzika vlákien*. Alfa, Bratislava 1987.
10. Strecký J.: *Odevné tovaroznalectvo*. Alfa, Bratislava 1996.
11. Jambrich M.: *Chemické technológie celulózových vlákien*. študijný materiál FPT TnU AD, Púchov 2005
12. Ščasníkova K., Balogová J., Benčíková E., Jambrich M., Lučivjanský J., Vnenčáková J.: In: *Prednáška na konferencii TEXCO, Ružomberok, 2010.*

P-48
MODELLING OF TRANSIENT THERMAL STRESS IN POLYMER LAYERED WALLS

OLDŘICH ŠUBA and LIBUŠE SÝKOROVÁ

Tomas Bata University in Zlín, Faculty of Technology, Department of Production Engineering, T. G. Masaryka 275, 762 72 Zlín, Czech Republik
suba@ft.utb.cz

Abstract

Results of FEM modelling of transient thermal stress analysis in layered walls are given in the article. It is shown that thermal stress alone is not solely caused by differences in coefficients of thermal expansion of individual layers. The emergence of transient thermal stress is subject to both the layered structure of the wall and given boundary conditions, as well as the existence of a temperature gradient in the direction normal to the surface of the wall.

Transient thermal stress due to the temperature gradient

Now consider generally layered wall, i.e. a wall with generally varying properties along its thickness, exposed to thermal effects with random thermal profile ΔT(y) corresponding to a certain moment of transient heat transfer through the wall – Fig. 1.

Not only the elastic constants but also the coefficient of linear thermal expansion generally changes both discontinuously at the layer interface and continuously within each layer due to possible dependences of constants on temperature.

This task can be seen as a wall imaginary composed of an infinite number of layers of elementary thickness dy; each layer has its own values of elastic constants and thermal expansion coefficient. The value ΔT(y) expresses the difference between the real temperature at place y and the reference temperature of the wall, i.e. temperature at which zero stress of the wall is assumed.

Let the wall be gripped again in a way which prevents its warpage but allows membrane deformations, i.e. deformations in the directions of the reference surface are possible. The resulting membrane forces in the wall sections then equal to zero, so that

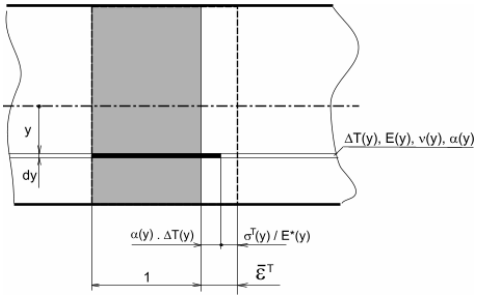

Fig. 1. **Generally layered wall**

$$\int_{(s)} \sigma^T(y)dy = 0. \qquad (1)$$

Unless there is warpage of the wall, the sum of thermal expansion and elastic deformation, which is in each imaginary layer dy constant, equals to ε^T. Considering that this is an equibiaxial stress, so that

$$\varepsilon^T = \frac{\sigma^T(y)}{E^*(y)} + \alpha(y)\,\Delta T(y) \qquad (2)$$

When using (*1*), the final uniaxial wall deformation can be expressed by the following relation

$$\varepsilon^T = \frac{\int_{(s)} E^*(y)\;\alpha(y)\;\Delta T(y)\;dy}{\int_{(s)} E^*(y)\;dy}. \qquad (3)$$

Thus equibiaxial stress in the area of ordinate y will be

$$\sigma^T(y) = E^*(y)\left[\varepsilon^T - \alpha(y)\,\Delta T(y)\right]. \qquad (4)$$

The expression (*4*) does not apply in areas of free edges of the double-layer wall, where the boundary stress-tops form, especially those of shear stress components at the layers interface. Tension given by the relation (*4*) is transient (time dependent) in cases of time-variable temperature field. After disappearance of the temperature gradient, stress also disappears.

FEM modelling of transient thermal stress

In recent years the development of consumer electronics has brought the necessity of electrical waste recycling due to falling prices of electronics, and thus its massive consumption, and also a decrease of its lifetime[1].

Although the formation of thermal stress can be generally regarded as a negative phenomenon in terms of utility properties of plastic and composite products, in practice there are cases in which thermal stress is formed deliberately. This is the case of PCB boards recycling; the aim is to break the interface and thus separate individual layers with the use of thermal stress. The role of thermal stress modelling in this area lies in predicting the possibility of separation in dependence on the type of thermal stress and material parameters of the layers.

FEM modelling of transient thermal stress states runs in two stages. Firstly, the appropriate thermal boundary conditions of the board are set and the instantaneous profiles of the temperature field are calculated in the chosen time steps. Time-variable thermal boundary conditions are entered via so-called time-curves. Secondly, the appropriate mechanical boundary conditions are set and the instantaneous values of transient thermal stress components are calculated for the chosen time frames of the course of the temperature in the board. Whereas the mechanical and thermal parameters of the material layer 1 (Cu) can be considered to be temperature-independent in calculation, the layer of polymer composite 2 shows strong temperature dependences of physical properties on temperature, especially that of the modulus of elasticity.

Therefore these dependencies were generalized by appropriate temperature curves in calculation. Thus the composite layer becomes quasi-layered during pull of the temperature gradient on its thickness; it means that the individual equidistant planes, respectively imaginary layers of elementary thickness, show different values of thermoelastic properties at the given instant of time.

Time curve of the chosen model of thermal process is shown in Fig. 2. The PCB board is heated to the temperature of 200 °C. By the immersion into brine of the temperature of −10 °C the surface is rapidly cooled to this temperature in the time interval of 1–2 seconds. Then the board remains in the bath until the disappearance of the thermal gradient, i.e. until the temperature fully reaches the value of −10 °C.

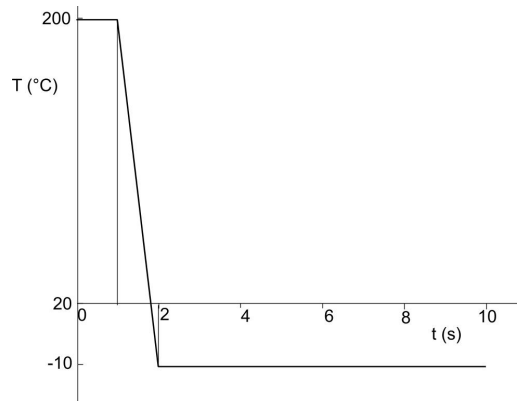

Fig. 2. **Time curve of the temperature on the PCB board surface for modelling of rapid, i.e. non-homogenous, cooling**

Conclusions

After the analysis of the time-variable temperature field the results of chosen time moments are used for the analysis of thermal stress. Values of biaxial normal stress in individual layers according to (*4*) do not themselves affect the separation of the layers. It depends on the existence of peaks of shear components on the edges of layers at their interface directly proportional to normal thermal stress. Type of course of shear stress at the layers interface is shown in Fig. 3. In a certain instant of time stress reaches its maximal value at the edge of the layer 1(Cu). Stress extends in direction from the edge to the distant L_0, which is the same order of magnitude with the thickness of polymer layer (*2*). If the maximal value of shear stress at the interface reaches the limit value – shear strength of interface, the separation begins. The resulting course of time dependence τ_{MAX} from the beginning of the board cooling is shown in Fig. 4. As can be seen, in process of rapid, i.e. non-homogenous, cooling there is the instant of time tmax in which the peak of shear stress reaches its maximal value.

Since the beginning of cooling the values are increasing to this value and after reaching it they decrease to the zero value when the temperatures in the board evened out. The

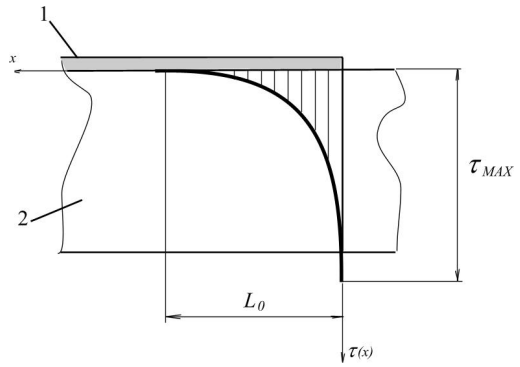

Fig. 3. **Dependence of shear stress at distance x from the edge of the layer 1 (Cu)**

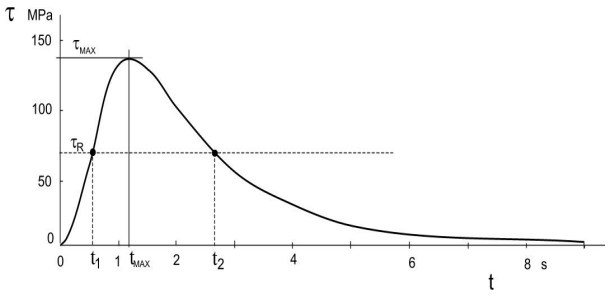

Fig. 4. **Time course of boundary maximal shear stress at the layers interface**

separation process can be characterized as follows: separation begins after rising of τ_{MAX} to the value of shear strength at the interface τ_R – instant of time t_1. The edge of Cu layer starts to peel, whereas the edge of layers joints moves in direction of separation and has a value τ_{MAX} variable in time. The process of peeling of Cu layer stops in time corresponding to decrease of τ_{MAX} to the value τ_R in time t_2.

This work was supported by the Ministry of Education and Youth of the Czech Republic under grant MSM 7088352102.

REFERENCE

1. Janáčová D., Kolomazník K., Vašek V., Mokrejš P.: *The 5th WSEAS Conference on Heat Transfer, Thermal Engineering and Environment HTE'07, Athens, 2007,* 268–271. WSEAS World Science and Engineering Academy and Science 2007.

P-49
EVALUATION OF TENSILE TESTS OF SHORT-FIBRE REINFORCED POLYMERS BY MICROSTRUCTURE FEM MODELLING

OLDŘICH ŠUBA and LIBUŠE SÝKOROVÁ

Tomas Bata University in Zlín, Faculty of Technology, Department of Production Engineering, T. G. Masaryka 275, 762 72 Zlín, Czech Republic
suba@ft.utb.cz

Abstract

The paper gives modelling results of elastic constants dependences on fibre volume ratio and its aspect ratio. 3D totally oriented short-fibre structure is expected. The results are compared with evaluation of stiffness experimental data of injection moulded polymer specimens reinforced with short fibres.

Introduction

Unlike isotropic materials, application of experimental data, obtained in standard tensile tests for the needs of the stress and deformation analysis and practical dimensioning of products made of short-fibre composites is a more complex problem. The result of a standard tensile test is only a value of elastic stiffness in the direction of the sample axis. The injection moulded sample represents, owing to its geometry, a highly oriented structure, which differs as a rule from the structure of products with more complex geometry. It is well known[1] that at higher velocities of the melt stream a „sandwich-type" structure arises. It consists of two surface layers and a central layer – „core". The fibres within both surface layers are oriented almost exclusively in the melt flow direction, while the fibres in the central layer are oriented transversally. Elastic behaviour of the short-fibre composite depends, next to the aspect ratio, on the basic parameter of the short-fibre structure – fibres orientation. In a certain dependence on the degree of orientation, both effective elastic constants and other physical and macroscopic properties are changed. Fibres orientation within the sample is influenced in its different parts by the location of the type of the gate and the shape of the body, or the mould cavity.It is practically impossible to ascertain the set of effective elastic constants of a monotropic- fully oriented short-fibre structure only on the use of experimental measurements. Therefore, a theoretical prediction of elastic constants of the short-fibre composite is very important here. We are presenting experience and results obtained at our department in micromechanics of 3D totally oriented short-fibre structures. These results are then used for the construction of macroscopic module of injection moulded sample stressed by a uniaxial strain. This model is then used to evaluate tensile tests of samples of polymers filled with short fibres.

Modelling of Elastic Constants of Particle Composite with Totally Oriented Fibres

Model structure of the composite with fully oriented short fibres represents a so called representative volume. Individual states of loading of the model volume were processed by means of the FEM software system. Results in a form of dependences of elastic constants of the oriented short fibre structure upon volume concentration of fibres are provided in the following diagrams.

Fig. 1 shows dependence of a longitudinal elasticity modulus in the practical area within the fibres volume ratio 50–100. The result provided in Fig. 2 for the transversal modulus confirms the well- known experience that E_T practically does not depend on fibres volume ratio.

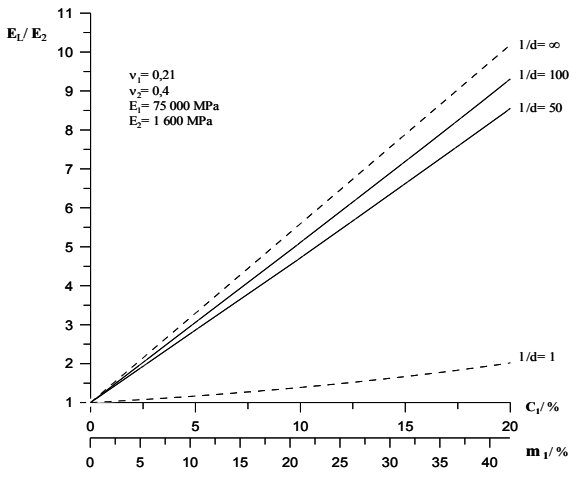

Fig. 1. **Young's modulus in fibres E_L direction in dependence on volume ratio c_1 and aspect ratio *l/d***

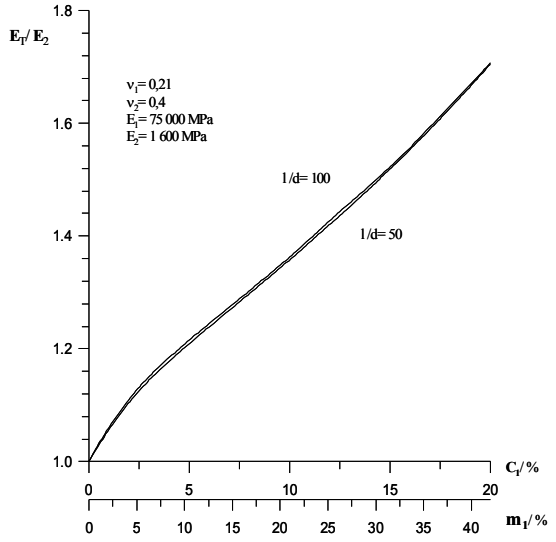

Fig. 2. **Young's modulus in direction transversal to fibres orientation E_L in dependence on volume ratio c_1 and aspect ratio *l/d***

Effective Elastic Constants of Injection Moulded Elements

The values of effective Young's modulus of injection moulded standard testing elements, found out by means of an experiment, were compared with two model imaginations, differing in the assumption of idealization of fibres orientation distribution after the cross-section. In the first case statistically isotropic structure without priority orientation after the cross section area was modelled. This effect was reached by simulation of a higher number of *n* layers, with totally oriented fibres, with a mutual angular displacement π/n. In the second case the relation between the surface layers area (with 0 orientation) and the core (with $\pi/2$ orientation) was supposed to be 2:1.

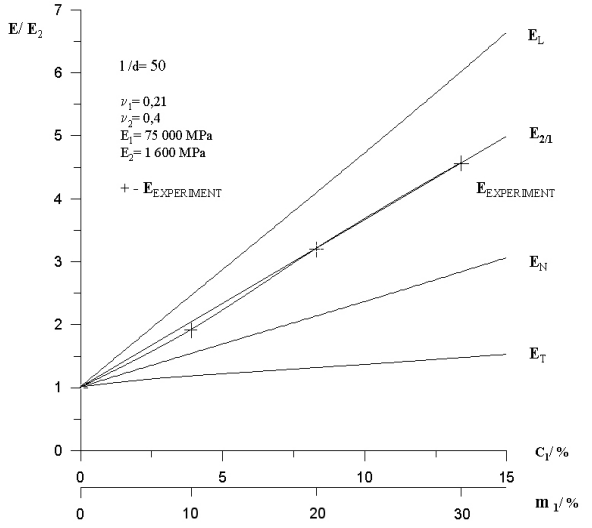

Fig. 3. **Comparison of dependence of effective Young's moduli of model structures with experimental results**

The results are shown in Fig. 3. Experimental data of samples with a different degree of fibres concentration ($E_{EXPERIMENT}$) are compared with theoretical values of the modulus of the totally oriented structure for the longitudinal (E_L) and transversal (E_T) direction, for non-oriented structure (E_N) and layer structure ($E_{2/1}$).

As evident, tensile stiffness found out in experimental measurements approaches the model values of the layer structure the most.

Conclusions

Results of micromechanical and macromechanical modelling of the elastic behaviour of short-fibre composites reached in tests enable to predict elastic behaviour of walls of injection moulded products made on the basis of these materials. In this case the theoretical predictions of elastic constants of short-fibre composite materials were used for determination of an effective Young's modulus in tension at real injection moulded testing products.

This work was supported by the Ministry of Education and Youth of the Czech Republic under grant MSM 7088352102.

REFERENCE

1. Bright P. F.: J. Mat. Sci. *13*, 2497 (1978).

P-50
POLYMER BLENDS OF POLYETHYLENE TEREPHTHALATE AND POLYLACTIC ACID

KATARÍNA TOMANOVÁ, MIROSLAVA PAVLAČKOVÁ, PETER BUGAJ, FRANTIŠEK BENOVIČ, and PAVOL ALEXY

Ústav polymérnych materiálov, Fakulta chemickej a potravinárskej technológie, Slovenská technická univerzita, Radlinského 9, 812 37 Bratislava, Slovak Republic
katarina_tomanova@stuba.sk

Introduction

Polyethylene terephthalate (PET) is a commercially important engineering thermoplastic with good thermal and mechanical properties, low permeability, and chemical resistance. It is used in bottle containers, food packaging, textile fibers, engineering plastics in automobiles, electronics and blood vessel tissue engineering[1]. But it is non-biodegradable and its amount in landfill is still growing, of course, with other synthetic and petroleum-based plastics. A proposed alternative is to develop blends of PET with naturally renewable units like polylactic acid (PLA)[2]. Unlike petroleum-based plastics, PLA is biodegradable green plastic derived from renewable resource, such as starch. PLA is biodegradable polyester with high strength and high modulus. It has

various applications in drug delivery, tissue engineering, food packing and bottle containers. PLA bottles have many advantages such as biodegradability, plentiful material source, and lower processing cost during blow-molding due to its lower glass transition temperature[1]. However, PLA has not good barrier properties and has relatively high cost. Therefore its usage in bottles is still limited. In the present work, mechanical and processing properties of PET/PLA blends were studied. PLA content in the blends gradually changed from 0 % to 100 %wt. Triacetine was used as plasticizer.

Experimental

Materials

- Polylactic acid – PLA 4042D from NatureWorks, LLC, USA
- Polyethylene terephthalate (PET)
- Triacetine as PLA plasticizer

PET/PLA blends preparation

Both polymers PET and PLA were dried 120 minutes at the temperature of 80 °C in hot-air chamber. PET/PLA blends were prepared using twin-screw extruder. PLA content in the blends gradually changed from 0 % to 100 % wt. Thermal profile of extrusion in the direction from feeder to die was set on 250 – 260 – 260 – 260 – 260 – 260 – 255 – 250 – 245 – 240 °C and extrusion speed was 80 rpm. Extruded material was cooled down with cold water and then it was granulated into small pellets.

PET/PLA monofils preparation

Granulated material was dried again 120 minutes at the temperature of 80 °C in hot-air chamber. Dried granules were used to PET/PLA monofils preparation on single-screw extruder, where one – hole die was used. Extrusion speed was 10 rpm.

Measurement of mechanical properties of prepared monofils

Yield strength (σy), tensile strength (σb) and the elongation at break (εb) were measured with Zwick machine at cross-head speed 1 mm/min in the deformation range of 0–3 % and after this value of elongation the speed increased up to 50 mm/min. These properties were determined based on recorded tensile curves.

Results and discussion

At first, monofils from pure PET were prepared at thermal profile 240 – 250 – 270 – 260 °C in the direction from feeder to die. Mechanical properties of prepared PET monofils were measured and Table I shows obtained results.

Also blends PET/PLA with various content of PLA were prepared at the same conditions. Fig. 1–3 show dependencies of tensile strength at yield, tensile strength at break and elongation at break on PLA content in PET/PLA blends.

Table I
Mechanical properties of pure PET monofils

PET [%]	σy [MPa]	σb [MPa]	εb [%]
100	52.61	81.59	919.54

Fig. 1 and 2 show that tensile strength at yield (σy), which is very important property of prepared blends because of their planned application, was minimally decreased at the range of PLA content in blends from 5 to wt.20 % At higher content of PLA in blends, except pure PLA, there was recorded no yield point. Tensile strength at break (σb) of PET/PLA blends was decreased with an addition of PLA nearly to the half.

Fig. 3 shows dependency of elongation at break (εb) on PLA content in PET/PLA blends. Effect of PLA content in blends has already been achieved in its content of 5%. The

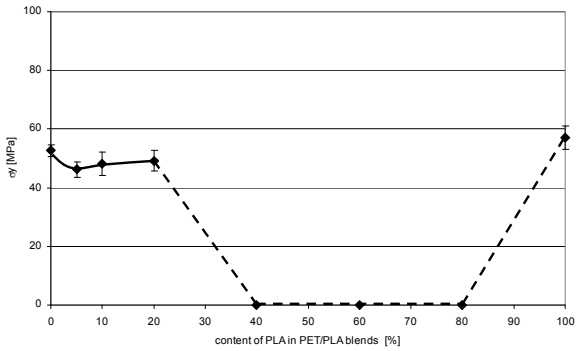

Fig. 1. **Dependence of tensile** strength at yield on PLA content in PET/PLA blends. Zero values of σy mean, that no yield points were observed on tensile curves

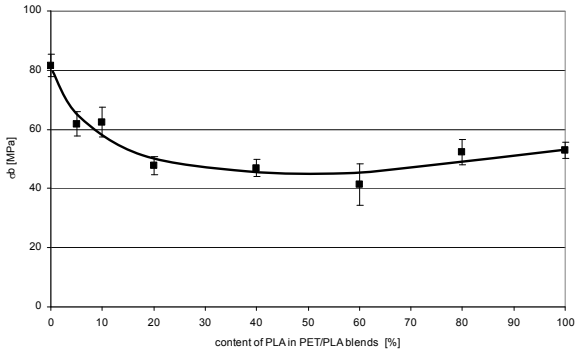

Fig. 2. **Dependence of tensile** strength at break on PLA content in PET/PLA blends

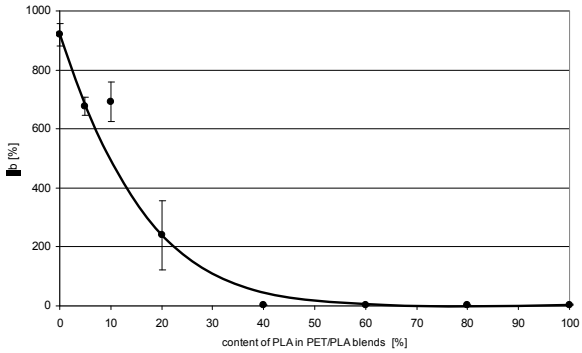

Fig. 3. **Dependence of elongation at** break on PLA content in PET/ PLA blends

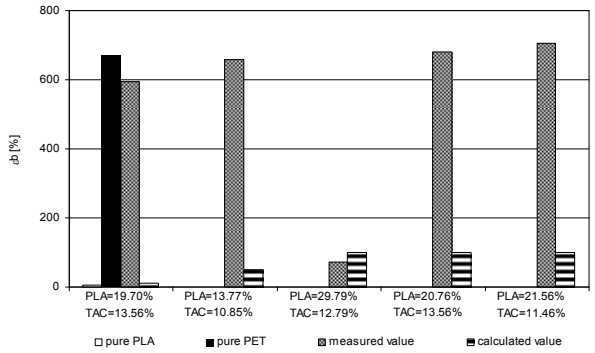

Fig. 6. **Elongation at break** of optimalized PET/PLA blends with various composition

value of εb decreased from 920 % to 3 %. This trend corresponded to elongation of pure PLA.

After research of basic properties of PET/PLA blends, Design of experiment (DoE) method was used in the next part of this work. PLA content in blends varied from 5 to 30 wt.%, triacetine (TAC) was used as PLA plasticizer and its content varied from 6 to 20 wt.%. Thereafter, optimalization of DoE followed. Fig. 4–6 show results of mechanical properties measurements.

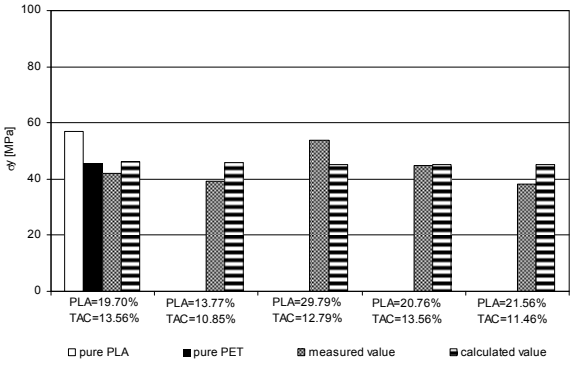

Fig. 4. **Tensile strength at** yield of optimalized PET/PLA blends with various composition

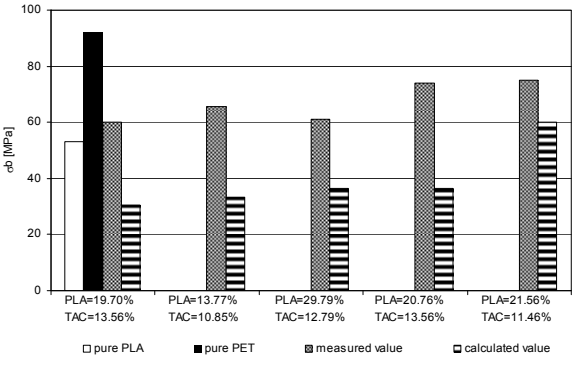

Fig. 5. **Tensile strength at break of optimalized PET/PLA** blends with various composition

Obtained results presented on Fig. 4–6 show coincidence between calculated values and experimental obtained results in case of tensile strength at yield. Worse coincidence can be observed in case of tensile strength at break and the worst one is in case of elongation at break. The differencies between experimental values and values predicted based on mathematical model have origin in relative high regression inadequacy as well as high value of experimental error in case of elongation at break. Nevertheless, experimentally obtained values are much better then calculated values in the most of blends. The positive effect of TAC can be observed mainly in case of elongation at break. Blends containing up to 20 wt.% of PLA reached εb values higher than 600 % in comparison with the blends with same quantity of PLA, but without TAC which exhibit around 200 % of εb. Also tensile strength at break was improved by application of TAC in PET/PLA blends. While TAC free blends of PET/PLA exhibit σb around 50 MPa when PLA content was 20 wt.%, the same blends with TAC reached σb higher than 70 MPa.

Conclusion

Based on reached results it can be concluded that addition of PLA to PET causes significant drop of elongation at break as well as tensile strength at break. This deterioration of mechanical properties can be supressed by addition of TAC as plasticizer. Optimised blends based on DoE results exhibit similar mechanical properties like pure PET up to 20 wt.% of PLA. In the next work processing properties as well as barier properties of PET/PLA/TAC blends will be studied.

This project is supported by Norwegian Financial Mechanism, Financial Mechanism of EEA and State budget of Slovakia – project No. SK 0094.

REFERENCES

1. Huipeng C. H., Pyda M., Cebe P.: Thermochim. Acta 492 (2009).
2. Gipija B. G., Sailaja R. R. N., Madras G.: Polym. Degrad. Stab. 90 (2005).

P-51
THE PHYSICAL MODIFICATION OF PP FIBRES FOR THE TECHNICAL APPLICATIONS

ANNA UJHELYIOVÁ[a], JOZEF RYBA[a], PETER MICHLÍK[b], ĽUBA HORBANOVÁ[a], PETER KRAJŇÁK[b], and JÁN LOKAJ[a]

[a] Faculty of Chemical and Food Technology, Slovak University of Technology in Bratislava, Radlinského 9, 812 37 Bratislava, [b] Research Institute for Man-Made Fibres, a. s., Štúrova 2, 059 21 Svit, Slovakia
anna.ujhelyiova@stuba.sk

Introduction

Concrete is the most widely used construction material in the world. Its need and use will increase in the future. Concrete is use in different areas from civil to engineering construction. Different methods of material preparation of concrete composite with improved special properties are developed and used nowadays. Reinforcing concrete with fibres is one of the methods to improve its specific properties[1]. Different types of fibres are used as the reinforcing components – steel (metal), glass, polymer (synthetic and natural – polyethylene (PE), polypropylene (PP), polyvinyl alcohol (PVA), polyamide (PA) and polyester (PES)) and their mixtures. Application of these fibres depends on improving of required specific properties of concrete[2–4].

Dispersed fiber reinforcements in the matrix of concrete have significant influence upon general properties of concrete. The properties that the dispersed fibre reinforcements influence negatively are workability of concrete, rheological properties, extending the mixing and blending period. By using fibers in concrete, it becomes more resistant to sudden temperature changes and the impermeability of concrete is increased. Good dissipation of reinforcements leads to increase the fire resistance and life cycle of construction, improvement of frost resistance, chemical resistance, the speed of carbonatation and waterproofing[3,5,8,9].

The addition of PP fibers into concrete is very interesting from construction point of view which includes the effect of reinforcement and concrete microarmouring, thereby eliminating the creation of micro cracks within hardening building materials[3]. Polymer fills pores and micro-cracks created in the concrete and reduce porosity, stop the spread of micro-cracks and thus improve the internal tensile strength and adhesion ability[5,6,10]. The hardening and setting of concrete, which is related to hydration is accompanying by significant evaporation of water[7]. Fibers in the matrix of concrete provide higher porosity and therefore better evaporation of water and also decrease stress during hardening. This effect also provides higher destruction resistance by burning (eg in tunnels). Fire melts PP fibers which melting temperature is about 165 °C and by this dense net is created this leads to leak of the water vapor.

The disadvantages of using pure PP fibers for reinforce concrete is that no molecular bond occur between the cement matrix and fibre reinforcement. Low affinity of PP fibers to silicate matrix is result of non-polar, physically (low specific surface area, smooth surface), and chemically inactive polyolefinic character of the material. The ability to absorb deformation energy by tensile and flexural straining of silica composites is reduced because of statistic possibilities of releasing (pulling) fibers from composites instead of deformation fibers[8].

This article deals with influence of the modifdication of PP fibres by inorganic fillers or by change of their cross-section profile on their macromorphological structure and mechanical properties as well as on the end-used properties of concrete composite prepared with PP fibres.

Experimental

Materials used

For the preparation of non-modified (PP) and modified PP (mPP) fibres was used polypropylene Tatren HT 1810 with MFI = 20.9 g/10 min from Slovnaft a.s., Slovakia and micronized inorganic filler (8.4 wt.%). From these materials were prepared undrawn fibres with circle shape cross-section without (sample 001) and with (sample 002) inorganic fillers and with five pointed star shape cross-section without inorganic fillers (sample 003) on the laboratory spinnig machine. Next, the undrawn PP fibres have been drawn to the drawing ratio $\lambda = 3$ and to cut on the length of 12 mm.

Method used

Evaluation of surfaces was provided using microanalyzer JXA-840A with EDS and WDS system, produced by JEOL, Japan. Measurement conditions were following: accelerating voltage 15 kV, sample current $1 \cdot 10^{-10}$ A.

Mechanical properties were measured on INSTRON 1122 and evaluated according to STN EN ISO 1973, 5079, 2062 – standard methods for evaluation of mechanical parameters.

Evaluation of end-used properties of concrete composites in accordance with STN EN 12350-6:2009 – volume mass, rheology of fresh concrete: Reometer Brio and STN EN 14651+A1: 2008 Measurements of strength in tension in flexure (flexural strength).

Results

The evaluation of macromorphological structure of the surfaces of prepared nonmodified and modified PP fibres with circle shape cross-section without and with inorganic filler and with five pointed star shape cross-section without inorganic filler was provided using microanalyzer. These obtained pictures are shown at Fig. 1. Surface of nonmodified PP fibers with circle shape cross-section without inorganic filler is smooth (Fig. 1a). Surface of modofied PP with circle shape cross-section with inorganic filler can be seen roughage caused by participation of inorganic filler particles (Fig. 1b). On the Fig. 1c it is shown of changed profile of the modified PP fibre with five pointed star shape cross-section without inorganic filler.

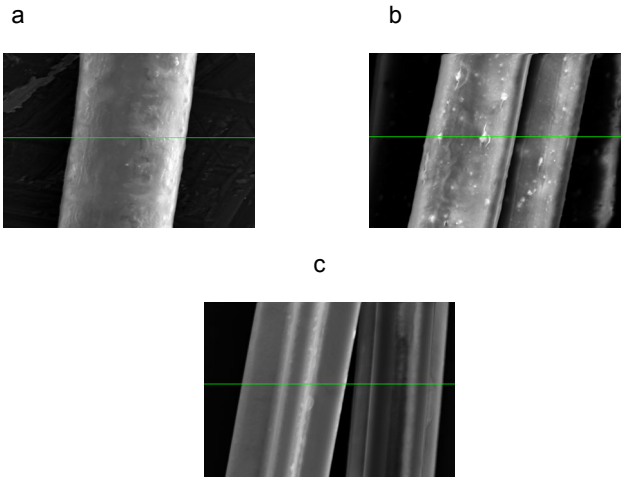

Fig. 1. **Surfaces PP fibres with circle shape cross-section without (a) and with (b) inorganic filler and with five pointed star shape cross-section without inorganic filler (c) with draw ratio λ = 3**

Mechanical properties of non-modified and modified PP fibres are shown in Table I. Although the macromorphological structure of prepared modified PP fibres had been changed the mechanical properties – tenacity (σ) at the break and Young's modulus (E) are practically unchanged. The low decrease of tenacity can be provided by minor decrease of fineness. The Young's modulus (E) of modified PP fibres is higher than the nonmodified PP fibre. The higher Young's modulus (E) of modified PP fibres had been caused by inorganic fillers which effects as the reinforcement additive. Over the way the inorganic filler had been induced the decrease of elongation of the modified PP fibre because the particles of filler decrease the sufficiency of drawing of polymer matrix. This confirms the theoretical knowledge, that the addition of micronized filler to the oriented polymer matrix decreases their mechanical properties.

The prepared nonmodified and modified PP fibres had been used to preparation of concrete composites. There had been evaluated the some end-used properties of these composite with PP fibres. The obtained results can be shown on the Fig. 2 and 3.

The nonmodified PP fibre used in the concrete composite had increased the rheological properties of the fresh concrete (Fig. 2). It makes worse its processability. The rheological properties of fresh concretes with the modified (by inorganic filler or change of profile) PP fibres are practically on the level of rheological properties of fresh concrete without fibres.

Table I
Fineness (T_d), tenacity (σ) and elongation (ε) at the break, Young's modulus (E) of the non-modified and modified PP fibres

Sample	T_d [dtex]	σ [cN/dtex]	ε [%]	E [cN/dtex]
001	6,2	3,6	204	22,3
002	6,1	3,3	152	23,1
003	6,1	3,5	174	27,0

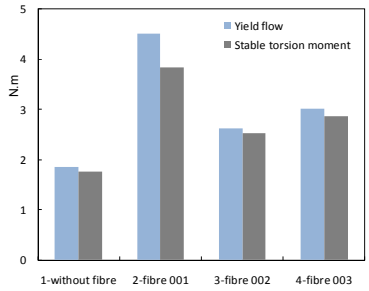

Fig. 2. **The effect of non-modified and modified PP fibres on the rheological properties of fresh concrete**

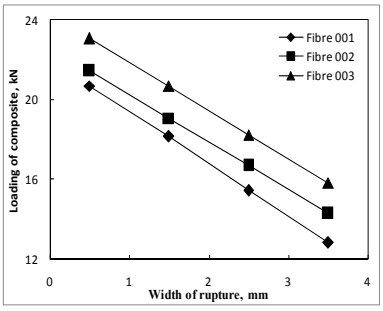

Fig. 3. **The effect of non-modified and modified PP fibres on the flexural strength of concrete composites**

The modification of PP fibres by inorganic filler or by change of their cross-section profile improves the flexural strength of concrete composites prepared using those fibres in comparison with the flexural strength of concrete composite with nonmodified PP fibre (Fig. 3).

Conclusion

The experimentally obtained results can be concluded as follows:

- The particles of inorganic filler are situated on the PP fibre surface. These particles can improve the adhesion of PP fibres to concrete matrix.
- The mechanical properties of modified PP fibres are practically same as the mechanical properties of non-modified PP fibres.
- The concrete composites with nonmodified or modified PP fibres have improved end-used properties in comparison with the concrete composite without fibres.

This work was supported by the VMSP-P-0007-09 and VEGA 1/0444/09.

REFERENCES
1. Sideris K. K, Manita P., Chaniotakis E.: Construction and Building Materials *23*, 1232 (2009).
2. Hsiea M., Tua Ch., Song P. S.: Mater. Sci. Eng., A *494*, 153 (2008).
3. Sun Z., Xu Q.: Mater. Sci. Eng., A *527*, 198 (2009).
4. Wang W., Wu S., Dai H.: Mater. Sci. Eng. A *434*, 347 (2006).
5. Wang R., Wang P. M., Li X. G.: Cem. Concr. Res. *35*, 900 (2005).
6. Schorn H., Butler M., Hempel S.: In: *Proceedings of the 11th Congress on Polymers in Concrete*, pp. 8–11. BAM editions, Berlin 2004.
7. Liu X., Ye G., De Schutter G., Yuan Y., Taerwe L.: Cem. Concr. Res. *38*, 487 (2008).
8. Liao K. Y., Chang P. K., Peng Y. N., Yang C. C.: Cem. Concr. Res. *34*, 977 (2004).
9. Toutanji H., Xua B., Gilbert J., Lavin T.: Construction and Building Mater. *24,* 1 (2010).
10. Han C.-G., Hwang Y.-S., Yang S.-H., Gowripalan N.: Cem. Concr. Res. *35*, 1747 (2005).

P-52
AN IMPROVEMENT OF HYDROPHOBICITY OF PES AND PES/COTTON FABRICS USING SOL-GEL TECHNOLOGY

MARIAN VALENTIN[a], IGOR KRUPA[a]*, PETER DEANKO[b], and JOZEF ŠESTÁK[b]

[a] Polymer Institute, Slovak Academy of Sciences, Dúbravská cesta 9, 84541 Bratislava, Slovakia, [b] VÚTCH-CHEMITEX, spol. s r. o., Rybníky 954, 011 68 Žilina, Slovakia
marian.valentin@savba.sk, *upolkrup@savba.sk*

In this work, a diffuse coplanar surface barrier discharged (DCSBD) plasma generated by atmospheric pressure has been used to modify fabrics (PES, PES-cotton) followed by the treatment with sol-gel silane solution. Modified surfaces were conditioned at 180 °C during 5 minutes. The plasma discharge was applied to ensure washing resistance of fabrics. The hydrophobicity was characterised through wetting-angle measurements. Fabrics treated with solutions containing fluorsilane portion reached significantly higher hydrophobicity than those ones modified by alkylsilane only. The highest hydrophobicity was obtained for PES-cotton fabric where the contact angle of distilled water before washing was 154° and 151° after standardised washing. Surfaces were also analysed by XPS, FTIR and SEM.

The research was supported by the Scientific Grant Agency of the Ministry of Education of Slovak Republic and the Slovak Academy of Sciences (project No. 2/0063/09) and by Science and Technology Assistance Agency under the contract VMSP-P-0023–09.

P-53
CHANGE OF WETTABILITY OF WOOL TEXTILE SURFACES AFTER PLASMA TREATMENT

PETRONELA VENCELOVÁ*, ANNA UJHELYIOVÁ, and ĽUDMILA ČERNÁKOVÁ

Slovak University of Technology in Bratislava, FCHFT, IPM, Department of Fibres and Textile Chemistry, Radlinského 9, 812 37 Bratislava, Slovak Republic
petronela.vencelova@stuba.sk

Introduction

The presence of scale on a wool fibre surface introduces a number of problems such as felting and a surface barrier to dyestuffs in the wool industry. In the past, chemical methods were the major treatment for eliminating those problems[1]. Plasma surface modification does not require the use of water and chemicals, resulting in a more economical and ecological process. The enormous advantage of plasma processes concerns the drastic reduction in pollutants and a corresponding cost reduction for effluent treatment, so it can be considered as an environmentally benign technology[2].

As a result, a low temperature plasma (LTP) method developed rapidly over the last decade has been introduced to the textile industry[1]. Plasma modification of textiles represents great opportunity for improvement of older, energetically demanding, slow and sometimes not very eco-friendly treatment technologies. Application of plasma is ecological and friendly for production costs due to energy savings and reduction of processing times. Compared to other scientific works describing increase of hydrophilicity of hemp, wool or PP textiles or decrease of felting shrinkage of wool[3].

Low temperature plasma is a partially ionized gas with electron temperatures much higher than ion temperatures. The high-energy electrons and low-energy molecular species can initiate reactions in the plasma volume without excessive heat causing substrate degradation. Low temperature plasmas are particularly suited to apply to textile processing because most textile materials are heat sensitive polymers. In addition, it is a versatile technique, where a large variety of chemically active functional groups can be incorporated into the textile surface. The possible aims of this are improved wettability, adhesion of coatings, printability, shrink resistance, dyeing properties, induced hydro- and/or oleophobic properties, changing physical and/or electrical properties, cleaning or disinfection of fibre surfaces etc. Moreover, non-thermal plasma surface modifications can be achieved over large textile areas[2,4].

Plasma can be used to modify different types of textile products. It has been used to modify the fibre surface such as: increase the failure stress and strain of carbon fibre and to improve shrink resistance of wool fabric. It has been reported that exposure of cotton yarn to the plasma of an electrical glow discharge resulted in an increase in breaking strength of the yarn. Plasma treated wool top offers a number of processing benefits at different stages of the wool pipeline including significant improvements in spinning performance and dyeing properties. The production of woven fabrics from plasma

treated tops offers considerable potential for the production of machine washable products minimising the conventional wet oxidation techniques. With the reference to previous research, exposure natural fabrics to a plasma environment can produce more reactive surfaces[3].

In addition to plasma processing is a clean (dry) and sustainable technology that generates minimal amounts of waste. It is also characterized by much lower materials and energy consumption in comparison to wet chemical-based finishing methods. Finally, because plasma processing results in a nanoscaled surface modification, it has the advantage of preserving the bulk properties as well as the touch of textiles[5].

In this paper the effect of the various conditions of low temperature plasma activation of wool textile materials will be presented. There will determine the change of wettability of untreated and treated wool textile materials.

Experimental

Material used

The woven fabrics from sizing and desizing wool were used as a substrate for the treatment of low temperature plasma.

Methods used

The samples of sizing and desizing wool textile were activated by low temperature plasma generated discharged at the atmospheric pressure for 3 and 5 seconds during different time of ageing. Next were measured wettability of wool untreatment and treatment fabrics.

The equipment See System (Surface Energy Evaluation System) was used for measuring of contact angles.

Contact angle measurement

An experimental equipment See System is a portable computer-based instrument consisting of rugged aluminium body, colour USB 2.0 camera with 1,3 Mpix resolution movable in vertical direction and 2D horizontally movable table for samples. This measuring equipment was designed primarily for contact angle measurement and surface energy determination. Liquid drops were dispersed on each fabric sample using a micrometer pipette. The image of each drop was captured by the camera connected with a computer. The captured images were viewed at the monitor. The images were captured after liquid droplets which were placed onto the sample surface and were photographed in 1 s. One specimen of untreated and seven specimens of treated wool fabrics were used for this experiment. Water, glycerol and ethylene glycol were used as measuring liquids.

Results and discussion

The results of contact angle of plasma treated and untreated wool samples are shown in Tables I–IV.

Contact angles for water and glycerol of untreated and treated specimens are comparable and higher than for ethylene glycol. By increasing of plasma ageing the contact angles of treated wool fabrics were increased compared to untreated fabric until 15 min. After 15 min of ageing the contact angles were decreased and after 60 min values of contact angles were similar to untreated wool specimen. Measured contact angles of treated wool textiles were lower by using ethylene glycol mainly after 10 and 15 min. After 60 min contact angles were increased but they didn't reach the values of untreated wool textile.

Table I
Contact angle of desizing wool fabrics after 3 s of plasma treatment

Ageing of plasma [min]	Contact angle [°]		
	water	glycerol	ethylene glycol
0	118,7	116,4	116,9
7	120,4	120,6	83,9
10	115,4	118,1	72,7
15	122,9	119,5	113,4
20	114,6	109,5	105,7
30	111,7	106,7	109,7
60	117,3	108,4	79,9
1440	116,5	112,3	108,3

Table II
Contact angle of sizing wool fabrics after 3 s of plasma treatment

Ageing of plasma [min]	Contact angle [°]		
	water	glycerol	ethylene glycol
0	98,84	121,31	120,94
7	82,48	106,94	85,45
10	93,19	101,67	70,70
15	95,69	100,54	75,83
20	102,45	105,54	80,48
30	99,73	112,60	86,67
60	96,50	116,44	98,43
1440	120,72	122,17	100,52

For sizing wool fabrics after 3 s of plasma treatment similar results were obtained. However, contact angles of sizing wool fabrics are lower than desizing wool materials. Measured values show that contact angles of treated specimen are lower at longer time of plasma ageing but at longer time of ageing the contact angles are approaching to values of untreated fabrics.

Similar results were obtained for desizing and sizing wool materials after 5 s of plasma activation where contact angles were higher for sizing specimens at 3 s of plasma treatment as we can show in Tables III and IV.

From the results we can see that contact angles of sizing wool textile materials were higher than contact angles of de-

Table III
Contact angle of desizing wool fabrics after 5 s of plasma treatment

Ageing of plasma [min]	Contact angle [°]		
	water	glycerol	ethylene glycol
0	118,7	116,4	116,9
7	116,6	113,2	101,0
10	115,6	108,5	66,0
15	104,8	111,1	79,5
20	116,3	112,1	90,5
30	106,0	104,2	92,3
60	115,0	116,9	100,8
1440	117,4	116,0	113,8

Table IV
Contact angle of sizing wool fabrics after 5 s of plasma treatment

Ageing of plasma [min]	Contact angle [°]		
	water	glycerol	ethylene glycol
0	98,84	121,31	120,94
7	105,96	106,13	87,27
10	104,14	109,81	81,32
15	109,30	111,75	84,07
20	93,91	109,51	90,94
30	110,40	99,11	86,02
60	109,13	116,78	88,28
1440	105,33	117,91	104,21

sizing wool fabrics which are shown in Tables I and II. This indicates that sizing could increase hydrophility of wool materials. As it can be observed from Table I–IV, the contact angles decreased after plasma treatment compared with the untreated wool samples in both the sizing and desizing wool textile materials after 3 and 5 s of plasma activation. This indicates that the surface free energy is increased for the plasma treated fabrics compared with the untreated. Changes of wettability by this modification are small and, in general, not important. Plasma oxidation reactions produce oxygen containing functional groups, which are attached to the polymer surface. These functional groups play an important role in increasing the hydrophilic properties of the fabrics[6]. The improved wettability might possibly be due to the removal of the outermost hydrophobic part of the wool fabric specimen[6]. As a result, the wettability of the plasma treated wool textile materials were improved.

Conclusions

By using LTP plasma for treating of wool textile materials, the wettability improved indicating penetration of plasma into the fabric. In this experiment was studying the effect of various treatment parameters on the wool specimens. From results were found that LTP treatment has positively effect to modify surface properties for improving the wettability. In this study was determined the effect of LTP treatment on the surface properties of wool textile materials.
Contact angle of desizing and sizing wool textile materials decreased to 10-30 min after plasma activation in both time of plasma treatment (3 and 5 s).

At lower values of contact angles the wettability is higher. The better wettability was obtained for the desizing and sizing wool materials. These properties can affect dyeing and finishing processes.

This work was supported by the Slovak Research and Development Agency under the contract No. VMSP-P-014-09.

REFERENCES

1. Kan C. W., et al: J. Mater. Process. Technol. *83*, 180 (1998).
2. Morent R., et al: Surf. Coat. Technol. 202, 3427 (2008).
3. Sun D., Stylios G. K.: J. Mater. Process. Technol. 173, 172 (2006).
4. Molina R.: Appl. Surf. Sci. *252*, 1417 (2005).
5. Guimond S., et al: Pure Appl. Chem. 82, 1239 (2010).
6. Yip J.: J. Mater. Process. Technol. 123, 5 (2002).

P-54
SYNTHESIS AND CHARACTERISTICS OF MAGNETIC CORE-SHELL NANOPARTICLES FOR ANISOTROPIC COMPOSITES

PIOTR WAGNER[a], TIMO STEINKE[a], MARKUS M. MÖWES[a], JENNIFER MCINTYRE[a], DIRK MENZEL[b],THOMAS ALSUTH[a], and ROBERT H. SCHUSTER[a]

[a] German Institute of Rubber Technology (DIK), Eupener Straße 33, D-30519 Hannover, Germany, [b] Institut für Physik der Kondensierten Materie, Technische Universität Braunschweig, Mendelssohnstraße 3, D-38106 Braunschweig, Germany
piotr.wagner@dikautschuk.de

Introduction

In the past 15 years there has been rapid progress in nanotechnology research. It has been proved that nanoparticles possess different physical and chemical properties than the bulk materials. Nanoparticles posses special optical properties due to the interaction between Π-orbitals of nanoparticles and electromagnetic waves of light. There are also different magnetic and quantum mechanical properties. The huge specific surface area causes high reactivity. The significance of the Van der Waals forces becomes more important due to

high mass-volume ratio and surface charge (zeta-Potential), as well of thermodynamical effects (Brownian motion). All of these properties lead to stable suspensions, but they may also cause aggregation of nanomaterials. The aim of this study is to generate a Composite with anisotropic magnetic properties incorporating magnetic nanoparticles into an elastomer matrix.

Experimental

The magnetic $MnFe_2O_4$ Nanoparticles were syntetheised in Bottom-Up process from their metallic salts[1,2]. Then the nanoparticles were functionalized with silanes. For the elastomer matrix a composite of silicone rubbers was selected. No vulcanization is required and it is easy to blend nanoparticles and elastomer. Another positive aspect was that polymerization was possible at room temperature. The nanoparticles were aligned in the same direction as the magnetic field lines.

Results and discussion

The synthesis of nanoparticles was optimized. High cristallinity was obtained using XRD measurements at 2 h and 80 °C as reaction conditions were investigated (Fig. 1). TEM analysis of $MnFe_2O_4$ nanoparticles showed that they were spherical. The average diameter of material was investigated and was found to be between 10 and 30 nm. This was confirmed by Debye-Scherrer equation from XRD Data. TGA and FT-IR analysis gave information about the functionalization grade. Rheometer measurements were necessary in order to investigate the frequency dependent dynamic material properties. A slurry of nanoparticles in silicone oil was tested.

Switching the magnetic field on and off during the measurement provides information about the changes in storage modulus (Fig. 2).

SQUID measurements were done to define magnetic hysteresis curves of $MnFe_2O_4$ nanoparticles.

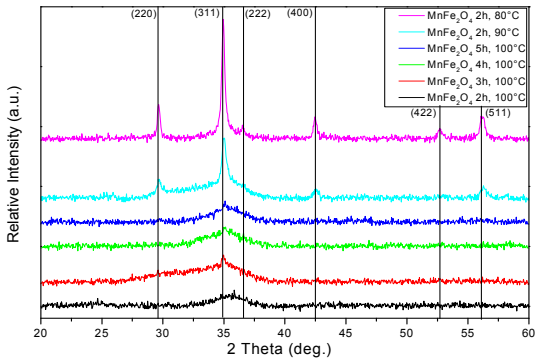

Fig. 1. **XRD spectra of $MnFe_2O_4$ nanoparticles synthesized at different conditions**

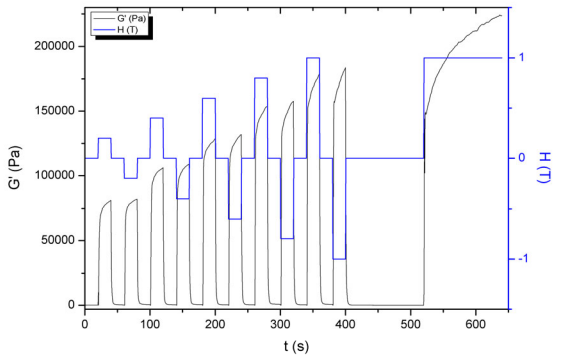

Fig. 2. **Rheometeric measurements of $MnFe_2O_4$ nanoparticles in silicone oil slurry**

Conclusion

The experiments carried out show that it is possible to create a stable anisotropic elastomer-nanoparticles composite. The high effect of magnetic nanoparticles on storage modules was proved in rheometric measurements.

We acknowledge BMBF and thank them for their support for the MAGNANO research project.

REFERENCES

1. Chinnasamy C. N., Jeyadevan B., Perales-Perez O., Shinoda K., Tohji K., Kasuya A.: IEEE Trans. Mag. *38*, 2640 (2002).
2. Caruntu D., Remond Y., Chou N., Jun M., Caruntu G., He J., Goloverda G., O'Connor C., Kolenichenko V.: Inorg. Chem. *41*, 6137 (2002).

P-55
TEXTILE MATERIALS MODIFIED WITH CYCLODEXTRINS

MAGDALENA WOLFOVA[a] LUDMILA CERNAKOVA[a] PETRA MICHALOVYCHOVA[a], and MIRKO CERNAK[b]

[a] Institute of Polymer Material, Slovak University of Technology, Radlinského 9, Bratislava 812 37, Slovakia, [b] R&D Center for Low-cost Plasma and Nanotechnology Surface Modifications, Masaryk University, Kotlarska 2, 611 37 Brno, Czech Republic
magdalena.wolfova@stuba.sk
cernak@fmph.uniba.sk

Introduction

During recent years many textile applications of cyclodextrins (CDs) in various industry sectors have been reported. This is because mainly the ability of CDs to form complexes

with perfumes or fragnances which can be stored over a long period without loss of these substances. On the other hand unpleasant odours of textiles can be removed by the complexation with cyclodextrins[1].The permanent fixation of CDs to the fibre surface leads to new odour absorbing textile material.

Cyclodextrins are natural, starch derived oligosaccharides. They are composed of α-1,4-coupled D-glucose units, which contain a hydrophobic internal cavity that can act as a host for various, generally lipophilic, guest molecules. Their specific shape is responsible for their original properties that consist of the possibility for organic substrates to penetrate spontaneously and reversibly inside their central cavity[2]. Therefore, molecules such as fragnances, drugs, pesticides and textile dyestuffs can be compexed by CDs.

The functionalisation of textile supports by cyclodextrins is a challenge that has been investigated in the last decade. Several interesting approaches in the textile functionalisation by CDs have been reported by Schollmeyer et al.[3,1] . The permanent fixation on fibres made from polyester is only possible with cyclodextrine derivates with long alkyl chains or other hydrophobic groups. Comparable with disperse dyeing, the hydrophobic part of the substitued cyclodextrins migrates into the fibre above the glass transition temperature. The polar cyclodextrins molecule remains on top of the fibre surface[1].

Martel[4] introduced a new method of immobilization of CDs onto PP consists of two steps. The PP is first submitted to electron beam irradiation, followed by the graft polymerization of glycidyl methacrylate (GMA). A PP nonwoven carrying polymerized GMA was the intermediate product. In a second step, the epoxide groups react with CDs´molecules to create the covalent linkage of the former, leading to the final product. Le Thuaut[5] et al. have recently reported a new way of immobilization of CDs onto PP nonwoven fabrics particularly adapted for filtration processes.

The use of cyclodextrins as a finishing agent of polyamide fibers was studied also. The finishing process involved polymerization between citric acid and CDs, which yielded a cross-linked polymer that physically adhered to the surface of PA fibers[6].

The aim of present work was to prepare polypropylene nonwoven surface modified with cyclodextrins. Before coating with CDs, textiles were pretreated by diffuse coplanar surface dielectric barrier discharge (DCSBD)[7].

Experimental

The polypropylene nonwoven (PPNW) was activated by an atmospheric-pressure plasma treatment in N_2 or ambient air. Based on our previous results, the times of activation was 5 seconds on both sides. The activated samples were immersed in solution of β-CDs/ γ-aminopropyltriethoxysilane (1 ml APTES: 90 ml EtOH: 9 ml H_2O). The concentration of cyclodextrins were 6, 12, 18 g l^{-1}. The drying process was realized in two ways, The PP samples were dried in the air at laboratory temperature or in drying chamber at temperature 125 °C.

Surface modification was confirmed gravimetrically and using SEM and ATR-FTIR spectroscopy.

Results

At first, the plasma activated PPNW were coated only with water solution of β-cyclodextrins and after drying the modified samples were washed in distilled water. It was found by gravimetric analysis, that 98 % from all coated amount of β-cyclodextrins was removed.

Because of that fact, it was chosen the possibility to modify the PPNW with cyclodextrins in combination with γ-aminopropyltriethoxysilane (APTES). Three parameters were studied, the concentration of CD solution, the drying temperature of samples and working atmosphere during plasma activation. The type of functionalization of PP imparted by plasma can be varied by selection of plasma gas and operating parameters. Air plasma has been used to oxidize polymer surface and nitrogeen plasmas has been used to ipart also amine group to the surface.

Fig. 1 indicated that the amount of β-cyclodextrins/ γ-aminopropyltriethoxysilane adhered to the PP fibers increases to the concentration of β-cyclodextrin in solution and depend on drying conditions (125 °C, 25 °C).

Contrary, plasma activation of PPNW samples in nitrogen atmosphere leads to almost the same content of β-cyclodextrins/ γ-aminopropyltriethoxysilane independently on method of drying (Fig. 2).

The modification of PPNW by CD/APTES was analysed by infrared spectroscopy (Fig. 3). The characteristic peaks in the region 1000–1200 cm^{-1} and 3000 cm^{-1}can be seen. The bands detected in the region 1000–1200 are associated with C-O vibrations of β-cyclodextrine. In this region are also characteristic peaks of Si-O valence from APTES.The presence of band at 1590 cm^{-1} correspond to APTES amine groups.

SEM pictures point out that fibres of polypropylene nonwoven are efficiently coated with cyclodextrin siloxane multilayer thin films (Fig. 4).

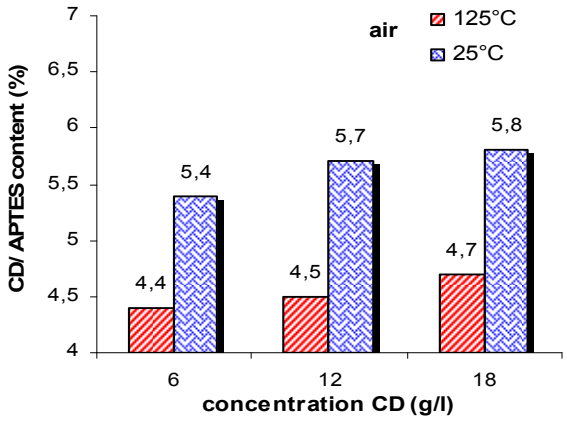

Fig. 1. **The dependence of CD/APTES content on concentration of CD solution, plasma activated in air atmosphere**

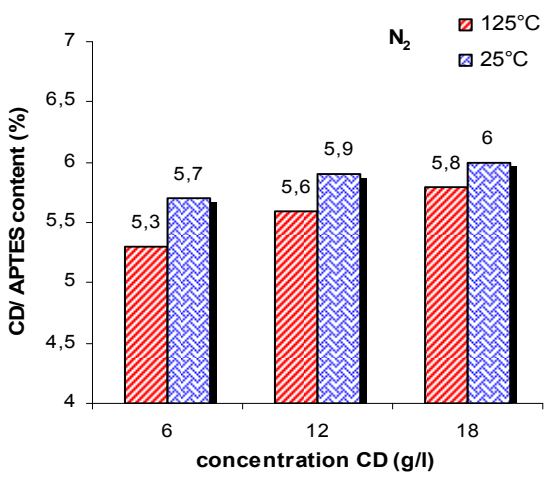

Fig. 2. **The dependence of CD/APTES content on concentration of CD solution, plasma activated in nitrogen atmosphere**

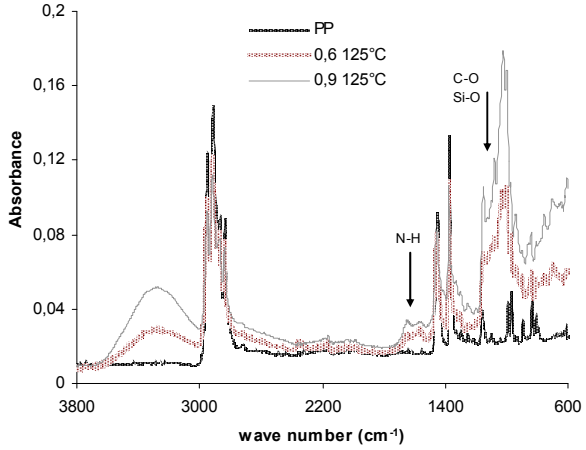

Fig. 3. **Spectrum of polypropylene non-woven, non- woven coated with layer of CD/APTES** (concentration of CD in solution was12 and 18 g l^{-1})

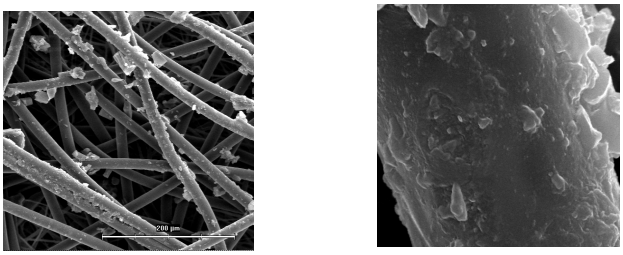

Fig. 4. **SEM images of the plasma-activated samples coated by CD/APTES**

The structure of siloxane film depend on the pH and drying condition. At pH 11, important observation is the frequency shift of the NH_2 deformation mode from 1601 to 1591 cm^{-1} upon heating. Before heating the samples, the amine groups are hydrogen bonded with the silanol groups. Upon heating the hydrogen bond is broken; the silanol groups condense and form Si-O-Si linkages as indicated by the splitting of the bands at 1035 and 1135 cm^{-1}. The amine groups become free.

When the siloxane film was dried in air, a bicarbonate structure can be formed[8] causing the appearance of bands at 1630, 1575, 1488, and 1332 cm^{-1}.

Conclusion

Plasma can be used as a precursor to other surface modification techniques, for example, plasma activation followed by silanization. The hydroxyl (carboxyl or amine) groups introduced by plasma activation to inert PP polymer surface can participate in the siloxane bond formation process and improve the adhesion of CD/APTES films to polypropyene nonwoven.

REFERENCES

1. Buschmann H.-J., Knittel D., Schollmeyer E.: J.Inclusion Phenom *40*, 169 (2001).
2. Manakker F., VermondenT.,Nostrum C.F., Hennink W. E.: Biomacromolecules *10*, 3157 (2009).
3. Schollmayer E., Grechin A., Buschmann H. J.: Functionalisation of textile materials using cyclodextrins, 3th *Int. Text. Clothing & Design Conference Oct. 2006*, *Dubrovnik,* Croatia, p. 351.
4. Martel B., at all: J. Appl. Polym. Sci. *78*, 2166 (2000).
5. Le Thuaut P., Martel B., Crini G., Maschke U., Coqueret X., Morcellet M.: J.Appl. Polym. Sci. *77*, 2118 (2000).
6. Ghoul Y.E. at all: Acta Materiala *4*, 1392 (2008).
7. Černák M., Černáková Ľ., Hudec I ., Kováčik D., Zahoranová A.: Eur. Phys. J. Appl. Phys. *47*, 22806 (2009).
8. Somsak Naviroj, Jack L. Koenig, Hatsuo Ishida: *Technical report 1981*, University Cleveland.

P-56
SPACE ANALYSIS OF THE MODEL STRUCTURE OF POLYMERS FILLED BY SPHERICAL PARTICLES

J. ZIDEK and J. KUCERA*

Brno University of Technology,Purkynova 118, 612 00 Brno Polymer Institute Brno, Tkalcovska 2, 656 49 Brno, Czech Republic
kucera@polymer.cz

The space distribution of particles is an important factor in a study of filled polymers. It can be used for interpretation of macroscopic properties. Mostly, the interpretations are based on 2D schematic pictures. Such schematic models may lead to some misinterpretation of structure-properties relation.

The real interpretation can be made from real 3D model. The real model was generated by AGLOMER software[1]. The particles in the real model were represented by hard spheres with prescribed volume fraction, particle size distribution and

local intensity of mixing. The results of modeling are positions and radii of given particles. They are visualized in Fig. 1.

The numerical model usually contains 100 000 spheres, which occupy volume cell with defined volume fraction (from 0 to 50 %). The raw data were applied to calculation of different functions. The resulting structural properties can be classified to three groups: analysis of particles agglomerates, analysis of void interparticle space and some special analysis (percolation, worm like chains).

In the first group there are the nearest particle distance (NPD) and agglomerates analyzed. For example NPD is useful in the analysis of nanocomposites. In the case when the interparticle distances start to be comparable to the radii of gyration of chains, it is observed connection of "particle – macromolecular chain – particle". The connection is relatively strong, however, it is separable. The separation and reconnection is characterized by long relaxation times[2].

Then the analysis of size and shape of agglomerates can be performed. The effect of agglomeration to the elastic modulus is very frequently reported in literature and leads for example to the Kerner-Nielsen theory, where one geometrical constant is replaced by a function of agglomeration[3]. The distribution of agglomerate size depended on effective volume. The effective volume is a volume of particle with certain interphase layer around particles. Concerning the shape, the aspect ratio was 2 with large variance. This value was observed independently on agglomerate size. That means that the agglomerates have usually shape of slightly elongated ellipsoids. Their shapes vary from sphere to jet-shape, but they never formed any chainlet or fiber structure.

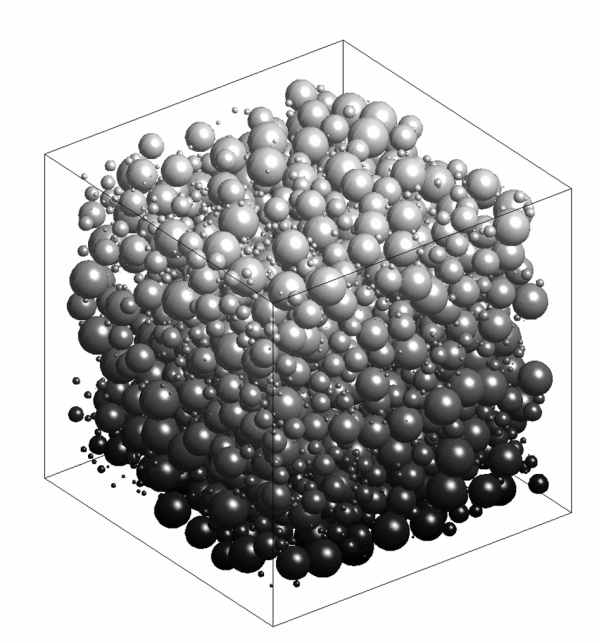

Fig. 1. **Visualization of hard-spheres model with given size distribution and volume fraction of spheres (50 %); basic model outputs are coordinates and radii of spheres**

The results of the second group of analysis concern the distribution of interparticle space. It can be determined by Voronoi analysis of interparticle cells. It was found that volume of interparticle cells have relatively broad distribution. There exist space cells much larger than the spaces in regular cubic lattice[4]. The next method of determination of interparticle space distribution is triangulation of particle positions. The distribution of lines connecting two triangulated particles is an image print of void places in the interparticle space. It can be related to the viscosity[5].

The third group of analysis contains a percolation and behavior of worm like chains in the free volume. The percolation probability increased rapidly after reaching certain particles concentration. The analysis by the worm like chains gives results which (together with Voronoi analysis) give information about restriction of macromolecular chains in nanocomposites.

This research was supported by Ministry of Education, Youth and Sports of the Czech Republic under research project MSM 0021630501 and Ministry of Industry and Trade under project FR-TI/232.

REFERENCES

1. Zidek J., Kucera J., Jancar J.: Computers, Materials & Continua *450*, 1 (2010).
2. Kalfus J., Kucera J., Jancar J.: Polym. Eng. Sci. *48*, 889 (2008).
3. Wu G., Lin Q. J., Zheng M. Z.: Polymer *47*, 2442 (2006).
4. Zidek J., Kucera J., Jancar J.: J. Nanoparticle Res., *in press*.
5. Hausnerova B., Zidek. J.: *International Conference on Injection Molding of Metals, Ceramics and Carbides; Orlando, Florida 2011*.

CONTENTS

Main Lectures

Key Lectures

Contributed Lectures

Posters

AUTHOR INDEX

SHIMADZU

Solutions for Science

since 1875

UV-VIS-NIR spectrophotometer UV 3600

CONTENTS

CHEMICKÉ LISTY • ročník/volume 105 (S), čís./no. Symposia • LISTY CHEMICKÉ roč./vol. 135, ČASOPIS PRO PRŮMYSL CHEMICKÝ, roč./vol. 121 • ISSN 0009-2770, ISSN 1213-7103 (e-verze), ISSN 1803-2389 (CD verze) • evidenční číslo MK ČR E 321 • Vydává Česká společnost chemická jako časopis Asociace českých chemických společností ve spolupráci s VŠCHT Praha, s ČSPCH a ÚOCHB AV ČR za finanční podpory Nadace Český literární fond a kolektivních členů ČSCH • IČO 444715 • Published by the Czech Chemical Society • VEDOUCÍ REDAKTOR/EDITOR-IN-CHIEF: B. Kratochvíl • REDAKTOŘI/ EDITORS: J. Barek, Z. Bělohlav, P. Drašar, J. Hetflejš, P. Holý, J. Horák, P. Chuchvalec, J. Podešva, P. Rauch, J. Volke; Bulletin: I. Valterová; Webové stránky: R. Liboska, P. Zámostný • ZAHRANIČNÍ A OBLASTNÍ REDAKTOŘI/FOREIGN AND REGIONAL EDITORS: F. Švec (USA), Z. Kolská (Ústí nad Labem) • KONZULTANT/ CONSULTANT: J. Kahovec • TECHNICKÁ REDAKTORKA/EDITORIAL ASSISTANT: R. Řápková • REDAKČNÍ RADA/ADVISORY BOARD: K. Bláha, L. Červený, E. Dibuszová, J. Hanika, Z. Havlas, J. Káš, M. Koman, J. Koubek, T. Míšek, V. Pačes, O. Paleta, V. Růžička, I. Stibor, V. Šimánek, R. Zahradník • ADRESA PRO ZASÍLÁNÍ PŘÍSPĚVKŮ/MANUSCRIPTS IN CZECH, SLOVAK OR ENGLISH CAN BE SENT TO: Chemické listy, Novotného lávka 5, 116 68 Praha 1; tel./phone +420 221 082 370, +420 222 220 184, e-mail: chem.listy@csvts.cz • INFORMACE O PŘEDPLATNÉM, OBJEDNÁVKY, PRODEJ JEDNOTLIVÝCH ČÍSEL A INZERCE/INFORMATION ADS: Sekretariát ČSCH, Novotného lávka 5, 116 68 Praha 1; tel. +420 222 220 184, e-mail: chem.spol@csvts.cz, chem.ekonom@csvts.cz • PLNÁ VERZE NA INTERNETU/FULL VERSION ON URL: http://www.chemicke-listy.cz • TISK: Rodomax s.r.o., Rezecká 1164, 549 01 Nové Město nad Metují • Redakce čísla Symposia (ISSUE EDITOR): Ľ. Černáková • SAZBA, ZLOM: ČSCH, Chemické listy • Copyright © 2011 Chemické listy/Česká společnost chemická • Cena výtisku 170 Kč, roční plné předplatné 2011 (12 čísel) 1730 Kč, individuální členské předplatné pro členy ČSCH 865 Kč. Roční předplatné ve Slovenské republice 92 EUR (doručování via SCHS), individuální členské předplatné pro členy ČSCH 70 EUR (doručování via SCHS), 258 EUR (individuální doručování), ceny jsou uvedeny včetně DPH • DISTRIBUTION ABROAD: KUBON & SAGNER, POB 34 01 08, D-80328 Munich, FRG; Annual subscription for 2011 (12 issues) 225 EUR • This journal has been registered with the Copyright Clearance Center, 2322 Rosewood Drive, Danvers, MA 01923, USA, where the consent and conditions can be obtained for copying the articles for personal or internal use • Pokyny pro autory najdete na http://www.chemicke-listy.cz , zkratky časopisů podle Chemical Abstract Service Source Index (viz http://cassi.cas.org/search.jsp) • Chemické listy obsahující Bulletin jsou zasílány zdarma všem individuálním a kolektivním členům ČSCH a ČSPCH v ČR i zahraničí, do všech relevantních knihoven v ČR a významným představitelům české chemie a chemického průmyslu; v rámci dohod o spolupráci i členům dalších odborných společností • Molekulární námět na obálce: P. Holý • Dáno do tisku 18.3.2011.

Universal testing machine

Electromechanical
High precision UTM AG-X
(up to 1500 kN)

Standard precision UTM
AGS-J (up to 10 kN)

Table top UTM (up to 5 kN)
EZ test

Servohydraulic UTM
Hydraulic UTM UH (up to 32 000 kN)

Hardness tester

High Speed Video Camera

Capilary Rheometer

Thermal Analyzers

SALD

SHIMADZU

Solutions for Science

since 1875